MECHANISTIC UNDERSTANDING OF RIBONUCLEOTIDE REDUCTASE INHIBITION BY HALOGENATED NUCLEOTIDE ANTICANCER AGENTS

A Dissertation

Presented to the Faculty of the Graduate School

of Cornell University

In Partial Fulfillment of the Requirements for the Degree of

Doctor of Philosophy in Chemistry

by

Somsinee Wisitpitthaya

May 2017

MECHANISTIC UNDERSTANDING OF RIBONUCLEOTIDE REDUCTASE INHIBITION BY HALOGENATED NUCLEOTIDE ANTICANCER AGENTS

Somsinee Wisitpitthaya, Ph. D.

Cornell University 2017

ABSTRACT

Ribonucleotide reductase (RNR) is an enzyme that catalyzes the conversion of ribonucleotides to C2′-deoxyribonucleotides, the building blocks for both DNA synthesis and repair in all living organisms, via controlled radical chemistry. Since RNR expression is elevated in many cancers, this enzyme is a major target of anticancer drugs. Until recently, the only clinically proven RNR-inhibition pathway was a suicide inactivation in which synthetic substrate analogues, for instance, gemcitabine diphosphate (F2CDP), irreversibly inactivate the RNR-$\alpha_2\beta_2$ heterodimeric complex. Recently, Clofarabine (ClF) nucleotides have been shown to reversibly inhibit the enzyme by targeting the large subunit of RNR (RNR-α) and inducing RNR-α-persistent hexamerization. To date, ClF nucleotides are the only known examples of this mechanism. In order to establish whether this reversible inhibition is a common mode of inhibition among nucleotide-derivative drugs, the active forms of two other drugs, Cladribine (ClA) and Fludarabine (FlU), were chemoenzymatically synthesized and their mechanism(s) of inhibition of RNR were evaluated. Enzyme inhibition and fluorescence anisotropy assays show that di- and triphosphates of these two nucleosides reversibly inhibit RNR with diverse K_i values, fairly dispersed in a range of 0.5–10 μM, and bind to the catalytic site (C-site) and the allosteric activity site (A-site) of RNR-α, respectively. Our EM studies, gel filtration, FRET, and protease digestion assays suggest that RNR-inhibition is coupled with the formation of

conformationally distinct hexamers. Studies in Flp-In HEK293 T-REx cells capable of selectively inducing either wild-type or oligomerization-defective mutant RNR-α overexpression define the central role of RNR-α oligomerization in drug activity, and highlight a potential resistant mechanism to these drugs. The results of these studies set the stage for new interventions targeting RNR oligomeric regulation.

Thesis Advisor: Yimon Aye

Title: Assistant Professor of Chemistry and Chemical Biology

BIOGRAPHICAL SKETCH

EDUCATION

Cornell University **Ithaca, NY**

Doctor of Philosophy in Chemistry (Spring 2017)
Cumulative GPA 3.76/4.00

Chulalongkorn University **Bangkok, Thailand**

Bachelor of Science in Chemistry (2011, Honors Program)
Cumulative GPA 3.99/4.00

SCHOLARSHIPS

- Granted a scholarship for Graduate study abroad from the Anandamahidol Foundation (2012-2017)
- Granted a full scholarship from "the Development and Promotion of Science and Technology Talents Project" (DPST) (2004-2011)

HONORS AND AWARDS

- Bayer Teaching Excellence prize, Cornell University (2014)
- First Class Honors with Gold Medal, Chulalongkorn University (2011)
- Professor Dr. Tab Nilanidhi Foundation Prizes, Chulalongkorn University (2011 and 2008)
- Prize for the highest GPA in Chemistry throughout Bachelor's degree course (2011)

PUBLICATIONS

[1] Wisitpitthaya, S., Zhao, Y., Long, M. J., Li, M., Fletcher, E. A., Blessing, W. A., Weiss, R. S., and Aye, Y. (2016) Cladribine and Fludarabine Nucleotides Induce Distinct Hexamers Defining a Common Mode of Reversible RNR Inhibition. *ACS Chem. Biol. 11*, 2021-2032.

[2] Fu, Y., Lin, H. Y., Wisitpitthaya, S., Blessing, W. A., and Aye, Y. (2014) A fluorimetric readout reporting the kinetics of nucleotide-induced human ribonucleotide reductase oligomerization. *ChemBioChem 15*, 2598-2604.

CONFERENCES

[1] Wisitpitthaya, S., Inayat, H., Zhao, Y., Long, M. J., Li, M., Fletcher, E. A., Blessing, W. A., Weiss, R. S., Ortega, J., and Aye, Y. (2016) Mechanism of Action of RNR Inhibition by Halogenated Nucleotide Anticancer Agents. The 252nd American Chemical Society (ACS) conference, Philadelphia, PA.

[2] Wisitpitthaya, S., Inayat, H., Zhao, Y., Li, M., Weiss, R. S., Ortega, J., and Aye, Y. (2015) Oligomeric Regulation of Ribonucleotide Reductase (RNR) by Antileukemic Nucleotides. The American Society for Biochemistry and Molecular Biology (ASBMB) conference, Boston, MA.

To His Majesty King Bhumibol Adulyadej

and my family

ACKNOWLEDGMENTS

I would like to thank the Anandamahidol Foundation, which was established by His Majesty King Bhumibol Adulyadej of Thailand, and all staff for their support in every way as well as their concern about my life in the United States.

Without support from my family, nanny, and lifelong friends, I would not have come this far in life. I would specifically like to thank my father for everything he has done for me, *i.e.*, encouragement, guidance, emotional support, and time.

I am lucky to have fantastic friends in graduate school, especially Joseph A. Haegele and Saba Parvez, who are also fellow graduate students in the Aye laboratory; they are both reliable and trustworthy friends that made the lab environment fun and supportive.

I would like to thank my advisor of this thesis, Professor Yimon Aye, my thesis committee, Professor Geoffrey Coates and Professor Hening Lin, and the director of graduate studies, Professor H. Floyd Davis, for their support in various ways.

My fluorescence anisotropy assays would not have been accomplished without a Fluorescence Spectrophotometer from Professor Chen's laboratory. There were many times during the revision of this manuscript when I urgently needed the instrument, and his students were always flexible with my use of it.

Lastly, I would like to thank all the members of the Aye laboratory whom I worked with throughout the years. In particular, I would like to thank Dr. Yuan Fu and Dr. Xinqiang Fang who taught me so much during my first year.

TABLE OF CONTENTS

LIST OF FIGURES

LIST OF TABLES

LIST OF SCHEMES

LIST OF ABBREVIATIONS

17-AAG	17-(Allylamino)-17-demethoxygeldanamycin
2D	two-dimensional
3-AP	Triapine
5-IAF	5-iodoacetamidofluorescein
5-TMRIA	tetramethylrhodamine-5-iodoacetamide dihydroiodide
A	absorbance
A	adenine
A	adenosine
AB	assay buffer
Ac	acetate
ADA	adenosine deaminase
ADP	adenosine diphosphate
AM	assay mixture
AMC	7-amino-4-methylcoumarin
AMP	adenosine monophosphate
AMPPNP	adenylyl-imidodiphosphate
APIM	AlkB homologue 2 PCNA-interacting motif
araA	9-β-D-arabinofuranosyladenine
ara-C	arabinosylcytosine
Arg	arginine
A-site	allosteric activity site
ATP	adenosine triphosphate
B	nucleobase
BCS	bovine calf serum
BME	β-mercaptoethanol
BSA	bovine serum albumin
Bu	butyl
BV	bed volume
Bz	benzoyl
C	cysteine
C	cytidine
C	cytosine
CAR	caracemide
CBZ	carboxybenzyl group
CDI	carbonyl diimidazole
CDP	cytidine diphosphate
ClA	Cladribine
CIP	alkaline phosphatase

	calf intestinal
ClF	Clofarabine
conc.	concentrated
cpm	count per minute
C-site	catalytic site
CV	column volume
Cys	cysteine
D	aspartic acid
d	doublet
dA	deoxyadenosine
dATP	deoxyadenosine triphosphate
dC	deoxycytidine
dC	deoxycytosine
dCDP	deoxycytidine diphosphate
dCK	deoxycytidine kinase
DFO	deferrioxamine
DFT	density functional theory
dGTP	deoxyguanosine triphosphate
DMF	dimethylformamide
DMSO	dimethyl sulfoxide
DNA	deoxyribonucleic acid
dNMP	deoxynucleoside monophosphate
dNDP	deoxynucleoside diphosphate
dNTP	deoxynucleoside triphosphate
DP	diphosphate
DTNB	5,5'-dithio-*bis*-(2-nitro-benzoic acid)
DTT	dithiothreitol
dTTP	deoxythymidine triphosphate
E	glutamic acid
E_0	standard oxidation-reduction potential
EC_{50}	half maximal effective concentration
EDTA	ethylenediamine-tetraacetic acid
em	emission
EM	electron microscopy
EPR	electron paramagnetic resonance
Eq.	equation
ESI	electrospray ionization
Et	ethyl
ex	excitation

F	phenylalanine
F2C	Gemcitabine
FA	fluorescence anisotropy
FAD	flavin adenine dinucleotide
FBS	fetal bovine serum
FDA	the US Food and Drug Administration
FLIP	flippase
FlU	Fludarabine
FPLC	fast protein liquid chromatography
FRET	fluorescence resonance energy transfer
FRT	flippase recognition target
G	guanine
G	glycine
GAPDH	glyceraldehyde 3-phosphate dehydrogenase
GDP	guanosine diphosphate
Gly	glycine
Grx	glutaredoxin
GrxR	glutathione reductase
GSH	glutathione
GSSG	glutathione disulfide
h	hour
h	human
H	histidine
HCl	hydrochloric acid
Hepes	4-(2-hydroxyethyl)-1-piperazineethanesulfonic acid
His	histidine
HPLC	high performance liquid chromatography
HRMS	high resolution mass spectrometry
HRP	horseradish peroxidase
HSP90	heat shock protein 90
HU	hydroxyurea
IM	inhibition mixture
IPTG	isopropyl β-D-thiogalactopyranoside
K	lysine
K	Kelvin
K_d	dissociation constant
K_i	inhibition constant
K_m	Michaelis-Menten constant
LB	Luria Broth
Leu	leucine

M	methionine
M	molecular weight marker
m	mouse
m	multiplet
m/z	mass/charge ratio
Me	methyl
min	minute
mM	millimolar
MMOH	methane monooxygenase
MP	monophosphate
mRNA	messenger ribonucleic acid
M.W.	molecular weight
N	asparagine
N	nucleoside
N/A	not applicable
NaCl	sodium chloride
NADPH	nicotinamide adenine dinucleotide phosphate reduced form
NDP	nucleoside diphosphate
NMP	nucleoside monophosphate
NMR	nuclear magnetic resonance spectroscopy
NMWL	nominal molecular weight limit
NTD	N-terminal domain
NTP	nucleoside triphosphate
OD	optical density
PCET	proton-coupled electron transfer
PDA	photodiode array
PDB	protein data bank
PELDOR	pulsed-electron double resonance
Phe	phenylalanine
PIP	PCNA-interacting protein
PMSF	phenylmethane sulfonyl fluoride
PP_i	inorganic pyrophosphate
ppm	part per million
PPP	triphosphate
psi	pounds per square inch
pyH^+	pyridinium ion
Q	glutamine

R	arginine
Ref.	reference
RNA	ribonucleic acid
RNR	ribonucleotide reductase
rpm	rounds per minute
RT	room temperature
s	singlet
S	serine
S•	thiyl radical
SA	specific activity
SAXS	small-angle X-ray scattering
Sc	*S. cerevisiae*
SD	standard deviation
SDS-PAGE	sodium dodecyl sulfate polyacrylamide gel electrophoresis
SEC	size exclusion chromatography
SH	sulfhydryl group
S-site	specificity site
t	triplet
T*-dATP	Texas Red®-5-dATP
TBAP	tributylammonium phosphate
TBAPP	tributylammonium pyrophosphate
TEAB	triethylammonium bicarbonate
TEM	transmission electron microscope
tet	tetracycline
TLC	thin layer chromatography
TP	triphosphate
TPS-TAZ	triisopropyl-Benzenesulfonyl Tetrazolide
Tris	tris(hydroxymethyl)-aminomethane
Trx	thioredoxin
TrxR	thioredoxin reductase
Tyr	tyrosine
U	unit
UDP	uridine diphosphate
UV	ultraviolet
Val	valine
W	tryptophan
wt	weight
wt	wild-type
Y	tyrosine
Y•	tyrosyl radical

ZRANB3	zinc finger Ran-binding domain-containing protein 3

LIST OF SYMBOLS

Å	angstrom	m	meter
α	large subunit of RNR	m	milli-
β	small subunit of RNR	M	mega-
c	centi-	M	molar
°C	Celsius	n	nano-
Ci	curie	T-α	5-TMRIA labeled hRNR-α
Da	Dalton		
δ	chemical shift	υ	velocity
Δ	deletion	v	volume
Δ^x	double bond located on the x^{th} C–C, counting from the carboxylic acid end of fatty acids	V	volt
		V_{max}	maximum velocity
		W	watt
ε_0	molar extinction coefficient		
F-α	5-IAF labeled hRNR-α		
g	gram		
g	gravity		
G	gauss		
Hz	hertz		
k	kilo-		
L	liter		
λ	wavelength		
μ	micro-		

PREFACE

My work presented in chapters 2, 3, 4 and portions of the Appendix have appeared in the following publication:

Wisitpitthaya, S., Zhao, Y., Long, M. J., Li, M., Fletcher, E. A., Blessing, W. A., Weiss, R. S., and Aye, Y. (2016) Cladribine and Fludarabine Nucleotides Induce Distinct Hexamers Defining a Common Mode of Reversible RNR Inhibition. *ACS Chem. Biol. 11*, 2021-2032.

CHAPTER 1

Ribonucleotide Reductases

1.1 General overview

Ribonucleotide reductases (RNRs) are enzymes responsible for the reduction of ribonucleotides to C2′-deoxyribonucleotides, the building blocks for both DNA synthesis and repair in all living organisms (Figure 1-1).[1-4] Since either elevated or unbalanced levels of the four deoxynucleoside triphosphates (dNTPs) increase the mutation rate dramatically, cell thus must have a tight control over the synthesis of these DNA precursors.[5]

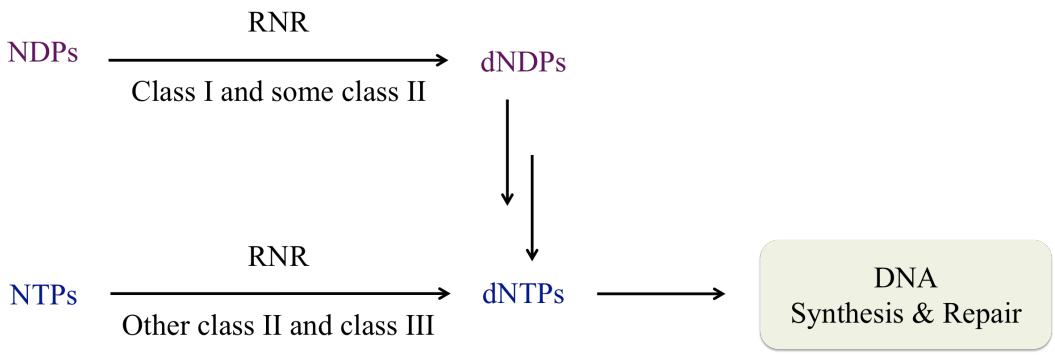

NDPs, Nucleoside Diphosphates; NTPs, Nucleoside Triphosphates.

Figure 1-1. Class I and some class II RNRs catalyze the reduction of NDPs, whereas class III and other class II RNRs operate at the NTPs level.[5,6] However, all RNRs provide precursors for DNA synthesis and repair.

As RNR plays a central role in this *de novo* synthesis, Nature invented sophisticated mechanisms, *e.g.*, gene transcription, protein degradation, mRNA stability, specific inhibitors as well as a unique allosteric control, to regulate the enzyme activity on many levels.[1,5] Under a scope of this study, we will only focus on enzyme allosteric regulation.

In nearly all cellular organisms and many viruses, RNRs initiate the reduction process of nucleotides by utilizing an essential thiyl radical, which is adjacent to the substrate at the active site, to subtract a 3′-hydrogen from the substrate (*more detail about RNR catalysis is discussed below, Figure 1-4*).[1,7,8] RNRs have been classified into three major classes and a few subclasses (Table 1-1, Figure 1-2)[9] largely based on how this radical can be (re)generated in each catalysis cycle.[1,5,10,11] Class I RNRs have a tyrosyl radical that is generated and stabilized by an oxo-bridged binuclear complex located in another subunit (β). Since oxygen is required for the metal center formation, class I RNRs sometimes are called the aerobic RNRs. Class II RNRs utilize adenosylcobalamin to generate a deoxyadenosyl radical under both aerobic and anaerobic conditions.[4,6,12] Class III RNRs only function in anaerobic surroundings and require an oxygen-sensitive glycyl radical[5] generated by a process that involves [Fe–S] cluster and S-adenosyl methionine.[12] While the radical from either class II deoxyadenosyl radical or class III glycyl radical comes into direct contact with the active site cysteine in catalytic subunit (α)[5,13], the radical from class I tyrosyl radical needs to be transferred from the β subunit to the active site cysteine residue via the putative proton-coupled electron transfer (PCET) pathway. Other differences among RNRs, *e.g.*, oxygen dependency, subunit composition and allosteric regulation, are also used as criteria to classified RNRs (Table 1-1).[5]

Table 1-1. Three major classes of RNRs classified by their free radical chemistry, oxygen dependence, subunit composition, and allosteric regulation. Class I is further divided into three subclasses based on the identity of the metallocofactor.[1,5,10,11]

	Class I			Class II	Class III
	Class Ia	**Class Ib**	**Class Ic**		
Metals/cofactors	Fe^{III}–O–Fe^{III}	Fe^{III}–O–Fe^{III} Mn^{III}–O–Mn^{III}	Mn^{IV}–O–Fe^{III}	Co	Fe^{II}–S^{II}
Subunit structure	$\alpha_2\beta_2$	$\alpha_2\beta_2$	$\alpha_2\beta_2$	α or α_2	$\alpha_2 + \beta_2$
Radicals involve in turnover	Tyr, Cys	Tyr, Cys	Phe/Leu/Val, Cys	Deoxyadenosyl, Cys	Deoxyadenosyl, Gly, Cys
Oxygen dependence	Aerobic	Aerobic	Aerobic	No dependency	Anaerobic
Nucleotide substrates	NDP	NDP	NDP	NDP/NTP	NTP
Reductant	Thioredoxin, glutaredoxin	NrdH-redoxin, glutaredoxin	Unknown	Thioredoxin	Formate, Thioredoxin[§]
Allosteric sites	A- and S-sites	S-site	A- and S-sites	S-site (rarely A-site)	A- and S-sites
Distribution	Eukaryotes, eubacteria, archaea, bacteriophages, virus	Eubacteria	Eubacteria	Archaea, eubacteria, bacteriophages	Archaea, eubacteria, bacteriophages

[§]In 2014, Wei et al discovered a new subtype of class III RNRs in Neisseria bacilliformis. Unlike class III RNRs studied to date that utilize formate as a reductant, this subclass facilitates the nucleotide reduction using the ubiquitous thioredoxin/thioredoxin reductase/NADPH system.[14]

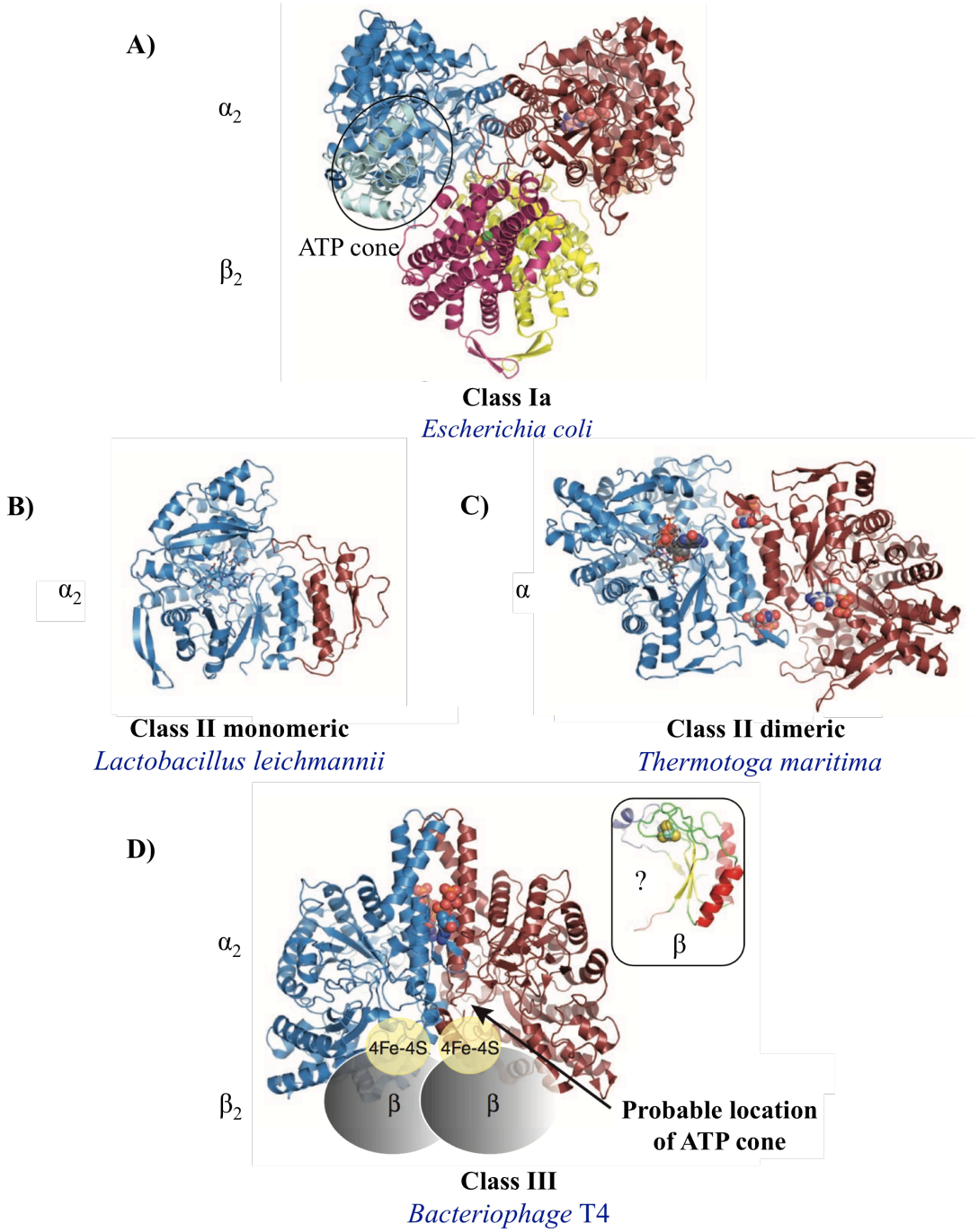

α, the catalytic subunit where the NDPs reduction occurs; β, the smaller subunit, assembles the metallocofactors in class I and class III.

Figure 1-2. Models of the three different classes of RNRs, taken from Ref. 9. Space-filling models represent substrates and allosteric effectors. **A)** The active $\alpha_2\beta_2$

holocomplex in class Ia. This model was made based on the crystal structures of *E. coli* RNR-α (PDB: 1RLR)[8] and *E. coli* RNR-β (PBD: 1RIB)[15] subunits. An N-terminal ATP cone is where ATP/dATP binds to the enzyme and regulates its activity. **B)** The monomeric class II from *L. leichmannii* (PDB: 1L1L).[16] There is a small structural extension in this monomeric class II enzyme substituting the specificity effector-binding site that, in the case of dimeric state, is constituted by another monomeric RNR-α.[1] **C)** The dimeric class II from *T. maritima* (PDB: 3O0O).[17] Stick models (in **B–C**) represent the adenosylcobalamin cofactors in the class II enzymes. **D)** *Bacteriophage* T4 Class III (PDB: 1HK8).[18] Inset shows a homology model of a β-monomer for this class.

Intriguingly, it is known that one organism can have multiple classes of RNRs, though, the expression of which depends on growth conditions.[11] For example, *E. coli* possesses three classes of RNRs (class Ia, Ib and III), where class Ia is expressed under typical conditions. Since *E. coli* class Ib RNR is not essential for *E. coli* growth, it is poorly expressed.[19,20] However, when the surrounding environment changes to microaerophilic or anaerobic conditions, *E. coli* class III RNR is instead expressed.[19] In this thesis, we will mainly focus on class Ia RNRs.

Class I RNRs are found almost in all eukaryotes and some eubacteria, viruses and bacteriophages.[3,21] They contain two dissimilar subunits, α and β, which both function as homodimers (α_2 and β_2) and are needed for enzyme activity. In all eukaryotes, interactions between α_2 and β_2 can lead to the formation of an $\alpha_n\beta_m$ complex, of which minimally active form is the $\alpha_2\beta_2$ heterodimeric complex.[21-25]

During the enzyme catalysis of class Ia RNRs, their stable tyrosyl radical required for enzymatic turnover is generated in the β subunit by the Fe^{III}–O–Fe^{III} center and subsequently transferred to the α subunit via the PCET pathway, generating

the active thiyl radical at the catalytic site (C-site) (Figure 1-3).[1,5,8] More detail of how this thiyl radical is generated and transferred to the active site cysteine is later discussed in *section 1.3*. In addition to the C-site, this larger subunit contains two allosteric sites, the allosteric activity site (A-site) and the specificity site (S-site). In the absence of nucleotides, the α subunit is present as a monomer.[21,22,25-29] However, upon binding of triphosphate effectors to the S-site, α dimerization is induced, which consequently primes α for substrate selection at the C-site. Binding of ATP (the positive activity effector) or dATP (the negative activity effector) to the A-site, on the other hand, controls the enzyme overall activity (Figure 1-3).[1,5,22]

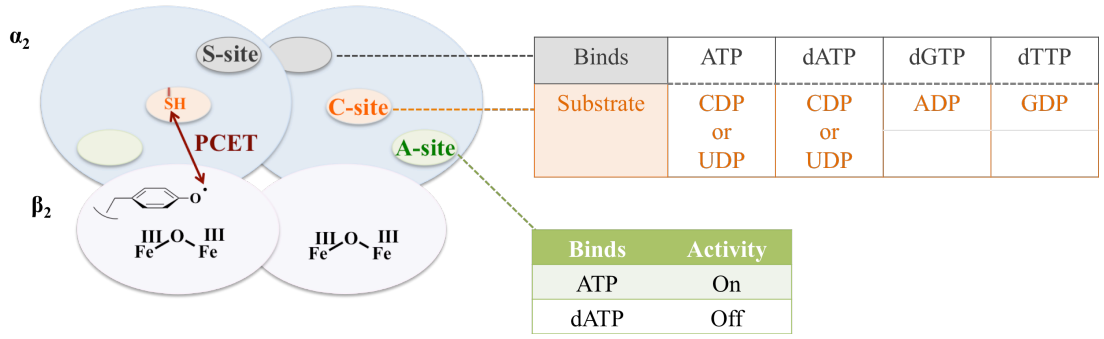

Binds	ATP	dATP	dGTP	dTTP
Substrate	CDP or UDP	CDP or UDP	ADP	GDP

Binds	Activity
ATP	On
dATP	Off

PCET, Proton-Coupled Electron Transfer.

Figure 1-3. The active $\alpha_2\beta_2$ holocomplex of class Ia RNRs. The radical from the transient tyrosyl radical in the β subunit is transferred to the catalytic site (C-site) cysteine residue in the α subunit via PCET pathway, initiating radical-based chemistry on the NDP substrates. Binding of effectors to the allosteric activity site (A-site) and the specificity site (S-site) controls the overall enzyme activity and which substrates are reduced at the C-site, respectively.[1,5]

The generic mechanism of NDPs reduction catalyzed by *E. coli* class Ia RNRs with its natural substrate is quite well established to date (Figure 1-4A).[6,14,24,30-32] The

substrate reduction is initiated by the abstraction of the C3′ hydrogen atom by a transient, conserved, top face thiyl radical[33] in the C-site, generating a substrate radical intermediate **2**.[34-36] A loss of water molecule from the C2′ position in the next step, which leads to the formation of a ketyl radical in state **3,** likely involves general base catalysis by a conserved glutamate. This radical can be subsequently reduced by the bottom face conserved cysteines[32], generating a C3′-keto nucleotide and a disulfide anion radical[37] (state **4)**. This anion radical then serves as the reductant for the substrate C3′-keto nucleotide, forming a C3′-deoxynucleotide radical and a disulfide bridge (state **5**). Regeneration of the top face thiyl radical finally leads to product formation.[14] The radical in this final state **6** is then transferred via the PCET pathway back to the β subunit, reforming the stable tyrosyl radical. However, for the complete turnover, the active site disulfide bridge at the bottom face must be reduced.[6] As shown in figure 1-4B, a disulfide exchange between the active site disulfide bridge and a pair of conserved cysteines on the C-terminal tail of α[32] occurs first, then enzyme thioredoxin (Trx) or glutaredoxin (Grx) re-reduces the consequent C-terminal tail disulfide bond. Trx (or Grx) would probably prefer to reduce the cysteine radical at the C-site (if there is any) rather than the disulfide bridge. This might explain why RNR utilizes a separate β-subunit to store the radical since Trx (or Grx) cannot access the tyrosyl radical buried inside the β-subunit.[6]

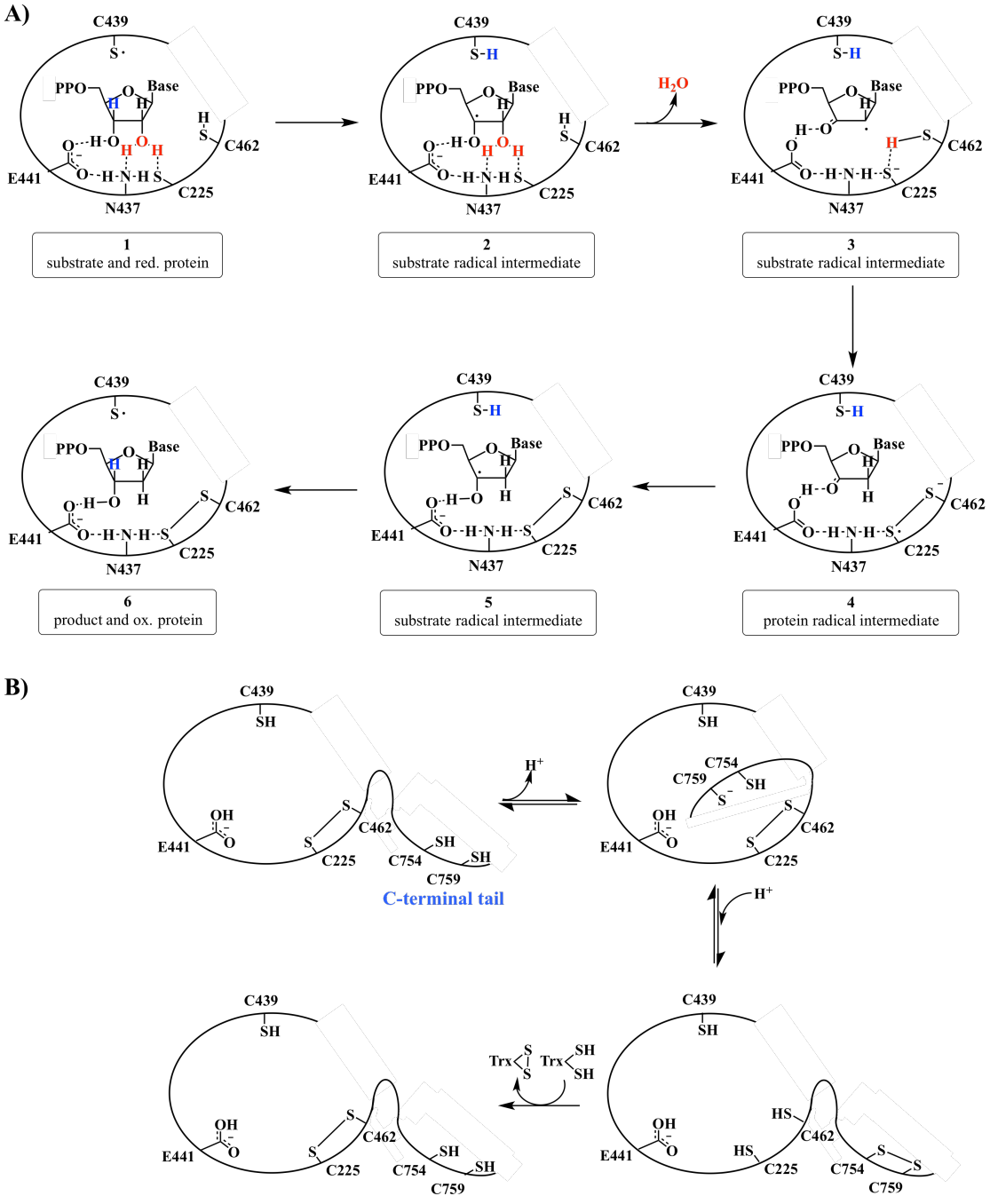

Base, nucleobases; red., reduced; ox., oxidized.

Figure 1-4. Mechanistic models for **A)** NDPs reduction catalyzed by class I RNRs, and **B)** re-reduction of the active site disulfide bond via a pair of conserved cysteine

residues on the C-terminal tail, which subsequently gets re-reduced by a ubiquitous enzyme thioredoxin (Trx). The existence of the two disulfide bridges in the α-subunit was first recognized by Thelander[38] in 1974. He shows that one disulfide bridge is formed after each NDP reduced in the *E. coli* class Ia system. However, two nucleotides can be reduced by the fully reduced enzyme in the absence of external reductants, indicating there are two disulfide bridges involved in the active monomer of *E. coli* class Ia RNR-α. This RNR catalysis is conserved from *E. coli* to *H. Sapiens*.[39] The shown amino acid numbering is from *E. coli* Class Ia RNR system.[14]

In order to regenerate the active Trx (or Grx) for the next turnover, the oxidized Trx-S_2 (or Grx-S_2) is re-reduced via a redox chain shown in Figure 1-5, which involves the NADPH binding flavoprotein thioredoxin reductase (TrxR) (or NADPH binding flavoprotein glutathione reductase (GrxR)).[40]

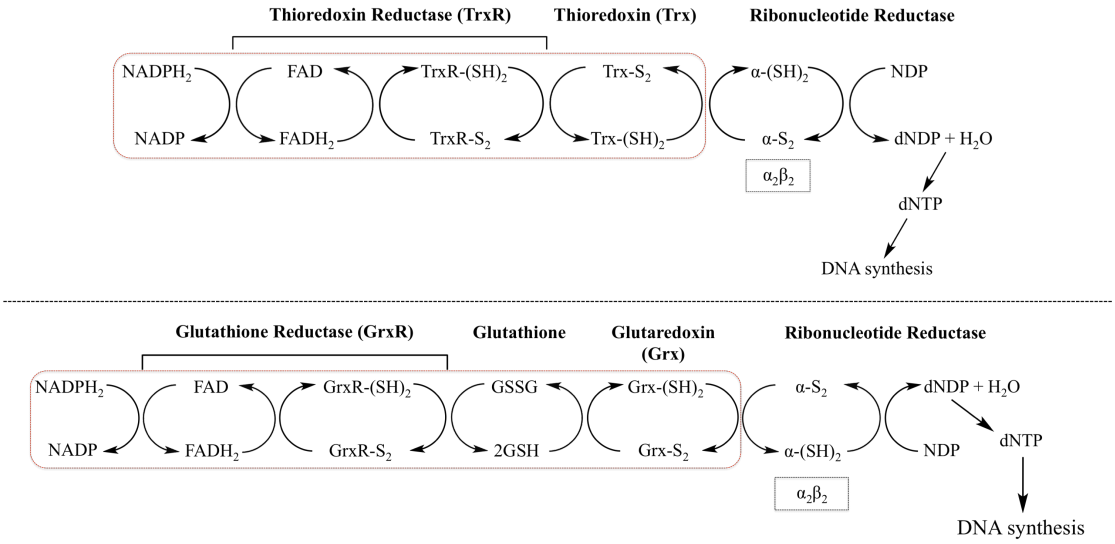

Figure 1-5. The thioredoxin system (*top*) and the glutaredoxin system (*bottom*) involving in RNR catalysis turnover.[40]

1.2 Allosteric regulation of class Ia RNRs

To ensure a balanced pool of deoxynucleotide monomer for DNA replication, the regulation of class Ia RNRs activity involves multiple allosteric sites, four different nucleotide effectors (ATP, dATP, dTTP, and dGTP), and changes in enzyme oligomeric state that accompany allosteric ligand binding.[41-43] In this section, we will discuss how these allosteric effectors regulate enzyme activity and substrate selection.

To date, it seems that the formation of α_n and $\alpha_n\beta_m$ oligomers plays an important role in the regulation of class I RNRs overall activity.[5] Once the allosteric effectors (ATP, dATP, dTTP, or dGTP) bind to the S-site, RNR-α is stimulated to dimerize and bind to the β_2 subunit to form an active $\alpha_2\beta_2$ holocomplex.[1,5,22] In 2006, Rofougaran *et al*[28] showed that in the presence of physiological concentrations of α and β subunits and under the physiologically relevant conditions where both A- and S-sites are occupied, an either active or inactive $\alpha_6\beta_2$ is formed depends on whether ATP or dATP is bound to the A-site. The ability of ATP and dATP to induce the same quaternary structure but have opposing effects on RNR activity had been a conundrum until Fairman *et al*[22] successfully crystallized a low-resolution (6.6 Å) X-ray structure of the dATP-bound hexamer from *S. cerevisiae* (Sc) class I RNR in 2011. Based on their results, the dATP-bound hexamer has a ring-like structure built up from three α-dimers. Their cryo-electron microscopy (cryo-EM) study of the inactive $\alpha_6\beta\beta'$ complex (in yeast, β_2 is $\beta\beta'$) showed that the $\beta\beta'$ subunit was bound in the center of the dATP-induced-ScRNR-hexamer ring, which prevents the $\beta\beta'$ to interact properly to the α subunit. As the results, this complex is inactive because the PCET can no longer occur under these structural settings. Also, a formation of complex other than $\alpha_6\beta\beta'$ is excluded in this case because only one $\beta\beta'$ can be accommodated inside the α_6-ring.

To investigate whether or not mutagenesis can target interactions at the observed hexamer interfaces and disrupt α-hexamerization, they also designed and purifed the D16R mutation in both *S. cerevisiae* (Sc) and human (h) RNR-α proteins. Based on their size exclusion chromatography (SEC) chromatograms, the D16R mutant proteins from both organisms cannot form dATP-induced hexamers. These results indicate that both ScRNR-α and hRNR-α utilize the same mechanism for dATP-induced α-hexamerization. However, the D16R hRNR-α retained its ability to hexamerize in the presence of ATP. It is unfortunate that to date there is no crystal structures available for the ATP-induced RNR-α-hexamer. However, by using gel filtration analysis, Wang *et al*[44] showed that ATP-induced α-hexamer can bind up to three p53β (an analogue of β in mammalian cells) dimers if the substrate analogue gemcitabine-5′-diphosphate (F2CDP) is added to the enzyme. Since a formation of an $\alpha_6\beta_6$ complex by fitting three β_2 in the center of the dATP-induced α_6-ring would not be possible as earlier discussed[22], these results altogether provided another solid evidence to support that ATP and dATP induce structurally different α-hexamers. Recently, Ando *et al*[45] crystalized a low-resolution (9.0 Å) crystal structure of the dATP-induced hRNR-α_6 where the C-sites align close to the inner hole (Figure 1-6, A–B). Based on their small-angle X-ray scattering (SAXS) data, ATP and dATP induce hRNR-α to form a similar hexamer. However, addition of equimolar β to both samples led to a loss of features representing hexamer in ATP-treated sample, while SAXS profile of dATP-treated sample still shared similar features as that of the one without β subunit. To correlate α-oligomerization with the specific activity of α, they performed assays for CDP reductase activity in the absence or presence of ATP or dATP. At the concentrations where both ATP and dATP induce hRNR-α_6, determined by their SAXS profiles, α activity remains activated in the case of ATP, but mostly inhibited by dATP. Differences in the ATP- and dATP-induced α_6 are thus verified. The authors also

proposed a model to answer a long-lasting question about why the ATP- and dATP-induced α_6 have opposing effects on α-activity (Figure 1-6C).

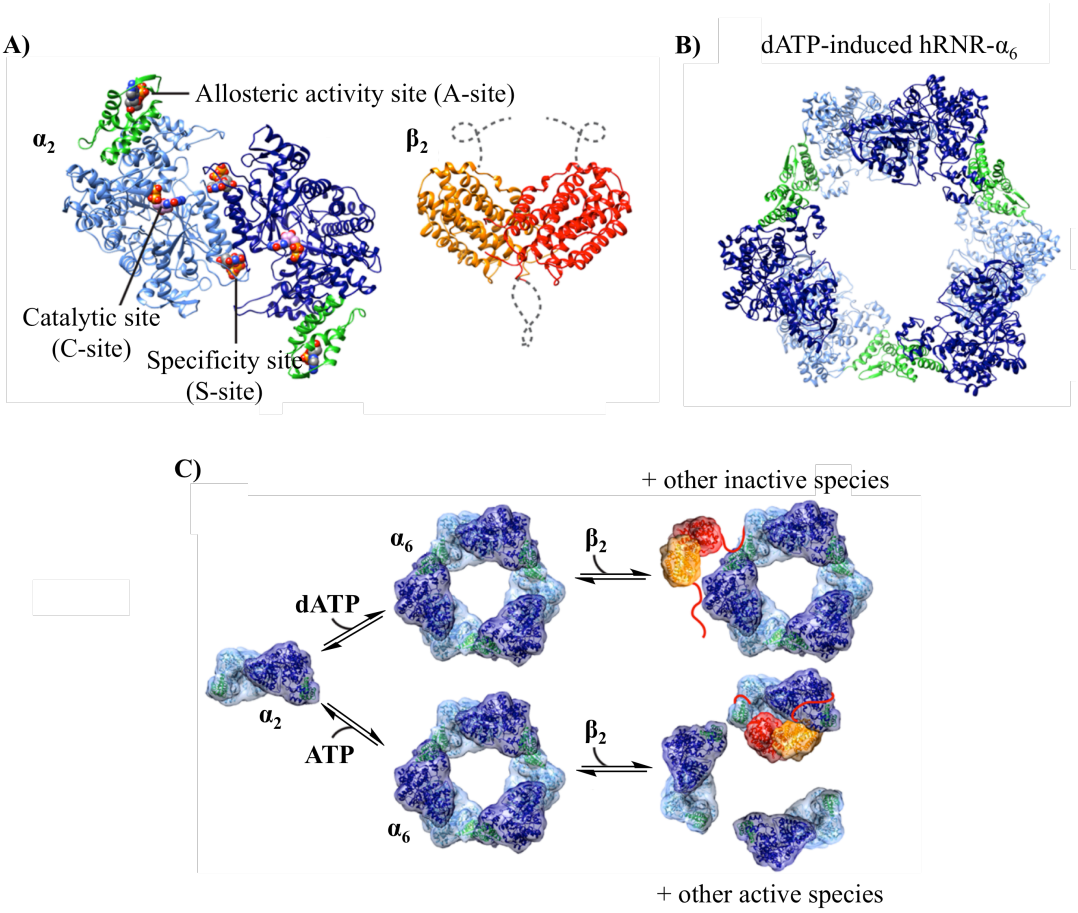

This figure is taken and modified form Ref. 45.

Figure 1-6. A) Structures of hRNR-α_2 and hRNR-β_2 subunits. Each monomer of hRNR-α_2 houses three nucleotide binding sites, C-site (PDB: 3HND), A-site (PDB: 3HNE) and S-site (PDB: 3HNC).[22] Green colored ribbon structures indicate the N-terminal ATP cone domain, where the A-site is located. Dotted lines shown in hRNR-β_2 structure represent the disordered C-terminus and N-terminus (PDB: 2UW2; To be published data of Welin *et al*). **B)** Crystal structure of the dATP-induced α_6 (PDB: 5D1Y).[45] **C)** Model of the ATP- and dATP-induced α_6, of which their stability is variable. In hRNR, binding of ATP or dATP to α subunit can promote the formation

of ring-shaped α_6 in the absence of β_2. Since the ATP-induced α_6 is less stable than the dATP-induced α_6, β_2 can disrupt the ATP-induced α_6 but cannot do so to the dATP-induced α_6 ring. As the results, access of β subunit to the C-site of α is prevented in the case of the dATP-induced α_6.

In contrast to the A-site, the S-site has the ability to bind dGTP and dTTP in addition to ATP and dATP. Specificity of NDP substrate binding to the C-site depends on the occupancy of this site. Binding of ATP or dATP to this site stimulates reduction of CDP or UDP at the C-site, while binding of dGTP and dTTP direct the enzyme toward to reduction of ADP and GDP, respectively.[1,4,5,43] This general model for substrate selection is well-supported by biochemical and structural data.[4,22,46-51]

Originally, it was unclear how the effectors bound to the S-site direct substrate binding since these two sites are approximately 15 Å apart from each other.[4] But, now, since many crystal structures of RNRs in the presence of allosteric effectors and substrates available[22,47-50,52], it is unambiguous that the S-site communicates with the C-site via a flexible loop 2 (residues 289–303 in *E. coli* or 283–298 in humans), which bridges these two sites[48] (Figure 1-7). When the allosteric effector binds to the S-site, the conformation of loop 2 is changed in such a way that it affects the C-site conformation in a highly specific manner, making it prone to bind one substrate over the others.[4, 5] Loop 2, as a consequence, becomes more ordered after the effector and substrate binding.[48,50] In addition to loop 2, there is an additional loop, so-called loop 1 (residues 259–278 in *E. coli*) (Figure 1-7), located near the S-site and is stabilized upon the effector binding.[50]

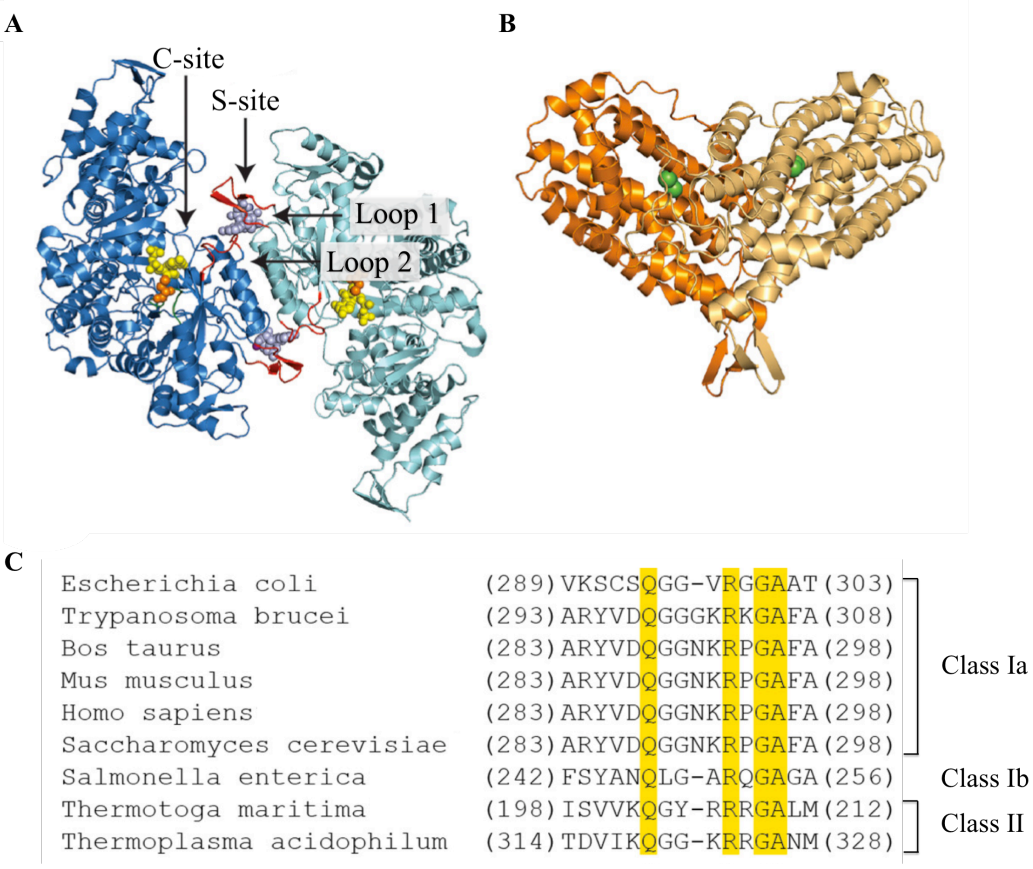

This figure is taken and modified from Ref. 48.

Figure 1-7. Ribbon representation of two subunits in the *E. coli* class Ia RNR, **A)** α-subunit (PDB: 3R1R)[50] and **B)** β-subunit (PDB: 1RIB)[15]. In **A)**, NDP substrate and dNTP specific effector are shown as spheres in yellow and purple, respectively. Orange spheres represent C439, where the active site thiyl radical is formed. Loop 1 and loop 2 are colored in red. In **B)**, one β chain is colored in orange and the other is in tan. Green spheres represent the diiron cofactor needed for the initial tyrosyl radical generation. **C)** Sequence alignment of loop 2 residues of characterized class Ia, class Ib, and class II RNRs. The absolutely conserved residues are highlighted.

In 2016, Zimanyi *et al*[48] determined their crystal structures of *E. coli* class Ia RNR with all four pairs of specificity effector–substrate bound (dATP–CDP, dATP–

UDP, TTP–GDP, and dGTP–ADP), and revealed the conformational rearrangements responsible for this allostery (Figure 1-8). Based on their composite omit electron density maps, they confirm that loop 2 is ordered after effector and substrate bind to the enzyme (Figure 1-8, *left panels*). The results also show a stabilized loop 2 that adopts three different conformations depending on which specific effector is bound to the S-site. In brief, dATP can hydrogen bond to S293, which subsequently makes Q294 orienting toward the C-site and stabilizing the binding of both CDP and UDP (Figure 1-8, A–B). Since cytidine deaminase provides another level of control for dCTP/TTP ratios, this lack of discrimination between CDP and UDP substrates by RNR should not be troublesome.[53,54] In contrast to dATP, binding of dGTP hydrogen bonds to Q294 and pulls it away from the C-site, creating a more expansive C-site for the larger purine substrates to bind and hydrogen bond to the carbonyl of G299. Even though binding of CDP and UDP is not prohibited in this case, the CDP/UDP binding would not be stabilized due to the absence of Q294 at the C-site (Figure 1-8, A–C). Likewise, binding of TTP to the S-site creates room at the C-site for purine substrates, even though TTP does not direct hydrogen bond to Q294 (Figure 1-8D). Specificity for ADP versus GDP appears to be modulated by the position of the carbonyl of G299. If effector-loop contact stabilizes the carbonyl of G299 in a forward position, ADP is favored, whereas stabilizing the carbonyl of G299 in a backward position favors GDP (Figure 1-8, C–D). Among the differences discussed above, R298 of loop 2 always forms a conserved charge-charge interaction with the β-phosphate of all four substrates.

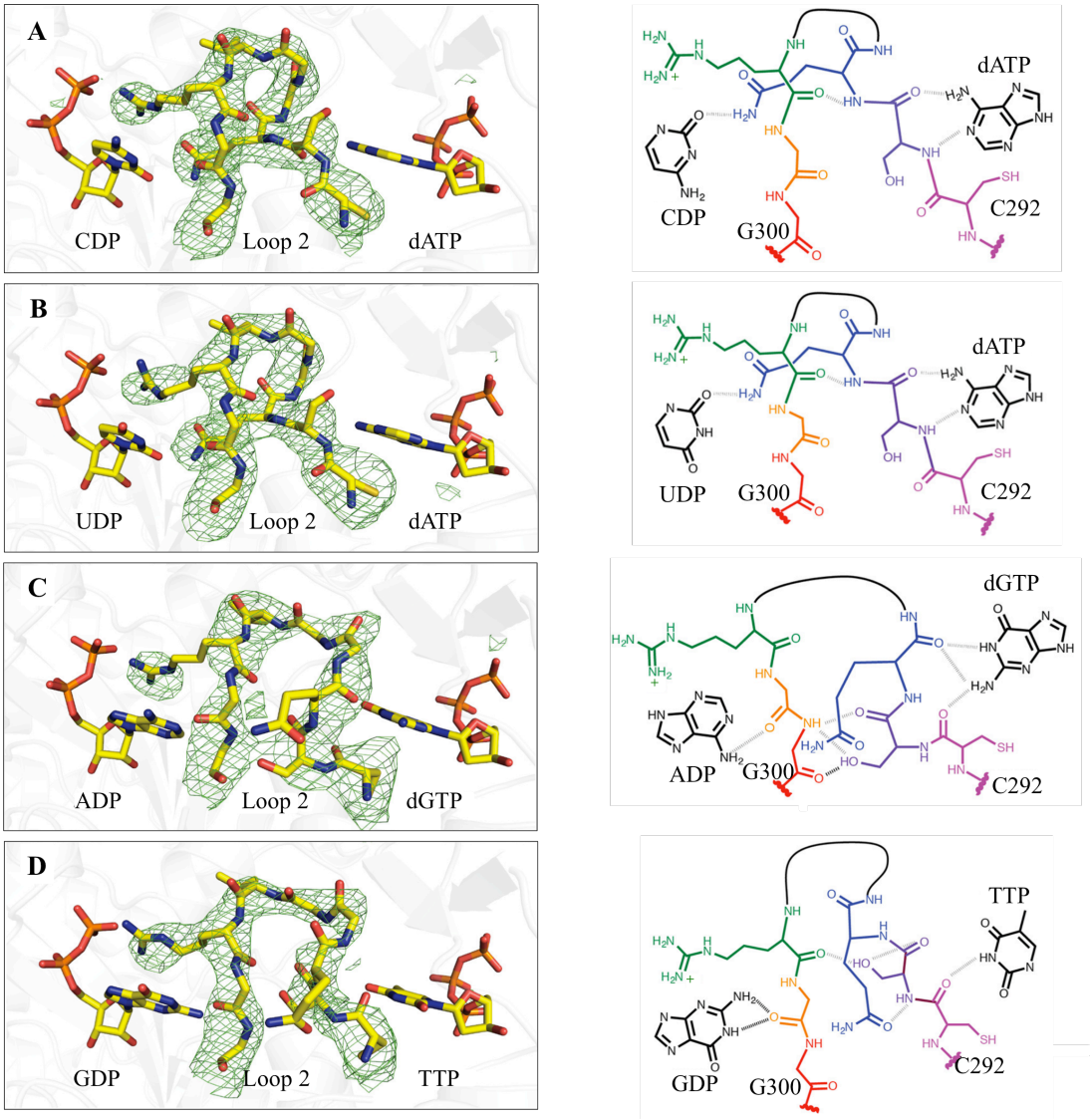

This figure is taken and modified from Ref. 48.

Figure 1-8. Conformations of *E. coli* RNR loop 2 in the presence of specificity effector–substrate pairs: **A)** dATP–CDP (PDB: 5CNS) **B)** dATP–UDP (PDB: 5CNT) **C)** dGTP–ADP (PDB: 5CNU), and **D)** TTP–GDP (PDB: 5CNV). Left panels show composite omit electron density maps. Carbon, oxygen, nitrogen, and phosphorus are colored in yellow, red, blue, and orange, respectively. Right panels, on the other hand, show 2D representations of hydrogen-bonding interactions. Each residue is colored

differently and residues 295–297 are shown as a black line. Hydrogen bonds are indicated with black dashed lines.

Soon after, Knappenberger *et al*[51] provided further information how functional groups of each specific effector drive hRNR substrate specificity. Based on crystal structures of eukaryotic class Ia RNRs bound to S-site effectors from previous studies[22,47] (Figure 1-9, A–C) and the sequence alignment of loop 2 across species (Figure 1-7C), there are three conserved amino acid residues, Q288, G289, and R293 (hRNR numbering), and one non-conserved amino acid residue, D287, proximal to the effector nucleobase. Similar to the results observed from *E. coli* RNR, binding of different specific effector affects the conformation of loop 2 in different way (Figure 1-9, A–C). In a crystal structure of hRNR with dTTP bound to the S-site (Figure 1-9A), the nucleobase does not contact D287 directly. Instead, the N3 group of dTTP contacts N270 that forms a hydrogen bond with D287.[47,55,56] In the structure of ScRNR containing dGTP in the S-site, the protonated N1 group of dGTP forms a hydrogen bond to the carboxylic acid side chain of D287 (Figure 1-9B). In contrast, the unprotonated N1 group of the adenosine nucleobase in the structure of ScRNR containing AMPPNP in the S-site acts as a hydrogen bond acceptor and contacts the backbone amide group of D287. The D287 side chain, in this case, is pointed away from the S-site (Figure 1-9C).[47,57] Until the study of Knappenberger *et al*, the functional groups proposed to drive substrate specificity had remained untested. To determine the molecular features of specific effectors that contribute to substrate discrimination, the authors examined hRNR substrate specificities directed by a series of purine and pyrimidine effector analogues using internal competition kinetics. Based on their results, the 5-methyl, O4 and N3 groups of dTTP direct specificity for GDP, whereas the exocyclic amine of dCTP acts as an antideterminant for overall effector

function. The O6 and protonated N1 of dGTP contribute to specificity for ADP, the unprotonated N1 of dATP, on the other hand, is the primary determinant for CDP substrate (Figure 1-9D).

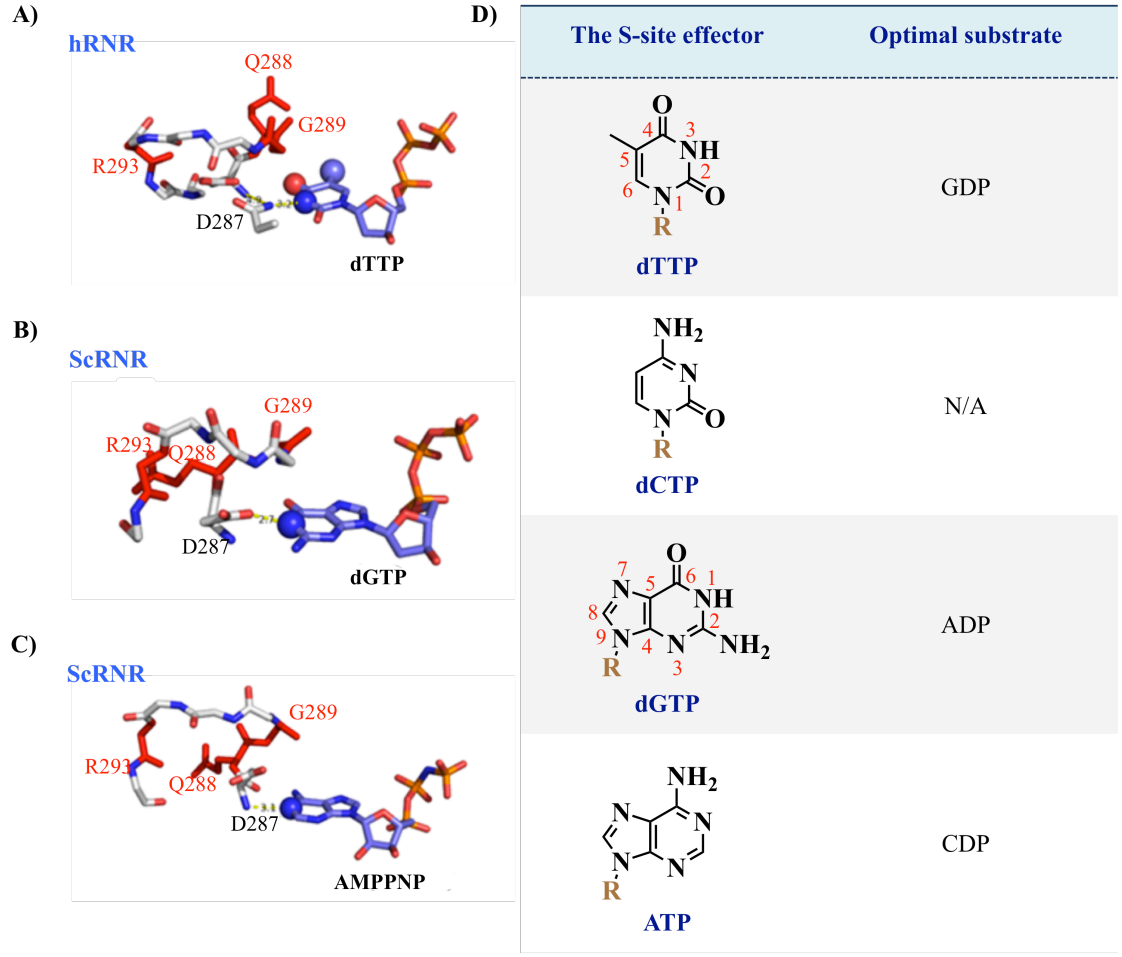

N/A, non-applicable; Figure A–C are taken and modified from Ref. 51.

Figure 1-9. A–C) Structures of eukaryotic RNRs bound to S-site effectors. **A)** Crystal structure of hRNR bound to dTTP and GDP (not shown) (PDB: 3HND).[22] **B)** Crystal structure of ScRNR bound to dGTP and ADP (not shown) (PDB: 2CVX).[47] **C)** Crystal structure of ScRNR bound to AMPPNP and CDP (not shown) (PDB: 2CVU).[47] S-site effectors are shown as dark blue sticks. Small spheres represent atoms that perturb specificity when modified. Loop 2 amino acids are shown as white sticks, while the

conserved Q288, G289, and R293 are shown as red sticks. Yellow dashes indicate potential contacts involving the non-conserved D287. Optimal substrate in response to the binding of each nucleotide effector is shown in **D)**. R denotes the deoxyribose triphosphate moiety, except that ATP has a ribose triphosphate moiety.

1.3 Formation of tyrosyl radical in class Ia RNR β subunit

The tyrosyl radical needed for RNRs (class Ia) catalytic cycle is generated in β subunit by the reaction of the diiron (II) cluster with O_2, according to equation 1.1 (Eq. 1.1). This equation describes the four-electron reduction of O_2 to its oxidation state O^{2-} in the best-studied *E. coli* β-subunit.[58] While the total of three electrons are obtained from the bound diiron cluster and Y122[59], another electron is from an external source, *i.e.*, exogenous Fe(II)[6,60] or a ferrous ion in the diiron site of the second β-subunit.[6,58]

$$[\text{Y122}, \text{Fe}^{\text{II}}\text{–}\text{Fe}^{\text{II}}] + \text{O}_2 + \text{e}^- \longrightarrow [\text{Y122}\bullet, \text{Fe}^{\text{III}}\text{–O–}\text{Fe}^{\text{III}}] + \text{OH}^- \quad \text{(Eq. 1.1)}$$

It is known that the activation of dioxygen by a ferrous diiron center is not unique for RNR-β. Very similar ferrous diiron centers are also found in other proteins such as the hydroxylase component of methane monooxygenase (MMOH) and Δ^9 stearoyl-acyl carrier protein desaturase. These proteins not only bind dioxygen, but also have very similar overall protein fold pattern. In most cases, the dioxygen is cleaved and used in the catalysis. However, in the oxygen carrier protein hemerythrin, the binding of dioxygen is reversible.[61-63]

The stable diferrous state, Fe^{II}–Fe^{II}, in *E. coli* β_2 is formed after adding ferrous ions to the apo protein under anaerobic conditions (Figure 1-10).[6,64] In 1996, Logan *et*

al reported the X-ray structure of this diferrous form of *E. coli* β_2 with 1.7-Å resolution.[65] Fe1 and Fe2 appear to coordinate with one histidine, H118 and H241, respectively. E115 and E238 bridge the two iron ions by using both oxygens from their carboxylic acid moieties. The distance between these iron ions (3.9 Å) is increased from what previously observed in the met state of RNR-β, which is a non-radical $Fe^{III}Fe^{III}$ state (3.3 Å).[15] The last ligand coordination of Fe1 and Fe2 is from a monodentate terminal ligand, D84 and E204**,** respectively. Due to their coordination number (n=4), these iron ions could be described as distorted tetrahedrons.

Under aerobic conditions, the molecular oxygen (O_2) will bind to diferrous β-subunit, generating a diferrous-oxygen complex. Though, a crystal structure of such complex has yet been observed in RNRs.[6] However, the indirect evidence for the existence of this intermediate is found in MMOH.[62,66]

Based on the homology between RNR-β and related diiron center containing proteins, it could be expected that oxygen atoms from O_2 instantly abstract an electron from each Fe(II) when it binds the diferrous center, forming a μ-1,2-peroxy diferric intermediate (**A**).[63,67] The homolytic O−O cleavage of this peroxo complex initially requires an electron from each Fe(III), leading to the formation of diiron(IV) intermediate **B**. This intermediate is stable in the absence of methane or other oxidizable substrates.[61,62,68] Again, the formations of these two intermediates have not yet been observed in RNR.

As intermediate **B** is considered as a very strong reductant, it can oxidize amino acid residues with sufficiently low redox potentials residing close to the diiron center, *e.g.*, tryptophans and tyrosines. W48, a member of the radical transfer chain, provides an electron to cleave the nearest $O-Fe^{IV}$ bond, generating intermediate **C**.[59,69] This red-colored intermediate has been observed in the reconstitution reaction of wild-type RNR-β under limiting iron source (less than 2.4 irons per β-subunit).[70] However,

the lifetime of this intermediate is too short to be observed when the reconstitution reaction is carried out under excessive amount of iron (more than five irons per β-subunit).[71] This could be explained by the fact that an exogenous Fe(II) immediately transfers an electron to $W48^{\bullet+}$ and, thus, intermediate **D** is directly observed. Intermediate **D** is stable for a few seconds time-scale. However, in the Y122F mutant where the key Y122 is replaced with non-oxidizable phenylalanine, the lifetime of intermediate **D** is doubled.[70-72]

By abstracting a hydrogen atom from a phenolic hydroxyl group in Y122, the iron site is left in the active Fe^{III}–O–Fe^{III} form and a stable tyrosyl radical (Y122•) is observed. After this reconstitution process, the stable inactive met RNR-β state and an intermediate mixed valence $Fe^{II}Fe^{III}$ state can be generated *in vitro*.[6]

All crystal structures of oxidized RNR-β have been of the met RNR-β state since this state is spontaneously obtained upon storing purified iron-containing protein in solution. However, selective reduction of Y122• by exogenous reductants, *i.e.,* hydoxyurea[73,74], various hydrazines[75,76] and alkoxyphenols[77], can also lead to the met RNR-β state formation.

Ascorbate or dithionite are used as reducing reagents to transfer an electron to the met RNR-β state, generating the mixed valence $Fe^{II}Fe^{III}$ state in mouse and herpes simplex type 1 RNR-β.[6,78] In the wild-type *E. coli* RNR-β, however, this mixed valence state has been observed after reduction by hydrazines at high pH[6,75] and radiolytic reduction at 77 K.[6,79-81] Up to date, no crystal structures of this $Fe^{II}Fe^{III}$ state from any organism have been obtained.

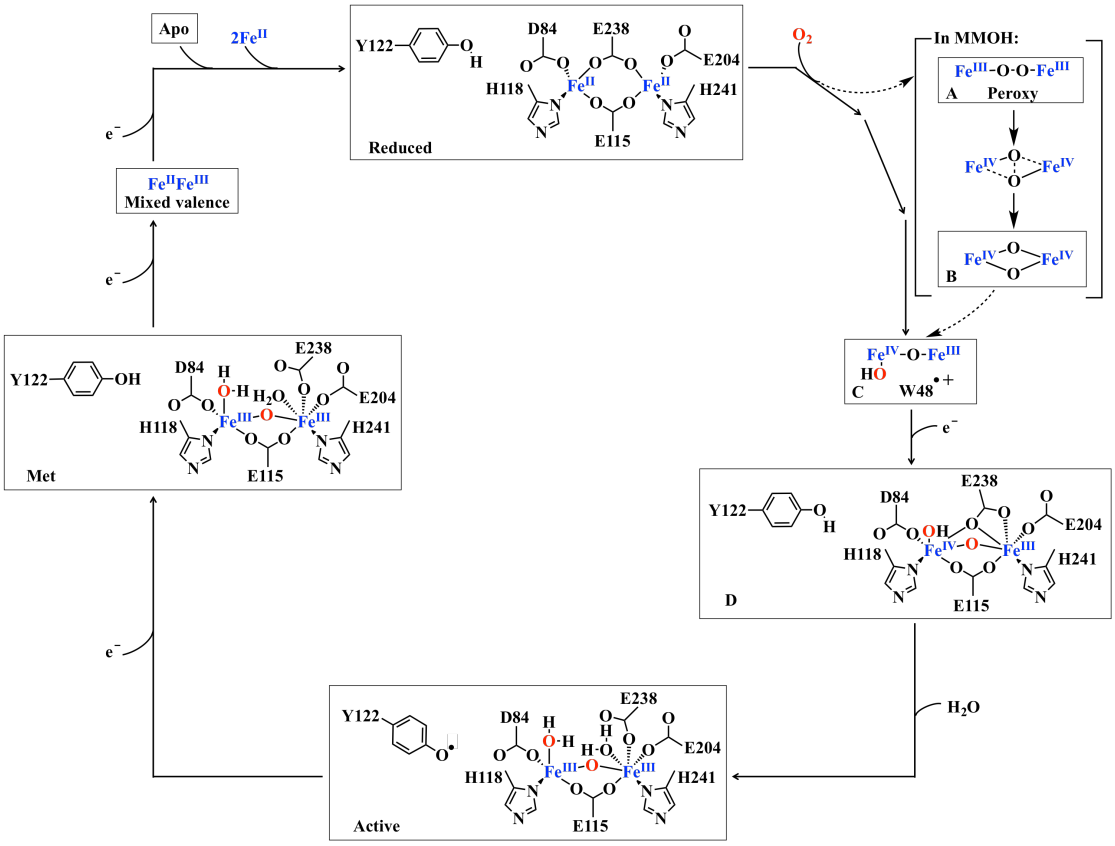

Figure 1-10. Formation of the stable tyrosyl radical in *E. coli* β-subunit.[6]

The docking models of crystal structures of *E. coli* RNR-α and RNR-β have shown that the radical of Y122 in RNR-β needs to be transferred no less than 35 Å to C439 at the C-site in RNR-α.[8,82] Kolberg *et al*[6] states that this unusual long radical transfer distance "is far beyond the reach of the pure electron tunnelling process found in most other biological electron transfer reactions". So, this radical has been proposed to be concertedly transferred via a chain of hydrogen bonded amino acid side chains instead.[83-87]

In order to understand the mechanism of this long-range PCET pathway in *E. coli* class Ia RNR, many studies have been actively refining our understanding of the residues involved.[11,84,88,89] These studies include site-directed mutagenesis[90,91], site-

specific replacement of Y356-β, Y730-α, and Y731-α with unnatural tyrosine analogues with modified redox properties[81,92], distance measurement between residues involved in the radical propagation pathway using pulsed-electron double resonance (PELDOR) spectroscopy[93], and others. The most recent study of Kasanmascheff and co-workers[94] in 2016 proposed a more detailed mechanism of PCET, involving a so-called "flipped" conformation of Y731-α (Figure 1-11). They believe that the flexibility of Y731-α and Y356-β, which is located in the flexible C-terminal tail of β_2 subunit, might be the key to drive the radical transfer at the subunit surface through water cluster.[95,96] Of note, these two contiguous residues have been suggested to communicate during PCET.[97]

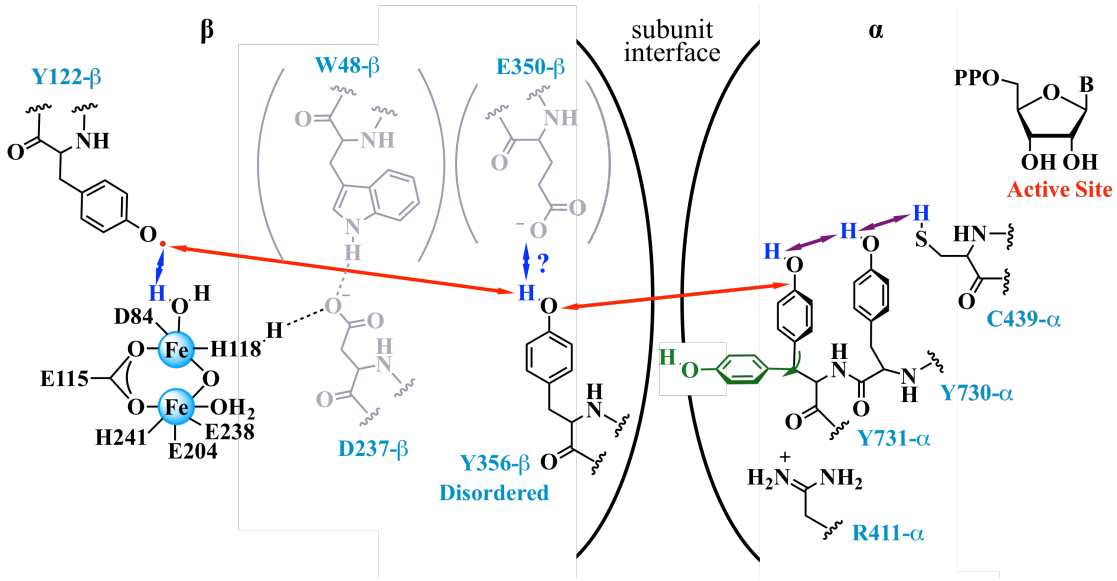

This model is adapted from Ref. 94.

Figure 1-11. Model for long-range (~35 Å), reversible radical transfer in *E. coli* class Ia RNR. The locations of Y356 and E350 are unknown since they are within the flexible C-terminal tail of β_2. W48, D237, and E350 are shown in grey because there is no published experimental data that supports their participation in this process.[94] Red, blue and purple arrows represent electron transfer, proton transfer and collinear

PCET pathways, respectively. The green tyrosine moiety shows the flipped conformation of Y731.

1.4 Inhibitors of class Ia RNRs

In 1953, Irwin and Schweigert[98] observed that dNTPs cannot be directly obtained from cell metabolism, but instead are synthesized from NTPs through catalytic reduction performed by RNRs. As DNA replication and repair are dependent on the availability of adequate and balanced pools of dNTPs[99], inhibition of RNRs can induce cell apoptosis.[12]

To form active RNRs, class Ia enzymes require subunit interactions, free radical chemistry, metallocofactor, and redox-active sulfhydryl (–SH) groups in the α subunit. Thus, to date, there are at least six important and useful types of inhibitors that could potentially inhibit class Ia RNRs in various ways (Figure 1-12).[12,61]

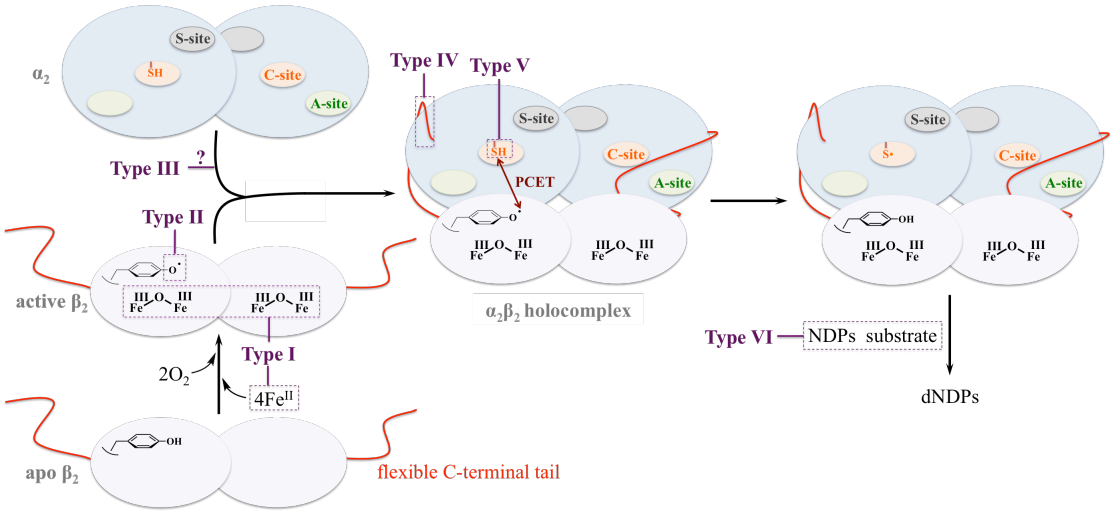

Figure 1-12. Six potential types of class Ia RNRs inhibitors.[12,61]

As the metallocofactor is indispensable for the radical formation in the β subunit, type I inhibitors inhibit enzyme activity by chelation of the cofactors either in solution (preventing the incorporation of the cofactor in the enzyme) or directly at the enzyme-bound metal center.[12] Some examples of this type include Triapine (3-aminopyridine-2-carboxaldehydethiosemicarbazone)[100], deferrioxamine (DFO)[101], and 2-hydroxy-1-naphthylaldehydeisonicotinoyl hydrazine[102]. Type II inhibitors diminish enzyme activity by donating electrons to quench the crucial tyrosyl radical, which is buried ~10 Å from the surface of the protein. In order to approach the free radical, these radical scavengers are normally small and planar[12], *e.g.*, hydroxyurea (HU)[103], acetohydroxamate[104], hydroquinone, and hydrazine derivatives[105]. Even though some inhibitors from type I and type II have already been largely used in cancer treatment, they have a main common disadvantage due to a short half-life of β subunit. As they will have time enough to find its target only in tumors that have an accelerated growth rate, their application is limited.[12] Type III inhibitors are nucleoside analogues that have similar chemical structures to ATP and are capable of inhibiting RNRs, *e.g.*, Cladribine (ClA)[106,107], Fludarabine (FlU)[108], and Clofarabine (ClF)[12,109]. Beside ClF, which inhibits RNR by alternation of RNR-α's quaternary structure[25,27], how the others inhibit RNR remained unknown by the time we started our study. Type IV inhibitors, which are oligopeptides, prevent the formation of an active $\alpha_2\beta_2$ holocomplex. These inhibitors exert their inhibition by competing with the β-subunit, via sequence homology to the β subunit's nine C-terminal residues. Some examples of type IV inhibitors for mammalian class Ia RNRs[110] are shown in Figure 1-13. Type V inhibitors are small compounds that can covalently modify sulfhydryl groups of the active site cysteines. One of the most popular is caracemide (CAR or *N*-acetyl-*N,O*-di(methylcarbamoyl)-hydroxylamine) (Figure 1-13).[12] CAR irreversibly inactivates the α-subunit of *E. coli* RNR, probably at an activated cysteine or serine residue, but

does not have any observable effects on the β subunit. The active $\alpha_2\beta_2$ complex, nevertheless, is more sensitive to CAR than the α subunit alone.[111] Type VI inhibitors, the so-called "suicide inhibitors", are recognized by RNRs as natural substrates. However, when they react with the C-site, they lead to abnormal products that subsequently inactivate the enzyme activity. Examples of this type include arabinosylcytosine (ara-C)[112], azidouridine[113], gemcitabine (F2C)[114,115] and other.[12]

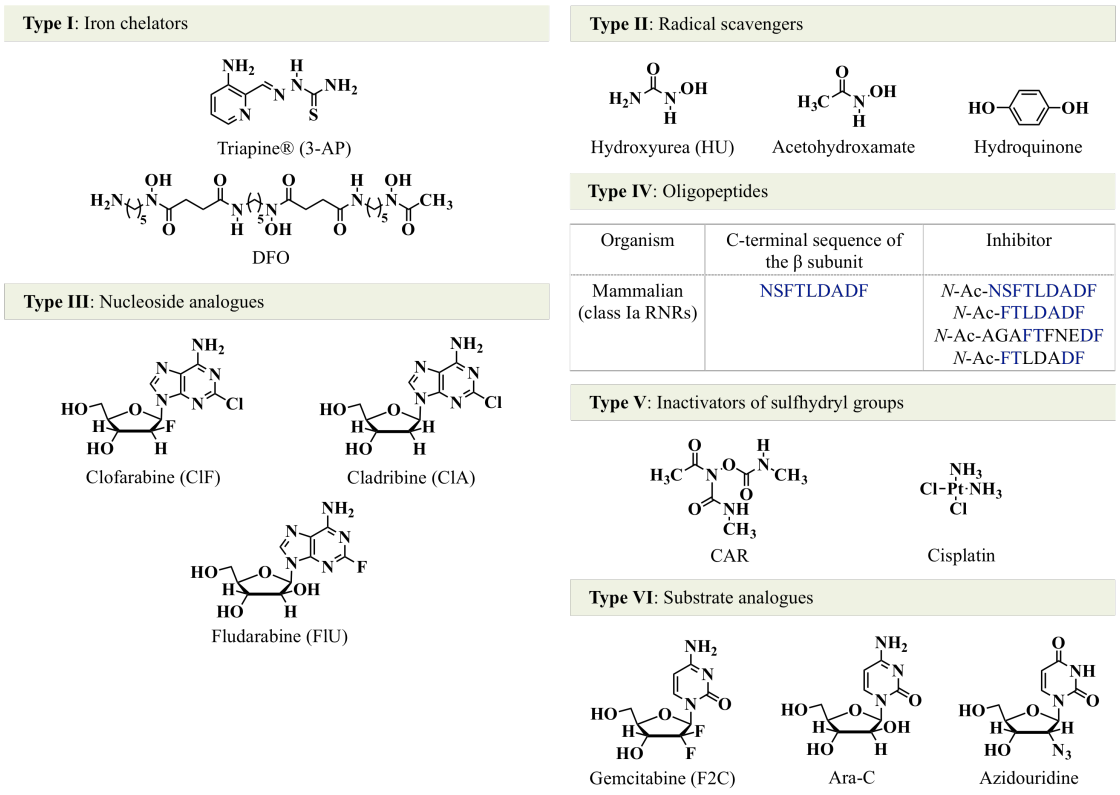

Figure 1-13. Examples of class Ia RNRs inhibitors.[12, 61, 110]

According to the US Food and Drug Administration (FDA), many drugs have been moved into clinical trials without understanding how they act, which sometimes leading to failures in late-stage clinical trials.[116] Thus, understanding a drug's mechanism could potentially help guide drug development. As mentioned above, there

were some type III RNR inhibitors of which their enzyme inhibition mechanisms had been unknown until this study, *e.g.*, ClA and FlU. Since di- and triphosphate of ClF have been shown to inhibit RNR by inducing RNR-α-subunit-hexamerization both *in vitro* and in cell[25,27], in this study we hypothesize that ClA and FlU might inhibit RNR via the same mechanism as ClF based on their similarities in structures as well as applications for the treatment of leukemia.[117]

REFERENCE

[1] Nordlund, P., and Reichard, P. (2006) Ribonucleotide reductases. *Annu. Rev. Biochem. 75*, 681-706.

[2] Cotruvo, J. A., and Stubbe, J. (2011) *Escherichia coli* class Ib ribonucleotide reductase contains a dimanganese(III)-tyrosyl radical cofactor in vivo. *Biochemistry 50*, 1672-1681.

[3] Rofougaran, R., Crona, M., Vodnala, M., Sjoberg, B. M., and Hofer, A. (2008) Oligomerization status directs overall activity regulation of the *Escherichia coli* class Ia ribonucleotide reductase. *J. Biol. Chem. 283*, 35310-35318.

[4] Reichard, P. (2002) Ribonucleotide reductases: the evolution of allosteric regulation. *Arch. Biochem. Biophys. 397*, 149-155.

[5] Hofer, A., Crona, M., Logan, D. T., and Sjoberg, B.-M. (2012) DNA building blocks: keeping control of manufacture. *Critical Reviews in Biochemistry and Molecular Biology 47*, 50-63.

[6] Kolberg, M., Strand, K. R., Graff, P., and Andersson, K. K. (2004) Structure, function, and mechanism of ribonucleotide reductases. *Biochim. Biophys. Acta. 1699*, 1-34.

[7] Stubbe, J. (1998) Ribonucleotide reductases in the twenty-first century. *Proc. Natl. Acad. Sci. U. S. A. 95*, 2723-2724.

[8] Uhlin, U., and Eklund, H. (1994) Structure of ribonucleotide reductase protein R1. *Nature 370*, 533-539.

[9] Logan, D. T. (2011) Closing the circle on ribonucleotide reductases. *Nat. Struct. Mol. Biol. 18*, 251-253.

[10] Torrents, E. (2014) Ribonucleotide reductases: essential enzymes for bacterial life. *Front. Cell Infect. Microbiol. 4*, 52.

[11] Cotruvo, J. A., and Stubbe, J. (2011) Class I ribonucleotide reductases: metallocofactor assembly and repair *in vitro* and *in vivo*. *Annu. Rev. Biochem. 80*, 733-767.

[12] Cerqueira, N. M., Pereira, S., Fernandes, P. A., and Ramos, M. J. (2005) Overview of ribonucleotide reductase inhibitors: an appealing target in anti-tumour therapy. *Curr. Med. Chem. 12*, 1283-1294.

[13] Lawrence, C. C., and Stubbe, J. (1998) The function of adenosylcobalamin in the mechanism of ribonucleoside triphosphate reductase from *Lactobacillus leichmannii*. *Curr. Opin. Chem. Biol. 2*, 650-655.

[14] Wei, Y., Funk, M. A., Rosado, L. A., Baek, J., Drennan, C. L., and Stubbe, J. (2014) The class III ribonucleotide reductase from *Neisseria bacilliformis* can utilize thioredoxin as a reductant. *Proc. Natl. Acad. Sci. U. S. A. 111*, E3756-3765.

[15] Nordlund, P., and Eklund, H. (1993) Structure and function of the *Escherichia coli* ribonucleotide reductase protein R2. *J. Mol. Biol. 232*, 123-164.

[16] Sintchak, M. D., Arjara, G., Kellogg, B. A., Stubbe, J., and Drennan, C. L. (2002) The crystal structure of class II ribonucleotide reductase reveals how an allosterically regulated monomer mimics a dimer. *Nat. Struct. Biol. 9*, 293-300.

[17] Larsson, K. M., Logan, D. T., and Nordlund, P. (2010) Structural basis for adenosylcobalamin activation in AdoCbl-dependent ribonucleotide reductases. *ACS Chem. Biol. 5*, 933-942.

[18] Logan, D. T., Mulliez, E., Larsson, K. M., Bodevin, S., Atta, M., Garnaud, P. E., Sjoberg, B. M., and Fontecave, M. (2003) A metal-binding site in the catalytic subunit of anaerobic ribonucleotide reductase. *Proc. Natl. Acad. Sci. U. S. A. 100*, 3826-3831.

[19] Torrents, E., Grinberg, I., Gorovitz-Harris, B., Lundstrom, H., Borovok, I., Aharonowitz, Y., Sjoberg, B. M., and Cohen, G. (2007) NrdR controls differential expression of the *Escherichia coli* ribonucleotide reductase genes. *J. Bacteriol. 189*, 5012-5021.

[20] Jordan, A., Aragall, E., Gibert, I., and Barbe, J. (1996) Promoter identification and expression analysis of *Salmonella typhimurium* and *Escherichia coli* nrdEF operons encoding one of two class I ribonucleotide reductases present in both bacteria. *Mol. Microbiol. 19*, 777-790.

[21] Kashlan, O. B., and Cooperman, B. S. (2003) Comprehensive model for allosteric regulation of mammalian ribonucleotide reductase: refinements and consequences. *Biochemistry 42*, 1696-1706.

[22] Fairman, J. W., Wijerathna, S. R., Ahmad, M. F., Xu, H., Nakano, R., Jha, S., Prendergast, J., Welin, R. M., Flodin, S., Roos, A., Nordlund, P., Li, Z., Walz, T., and Dealwis, C. G. (2011) Structural basis for allosteric regulation of human ribonucleotide reductase by nucleotide-induced oligomerization. *Nat. Struct. Mol. Biol. 18*, 316-322.

[23] Ingemarson, R., and Thelander, L. (1996) A kinetic study on the influence of nucleoside triphosphate effectors on subunit interaction in mouse ribonucleotide reductase. *Biochemistry 35*, 8603-8609.

[24] Uppsten, M., Farnegardh, M., Domkin, V., and Uhlin, U. (2006) The first holocomplex structure of ribonucleotide reductase gives new insight into its mechanism of action. *J. Mol. Biol. 359*, 365-377.

[25] Aye, Y., and Stubbe, J. (2011) Clofarabine 5'-di and -triphosphates inhibit human ribonucleotide reductase by altering the quaternary structure of its large subunit. *Proc. Natl. Acad. Sci. U. S. A. 108*, 9815-9820.

[26] Fu, Y., Lin, H. Y., Wisitpitthaya, S., Blessing, W. A., and Aye, Y. (2014) A fluorimetric readout reporting the kinetics of nucleotide-induced human ribonucleotide reductase oligomerization. *ChemBioChem 15*, 2598-2604.

[27] Aye, Y., Brignole, E. J., Long, M. J., Chittuluru, J., Drennan, C. L., Asturias, F. J., and Stubbe, J. (2012) Clofarabine targets the large subunit (α) of human ribonucleotide reductase in live cells by assembly into persistent hexamers. *Chem. Biol. 19*, 799-805.

[28] Rofougaran, R., Vodnala, M., and Hofer, A. (2006) Enzymatically active mammalian ribonucleotide reductase exists primarily as an $\alpha_6\beta_2$ octamer. *J. Biol. Chem. 281*, 27705-27711.

[29] Fu, Y., Long, M. J., Rigney, M., Parvez, S., Blessing, W. A., and Aye, Y. (2013) Uncoupling of allosteric and oligomeric regulation in a functional hybrid enzyme constructed from *Escherichia coli* and human ribonucleotide reductase. *Biochemistry 52*, 7050-7059.

[30] Licht, S., and Stubbe, J. (1999) *Mechanistic Investigations of Ribonucleotide Reductase* (Pourler, C. D., Ed.), pp 163-203, Elsevier, Amsterdam.

[31] Stubbe, J., and van Der Donk, W. A. (1998) Protein Radicals in Enzyme Catalysis. *Chem. Rev. 98*, 705-762.

[32] Mao, S. S., Holler, T. P., Yu, G. X., Bollinger, J. M., Jr., Booker, S., Johnston, M. I., and Stubbe, J. (1992) A model for the role of multiple cysteine residues involved in ribonucleotide reduction: amazing and still confusing. *Biochemistry 31*, 9733-9743.

[33] Licht, S., Gerfen, G. J., and Stubbe, J. (1996) Thiyl radicals in ribonucleotide reductases. *Science 271*, 477-481.

[34] Stubbe, J., and Ackles, D. (1980) On the mechanism of ribonucleoside diphosphate reductase from *Escherichia coli*. Evidence for 3'-C−H bond cleavage. *J. Biol. Chem. 255*, 8027-8030.

[35] Stubbe, J., Ackles, D., Segal, R., and Blakley, R. L. (1981) On the mechanism of ribonucleoside triphosphate reductase from *Lactobacillus leichmannii*. Evidence for 3' C−H bond cleavage. *J. Biol. Chem. 256*, 4843-4846.

[36] Stubbe, J., Ator, M., and Krenitsky, T. (1983) Mechanism of ribonucleoside diphosphate reductase from *Escherichia coli*. Evidence for 3'-C−H bond cleavage. *J. Biol. Chem. 258*, 1625-1631.

[37] Lawrence, C. C., Bennati, M., Obias, H. V., Bar, G., Griffin, R. G., and Stubbe, J. (1999) High-field EPR detection of a disulfide radical anion in the reduction of cytidine 5'-diphosphate by the E441Q R1 mutant of *Escherichia coli* ribonucleotide reductase. *Proc. Natl. Acad. Sci. U. S. A. 96*, 8979-8984.

[38] Thelander, L. (1974) Reaction mechanism of ribonucleoside diphosphate reductase from *Escherichia coli*. Oxidation-reduction-active disulfides in the B1 subunit. *J. Biol. Chem. 249*, 4858-4862.

[39] Stubbe, J., and van der Donk, W. A. (1995) Ribonucleotide reductases: radical enzymes with suicidal tendencies. *Chem. Biol. 2*, 793-801.

[40] Holmgren, A. (1988) Thioredoxin and glutaredoxin: small multi-functional redox proteins with active-site disulphide bonds. *Biochem. Soc. Trans. 16*, 95-96.

[41] Thelander, L., and Reichard, P. (1979) Reduction of ribonucleotides. *Annu. Rev. Biochem. 48*, 133-158.

[42] Cooperman, B. S., and Kashlan, O. B. (2003) A comprehensive model for the allosteric regulation of Class Ia ribonucleotide reductases. *Adv. Enzyme Regul. 43*, 167-182.

[43] Andersson, K. K. (2008) *Ribonucleotide Reductase*, Nova Science Publishers Inc., New York.

[44] Wang, J., Lohman, G. J., and Stubbe, J. (2009) Mechanism of inactivation of human ribonucleotide reductase with p53R2 by gemcitabine 5'-diphosphate. *Biochemistry 48*, 11612-11621.

[45] Ando, N., Li, H., Brignole, E. J., Thompson, S., McLaughlin, M. I., Page, J. E., Asturias, F. J., Stubbe, J., and Drennan, C. L. (2016) Allosteric Inhibition of Human Ribonucleotide Reductase by dATP Entails the Stabilization of a Hexamer. *Biochemistry 55*, 373-381.

[46] Brown, N. C., and Reichard, P. (1969) Role of effector binding in allosteric control of ribonucleoside diphosphate reductase. *J. Mol. Biol. 46*, 39-55.

[47] Xu, H., Faber, C., Uchiki, T., Fairman, J. W., Racca, J., and Dealwis, C. (2006) Structures of eukaryotic ribonucleotide reductase I provide insights into dNTP regulation. *Proc. Natl. Acad. Sci. U. S. A. 103*, 4022-4027.

[48] Zimanyi, C. M., Chen, P. Y. T., Kang, G., Funk, M. A., and Drennan, C. L. (2015) Molecular basis for allosteric specificity regulation in class Ia ribonucleotide reductase from *Escherichia coli*. *eLIFE*, e07141.

[49] Larsson, K. M., Jordan, A., Eliasson, R., Reichard, P., Logan, D. T., and Nordlund, P. (2004) Structural mechanism of allosteric substrate specificity regulation in a ribonucleotide reductase. *Nat. Struct. Mol. Biol. 11*, 1142-1149.

[50] Eriksson, M., Uhlin, U., Ramaswamy, S., Ekberg, M., Regnstrom, K., Sjoberg, B. M., and Eklund, H. (1997) Binding of allosteric effectors to ribonucleotide reductase protein R1: reduction of active-site cysteines promotes substrate binding. *Structure 5*, 1077-1092.

[51] Knappenberger, A. J., Ahmad, M. F., Viswanathan, R., Dealwis, C. G., and Harris, M. E. (2016) Nucleoside Analogue Triphosphates Allosterically Regulate Human Ribonucleotide Reductase and Identify Chemical Determinants That Drive Substrate Specificity. *Biochemistry*.

[52] Uppsten, M., Farnegardh, M., Jordan, A., Eliasson, R., Eklund, H., and Uhlin, U. (2003) Structure of the large subunit of class Ib ribonucleotide reductase from *Salmonella typhimurium* and its complexes with allosteric effectors. *J. Mol. Biol. 330*, 87-97.

[53] Wang, L., and Weiss, B. (1992) dcd (dCTP deaminase) gene of *Escherichia coli*: mapping, cloning, sequencing, and identification as a locus of suppressors of lethal dut (dUTPase) mutations. *J. Bacteriol. 174*, 5647-5653.

[54] O'Donovan, G. A., Edlin, G., Fuchs, J. A., Neuhard, J., and Thomassen, E. (1971) Deoxycytidine triphosphate deaminase: characterization of an *Escherichia coli* mutant deficient in the enzyme. *J. Bacteriol. 105*, 666-672.

[55] Ahmad, M. F., and Dealwis, C. G. (2013) The Structural Basis for the Allosteric Regulation of Ribonucleotide Reductase. *Progress in Molecular Biology and Translational Science 117*, 389-410.

[56] Xu, H., Faber, C., Uchiki, T., Racca, J., and Dealwis, C. (2006) Structures of eukaryotic ribonucleotide reductase I define gemcitabine diphosphate binding and subunit assembly. *Proc. Natl. Acad. Sci. U. S. A. 103*, 4028-4033.

[57] Ahmad, M. F., Kaushal, P. S., Wan, Q., Wijerathna, S. R., An, X., Huang, M., and Dealwis, C. G. (2012) Role of arginine 293 and glutamine 288 in communication between catalytic and allosteric sites in yeast ribonucleotide reductase. *J. Mol. Biol. 419*, 315-329.

[58] Miller, M. A., Gobena, F. T., Kauffmann, K., Munck, E., Que, J., L., and Stankovich, M. T. (1999) Differing Roles for the Diiron Clusters of

Ribonucleotide Reductase from Aerobically Grown *Escherichia coli* in the Generation of the Y122 Radical. *J. Am. Chem. Soc. 121*, 1096-1097.

[59] Baldwin, J., Krebs, C., Ley, B. A., Edmondson, D. E., Huynh, B. H., and Bollinger, J. J. M. (2000) Mechanism of Rapid Electron Transfer during Oxygen Activation in the R2 Subunit of *Escherichia coli* Ribonucleotide Reductase. 1. Evidence for a Transient Tryptophan Radical. *J. Am. Chem. Soc. 122*, 12195-12206.

[60] Coves, J., Laulhere, J., and Fontecave, M. (1997) The role of exogenous iron in the activation of ribonucleotide reductase from *Escherichia coli*. *J. Biol. Inorg. Chem. 2*, 418-426.

[61] Andersson, K. K., and Graslund, A. (1995) *DIIRON-OXYGEN PROTEINS in Advances in Inorganic Chemistry* (Sykes, A. G., Ed.), pp 359-408, Academic Press Inc., California.

[62] Waller, B. J., and Lipscomb, J. D. (1996) Dioxygen Activation by Enzymes Containing Binuclear Non-Heme Iron Clusters. *Chem. Rev.*, 2625-2657.

[63] Solomon, E. I., Brunold, T. C., Davis, M. I., Kemsley, J. N., Lee, S. K., Lehnert, N., Neese, F., Skulan, A. J., Yang, Y. S., and Zhou, J. (2000) Geometric and electronic structure/function correlations in non-heme iron enzymes *Chem Rev 100*, 235-350.

[64] Atkin, C. L., Thelander, L., Reichard, P., and Lang, G. (1973) Iron and free radical in ribonucleotide reductase. Exchange of iron and Mossbauer spectroscopy of the protein β_2 subunit of the *Escherichia coli* enzyme. *J. Biol. Chem. 248*, 7464-7472.

[65] Logan, D. T., Su, X. D., Aberg, A., Regnstrom, K., Hajdu, J., Eklund, H., and Nordlund, P. (1996) Crystal structure of reduced protein R2 of ribonucleotide reductase: the structural basis for oxygen activation at a dinuclear iron site. *Structure 4*, 1053-1064.

[66] Merkx, M., Kopp, D. A., Sazinsky, M. H., Blazyk, J. L., Muller, J., and Lippard, S. J. (2001) Dioxygen Activation and Methane Hydroxylation by Soluble Methane Monooxygenase: A Tale of Two Irons and Three Proteins A list of abbreviations can be found in Section 7 *Angew. Chem. Int. Ed. Engl. 40*, 2782-2807.

[67] Andersson, M. E., Hogbom, M., Rinaldo-Matthis, A., Andersson, K. K., Sjoberg, B.-M., and Nordlund, P. (1999) The Crystal Structure of an Azide Complex of the Diferrous R2 Subunit of Ribonucleotide Reductase Displays a Novel Carboxylate Shift with Important Mechanistic Implications for Diiron-Catalyzed Oxygen Activation. *J. Am. Chem. Soc. 121*, 2346-2352.

[68] Lipscomb, J. D., and Que, J., L. . (1998) MMO: P450 in wolf's clothing? *J. Biol. Inorg. Chem. 3*, 331–336.

[69] Krebs, C., Chen, S., Baldwin, J., Ley, B. A., Patel, U., Edmondson, D. E., Huynh, B. H., and Bollinger, J., J. M. (2000) Mechanism of Rapid Electron Transfer during Oxygen Activation in the R2 Subunit of *Escherichia coli* Ribonucleotide Reductase. 2. Evidence for and Consequences of Blocked Electron Transfer in the W48F Variant. *J. Am. Chem. Soc. 122*, 12207-12219.

[70] Bollinger, J. M., Jr., Tong, W. H., Ravi, N., Huynh, B. H., Edmondson, D. E., and Stubbe, J. (1994) Mechanism of Assembly of the Tyrosyl Radical-Diiron(III) Cofactor of *E. coli* Ribonucleotide Reductase. 3. Kinetics of the Limiting Fe^{2+} Reaction by Optical, EPR, and Mossbauer Spectroscopies. *J. Am. Chem. Soc. 116*, 8024-8032.

[71] Bollinger, J. M., Jr., Tong, W. H., Ravi, N., Huynh, B. H., Edmondson, D. E., and Stubbe, J. (1994) Mechanism of Assembly of the Tyrosyl Radical-Diiron(III) Cofactor of *E. coli* Ribonucleotide Reductase. 2. Kinetics of The Excess Fe^{2+} Reaction by Optical, EPR, and Mossbauer Spectroscopies. *J. Am. Chem. Soc. 116*, 8015-8023.

[72] Ravi, N., Bollinger, J., J. M., Huynh, B. H., Edmondson, D. E., and Stubbe, J. (1994) Mechanism of Assembly of the Tyrosyl Radical-Diiron(III) Cofactor of *E. Coli* Ribonucleotide Reductase. 1. Mossbauer Characterization of the Diferric Radical Precursor *J. Am. Chem. Soc. 116*, 8007-8014.

[73] Lassmann, G., Thelander, L., and Graslund, A. (1992) EPR stopped-flow studies of the reaction of the tyrosyl radical of protein R2 from ribonucleotide reductase with hydroxyurea. *Biochem. Biophys. Res. Commun. 188*, 879-887.

[74] Karlsson, M., Sahlin, M., and Sjoberg, B.-M. (1992) *Escherichia coli* ribonucleotide reductase. Radical susceptibility to hydroxyurea is dependent on the regulatory state of the enzyme. *J. Biol. Chem. 267*, 12622-12626.

[75] Gerez, C., and Fontecave, M. (1992) Reduction of the small subunit of *Escherichia coli* ribonucleotide reductase by hydrazines and hydroxylamines. *Biochemistry 31*, 780-786.

[76] Sarel, S., Fizames, C., Lavelle, F., and Avramovici-Grisaru, S. (1999) Domain-structured N^1,N^2-derivatized hydrazines as inhibitors of ribonucleoside diphosphate reductase: redox-cycling considerations. *J. Med. Chem. 42*, 242-248.

[77] Potsch, S., Drechsler, H., Liermann, B., Graslund, A., and Lassmann, G. (1994) *p*-Alkoxyphenols, a new class of inhibitors of mammalian R2 ribonucleotide reductase: possible candidates for antimelanotic drugs. *Mol. Pharmacol. 45*, 792-796.

[78] Atta, M., Andersson, K. K., Ingemarson, R., Thelander, L., and Graslund, A. (1994) EPR Studies of Mixed-Valent [Fe(II)Fe(III)] Clusters Formed in the R2 Subunit of Ribonucleotide Reductase from Mouse or Herpes Simplex Virus: Mild Chemical Reduction of the Diferric Centers. *J. Am. Chem. Soc. 116*, 6429-6430.

[79] Hendrich, M. P., Elgren, T. E., and Que, L., Jr. (1991) A mixed valence form of the iron cluster in the β_2 protein of ribonucleotide reductase from *Escherichia coli*. *Biochem. Biophys. Res. Commun. 176*, 705-710.

[80] Davydov, R. M., Smieja, J., Dikanov, S. A., Zang, Y., Que, L., Jr., and Bowman, M. K. (1999) EPR properties of mixed-valent mu-oxo and mu-hydroxo dinuclear iron complexes produced by radiolytic reduction at 77 K. *J. Biol. Inorg. Chem. 4*, 292-301.

[81] Krebs, C., Davydov, R., Baldwin, J., Hoffman, B. M., Bollinger, J., J. M., and Huynh, B. H. (2000) Mossbauer and EPR Characterization of the S = 9/2

Mixed-Valence Fe(II)Fe(III) Cluster in the Cryoreduced R2 Subunit of *Escherichia coli* Ribonucleotide Reductase. *J. Am. Chem. Soc. 122*, 5327-5336.

[82] Sjoberg, B.-M. (1995) Structure of Ribonucleotide Reductase from *Escherichia coli* (Eckstein, F., and Lilley, D. M. J., Ed.), pp 192-221, Springer-Verlag, Berlin-Heidelberg.

[83] Sjoberg, B.-M. (1997) Ribonucleotide Reductases-A Group of Enzymes with Different Metallosites and a Similar Reaction Mechanism, pp 139-173, Springer-Verlag, Berlin-Heidelberg.

[84] Stubbe, J., Nocera, D. G., Yee, C. S., and Chang, M. C. (2003) Radical initiation in the class I ribonucleotide reductase: long-range proton-coupled electron transfer? *Chem. Rev. 103*, 2167-2201.

[85] Rova, U., Goodtzova, K., Ingemarson, R., Behravan, G., Graslund, A., and Thelander, L. (1995) Evidence by site-directed mutagenesis supports long-range electron transfer in mouse ribonucleotide reductase. *Biochemistry 34*, 4267-4275.

[86] Ekberg, M., Potsch, S., Sandin, E., Thunnissen, M., Nordlund, P., Sahlin, M., and Sjoberg, B. M. (1998) Preserved catalytic activity in an engineered ribonucleotide reductase R2 protein with a nonphysiological radical transfer pathway. The importance of hydrogen bond connections between the participating residues. *J. Biol. Chem. 273*, 21003-21008.

[87] Ehrenberg, A. (2001) Free radical transfer, fluctuating structure and reaction cycle of ribonucleotide reductase. *Biosystems 62*, 9-12.

[88] Minnihan, E. C., Ando, N., Brignole, E. J., Olshansky, L., Chittuluru, J., Asturias, F. J., Drennan, C. L., Nocera, D. G., and Stubbe, J. (2013) Generation of a stable, aminotyrosyl radical-induced $\alpha_2\beta_2$ complex of *Escherichia coli* class Ia ribonucleotide reductase. *Proc. Natl. Acad. Sci. U. S. A. 110*, 3835-3840.

[89] Reece, S. Y., Hodgkiss, J. M., Stubbe, J., and Nocera, D. G. (2006) Proton-coupled electron transfer: the mechanistic underpinning for radical transport and catalysis in biology. *Philos. Trans. R. Soc. Lond. B. Biol. Sci. 361*, 1351-1364.

[90] Climent, I., Sjoberg, B. M., and Huang, C. Y. (1992) Site-directed mutagenesis and deletion of the carboxyl terminus of *Escherichia coli* ribonucleotide reductase protein R2. Effects on catalytic activity and subunit interaction. *Biochemistry 31*, 4801-4807.

[91] Ekberg, M., Sahlin, M., Eriksson, M., and Sjoberg, B. M. (1996) Two conserved tyrosine residues in protein R1 participate in an intermolecular electron transfer in ribonucleotide reductase. *J. Biol. Chem. 271*, 20655-20659.

[92] Seyedsayamdost, M. R., Xie, J., Chan, C. T., Schultz, P. G., and Stubbe, J. (2007) Site-specific insertion of 3-aminotyrosine into subunit α_2 of *E. coli* ribonucleotide reductase: direct evidence for involvement of Y730 and Y731 in radical propagation. *J. Am. Chem. Soc. 129*, 15060-15071.

[93] Seyedsayamdost, M. R., Chan, C. T., Mugnaini, V., Stubbe, J., and Bennati, M. (2007) PELDOR spectroscopy with DOPA-β2 and NH2Y-α2s: distance

measurements between residues involved in the radical propagation pathway of *E. coli* ribonucleotide reductase. *J. Am. Chem. Soc. 129*, 15748-15749.

[94] Kasanmascheff, M., Lee, W., Nick, T. U., Stubbe, J., and Bennati, M. (2016) Radical transfer in *E. coli* ribonucleotide reductase: a NH2Y731/R411A-a mutant unmasks a new conformation of the pathway residue 731. *Chem. Sci.*, 2170–2178.

[95] Bonin, J., Costentin, C., Louault, C., Robert, M., and Saveant, J. M. (2011) Water (in water) as an intrinsically efficient proton acceptor in concerted proton electron transfers. *J. Am. Chem. Soc. 133*, 6668-6674.

[96] Saveant, J. M. (2014) Concerted proton-electron transfers: fundamentals and recent developments. *Annu. Rev. Anal. Chem. (Palo Alto Calif) 7*, 537-560.

[97] Song, D. Y., Pizano, A. A., Holder, P. G., Stubbe, J., and Nocera, D. G. (2015) Direct interfacial Y731 oxidation in α_2 by a photoβ_2 subunit of *E. coli* class Ia ribonucleotide reductase. *Chem. Sci. 6*, 4519–4524.

[98] Rose, I. A., and Scheweigert, B. S. (1953) Incorporation of C14 totally labeled nucleosides into nucleic acids. *J. Biol. Chem. 202*, 635-645.

[99] Aye, Y., Li, M., Long, M. J., and Weiss, R. S. (2015) Ribonucleotide reductase and cancer: biological mechanisms and targeted therapies. *Oncogene. 34*, 2011-2021.

[100] Finch, R. A., Liu, M., Grill, S. P., Rose, W. C., Loomis, R., Vasquez, K. M., Cheng, Y., and Sartorelli, A. C. (2000) Triapine (3-aminopyridine-2-carboxaldehyde-thiosemicarbazone): A potent inhibitor of ribonucleotide reductase activity with broad spectrum antitumor activity. *Biochem. Pharmacol. 59*, 983-991.

[101] Juckett, M. B., Shadley, J. D., Zheng, Y., and Klein, J. P. (1998) Desferrioxamine enhances the effects of gamma radiation on clonogenic survival and the formation of chromosomal aberrations in endothelial cells. *Radiat. Res. 149*, 330-337.

[102] van Reyk, D., Sarel, S., and Hunt, N. (2000) Inhibition of *in vitro* lymphoproliferation by three novel iron chelators of the pyridoxal and salicyl aldehyde hydrazone classes. *Biochem. Pharmacol. 60*, 581-587.

[103] Elford, H. (1977) Inhibition of ribonucleotide reductase by analogs of hydroxyurea and their effect on L1210 leukemia. *Proc. Am. Assoc. Can. Res. 18*, 177-277.

[104] Mayhew, C. N., Mampuru, L. J., Chendil, D., Ahmed, M. M., Phillips, J. D., Greenberg, R. N., Elford, H. L., and Gallicchio, V. S. (2002) Suppression of retrovirus-induced immunodeficiency disease (murine AIDS) by trimidox and didox: novel ribonucleotide reductase inhibitors with less bone marrow toxicity than hydroxyurea. *Antiviral Res. 56*, 167-181.

[105] Han, J.-Y., Gräslund, A., Thelander, L., and Sykes, A. G. (1997) Kinetic studies on the reduction of the R2 subunit of mouse ribonucleotide reductase with hydroxyurea, hydrazine, phenylhydrazine and hydroxylamine. *J. Biol. Inorg. Chem. 2*, 287–294.

[106] Chunduru, S. K., Appleman, J. R., and Blakley, R. L. (1993) Activity of human DNA polymerases α and β with 2-chloro-2'-deoxyadenosine 5'-

triphosphate as a substrate and quantitative effects of incorporation on chain extension. *Arch. Biochem. Biophys. 302*, 19-30.

[107] Begleiter, A., Verburg, L., Ashique, A., Lee, K., Israels, L. G., Mowat, M. R., and Johnston, J. B. (1995) Comparison of antitumor activities of 2-chlorodeoxyadenosine and 9-β-arabinosyl-2-fluoroadenine in chronic lymphocytic leukemia and marrow cells *in vitro*. *Leukemia 9*, 1875-1881.

[108] Mansson, E., Spasokoukotskaja, T., Sallstrom, J., Eriksson, S., and Albertioni, F. (1999) Molecular and biochemical mechanisms of fludarabine and cladribine resistance in a human promyelocytic cell line. *Cancer Res. 59*, 5956-5963.

[109] Jeha, S., Gandhi, V., Chan, K. W., McDonald, L., Ramirez, I., Madden, R., Rytting, M., Brandt, M., Keating, M., Plunkett, W., and Kantarjian, H. (2004) Clofarabine, a novel nucleoside analog, is active in pediatric patients with advanced leukemia. *Blood 103*, 784-789.

[110] Yang, F. D., Spanevello, R. A., Celiker, I., Hirschmann, R., Rubin, H., and Cooperman, B. S. (1990) The carboxyl terminus heptapeptide of the R2 subunit of mammalian ribonucleotide reductase inhibits enzyme activity and can be used to purify the R1 subunit. *FEBS Lett. 272*, 61-64.

[111] Larsen, I. K., Cornett, C., Karlsson, M., Sahlin, M., and Sjoberg, B. M. (1992) Caracemide, a site-specific irreversible inhibitor of protein R1 of *Escherichia coli* ribonucleotide reductase. *J. Biol. Chem. 267*, 12627-12631.

[112] Creasey, W. A., Papac, R. J., Markiw, M. E., Calabresi, P., and Welch, A. D. (1966) Biochemical and pharmacological studies with 1-β-D-arabinofuranosylcytosine in man. *Biochem. Pharmacol. 15*, 1417-1428.

[113] Thelander, L., and Larsson, B. (1976) Active site of ribonucleoside diphosphate reductase from *Escherichia coli*. Inactivation of the enzyme by 2'-substituted ribonucleoside diphosphates. *J. Biol. Chem. 251*, 1398-1405.

[114] Heinemann, V., Xu, Y. Z., Chubb, S., Sen, A., Hertel, L. W., Grindey, G. B., and Plunkett, W. (1990) Inhibition of ribonucleotide reduction in CCRF-CEM cells by 2',2'-difluorodeoxycytidine. *Mol. Pharmacol. 38*, 567-572.

[115] Grem, J. L., Quinn, M. G., Keith, B., Monahan, B. P., Hamilton, J. M., Xu, Y., Harold, N., Nguyen, D., Takimoto, C. H., Rowedder, A., Pang, J., Morrison, G., and Chen, A. (2003) A phase I and pharmacologic study of weekly gemcitabine in combination with infusional 5-fluorodeoxyuridine and oral calcium leucovorin. *Cancer Chemother. Pharmacol. 52*, 487-496.

[116] (2010) Mechanism matters. *Nat. Med. 16*, 347.

[117] Damaraju, V. L., Damaraju, S., Young, J. D., Baldwin, S. A., Mackey, J., Sawyer, M. B., and Cass, C. E. (2003) Nucleoside anticancer drugs: the role of nucleoside transporters in resistance to cancer chemotherapy. *Oncogene. 22*, 7524-7536.

CHAPTER 2

Nucleotide Syntheses

2.1 Introduction

Nucleoside analogues in cancer therapy

Many cellular processes, *e.g.*, cell signaling, enzyme regulation and metabolism, demand nucleosides and nucleotides.[1] Particularly, during cell division, dNTPs are necessary for DNA and RNA synthesis. Maintaining balanced dNTP pools is thus pivotal for genomic stability since mutagenesis can be caused by misincorporation of an excess dNTP into DNA.[2]

The development of anticancer and antiviral drugs has been focused on the design and synthesis of chemically modified nucleosides and nucleotides, so-called nucleoside analogues. These agents have been developed to mimic physiological nucleosides and nucleotides and thus compete with their counterparts as antimetabolites.[1,3] By incorporation of nucleoside analogues into DNA and RNA, cell proliferation and viral replication can be inhibited.[1] Both pyrimidine and purine nucleoside analogues such as Cytarabine (Cytosar-U®), Gemcitabine (Gemzar®), Clofarabine (Clolar®), Cladribine (Leustatin®), Fludarabine (Fludara®) and Troxacitabine (Troxatyl™) are currently clinically used as antimetabolite drugs.[4]

Besides of behaving as antimetabolites, Gemcitabine (F2C) and Clofarabine (ClF) (Figure 2-1) were shown to have inhibitory activity towards enzyme ribonucleotide reductase (RNR) through different mechanisms (Figure 2-2).[5-10] While gemcitabine 5′-diphosphate (F2CDP) is a potent mechanism-based inhibitor of class I

and II RNRs[7], di- and triphosphates of ClF were the first group of nucleotide-based drugs that reversibly inhibit RNR by inducing RNR-α-subunit-hexamerization.[8]

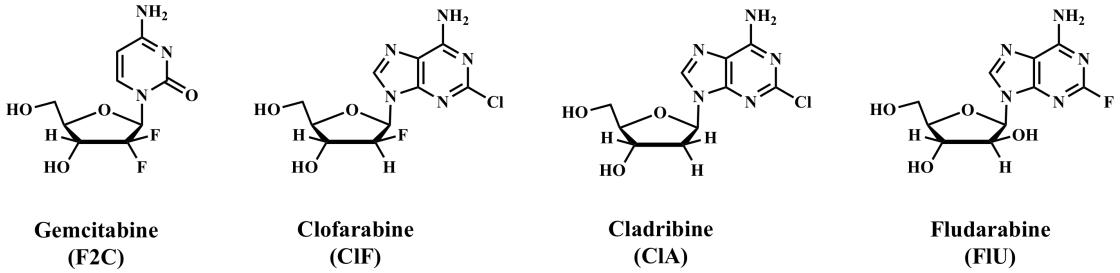

Figure 2-1. Structures of RNR-inhibiting nucleoside analogues of which mechanisms are know *in vitro* (F2C)[5,6] as well as in cells (ClF)[8-10] and unknown ClA and FlU[2,4].

In order to prove that this reversible mechanism is not limited to ClF, we sought for other nucleoside analogues that might have the ability to induce this RNR-α–subunit oligomeric regulation. ClF was developed after other deoxyadenosine analogues, ClA and FlU.[11,12] All of these adenosine analogues are shown to kill lymphocytes selectively.[13] As they have halogenated substitution at C2 of adenine ring (Figure 2-1), these agents are resistant to adenosine deaminase, a catabolic enzyme that may diminish the quantity of the active nucleoside analogues[1,4,14] (Figure 2-3). In addition to sharing the same adenosine backbone structure, these three compounds have been shown to target enzyme RNR and have similar effectiveness against hematologic malignancies (Table 2-1).[4,11,15-21]

In this work, by considering their similar structures, therapeutic functions, and common target enzyme, ClA and FlU were then hypothesized to reversibly inhibit enzyme RNR via the same oligomeric regulation as ClF.

i) Irreversible inhibition of $\alpha_2\beta_2$ holocomplex by F2CDP (active form of F2C in cell)[5-7]

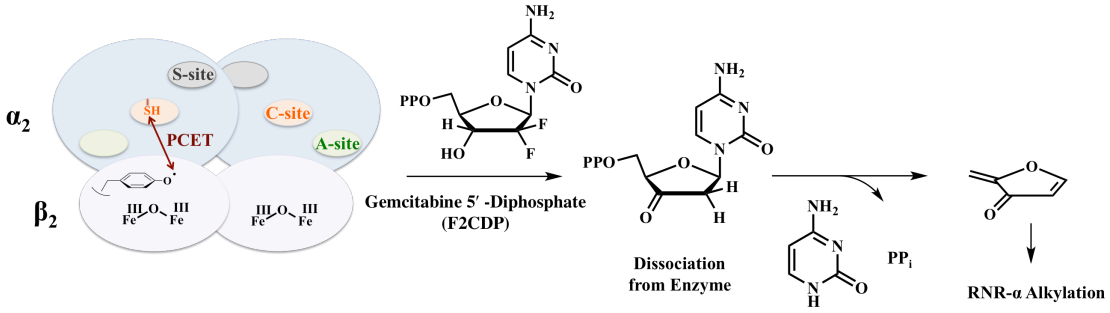

PCET, Proton-Coupled Electron Transfer.

ii) hRNR-α specific oligomeric regulation by ClA(D/T)P (active forms of ClF in cell).[8-10]

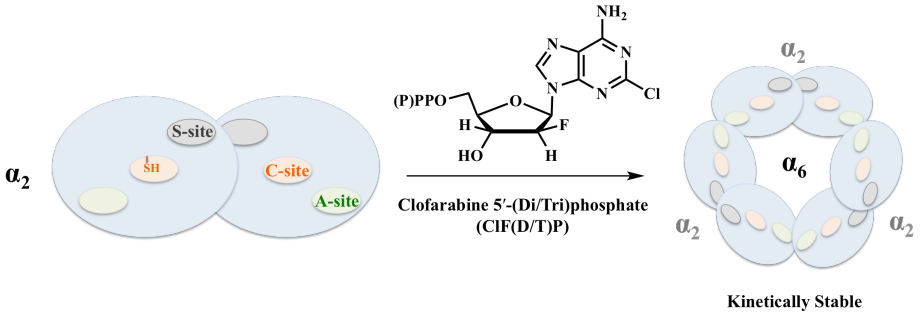

Figure 2-2. F2C (i) and ClF (ii) inhibit RNR via distinct mechanisms.

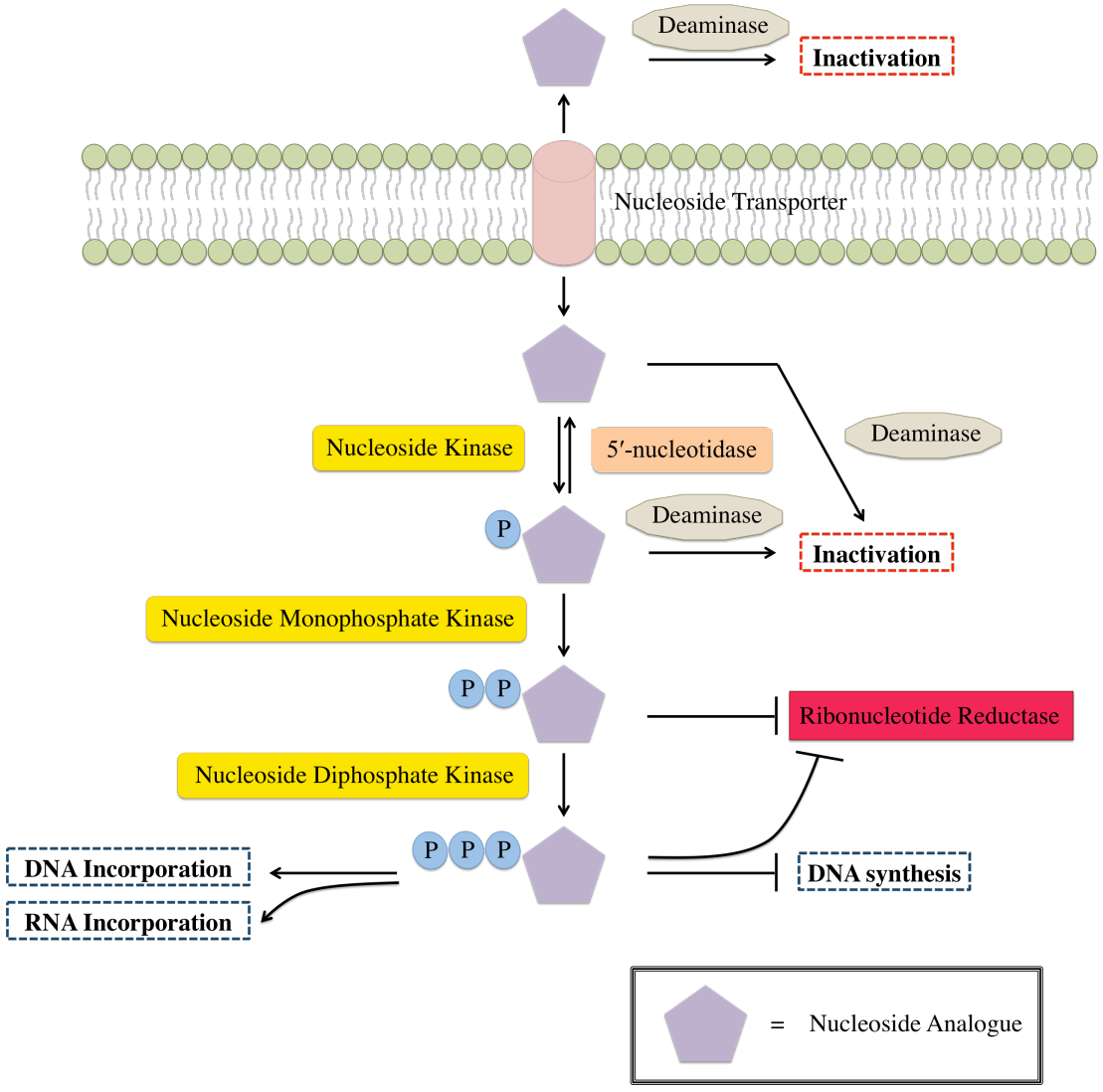

Figure 2-3. Mechanism of nucleoside analogues' activity in cell. Figure adapted from Ref. 1.

Table 2-1. Postulated target enzyme(s) and therapeutic function of triphosphorylated ClF, ClA and FlU. Adapted from Ref. 4.

Nucleoside Analogue	Active Form	Target Enzyme(s)	Disease
ClF	TP	DNA polymerases, ribonucleotide reductase	Acute lymphocytic leukemia, Pediatric refractory or relapsed acute myelogenous leukemia
ClA	TP	ribonucleotide reductase	Low-grade lymphoma, hairy cell leukemia, chronic lymphocytic leukemia, childhood leukemia
FlU	TP	DNA polymerase-α (mainly), ribonucleotide reductase, DNA primase	Lymphoproliferative disorders, low-grade lymphoma, chronic lymphocytic leukemia

TP, triphosphorylated nucleoside analogue.

Active forms of nucleoside analogues in cell

Cytotoxicity of nucleoside analogues is mainly associate with accumulation of their phosphorylated derivatives in cells[4,13,22-24] (Figure 2-3). Enzymes involved in the phosphorylation steps of ClF, ClA and FlU are listed in Table 2-2. Of note, fludarabine is clinically used in its monophosphorylated form (FlUMP). The additional phosphate group is important for drug solubility. However, FlUMP is dephosphorylated by plasma phosphatases and ecto-5′-nucleotidase to FlU right before it gets transported into cells by nucleoside transporters. Following entry into cells, FlU is initially phosphorylated to FlUMP by enzyme dCK, prior to further phosphorylation to FlUDP or FlUTP by other kinases.[4] Since dCK plays key roles in these drugs' activations, either by (1) providing a monophosphate metabolite reservoir for their di- and triphosphate active forms (for ClF and ClA)[23] or (2) catalyzing the rate-limiting step in FlU's activation[23,25] (Table 2-2), cell lines with drastically decreased level of dCK are resistant to these drugs.[26-28] In order to study the mechanism(s) through

which ClA and FlU inhibit RNR *in vitro*, the di- and triphosphorylated forms of ClA and FlU were synthesized in this thesis study. Monophosphorylated nucleoside analogues are not the primary focus of this thesis since RNRs bind to only nucleoside di- and triphosphates.

Table 2-2. Enzymes involved in cellular phosphorylation steps of ClF, ClA and FlU.

Nucleoside Analogue	Enzyme			Rate-limiting step[12,23,25]
	Nucleoside ⟶ MP	MP ⟶ DP	DP ⟶ TP	
ClF	dCK[4,15]	Nucleotide Kinases[15,23]	Nucleotide Kinases[12,15,23]	MP ⟶ DP
ClA	dCK[4]	Nucleoside Monophosphate Kinase[22]	Nucleoside Diphosphate Kinase[22]	MP ⟶ DP
FlU	dCK[4]	Adenylate Kinase[24]	Nucleoside Diphosphate Kinase[24]	Nucleoside ⟶ MP

dCK, deoxycytidine kinase; MP, monophosphorylated nucleoside; DP, diphosphorylated nucleoside; TP, triphosphorylated nucleoside.

Synthesis of nucleoside monophosphates (NMPs) in the literature

Synthetic approaches for nucleoside 5′-monophosphates have been developed by using either a P(III) or P(V) reagent as a phosphate source. The corresponding intermediates are shown in Figure 2-4.[29]

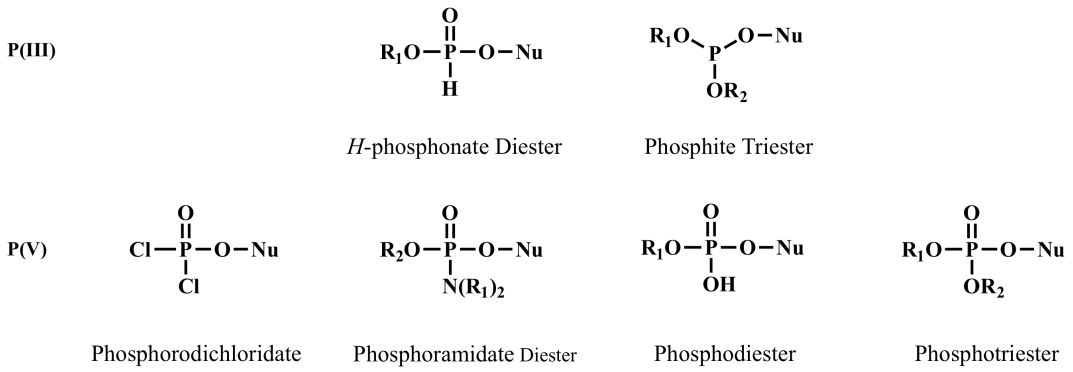

Nu, nucleoside; R_1 and R_2, alkyl groups.

Figure 2-4. P(III) and P(V) intermediates formed during monophosphorylation of nucleosides. Adapted from Ref. 29.

In 1967, Yoshikawa and co-workers reported a 5′-monophosphorylation of unprotected natural nucleosides. For substrate adenosine, phosphoryl chloride in triethylphosphate is used as a phosphate source and the reaction is carried out at 0−4 °C for 6 hours before hydrolysis (Scheme 2-1).[30] Formation of a nucleoside-trialkylphosphate complex (**1)** explains the reaction's regioselectivity.[30,31] However, formation of hydrochloric acid (HCl) during hydrolysis of **2** to NMPs could potentially lead to the acid-catalyzed cleavage of the glycosidic bond. Thus, triethylammonium bicarbonate (TEAB) buffer is used to maintain the reaction pH ~7.5.[29]

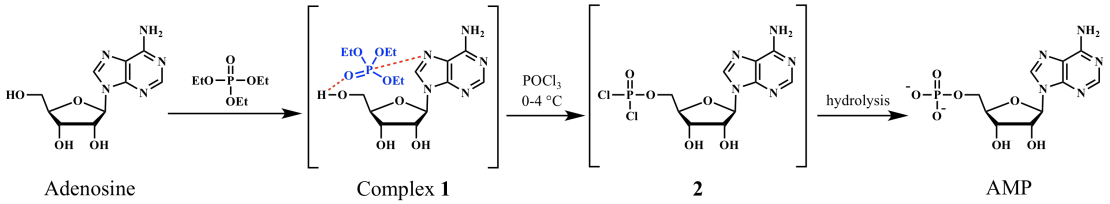

Scheme 2-1. Synthesis of monophosphorylated adenosine (AMP) using Yoshikawa's method.[30]

Nevertheless, Yoshikawa's method might not be ideal for nucleoside analogues of which their C2′ substituents are electronegative elements; for example, F2C (Figure 2-1). By having fluorines nearby, the C3′ hydroxyl group is acidic enough to initiate C3′, C5′-cyclic phosphate formation from unprotected nucleoside[32] (Figure 2-5).

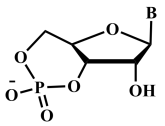

B, nucleobase.

Figure 2-5. Structure of C3′, C5′-cyclic phosphate nucleoside.[32]

In 2000, Taktakishvili and Nair developed another phosphorylating reagent, 2-*O*-(4,4′-dimethyoxytrityl)ethylsulfonylethan-2′-yl-phosphate (**3**) for phosphorylation of the primary and secondary alcohol of deoxyribonucleosides in the present of a coupling reagent, triisopropylbenzenesulfonyl tetrazolide (TPS-TAZ)[29,33] (Scheme 2-2). Syntheses of deoxynucleoside monophosphates (dNMPs) are accomplished after *in situ* deprotection of protecting groups at the phosphate and C3′ hydroxyl groups in 80−95% yield.[33]

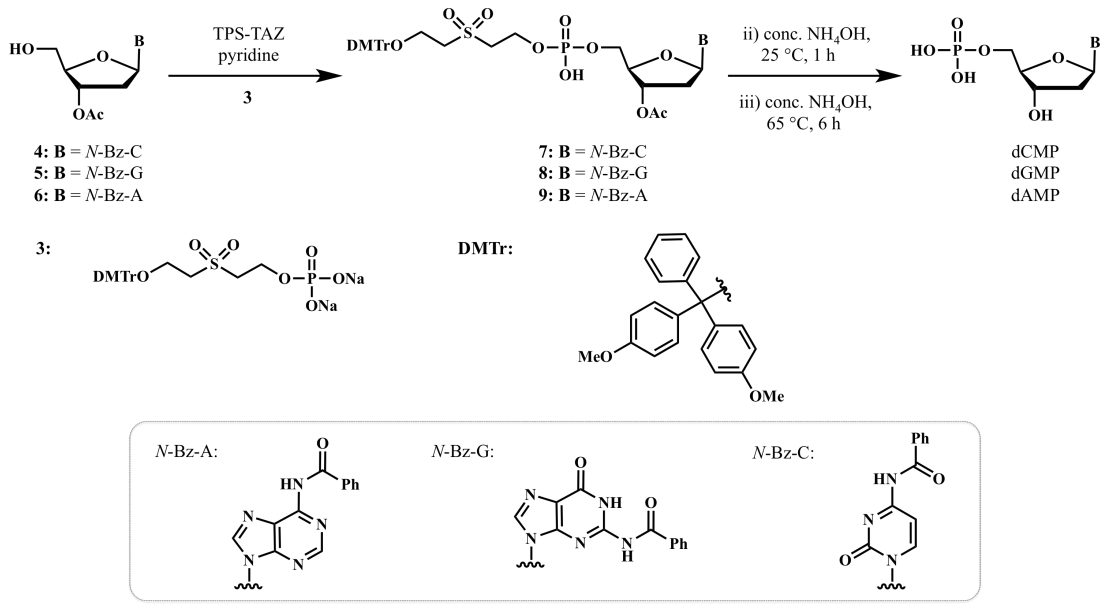

Scheme 2-2. Syntheses of dNMPs using an alternative phosphorylating reagent **3**.[33]

A drawback of this method is that protection for both the nucleobase and C3′ hydroxyl groups is required before the phosphorylation step (Scheme 2-2).[33]

As NMPs are synthesized in cells by nucleoside kinases[4,12,15,22-24,29], enzymatic syntheses of NMPs have also been reported. In 1997, Usova and Eriksson accomplished phosphorylation of nucleoside derivatives by using human deoxycytidine kinase (dCK) and a phosphate donor molecule, ATP.[34] In 2011, the same method was applied to ClFMP synthesis.[8] As ClF and ClA are both adenosine derivatives, human dCK was used to synthesize ClAMP in this present work under an assumption that the enzyme's catalytic function would remain for ClA substrate.

Synthesis of nucleoside diphosphates (NDPs) in the literature

Synthesis of NDPs via phosphorodichloride intermediate (**2**), by using a corresponding precursor based on Yoshikawa's method (Scheme 2-1), has been reported (Scheme 2-3). Tetra-*n*-butyl ammonium phosphate is used as a phosphate donor in this approach. After hydrolysis by TEAB buffer, NDP is obtained. However, the presence of a triphosphate derivative byproduct is reported in some cases.[29]

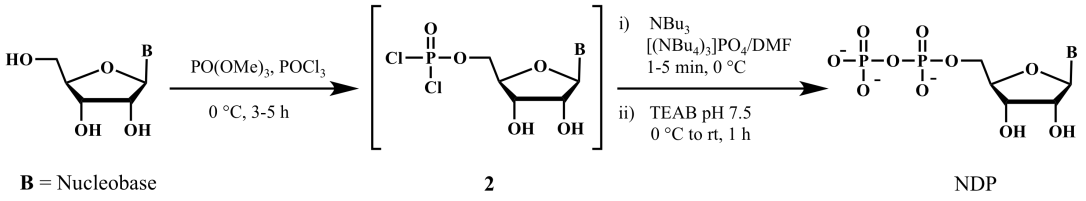

Scheme 2-3. NDP synthesis via NMP precursor obtained from Yoshikawa's procedure. Adapted from Ref. 29.

There are other approaches for NDP syntheses reported; for example, synthesis via a tosylate intermediate by the Poulter group[35] and synthesis via a phosphoramidate intermediate.[36,37] However, these approaches require either days for reaction completion or protecting groups at C2′ and/or C3′ hydroxyl groups. Moreover, all studies mentioned above reported only phosphorylation of natural (d)NMP substrates. Nucleoside derivatives that contained a modified base have not been studied.

Aye and Stubbe have developed a synthetic route to synthesize ClFDP from its precursor (ClFMP) after many of their attempts to utilize nucleotide monophosphate kinases failed (Scheme 2-4).[8] Before the addition of a phosphorylating agent, tributylammonium phosphate (TBAP), the phosphate group of ClFMP is initially

activated by carbonyl diimidazole (CDI) to form **10** (Scheme 2-4).[8,36] An advantage of this method is that there is no triphosphorylated byproduct observed.

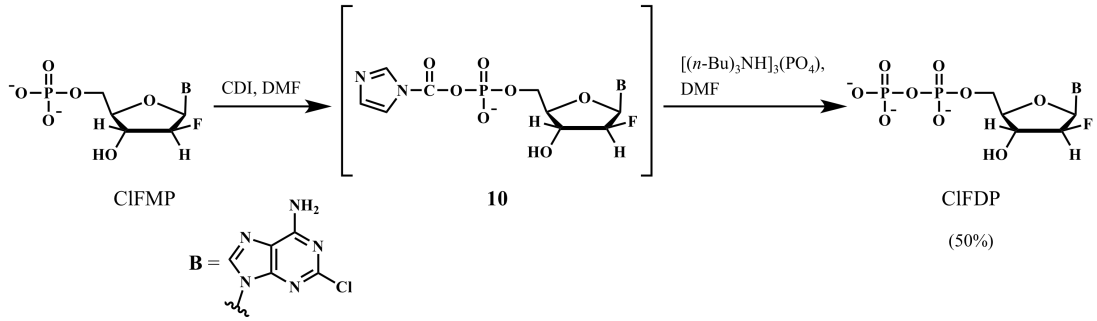

Scheme 2-4. ClFDP synthesis. Adapted from Ref. 8.

Synthesis of nucleoside triphosphates (NTPs) in the literature

In 1981, Ludwig revealed a route to synthesize (deoxy)adenosine 5′-triphosphates. The first step is (d)AMP synthesis using Yoshikawa's procedure (Scheme 2-1 and 2-5). Addition of tributylamine and an excess of bis(tri-*n*-butylammonium) pyrophosphate in dry DMF for 1 minute leads to a formation of cyclic **11**. Final product, (d)ATP, is obtained after hydrolysis with 1 M TEAB in excellent yield.[38]

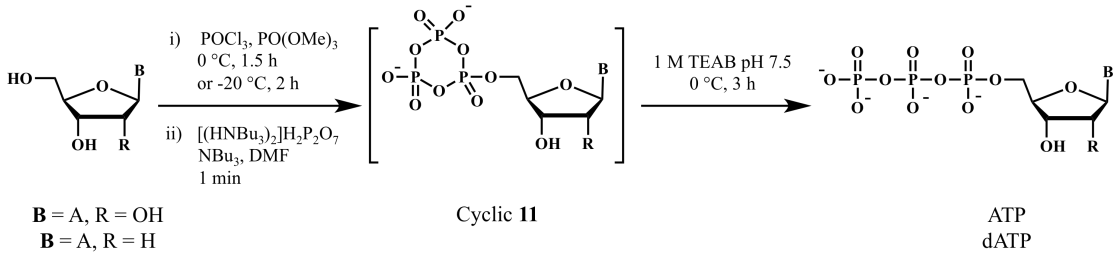

B, nucleobases; A, adenine.

Scheme 2-5. (d)ATP synthesis. Adapted form Ref. 29 and 38.

Aye and Stubbe also applied this method to their ClFTP synthesis shown in Scheme 2-6.[8]

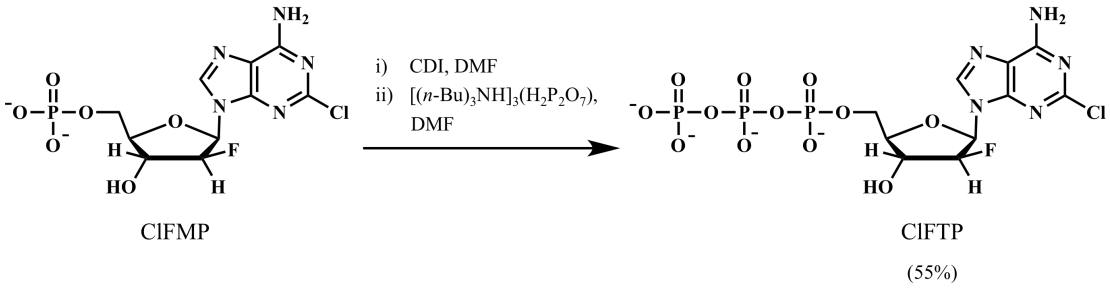

Scheme 2-6. ClFTP synthesis. Adapted from Ref. 8.

By taking structural similarity between ClF, ClA and FlU into account, Aye and Stubbe's procedure was chosen to be a synthetic route for di- and triphosphorylation of ClAMP and FlUMP in this work (Scheme 2-7).

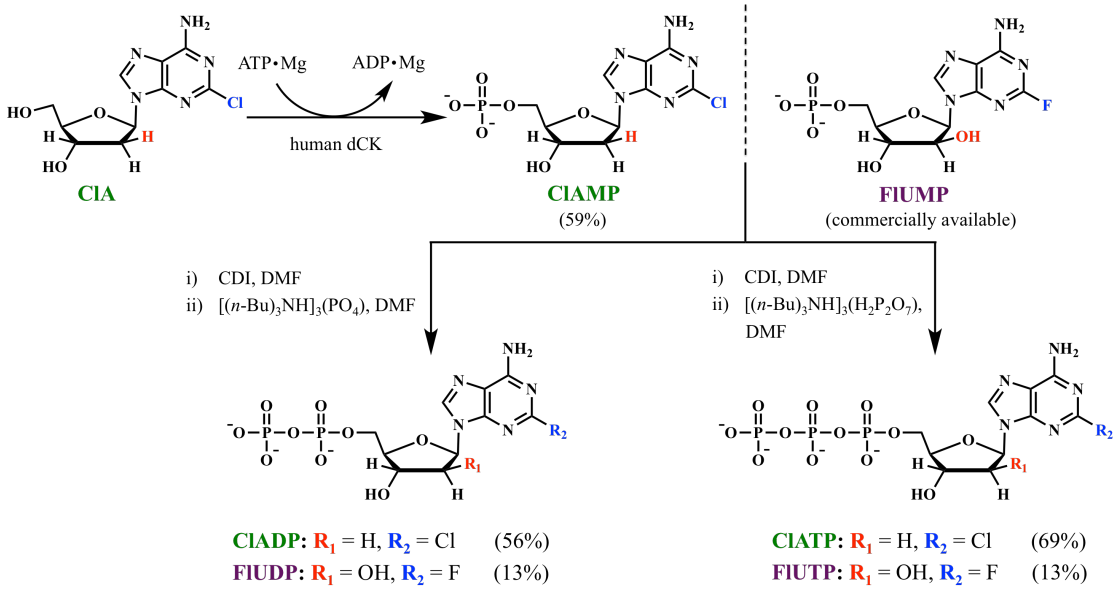

Scheme 2-7. Enzymatic synthesis of monophosphate of ClA and chemical syntheses of di- and triphosphates of ClA and FlU.

2.2 Experimental

General Materials and Methods. Cladribine (ClA), Fludarabine phosphate (FlUMP) and Clofarabine (ClF) were from AK Scientific. Streptomycin sulfate and isopropyl β-D-thiogalactopyranoside (IPTG) were purchased from Gold Biotechnology. DL-dithiothreitol (DTT) was from Amresco. All other chemicals were purchased from either Sigma Aldrich or Fisher in highest available purity and used without further purification. Sephadex G-25 resin for protein purification, DEAE-Sephadex A-25 chloride, TALON® metal affinity resin and Dowex® 50WX4 200−400 (H) were from GE Healthcare, Sigma life science, Clontech and Alfa Aesar, respectively. Centricons were from Millipore. The human deoxycytidine kinase (dCK) expression plasmid was kindly provided by Professor Staffan Eriksson (Swedish University of Agricultural Sciences, Uppsala, Sweden).[34] Analytical thin layer chromatography (TLC) was performed on Merck TLC silica gel 60 F_{254} glass plates. Compounds were visualized by exposure to UV light. Enzyme human dCK concentration was determined using its known absorption property: A_{280nm} = 1.0 at 0.55 mg/mL. Gel images were analyzed using Image Lab Version 4.1. Concentrations of ClA(M/D/T)P, FlU(M/D/T)P and ClF(M/D)P were determined by using their extinction coefficients: $\varepsilon_{265,\ ClA}$ = 15,700 $M^{-1}.cm^{-1}$, $\varepsilon_{263,\ FlU}$ = 16,400 $M^{-1}.cm^{-1}$ and $\varepsilon_{263,\ ClF}$ = 16,400 $M^{-1}.cm^{-1}$, respectively.

Purification of enzyme human deoxycytidine kinase (dCK)

The His_6-tagged human dCK plasmid[34] was transformed into the BL21-CodonPlus(DE3)-RIL *E.coli* host strain, selected with kanamycin, and inoculated in Luria Broth (LB) containing 50 μg/mL Kanamycin and 50 μg/mL Chloramphenicol. The expression of human dCK was induced when the OD_{600} reached 1.0 by the

addition of IPTG, to a final concentration of 1.0 mM. The media was incubated for another 4 hours at 37 °C. Cells were then harvested by centrifugation at 6,000×g for 20 minutes at 4 °C. *This cell pellet preparation was performed by a former member of the Aye lab, Tyler Charles Peterhansel.* The expression of human dCK was confirmed by SDS-PAGE gel (Figure 2-6).

Purification of His_6-tagged human dCK was carried out by a modified procedure of Usova and Eriksson.[34] The cell pellet was suspended in lysis buffer (20 mM Tris-HCl pH 7.9, 500 mM NaCl, 10 mM imidazole, 10 mM BME and 0.5 mM PMSF) in a ratio of 1 g cell pellet:5 mL lysis buffer. The suspension was then lysed at 13,000 psi by two passes through a French Pressure Cell Press. After centrifugation at 20,000×g at 4 °C for 30 minutes, streptomycin sulfate was slowly added to the supernatant to a final concentration of 2% (wt/v) within 15 minutes. The suspension was then gently stirred and incubated at 4 °C for another 15 minutes. The supernatant obtained after centrifugation at 20,000×g at 4 °C for 30 minutes was incubated with TALON® metal affinity resin, which was pre-equilibrated with 10 column volumes (CV) of lysis buffer, for 1 hour. The suspension was re-loaded on the column and the flow through was collected for SDS-PAGE. The resin was washed with 1 bed volume (BV) of wash buffer (20 mM Tris-HCl pH 7.9, 500 mM NaCl, 50 mM imidazole and 10 mM BME) to get rid of any non-specific binding proteins. This step was repeated two more times. Elution buffer (20 mM Tris-HCl pH 7.9, 500 mM NaCl and 150 mM imidazole) was then used to elute human dCK; 1.5 mL fractions were collected to a final volume of 48 mL. Fractions that had A_{280nm}:A_{260nm} ratios greater than 1.6 were pooled. Centricons with a membrane NMWL (nominal molecular weight limit) of 10 kDa were used to concentrate protein-containing fractions to a final volume of 9 mL before loading onto Sephadex G-25 resin, which had been pre-equilibrated with at least 5 BV of storage buffer (20 mM Tris-HCl pH 7.9, 500 mM NaCl, 10 mM DTT

and 20% glycerol). After elution, the protein-containing fractions, judged by Bradford protein assay[39,40], were concentrated using 10 kDa NMWL centricons to a final concentration of 5.1 mg/mL. His_6-tagged human dCK concentration was calculated using A_{280nm} = 1.0 at 0.55 mg/mL. The purity of the enzyme was determined using SDS-PAGE (Figure 2-6).

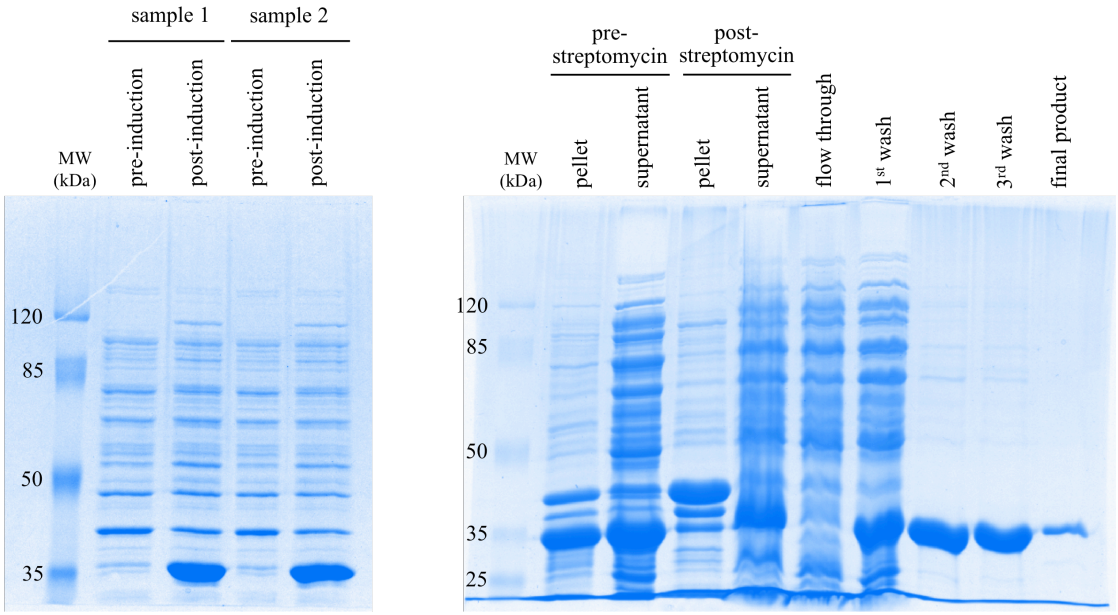

Figure 2-6. SDS-PAGE gels of (*left*) His_6-tagged human dCK expression induced by IPTG and (*right*) purified His_6-tagged human dCK (30 kDa[34]).

Syntheses of ClFMP, ClFDP, ClAMP, ClADP, ClATP, FlUDP, and FlUTP

ClFMP and ClFDP. Mono- and diphosphorylated ClF were synthesized as previously reported.[8] Anion exchange chromatography (DEAE-Sephadex) of the reaction of ClF with His_6-tagged human dCK and of the reaction of ClFMP with TBAP are shown in Figure 2-7 and 2-8, respectively. NMR spectroscopic, both ^{1}H and ^{31}P, and mass spectrometric analyses were verified with previously reported spectra.[8]

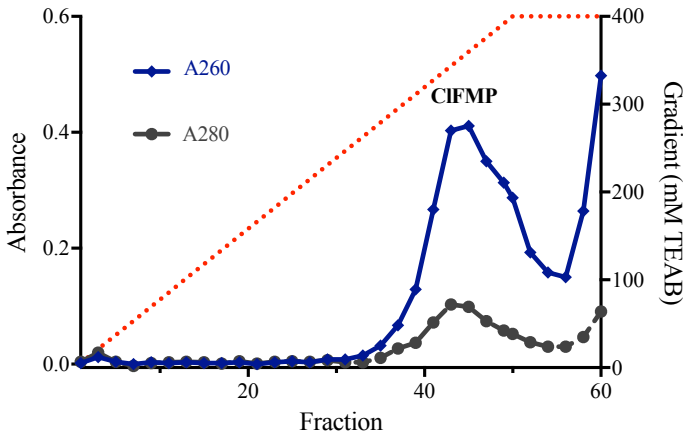

Figure 2-7. Anion-exchange purification of ClFMP.

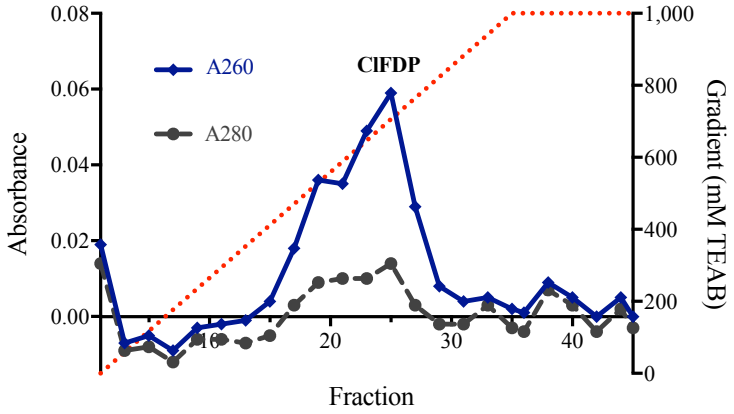

Figure 2-8. Anion-exchange purification of ClFDP.

ClAMP. The conversion of substrate ClA to ClAMP was achieved via enzymatic phosphorylation using human dCK (Scheme 2-7).[8,34] The 10 mL reaction mixture, containing 1 mM ClA, 10 mM ATP, 2 mM DTT, 100 mM KCl and 10 mM $MgCl_2$ in Tris-HCl (pH 7.6), was gently stirred at 37 °C for 2 minutes before His_6-tagged human dCK was added, to a final concentration of 0.25 mg/mL. The reaction was further incubated at 37 °C for another 45 minutes. Completion of the reaction was confirmed by silica gel TLC using 10% MeOH in ethyl acetate as the mobile phase. Anion-

exchange purification of ClAMP on 40 mL BV of DEAE A-25 Sephadex column, which had been pre-equilibrated with 200 mL of 5 mM TEAB (pH 7.0), was carried out at 4 °C. After a 150 mL×150 mL linear gradient from 5 mM to 400 mM TEAB (pH 7.0) was applied to the A-25 Sephadex column, the desired product was eluted (Figure 2-9). Product-containing fractions were pooled and solvent removed under vacuum using a lyophilizer.

ClADP. The triethylammonium salt (Et_3NH^+) of ClAMP (5.9 μmol) was dissolved in 500 μL H_2O and loaded onto 60 mL BV of Dowex® 50WX4 200−400 (H) column, which had been pre-equilibrated with 600 mL (or 10 BV) of 20% pyridinium (pyH^+) solution. The pyH^+ salt of ClAMP was eluted with H_2O and solvent removed under vacuum using a lyophilizer. The resultant salt (pyH^+ of ClAMP) was dissolved in 1 mL H_2O, then treated with 12 μmol of $(n\text{-Bu})_3N$. The reaction mixture was azeotroped with benzene (5×1.5 mL) to provide the anhydrous tributylammonium [$(n\text{-Bu})_3NH^+$] salt of ClAMP. 100 μL of anhydrous dimethylformamide (DMF) was added to the $(n\text{-Bu})_3NH^+$ salt of ClAMP (3.4 μmol) under argon (Ar) atmosphere, followed by CDI (16.8 μmol) in 100 μL DMF at room temperature (RT). The resultant clear solution was stirred overnight under Ar atmosphere at RT. Then, excess CDI was consumed by the addition of anhydrous MeOH (3 μmol). The suspension was further stirred at RT for 30 minutes before 32 μL of 0.27 M solution of TBAP (prepared as previously reported)[8,41,42] was added. The reaction suspension was stirred at RT for another 10 minutes at which point the reaction container was placed in a desiccator under house vacuum until dry-residue was observed. 200 μL of DMF was added to the resultant residue. After centrifugation (20,850×g, 1 minute, at RT), the supernatant was collected. The process was repeated 6 times before the combined supernatants were treated with an equal volume of MeOH, and subsequently concentrated in vacuo.

After dissolving the residue in 1 mL ddH_2O, ClADP was purified at 4 °C on 20 mL BV of DEAE-Sephadex A-25 column that had been pre-equilibrated with ddH_2O. ClADP was eluted with a 150 mL×150 mL linear gradient from 0 M to 1 M TEAB (pH 7.0). 5 mL fractions were collected and assayed for A_{260nm} and A_{280nm} (Figure 2-10). After pooling all ClADP-containing fractions, the solvent was removed using a lyophilizer.

ClATP. 5 μmol of anhydrous $(n\text{-Bu})_3NH^+$ salt of ClAMP was dissolved in anhydrous DMF (330 μL). 25 μmol CDI in 170 μL of anhydrous DMF was then added to the resultant cloudy suspension. After stirring at RT under Ar atmosphere for 19 hours, a colorless solution was obtained. The excess CDI was quenched by the addition of anhydrous MeOH (192 μmol), and was stirred for another 30 minutes. The resultant solution was treated with a 0.1 M solution of a commercially available tributylammonium pyrophosphate (TBAPP, 25 μmol) in anhydrous DMF, which had been freshly prepared. The resultant suspension was stirred at RT for another 10 minutes before placing it under vacuum overnight. Anion exchange chromatography of ClATP was carried out at 4 °C on a 20 mL BV DEAE-Sephadex A-25 column, which had been pre-equilibrated with ddH_2O. Upon applying a 200 mL×200 mL linear gradient from 0 to 1 M TEAB (pH 7.0) onto the column, 5 mL fractions were collected and assayed for A_{260nm} and A_{280nm} (Figure 2-11). The solvent was removed under vacuum using a lyophilizer after all ClATP-containing fractions were pooled.

FlUDP. The commercially available FlUMP (31.8 μmol) was dissolved in 1 mL of 5 mM TEAB (pH 7.0) and subsequently loaded on a 40 mL BV of DEAE-Sephadex A-25 column, which had pre-equilibrated with 200 mL of 5 mM TEAB (pH 7.0). This step was carried out at 4 °C. The desired product was eluted with a 150 mL×150 mL

linear gradient from 5 mM to 400 mM TEAB (pH 7.0). 6 mL fractions were collected and assayed for A_{260nm} and A_{280nm} (Figure 2-12). The solvent was removed under vacuum using a lyophilizer. The resultant Et_3NH^+ salt of FlUMP was evenly separated into three portions. Each portion was dissolved in ddH_2O and loaded on a 60 mL BV of Dowex® 50WX4 200−400 (H) column, which had been pre-equilibrated with 600 mL of 20% pyridinium (pyH^+) solution. ddH_2O was then used to elute the desired pyH^+ salt of FlUMP. All fractions containing the pyH^+ salt of FlUMP from three separate batches were combined and the solvent was removed using a lyophilizer. 13.6 μmol of the resultant pyH^+ salt of FlUMP was dissolved in 1 mL ddH_2O, followed by treatment with 27 μmol of $(n\text{-Bu})_3N$. In order to obtain the anhydrous $(n\text{-Bu})_3NH^+$ salt of FlUMP, the reaction mixture was azeotroped with benzene (5×1.5 mL). The amount of $(n\text{-Bu})_3NH^+$ salt of FlUMP was determined by using $\varepsilon_{263,\ FlU}$ = 16,400 $M^{-1}cm^{-1}$, and found to be 12.1 μmol. The synthesis of FlUDP was consequently accomplished by following the same protocol as mentioned in *ClADP synthesis*. A 20 mL BV of DEAE-Sephadex A-25 column was used for the purification of FlUDP. The column was pre-equilibrated with ddH_2O before use. The temperature during the purification process was kept constant at 4 °C. A sequence of different concentrations of TEAB (pH 7.0) used to elute the desired product comprised of a 150 mL×150 mL linear gradient from 0 to 300 mM TEAB (pH 7.0), an isocratic flow of 100 mL of 300 mM TEAB (pH 7.0), and a 200 mL×200 mL linear gradient from 300 to 700 mM TEAB (pH 7.0). 5 mL fractions were collected and assayed for A_{260nm} and A_{280nm} (Figure 2-13). After pooling all FlUDP-containing fractions, the solvent was removed under vacuum using a lyophilizer.

FlUTP. The protocol, identical to that of ClATP synthesis, was followed starting with 7.2 μmol of anhydrous $(n\text{-Bu})_3NH^+$ salt of FlUMP. The triphosphate of FlU was eluted

from a DEAE-Sephadex A-25 column with a 200 mL×200 mL linear gradient from 0 to 1 M TEAB (pH 7.0). 5 mL fractions were collected and assayed for A_{260nm} and A_{280nm} (Figure 2-14). FlUTP-containing fractions were pooled and subsequently solvent removed under vacuum using a lyophilizer.

2.3 Results and discussion

ClAMP. After lyophilizing the ClAMP-containing fractions (Figure 2-9), the resultant white powder (59 % isolated yield) was characterized by ^{1}H and ^{31}P NMR spectroscopic analyses: ^{1}H NMR (600 MHz, D_2O) δ (ppm) 8.38 (*s*, 1H), 6.38 (*t*, ^{3}J = 6.8 Hz, 1H), 4.65−4.71 (*m*, 1H), 4.22−4.28 (*m*, 1H), 4.02 (*m*, 2H); ^{31}P NMR (501 MHz, D_2O, H_3PO_4 external reference) δ 2.02 ppm (*see Appendix B)*. HRMS (ESI) exact mass calculated for $C_{10}H_{12}ClN_5O_6P$ $[M-H]^-$ requires *m/z*: 364.02192, found 364.02231.

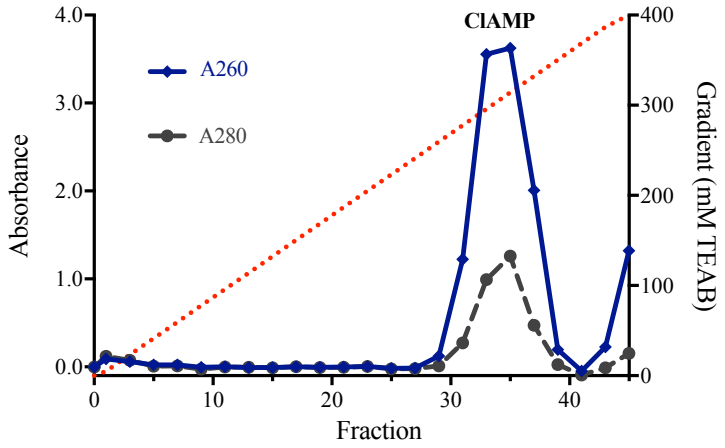

Figure 2-9. Anion-exchange purification of ClAMP using DEAE-Sephadex A-25 column.

ClADP. As shown in Figure 2-10, ClADP was eluted at 550 mM TEAB. The final product after lyophilizing, with overall 56% yield, was characterized by ^{1}H, ^{31}P NMR spectroscopic, and mass spectrometric analyses: ^{1}H NMR (600 MHz, D_2O) δ (ppm) 8.45 (*s*, 1H), 6.43 (*t*, ^{3}J = 6.8 Hz, 1H), 4.74−4.78 (*m*, 1H), 4.30 (*m*, 1H), 4.10−4.20 (*m*, 2H); ^{31}P NMR (501 MHz, D_2O, H_3PO_4 external reference) δ (ppm) -10.53 and -11.11; (*see Appendix B)*; HRMS (ESI) exact mass calculated for $C_{10}H_{13}ClN_5O_9P_2$ $[M-H]^-$ requires *m/z*: 443.98825, found 443.98973.

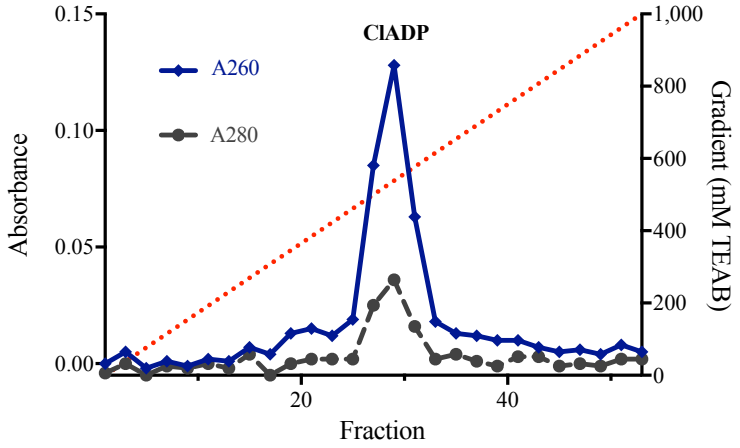

Figure 2-10. Anion-exchange purification of ClADP.

ClATP. The desired triphosphate of ClA was eluted at 630 mM TEAB (Figure 2-11). The resultant lyophilized residue, in overall 69% yield, was evaluated by ^{1}H, ^{31}P NMR spectroscopic, and mass spectrometric analyses: ^{1}H NMR (600 MHz, D_2O) δ (ppm) 8.50 (*s*, 1H), 6.46 (*t*, ^{3}J = 6.8 Hz, 1H), 4.31−4.33 (*m*, 1H), 4.15−4.28 (*m*, 2H), 4.10−4.20 (*m*, 2H); ^{31}P NMR (400 MHz, D_2O, H_3PO_4 external reference) δ (ppm) -10.54, -11.23 and -23.10 (*see Appendix B)*; HRMS (ESI) exact mass calculated for $C_{10}H_{14}ClN_5O_{12}P_3$ $[M-H]^-$ requires *m/z*: 523.95458, found 523.95505.

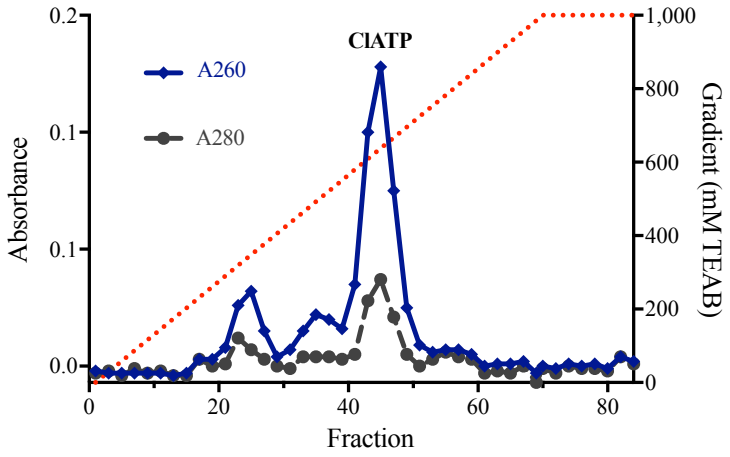

Figure 2-11. Anion-exchange purification of ClATP.

FlUDP. As described above, the diphosphate of FlU was synthesized from the lyophilized FlUMP-containing fractions (Figure 2-12). During the anion-exchange purification, FlUDP was eluted at 300 mM TEAB (Figure 2-13). The overall 13% yield material was characterized by ^{1}H, ^{31}P NMR spectroscopic, and mass spectrometric analyses: ^{1}H NMR (600 MHz, D_2O) δ (ppm) 8.43 (*s*, 1H), 6.34 (*d*, ^{3}J = 5.9 Hz, 1H), 4.61 (*t*, ^{3}J = 6.2 Hz, 1H), 4.49 (*t*, ^{3}J = 6.7 Hz, 1H), 4.32 (*m*, 2H), 4.19 (*m*, 1H); ^{31}P NMR (501 MHz, D_2O, H_3PO_4 external reference) δ (ppm) -10.24 and -11.01 (*see Appendix B)*; HRMS (ESI) exact mass calculated for $C_{10}H_{13}FN_5O_{10}P_2$ $[M-H]^-$ requires *m/z*: 444.01272, found 444.01374.

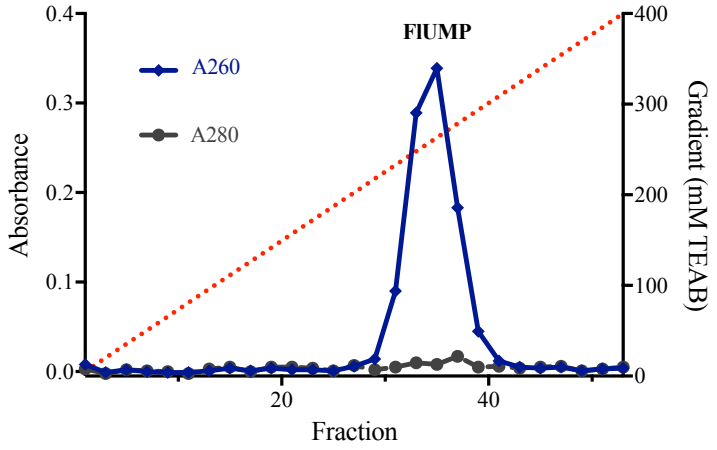

Figure 2-12. Anion-exchange chromatography (DEAE-Sephadex A-25) of FlUMP.

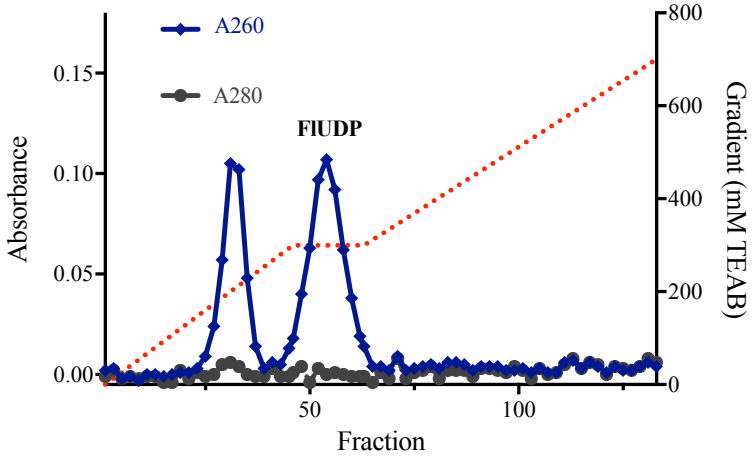

Figure 2-13. Anion-exchange (DEAE-Sephadex A-25) purification of FlUDP.

FlUTP. Shown in Figure 2-14, FlUTP-containing fractions were eluted at 600 mM TEAB (pH 7.0). The 13% lyophilized material was judged homogenous by ^{1}H, ^{31}P NMR spectroscopic, and mass spectrometric analyses: ^{1}H NMR (600 MHz, D_2O) δ (ppm) 8.63 (*s*, 1H), 6.35 (*d*, ^{3}J = 6.0 Hz, 1H), 4.62 (*t*, ^{3}J = 6.4 Hz, 1H), 4.49 (*t*, ^{3}J = 7.0 Hz, 1H), 4.34 (*m*, 2H), 4.19 (*m*, 1H); ^{31}P NMR (501 MHz, D_2O, H_3PO_4 external reference) δ (ppm) -10.47, -11.07, and -22.95 (*see Appendix B)*; HRMS (ESI) exact

mass calculated for $C_{10}H_{14}FN_5O_{13}P_3$ $[M-H]^-$ requires *m/z*: 523.97905, found 523.96014.

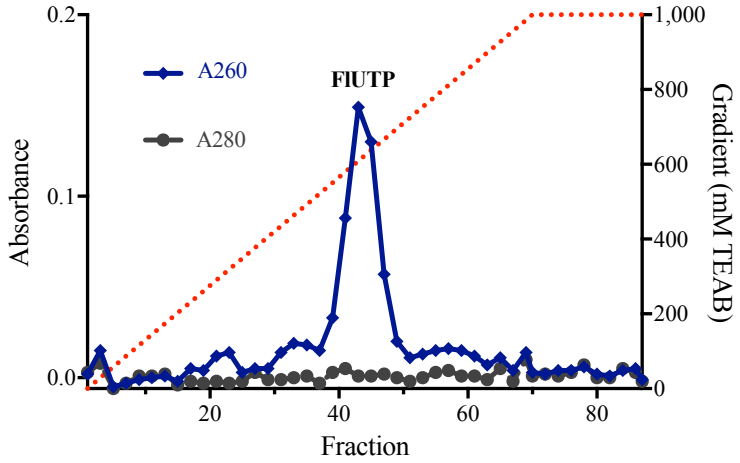

Figure 2-14. Anion-exchange purification of FlUTP.

Conclusions

Phosphorylated derivatives of ClA and FlUMP were successfully synthesized and characterized for a variety of *in vitro* biochemical studies. One advantage of using enzymatic phosphorylation is the enzyme's specificity towards its substrates, which circumvents the protection and deprotection steps used in standard chemical phosphorylation methods. Additionally, since enzymatic reactions do not generate any undesired byproducts, the reaction-yields tend to be much higher. Even though the syntheses of FlUDP and FlUTP were not achieved in high yields, this method was relatively straightforward and facile, when compared with other chemical methods.[35-37]

REFERENCE

[1] Jordheim, L. P., Durantel, D., Zoulim, F., and Dumontet, C. (2013) Advances in the development of nucleoside and nucleotide analogues for cancer and viral diseases. *Nat. Rev. Drug Discov. 12*, 447-464.

[2] Aye, Y., Li, M., Long, M. J., and Weiss, R. S. (2015) Ribonucleotide reductase and cancer: biological mechanisms and targeted therapies. *Oncogene. 34*, 2011-2021.

[3] Galmarini, C. M., Mackey, J. R., and Dumontet, C. (2002) Nucleoside analogues and nucleobases in cancer treatment. *Lancet. Oncol. 3*, 415-424.

[4] Damaraju, V. L., Damaraju, S., Young, J. D., Baldwin, S. A., Mackey, J., Sawyer, M. B., and Cass, C. E. (2003) Nucleoside anticancer drugs: the role of nucleoside transporters in resistance to cancer chemotherapy. *Oncogene. 22*, 7524-7536.

[5] Stubbe, J., and van der Donk, W. A. (1995) Ribonucleotide reductases: radical enzymes with suicidal tendencies. *Chem. Biol. 2*, 793-801.

[6] Licht, S., and Stubbe, J. (1999) *Mechanistic Investigations of Ribonucleotide Reductase* (Pourler, C. D., Ed.), pp 163-203, Elsevier, Amsterdam.

[7] van der Donk, W. A., Yu, G., Perez, L., Sanchez, R. J., Stubbe, J., Samano, V., and Robins, M. J. (1998) Detection of a new substrate-derived radical during inactivation of ribonucleotide reductase from *Escherichia coli* by gemcitabine 5'-diphosphate. *Biochemistry 37*, 6419-6426.

[8] Aye, Y., and Stubbe, J. (2011) Clofarabine 5'-di and -triphosphates inhibit human ribonucleotide reductase by altering the quaternary structure of its large subunit. *Proc. Natl. Acad. Sci. U. S. A. 108*, 9815-9820.

[9] Aye, Y., Brignole, E. J., Long, M. J., Chittuluru, J., Drennan, C. L., Asturias, F. J., and Stubbe, J. (2012) Clofarabine targets the large subunit (α) of human ribonucleotide reductase in live cells by assembly into persistent hexamers. *Chem. Biol. 19*, 799-805.

[10] Fu, Y., Lin, H. Y., Wisitpitthaya, S., Blessing, W. A., and Aye, Y. (2014) A fluorimetric readout reporting the kinetics of nucleotide-induced human ribonucleotide reductase oligomerization. *ChemBioChem 15*, 2598-2604.

[11] Jeha, S., Gandhi, V., Chan, K. W., McDonald, L., Ramirez, I., Madden, R., Rytting, M., Brandt, M., Keating, M., Plunkett, W., and Kantarjian, H. (2004) Clofarabine, a novel nucleoside analog, is active in pediatric patients with advanced leukemia. *Blood 103*, 784-789.

[12] Xie, C., and Plunkett, W. (1995) Metabolism and actions of 2-chloro-9-(2-deoxy-2-fluoro-β-D-arabinofuranosyl)-adenine in human lymphoblastoid cells. *Cancer Res. 55*, 2847-2852.

[13] Cohen, A., Hirschhorn, R., Horowitz, S. D., Rubinstein, A., Polmar, S. H., Hong, R., and Martin, D. W., Jr. (1978) Deoxyadenosine triphosphate as a potentially toxic metabolite in adenosine deaminase deficiency. *Proc. Natl. Acad. Sci. U. S. A. 75*, 472-476.

[14] Xie, K. C., and Plunkett, W. (1996) Deoxynucleotide pool depletion and sustained inhibition of ribonucleotide reductase and DNA synthesis after treatment of human lymphoblastoid cells with 2-chloro-9-(2-deoxy-2-fluoro-β-D-arabinofuranosyl) adenine. *Cancer Res. 56*, 3030-3037.

[15] Parker, W. B., Shaddix, S. C., Chang, C. H., White, E. L., Rose, L. M., Brockman, R. W., Shortnacy, A. T., Montgomery, J. A., Secrist, J. A., 3rd, and Bennett, L. L., Jr. (1991) Effects of 2-chloro-9-(2-deoxy-2-fluoro-β-D-arabinofuranosyl)adenine on K562 cellular metabolism and the inhibition of human ribonucleotide reductase and DNA polymerases by its 5'-triphosphate. *Cancer Res. 51*, 2386-2394.

[16] Keating, M. J., O'Brien, S., Plunkett, W., Robertson, L. E., Gandhi, V., Estey, E., Dimopoulos, M., Cabanillas, F., Kemena, A., and Kantarjian, H. (1994) Fludarabine phosphate: a new active agent in hematologic malignancies. *Semin. Hematol. 31*, 28-39.

[17] Krance, R. A., Hurwitz, C. A., Head, D. R., Raimondi, S. C., Behm, F. G., Crews, K. R., Srivastava, D. K., Mahmoud, H., Roberts, W. M., Tong, X., Blakley, R. L., and Ribeiro, R. C. (2001) Experience with 2-chlorodeoxyadenosine in previously untreated children with newly diagnosed acute myeloid leukemia and myelodysplastic diseases. *J. Clin. Oncol. 19*, 2804-2811.

[18] Chun, H. G., Leyland-Jones, B., and Cheson, B. D. (1991) Fludarabine phosphate: a synthetic purine antimetabolite with significant activity against lymphoid malignancies. *J. Clin. Oncol. 9*, 175-188.

[19] Dimopoulos, M. A., Kantarjian, H., Weber, D., O'Brien, S., Estey, E., Delasalle, K., Rose, E., Cabanillas, F., Keating, M., and Alexanian, R. (1994) Primary therapy of Waldenstrom's macroglobulinemia with 2-chlorodeoxyadenosine. *J. Clin. Oncol. 12*, 2694-2698.

[20] Lindemalm, S., Liliemark, J., Gruber, A., Eriksson, S., Karlsson, M. O., Wang, Y., and Albertioni, F. (2003) Comparison of cytotoxicity of 2-chloro-2'-arabino-fluoro-2'-deoxyadenosine (clofarabine) with cladribine in mononuclear cells from patients with acute myeloid and chronic lymphocytic leukemia. *Haematologica 88*, 324-332.

[21] Seymour, J. F., Kurzrock, R., Freireich, E. J., and Estey, E. H. (1994) 2-chlorodeoxyadenosine induces durable remissions and prolonged suppression of $CD4^+$ lymphocyte counts in patients with hairy cell leukemia. *Blood 83*, 2906-2911.

[22] Lotfi, K., Juliusson, G., and Albertioni, F. (2003) Pharmacological basis for cladribine resistance. *Leuk. Lymphoma 44*, 1705-1712.

[23] Bonate, P. L., Arthaud, L., Cantrell, W. R., Jr., Stephenson, K., Secrist, J. A., 3rd, and Weitman, S. (2006) Discovery and development of clofarabine: a nucleoside analogue for treating cancer. *Nat. Rev. Drug Discov. 5*, 855-863.

[24] Gandhi, V., and Plunkett, W. (2002) Cellular and clinical pharmacology of fludarabine. *Clin. Pharmacokinet 41*, 93-103.

[25] Lorkova, L., Scigelova, M., Arrey, T. N., Vit, O., Pospisilova, J., Doktorova, E., Klanova, M., Alam, M., Vockova, P., Maswabi, B., Klener, P., Jr., and

Petrak, J. (2015) Detailed Functional and Proteomic Characterization of Fludarabine Resistance in Mantle Cell Lymphoma Cells. *PLoS One 10*, e0135314.

[26] Mansson, E., Flordal, E., Liliemark, J., Spasokoukotskaja, T., Elford, H., Lagercrantz, S., Eriksson, S., and Albertioni, F. (2003) Down-regulation of deoxycytidine kinase in human leukemic cell lines resistant to cladribine and clofarabine and increased ribonucleotide reductase activity contributes to fludarabine resistance. *Biochem. Pharmacol. 65*, 237-247.

[27] Pandzic, T., Larsson, J., He, L., Kundu, S., Ban, K., Akhtar-Ali, M., Hellstrom, A. R., Schuh, A., Clifford, R., Blakemore, S. J., Strefford, J. C., Baumann, T., Lopez-Guillermo, A., Campo, E., Ljungstrom, V., Mansouri, L., Rosenquist, R., Sjoblom, T., and Hellstrom, M. (2016) Transposon Mutagenesis Reveals Fludarabine Resistance Mechanisms in Chronic Lymphocytic Leukemia. *Clin. Cancer Res. 22*, 6217-6227.

[28] Mackey, J. R., Galmarini, C. M., Graham, K. A., Joy, A. A., Delmer, A., Dabbagh, L., Glubrecht, D., Jewell, L. D., Lai, R., Lang, T., Hanson, J., Young, J. D., Merle-Beral, H., Binet, J. L., Cass, C. E., and Dumontet, C. (2005) Quantitative analysis of nucleoside transporter and metabolism gene expression in chronic lymphocytic leukemia (CLL): identification of fludarabine-sensitive and -insensitive populations. *Blood 105*, 767-774.

[29] Roy, B., Depaix, A., Perigaud, C., and Peyrottes, S. (2016) Recent Trends in Nucleotide Synthesis. *Chem. Rev. 116*, 7854-7897.

[30] Yoshikawa, M., Kato, T., and Takenishi, T. (1967) A novel method for phosphorylation of nucleosides to 5'-nucleotides. *Tetrahedron Lett. 50*, 5065-5068.

[31] Ikemoto, T., Haze, A., Hatano, H., Kitamoto, Y., Ishida, M., and Nara, K. (1995) Phosphorylation of Nucleosides with Phosphorus Oxychloride in Trialkyl Phosphate. *Chem. Pharm. Bull. 43*, 210–215.

[32] Genieser, H. G., Butt, E., Bottin, U., Dostmann, W., and Jastorff, B. (1989) Synthesis of the 3′,5′-Cyclic Phosphates from Unprotected Nucleosides. *Synthesis 1989*, 53-54.

[33] Taktakishvili, M., and Nair, V. (2000) A New Method for the Phosphorylation of Nucleosides. *Tetrahedron Lett. 41*, 7173-7176.

[34] Usova, E. V., and Eriksson, S. (1997) The effects of high salt concentrations on the regulation of the substrate specificity of human recombinant deoxycytidine kinase. *Eur. J. Biochem. 248*, 762-766.

[35] Davisson, V. J., Davis, D. R., Dixit, V. M., and Poulter, C. D. (1987) Synthesis of Nucleotide 5′-Diphosphates from 5′-O-Tosyl Nucleosides. *J. Org. Chem. 52*, 1794-1801.

[36] Zatorski, A., Goldstein, B. M., Colby, T. D., Jones, J. P., and Pankiewicz, K. W. (1995) Potent inhibitors of human inosine monophosphate dehydrogenase type II. Fluorine-substituted analogues of thiazole-4-carboxamide adenine dinucleotide. *J. Med. Chem. 38*, 1098-1105.

[37] Sun, Q., Gong, S., Sun, J., Liu, S., Xiao, Q., and Pu, S. (2013) A P(V)-N activation strategy for the synthesis of nucleoside polyphosphates. *J. Org. Chem. 78*, 8417-8426.

[38] Ludwig, J. (1981) A new route to nucleoside 5'-triphosphates. *Acta. Biochim. Biophys. Acad. Sci. Hung. 16*, 131-133.

[39] Bradford, M. M. (1976) A rapid and sensitive method for the quantitation of microgram quantities of protein utilizing the principle of protein-dye binding. *Anal. Biochem. 72*, 248-254.

[40] Stoscheck, C. M. (1990) Quantitation of protein. *Methods Enzymol. 182*, 50-68.

[41] Hoard, D. E., and Ott, D. G. (1965) Conversion of Mono- and Oligodeoxy-ribonucleotides to 5-Triphosphates. *J. Am. Chem. Soc. 87*, 1785-1788.

[42] Kozarich, J. W., Chinault, A. C., and Hecht, S. M. (1973) Ribonucleoside phosphates via phosphorimidazolidate intermediates. Synthesis of pseudo-adenosine 5'-triphosphate. *Biochemistry 12*, 4458-4463.

CHAPTER 3

In Vitro Biochemical Studies of Di- and Triphosphates of Cladribine and Fludarabine [ClA(D/T)P and FlU(D/T)P]

3.1 Introduction

Due to the key role of ribonucleotide reductase (RNR) in DNA synthesis and cell growth control[1], a wide range of strategies has been developed to inhibit RNR activity. Many known inhibitors are nucleoside analogues, of which their 5′-diphosphate (for class I and some class II RNRs) or 5′-triphosphate (for class III and some class II RNRs)[2,3] forms can act as mechanism-based or competitive inhibitors (Figure 3-1).[4-6] One of the most successful mechanism-based inhibitors that have developed into anti-tumor agents is gemcitabine (2′,2′-difluorodeoxycytidine, F2C).[7-9]

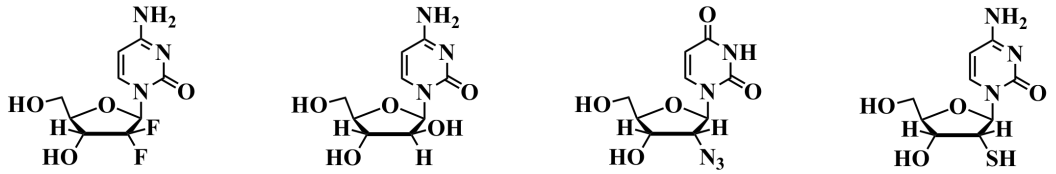

Figure 3-1. Some nucleoside analogue inhibitors of RNRs. Their active forms are either the 5′-diphosphates (for class I and some class II RNRs) or the 5′-triphosphates (for class III and some class II RNRs).[4-6]

In 2005, Cerqueira *et al*[5] proposed a mechanism by which gemcitabine 5′-diphosphate (F2CDP) utilizes to inhibit RNR activity in the absence of exogenous reductants (Figure 3-2). This mechanism is proposed based on density functional

theory (DFT) computational calculations modeling only the ribose ring (without base, pyrophosphates, or C5′ included) and key C-site side chains (cysteines as CH_3SH and the glutamate as formate), not the fully active catalytic site (C-site). The authors proposed a stable C4′ radical (**J**) to be a final product of this mechanism. However, the possibility of the top-face cysteine abstracting the C4′-hydrogen atom (**I**) to generate the C4′ radical (**J**) is later ruled out by the crystal structures of substrate-bound class I RNR-α.[10,11] These structures provide little support for the possibility that the C3′-keto nucleotide remains in the C-site long enough for the abstraction of the C4′-hydrogen atom. Instead, it is most likely released from the C-site and decomposes into furarone, which subsequently alkylates the enzyme as has been shown in the case of 2′-chloro-2′-deoxyuridine[12] (Figure 3-3).

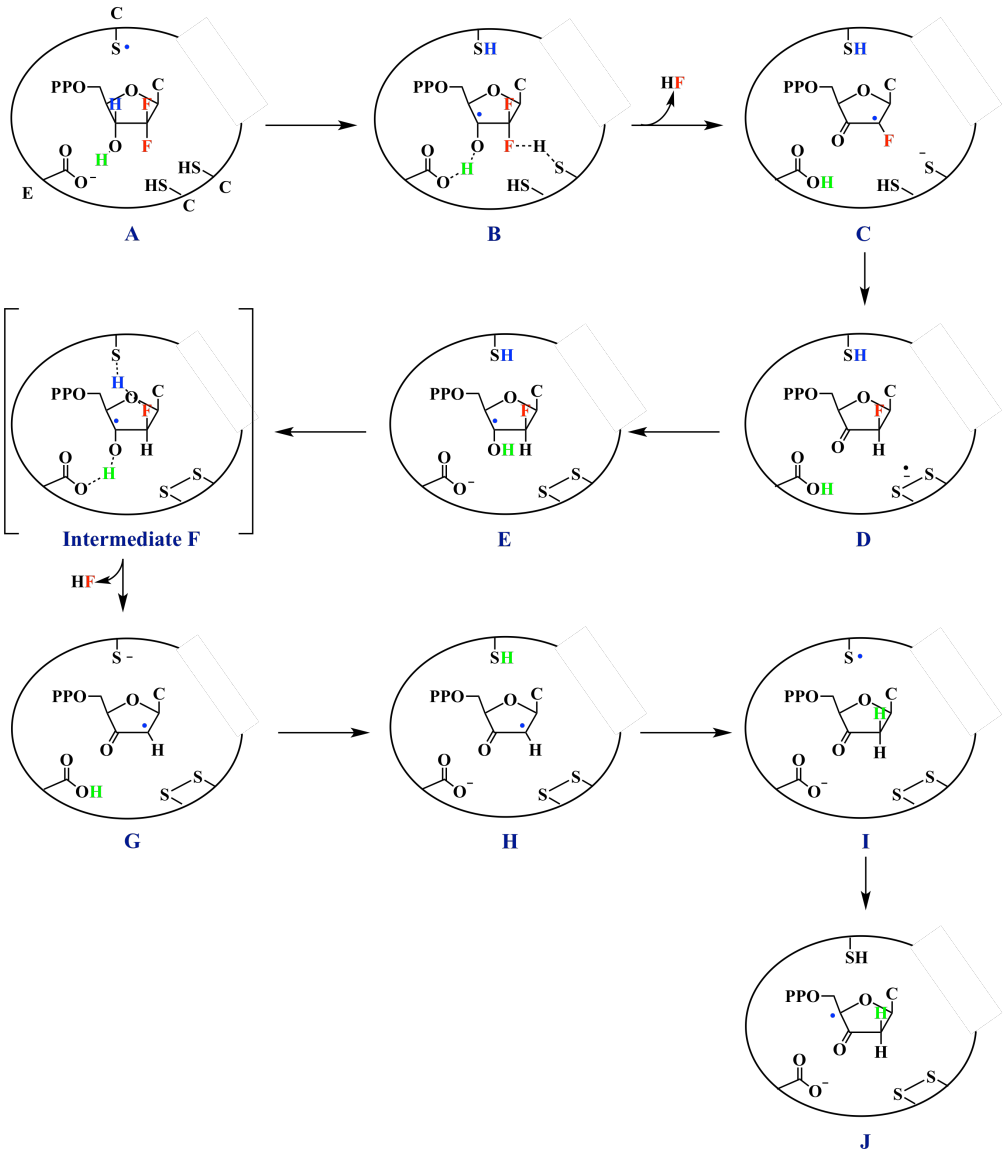

C (at the enzyme catalytic site), cysteine; E, glutamic acid; C (attached to a ribose ring), cytosine; PP, pyrophosphate.

Figure 3-2. Inhibitory mechanism of RNR by F2CDP proposed by Cerqueira *et al.*[5]

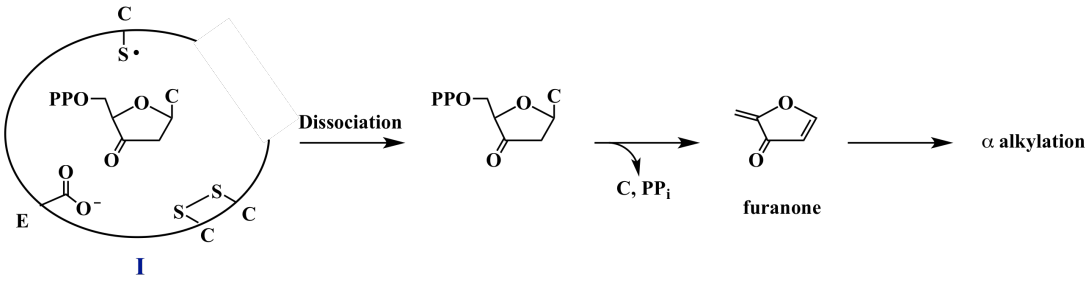

C (at the enzyme catalytic site), cysteine; E, glutamic acid; C (attached to a ribose ring), cytosine; PPi, inorganic pyrophosphate.

Figure 3-3. Upon a release of the C3′-keto nucleotide from the C-site (state **I** in Figure 3-2), it decomposes in solution into furanon, which subsequently alkylates the RNR-α.[6,10-12]

In addition to mechanism-based inhibitors that bind at the C-site of RNRs, there are also some synthetic nucleoside analogues that contain deoxyadenosine moiety similar to an enzyme inhibitory allosteric effector (dATP), *i.e.*, Clofarabine (ClF), Cladribine (ClA), and Fludarabine (FlU) (Figure 3-4). These compounds not only provide a potential RNR allosteric inhibition, but also have a low affinity to nucleotide-catabolizing enzymes such as adenosine deaminase, resulting in resistance to cell inactivation.[1] Their resistance to those catabolic enzymes arises from a halogenated substitution at C2 of their adenosine ring (Figure 3-4).[13-15]

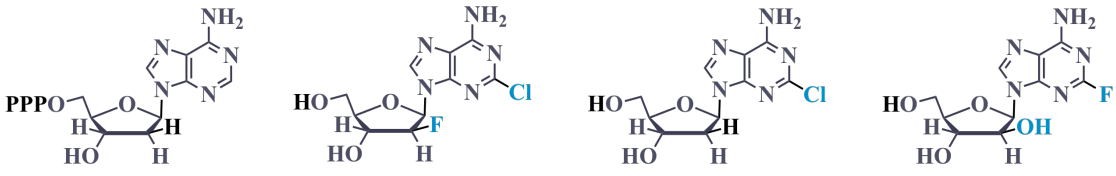

Figure 3-4. Chemical structures of dATP and its nucleoside analogues.

Mechanism(s) by which these three deoxyadenosine analogues use to inhibit RNR had been unknown until Aye and Stubbe[16] revealed a breakthrough on how ClF inhibits human (h)RNR in 2011. They have shown that di- and triphosphate of ClF induce inactive hRNR-α-hexamers (hRNR-α_6) (*see Figure 2-2, chapter 2*). This mechanism is different from the one used by F2CDP in two main aspects. First, it does not require the β-subunit. Second, this inhibition is reversible. As ClF, ClA, and FlU share a few common characteristics with respect to their structures and clinical use as antileukemic drugs[14,17-25], we hypothesized that these three deoxyadenosine analogues inhibit RNR via the same mechanism.

In this chapter, we report various *in vitro* experiments/techniques used to determine whether and how these di- and triphosphates of Cladribine and Fludarabine inhibit human RNR (hRNR) activity. For example, rapid CDP reductase activity assays[16,26] was used for the quantification of their binding affinities to the enzyme, fluorescence resonance energy transfer (FRET)[27], size exclusion chromatography (SEC) and electron microscopy (EM) were used for the determination of their enzyme-oligomerization inducing ability, and fluorescence anisotropy assays were used for the identification of their enzyme binding site preference, etc. Detailed explanations of all *in vitro* experiments are provided in the *experimental section 3.2.2*.

3.2 Experimental

General Materials and Methods. 5-iodoacetamidofluorescein (5-IAF) and tetramethylrhodamine-5-iodoacetamide dihydroiodide (5-TMRIA) were from Invitrogen. Texas Red®-5-dATP (T*-dATP) was obtained from PerkinElmer®. Streptomycin sulfate and isopropyl β-D-thiogalactopyranoside (IPTG) were from Gold Biotechnology. DL-dithiothreitol (DTT) and sodium phosphate monobasic

monohydrate were obtained from Amresco. 7-amino-4-methylcoumarin (AMC) was purchased from Alfa Aesar. *N*-alpha-CBZ-arginine 7-amino-4-methylcoumarin hydrochloride (z-Arg-AMC) was purchased from Santa Cruz Biotechnology. Alkaline Phosphatase Calf Intestinal (CIP) (10,000 U/mL) was from New England Biolabs. Sequencing grade modified trypsin was purchased from Promega. All other chemicals were obtained from either Sigma Aldrich or Fisher in highest available purity and used without further purification. NH_4^+ salt of [5-^{3}H]-CDP (19.4 Ci/mmol) was from ViTrax. AG® 1-X8 resin acetate form was purchased from BioRad. PD-10 desalting columns, Sephadex G-25 resin and protein molecular weight (M.W.) standards were from GE Healthcare. DEAE-Sephadex A-25 chloride and TALON® metal affinity resin were from Sigma life science and Clontech, respectively. Ultrafiltration membranes (YM-30 and -10), Centricons and Minicons were from Millipore.

Gel images were analyzed using Image Lab Version 4.1. The ^{3}H-counting was operated using LS 6500 multipurpose Scintillation Counter (Beckman Coulter). Absorbances were measured using a UV-2600 spectrophotometer from Shimadzu. Curve fittings and data analyses were evaluated using Prism v6.0 and v7.0 (Graphpad) and Kaleida Graph Version 4.1.2 (Synergy Software). Fluorescence anisotropy assays were performed using Varian Cary Eclipse Fluorescence Spectrophotometer. In fluorescence resonance energy transfer (FRET) experiments, fluorescence intensities were measured using Cytation™ 3 from BioTek®.

ClFTP and F2CDP used in these studies were previously synthesized and determined the concentrations using extinction coefficients previously reported.[16,27,28] Concentrations of ClA(M/D/T)P, FlU(M/D/T)P and ClF(M/D)P were determined by using their extinction coefficients: $\varepsilon_{265,\ ClA}$ = 15,700 $M^{-1}.cm^{-1}$, $\varepsilon_{263,\ FlU}$ = 16,400 $M^{-1}.cm^{-1}$ and $\varepsilon_{263,\ ClF}$ = 16,400 $M^{-1}.cm^{-1}$, respectively.

General Mammalian Expression Plasmids. Expression plasmids encoding *E. coli* thioredoxin A (His_6-Trx)[27], hRNR α-subunit (His_6-α)[27], hRNR β-subunit (His_6-β)[27], hRNR D57N α-subunit (His_6-D57N-α)[16] and the N-terminal domain of hRNR α-subunit (His_6-H-NTD)[29] were generous gifts from different sources (*see references*).

3.2.1 Protein purifications and their activity tests

General Recombinant Protein Expressions. Plasmid containing gene of interest was transformed into BL21-CodonPlus(DE3)-RIL competent cells, or non-codon enhanced BL21 competent cells in the case of His_6-Trx. Cells were grown at 37 °C overnight on an LB-agar plate containing 50 μg/mL Kanamycin. A single colony was picked and inoculated in 5 mL LB containing 50 μg/mL Kanamycin (and 50 μg/mL Chloramphenicol if CodonPlus cells were used). The culture tube was incubated overnight at 37 °C before diluting into 1.2 L LB media containing 50 μg/mL Kanamycin. Once OD_{600} reached 0.6–0.8, 1.0 mM IPTG (or 0.3 mM in the case of His_6-β and His_6-Trx) was added to induce the expression of a desired protein. The media were incubated at 19 °C for another 16 hours (or at 30 °C for 6 hours in the case of His_6-β.[30] Cells were then harvested by centrifugation for 20 minutes at 4 °C (6,000×g). The expression of desired protein was confirmed by 10% SDS-PAGE gel (or 15% SDS-PAGE gel for His_6-Trx and His_6-H-NTD).

General Protein Purifications. All buffer components used to purify protein of interest are listed in Table 3-1. The cell pellet was suspended in lysis buffer in a ratio of 1 g cell pellet:5 mL lysis buffer. The suspension was then lysed at 13,000 psi by two passes through a French Pressure Cell Press. After centrifugation at 20,000×g at 4 °C for 30 minutes, streptomycin sulfate was slowly added to the supernatant to a final

concentration of 2% (wt/v) within 15 minutes. The suspension was then gently stirred and incubated at 4 °C for another 15 minutes. The supernatant obtained after centrifugation at 20,000×g at 4 °C for 30 minutes was incubated with TALON® metal affinity resin, which was pre-equilibrated with 10 column volumes (CV) of lysis buffer, for 1 hour. The suspension was re-loaded on the column and the flow through was collected for SDS-PAGE. The resin was washed with 1 bed volume (BV) of wash buffer to get rid of any non-specific binding proteins. This step was repeated two more times. Elution buffer was then used to elute desired protein; 1.5 mL fractions were collected to a final volume of 48 mL. Fractions that had A_{280nm}:A_{260nm} ratios greater than 1.6 were pooled. 30 kDa (or 10 kDa for His_6-Trx and His_6-H-NTD) molecular weight cut-off Centricons were used to concentrate protein-containing fractions to a final volume of 9 mL before loading onto Sephadex G-25 resin, which had been pre-equilibrated with at least 5 BV of storage buffer. After elution, the protein-containing fractions, judged by Bradford protein assay[31,32], were concentrated using centricons. The enzyme purities were determined using SDS-PAGE (Figure 3-5, 3-7, 3-9, 3-10 and 3-12).

Table 3-1. Buffer components for each protein purification.

	His_6-α, His_6-D57N-α, His_6-H-NTD	**His_6-β**	**His_6-Trx**
Lysis buffer	50 mM NaH_2PO_4 10 mM imidazole 5 mM BME 1 mM PMSF 0.1% Triton X-100 (pH 7.0)	50 mM NaH_2PO_4 10 mM imidazole 5 mM BME 1 mM PMSF 0.1% Triton X-100 (pH 7.0)	50 mM NaH_2PO_4 10 mM imidazole 5 mM BME 1 mM PMSF (pH 7.0)
Wash buffer	50 mM NaH_2PO_4 800 mM NaCl 50 mM imidazole 5 mM BME 0.1% Triton X-100 (pH 7.0)	50 mM NaH_2PO_4 800 mM NaCl 50 mM imidazole 5 mM BME 0.1% Triton X-100 (pH 7.0)	50 mM NaH_2PO_4 800 mM NaCl 50 mM imidazole 5 mM BME (pH 7.0)
Elution buffer	50 mM NaH_2PO_4 300 mM NaCl 125 mM imidazole 1 mM BME (pH 7.0)	50 mM NaH_2PO_4 300 mM NaCl 125 mM imidazole 1 mM BME (pH 7.0)	50 mM NaH_2PO_4 150 mM NaCl 125 mM imidazole 5 mM BME (pH 7.0)
Storage buffer	50 mM Tris-HCl 100 mM KCl 15 mM $MgCl_2$ 5 mM DTT 5% glycerol (pH 7.6)	50 mM Tris-HCl 100 mM KCl 5% glycerol (pH 7.6)	50 mM NaH_2PO_4 150 mM NaCl 5 mM BME 5% glycerol (pH 7.6)

*** *His_6-TrxR was purified and tested its activity by Saba Parvez, a Ph. D. candidate in the Aye Lab.*

hRNR α-subunit (His$_6$-α).

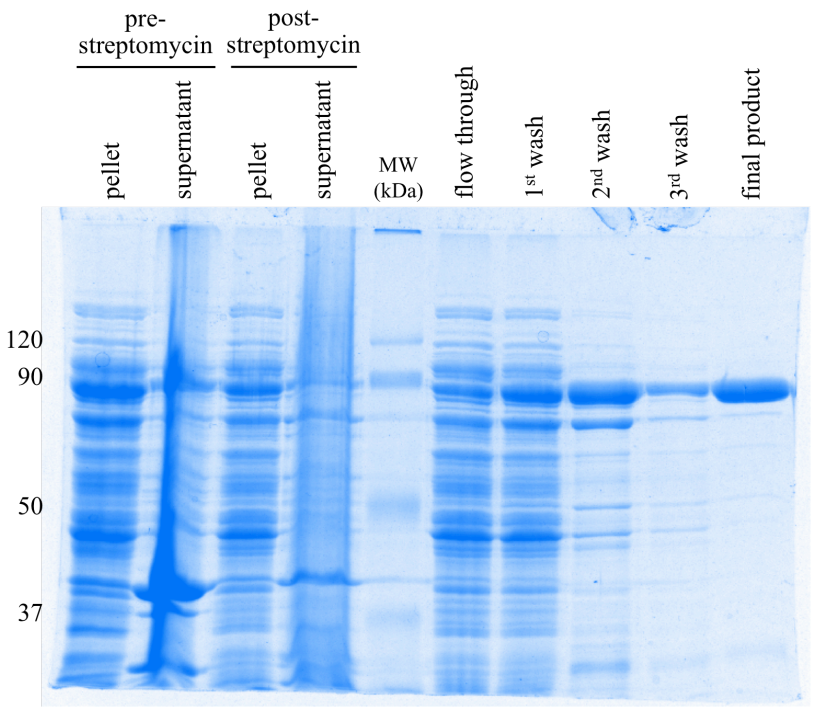

Figure 3-5. 10% SDS-PAGE gel of purified His$_6$-α (90 kDa).

Activity test. In 1970, Steeper and Steuart reported a rapid assay to measure RNR activity in mammalian cell extracts using a tritium (^{3}H)-labeled CDP substrate. The enzyme activity was determined based on the amount of ^{3}H-dCDP produced at certain incubation time. Upon loading the reaction mixture on borate column, which had been pre-equilibrated with saturated $K_2B_4O_7$ and rinsed off the excess salt with water, all vicinal diols left in the assay mixture were trapped. The amount of ^{3}H-dCDP was then determined by using liquid scintillation counting.[26]

Later, Aye and Stubbe[16] adapted this assay to study the binding affinity of di- and triphosphorylated Clofarabine [ClF(D/T)P] for purified recombinant RNR (Scheme 3-1).

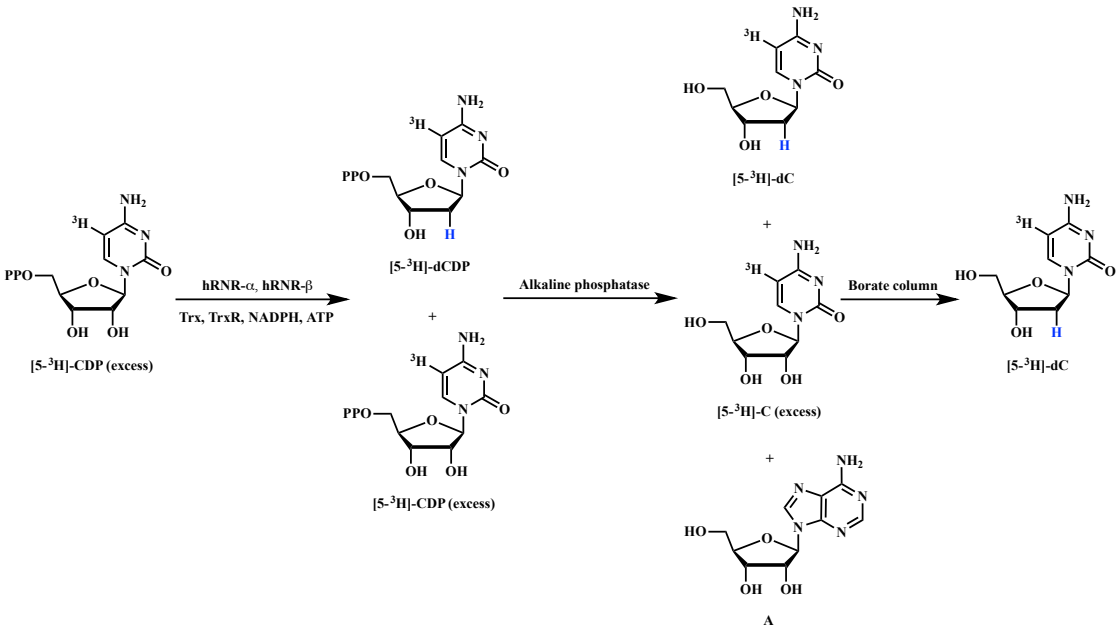

DP, diphosphate; PP, diphosphate; C, cytidine; dC, deoxycytidine; A, adenosine; dA, deoxyadenosine.

Scheme 3-1. A CDP reductase assay used to determined hRNR activity *in vitro*.

In order to determine a reductase activity of purified recombinant RNR-α, Aye and Stubbe's protocol[16] was followed. Typical assay mixture (AM) for CDP reduction in a 135 µL final volume contained: assay buffer (AB) [50 mM Hepes (pH 7.6), 15 mM $MgCl_2$, 3 mM ATP, 2 mM NADPH, 200 µM *E. coli* Trx, 1 µM *E. coli* TrxR, 0.5 mM [5-^{3}H]-CDP [specific activity (SA): 21,532 cpm.nmol^{-1}], 0.3 µM hRNR-α and 2.1 µM hRNR-β. The AM without the substrate was incubated at 37 °C for 2 minutes before the nucleotide reduction was initiated by the substrate addition. 30 µL-aliquots were removed at four different time points (40, 80, 130 and 180 seconds) post initiation, and immediately quenched with 30 µL 2% (v/v) $HClO_4$. The pH of the reaction mixture was neutralized by adding 30 µL of 0.4 M NaOH. Dephosphorylation of the resultant [5-^{3}H]-dCDP was achieved by adding 410 µL of dephosphorylation

mixture containing 10 units calf intestinal alkaline phosphatase (CIP), 1.2 mM deoxycytidine (dC), 100 mM Tris-HCl (pH 8.6), and incubating the mixture at 37 °C for 2 hours. [5-^{3}H]-C and adenosine were separated from the resultant mixture by loading 450 μL of the mixture on a borate column (prepared as previously described[26]), followed by an addition of 7.55 mL of ddH_2O. 1 mL of the [5-^{3}H]-dC solution was mixed with 9 mL scintillation cocktails. The amount of [5-^{3}H]-dC, which referred to the [5-^{3}H]-dCDP formed, at each time point was then analyzed by liquid scintillation counting.

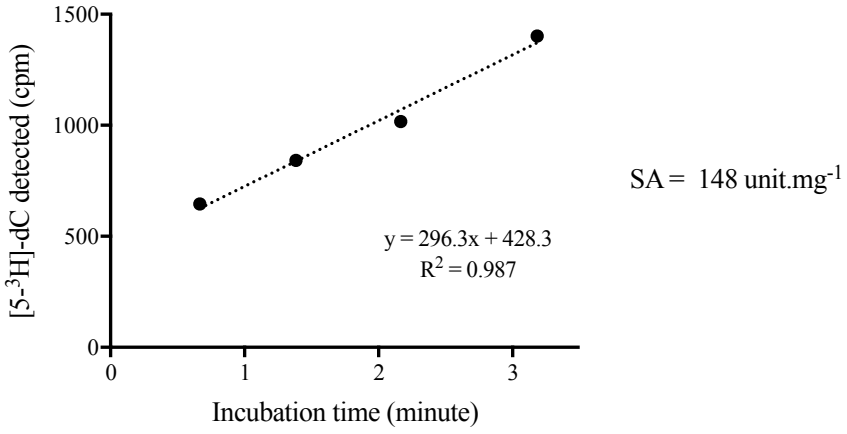

Unit, nmol.min^{-1}.

Figure 3-6. Purified recombinant hRNR-α activity test. The specific activity (SA) was calculated from the slope of the fitting curve.

This batch of hRNR-α was shown to have a specific activity (nmol.min^{-1}.mg^{-1}) of 148 unit.mg^{-1}, for the reduction of [5-^{3}H]-CDP to [5-^{3}H]-dCDP.

His_6-D57N-α.

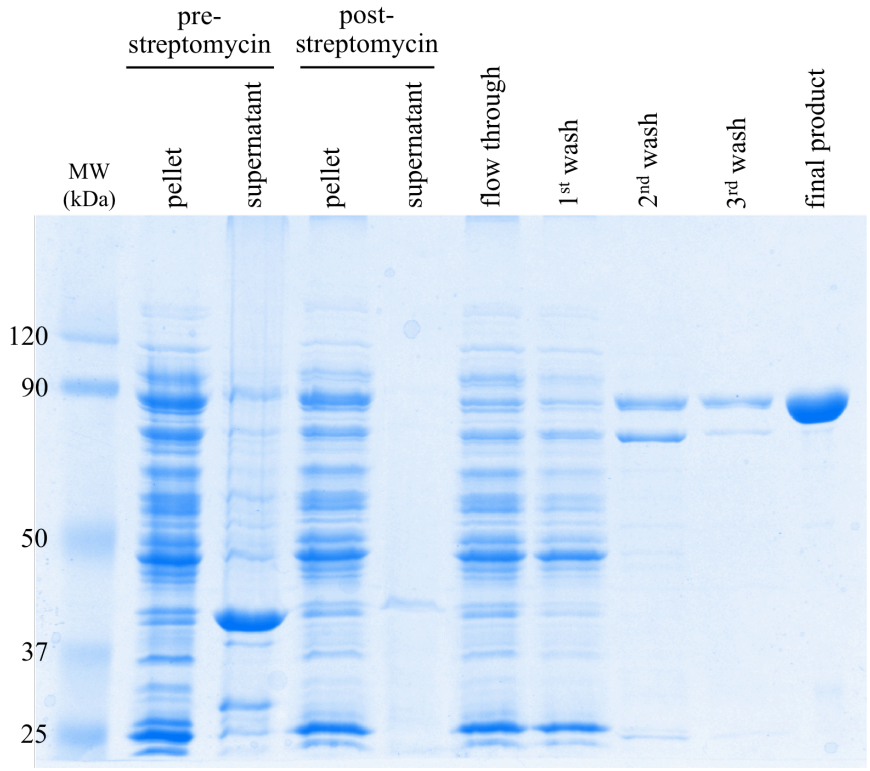

Figure 3-7. 10% SDS-PAGE gel of purified His_6-D57N-α (90 kDa).

Activity test. The same protocol as described in hRNR-α activity test was followed. However, 0.3 μM D57N-α was used instead of 0.3 μM hRNR-α.

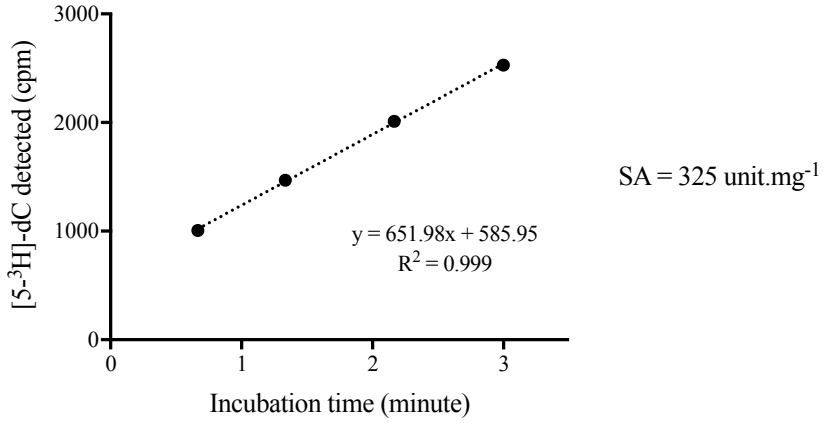

Unit, nmol.min^{-1}.

Figure 3-8. Purified recombinant D57N-α activity test. The specific activity (SA) was calculated from the slope of the fitting curve.

Based on the activity curve shown above, this batch of D57N-α showed an SA for the reduction of [5-^{3}H]-CDP to [5-^{3}H]-dCDP of 325 unit.mg^{-1}.

His_6-H-NTD.

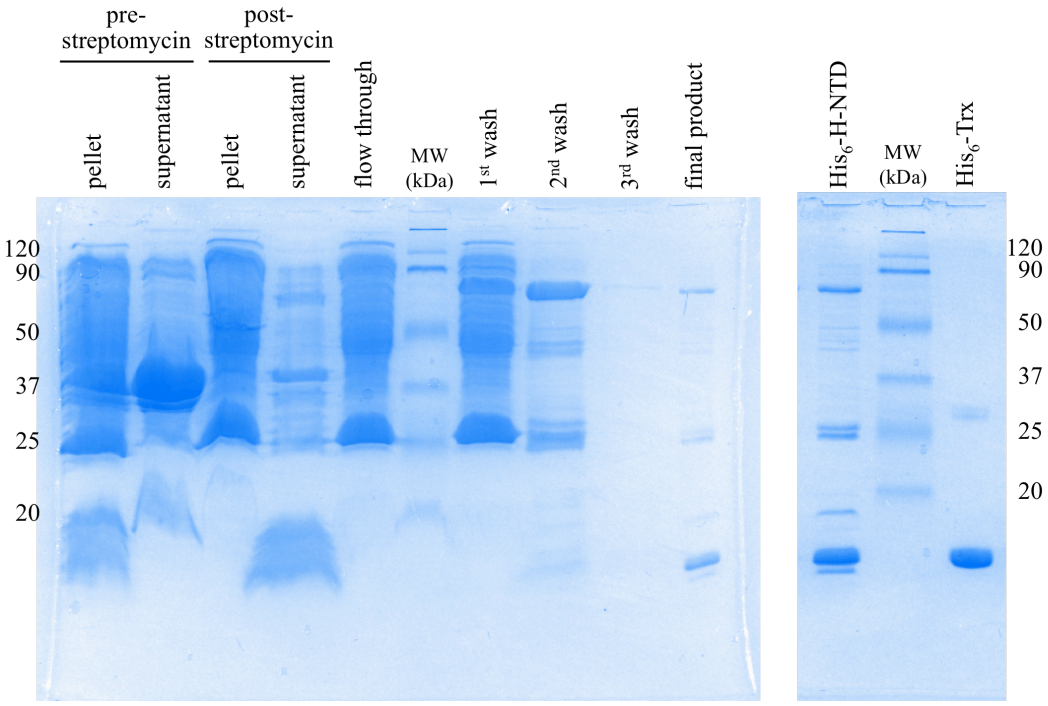

Figure 3-9. 15% SDS-PAGE gels of (*left*) purified His_6-H-NTD (11 kDa) (*right*) and a comparison between His_6-H-NTD and His_6-Trx (14 kDa).

hRNR β-subunit (His$_6$-β).

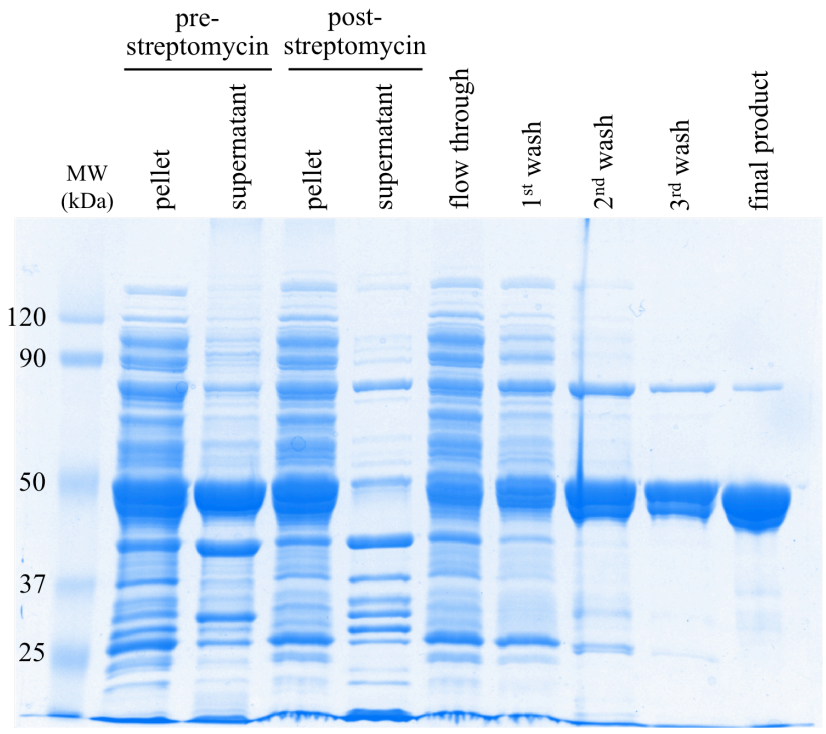

Figure 3-10. 10% SDS-PAGE gel of purified His$_6$-β (45 kDa).

Reconstitution of hRNR-β.[33,34] Stock apo-hRNR-β was diluted with argon (Ar)-saturated hRNR-β storage buffer (Table 3-1) to make a roughly 55 μM apo-hRNR-β. The resultant solution was then degased by exposing the solution to Ar for 30 seconds before switching to a vacuum for a second. This step was repeated 5 times before the solution was left under Ar atmosphere during the last cycle. The resultant mixture was gently added 22 μM ferrous ammonium sulfate hexahydrate (Mohr's salt), and incubated for another 20 minutes under anaerobic condition before O_2 saturated storage buffer was added. The amount of O_2 saturated storage buffer needed was calculated as previous reported.[30] The reaction mixture was then loaded onto the G-25 column, which had been pre-equilibrated with at least 4 CV of hRNR-β storage buffer.

Protein-containing fractions, determined by Bradford dye[31,32], were pooled and concentrated using centricons. All steps mentioned above were carried out on ice (or at 4 °C).

Verification of tyrosine radical in hRNR-β.[35] Electron paramagnetic resonance (EPR) spectra of the reconstitutued RNR-β were collected at the National Biomedical Research Center for AdvanCed ESR Technology (ACERT) at Cornell University. Instrument settings were as following: sweep time, 61 seconds; time constant, 0.163 seconds; modulation amplitude, 1.0 G; modulation frequency, 100 kHz; microwave power, 25 dB (0.6325 mW); temperature, 50 K. An average spectrum was calculated from 10 scans. The tyrosyl free radical in a 45 μM reconstituted hRNR-β sample was compared with a 45 μM *E. coli* RNR-β standard sample, which was purified and reconstituted by *William A. Blessing* (Figure 3-11).

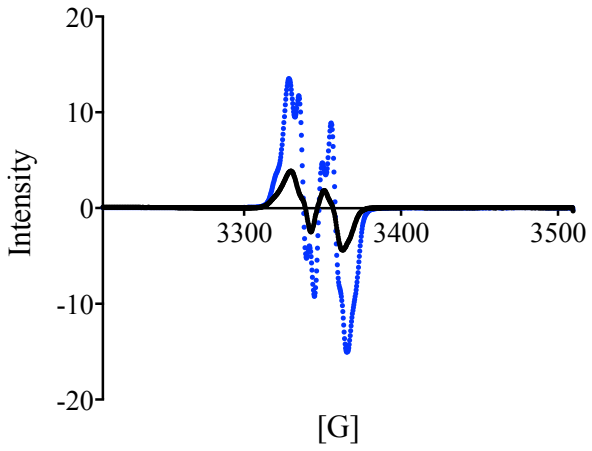

Figure 3-11. Overlaid EPR spectra of tyrosyl radicals from the reconstituted human (*blue*) and *E. coli* (*black*) RNR-β (45 μM) recorded at 50 K.

The EPR pattern of the reconstituted hRNR-β was similar to the previously reported EPR signal of a tyrosyl radical in hRNR-β.[34,36] This indicated the presence of the tyrosyl radical in the sample. Moreover, the activity of this reconstituted hRNR-β was confirmed by its significantly increased signal intensity compared to the standard sample.

His_6-Trx.

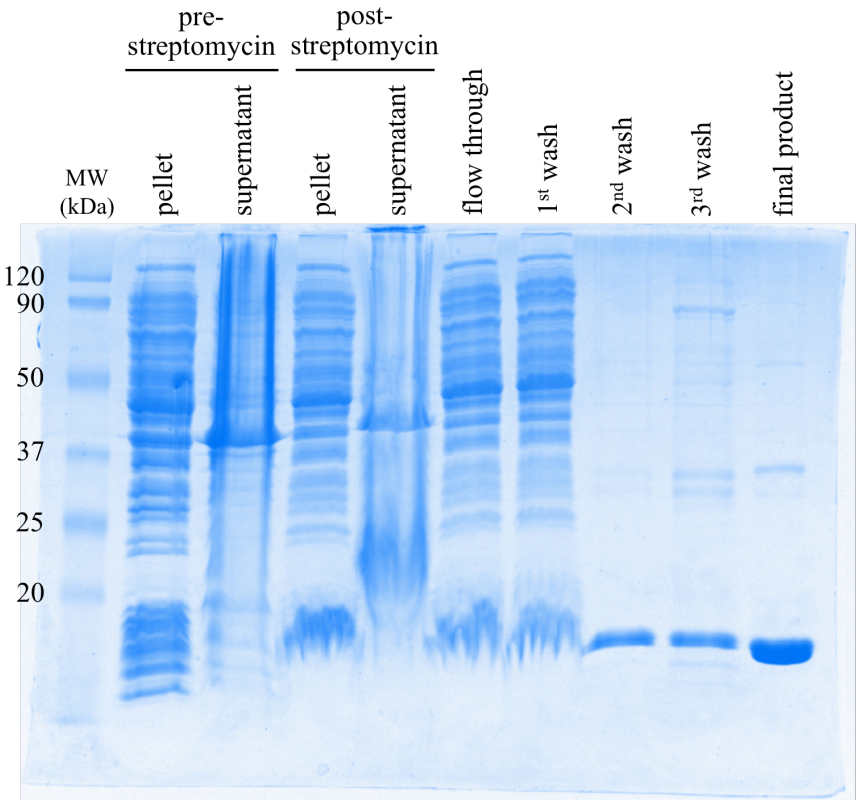

Figure 3-12. 15% SDS-PAGE gel of purified His_6-Trx (14 kDa).

Activity test. Ellman's reagent or 5,5′-dithio-*bis*-(2-nitrobenzoic acid) (DTNB) was used as a substrate in Trx activity assay (Figure 3-13).

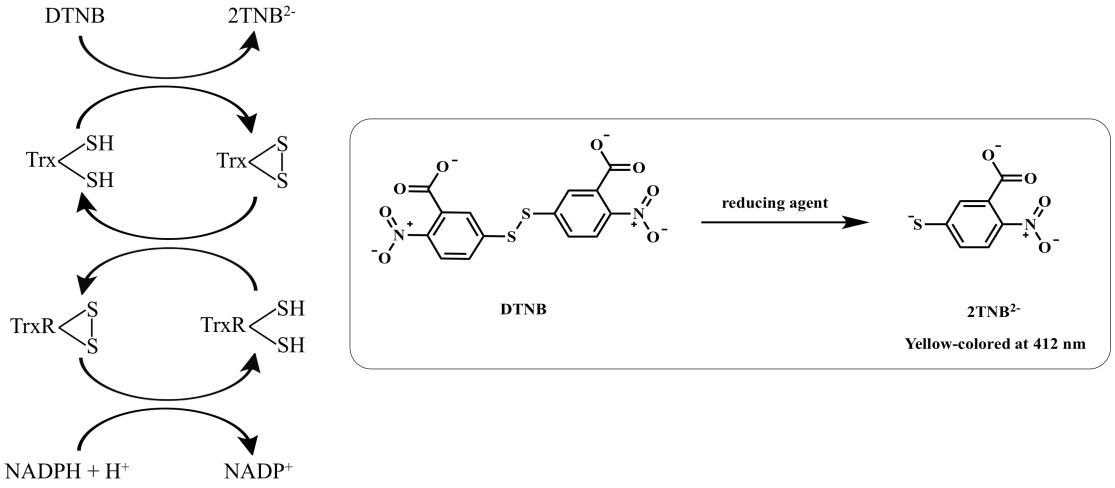

Figure 3-13. Introduction of thioredoxin (Trx) activity assay.[37]

Typical AM for Trx activity assay contained in a 300 μL final volume of 100 mM Tris-HCl (pH 8.0), 25 mM EDTA, 0.1 μM *E. coli* TrxR, 0.1 mM NADPH, 0.15 mM DTNB and 25 μM *E. coli* Trx. The AM without *E. coli* Trx was incubated at 37 °C 1 minute prior to the addition of *E. coli* Trx. For blank, the protein storage buffer was used instead of *E. coli* Trx. Absorbance at 412 nm (A_{412nm}) of AM was collected throughout all time using a UV-2600 spectrophotometer (Shimadzu). By plotting A_{412nm} against incubation time, the amount of TNB^{2-} generated per second was calculated by using TNB^{2-} molar extinction coefficient (ε_0): 14,150 $M^{-1}.cm^{-1}$.[38] (Figure 3-14).

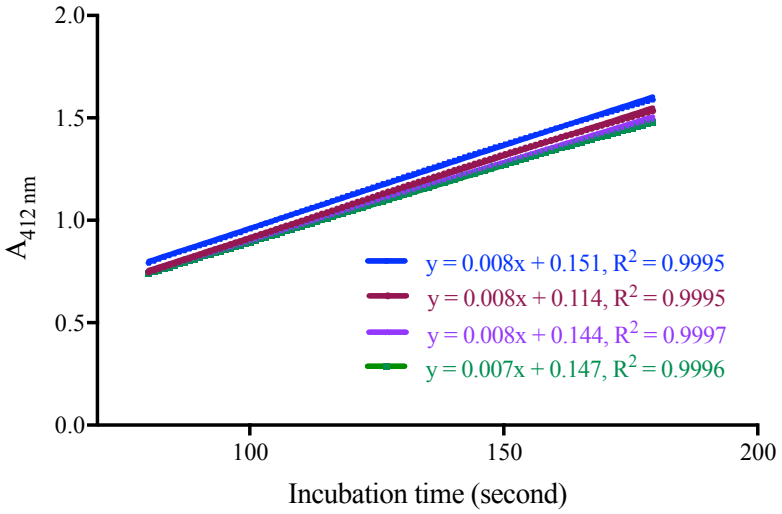

Figure 3-14. Thioredoxin (Trx) activities were reproducible among 4 technical replicates. The averaged activity of this batch of Trx was 95 unit.mg^{-1}, or 1 mg of Trx can reduce DTNB to 95 nmol TNB^{2-} in one minute.

3.2.2 *In vitro* biochemical studies of ClA(D/T)P and FlU(D/T)P

Radioactive assays for [5-^{3}H]-CDP reduction in isolate system

Dose-dependent inhibition assays for wild-type (wt) hRNR-α and D57N-α (Figure 3-21 and 3-35). Typical inhibition mixture (IM) in a 50 µL final volume contained 3 mM ATP, 2 mM NADPH, 15 mM $MgCl_2$, 0.5 mM [5-^{3}H]-CDP, 100 µM *E. coli* Trx, 1 µM *E. coli* TrxR, 3 µM hRNR-β, 1 µM wt hRNR-α (or D57N-α) in 50 mM Hepes (pH 7.6). The IM without [5-^{3}H]-CDP was pre-incubated at 37 °C for 2 minutes prior to the addition of substrate and a particular inhibitor (ClADP, or ClATP, or FlUDP, or FlUTP) at various concentrations (as shown in Figure 3-21). After further incubation at 37 °C for 3 minutes, 30 µL of 2% (v/v) $HClO_4$ was added to quench the enzymatic

reaction and the reaction pH was subsequently neutralized by adding 30 μL of 0.4 M NaOH. Upon adding 390 μL of dephosphory-lation mixture [10 units CIP, 1.2 mM dC, 100 mM Tris-HCl (pH 8.6)] and incubating the mixture at 37 °C for 2 hours, all phosphorylated nucleotides got dephosphorylated. The amount of [5-^{3}H]-dC was analyzed as described under *hRNR-α activity test*. To derive an inhibition constant (K_i) of each nucleotide analogue, in the case of wt hRNR-α, the obtained data were fitting to the tight-binding equation (Eq. 3.1)[39].

$$\frac{\upsilon_i}{\upsilon_0} = 1 - \left[\frac{([E]_T + [I]_T + K_i) - \sqrt{([E]_T + [I]_T + K_i)^2 - 4[E]_T[I]_T}}{2[E]_T} \right] \quad \text{(Eq. 3.1)}$$

In this equation, υ_0 and υ_i represent enzyme activity in the absence or in the presence of inhibitor at particular concentration, respectively; $[E]_T$ represents the total concentration of enzyme; $[I]_T$ represents the total concentration of inhibitor; and K_i represents an inhibition constant.

Time-dependent inhibition assays for wt hRNR-α (Figure 3-22). Typical IM in a 250 μL final volume contained 3 mM ATP, 2 mM NADPH, 15 mM $MgCl_2$, 0.5 mM [5-^{3}H]-CDP, 100 μM *E. coli* Trx, 1 μM *E. coli* TrxR, 3 μM hRNR-β, 1 μM hRNR-α and a particular concentration of nucleotide inhibitor [ClADP (5 μM), ClATP (5 μM), FlUDP (50 μM), or FlUTP (12.5 μM)] in 50 mM Hepes (pH 7.6). The IM without [5-^{3}H]-CDP was pre-incubated at 37 °C for 2 minutes prior to the addition of the substrate. After further incubation at 37 °C, 30 μL-aliquots of IM were taken out at different time points (0, 0.5, 1, 3, 7, 10 and 15 minutes) and immediately quenched with 30 μL of 2% (v/v) $HClO_4$. The reaction pH was then neutralized by an addition of 0.4 M NaOH (30 μL). Dephosphorylation of [5-^{3}H]-dCDP and a measurement of the

amount of [5-^{3}H]-dC generated were achieved as previously described under *hRNR-α activity test*.

Time-dependent inhibition assays for hRNR-β subunit

Two mixtures required for this assay were separately prepared. First, a typical IM in a final volume of 70 µL (for Triapine® (3-AP), FlUDP, FlUTP and control) or 35 µL (for ClADP and ClATP) contained 2 µM hRNR-α, 2 µM hRNR-β, 3 mM ATP, 15 mM $MgCl_2$, 10 mM DTT, 6 µM of indicated inhibitor or buffer alone (for control) in 50 mM Hepes (pH 7.6). Second, a typical AM in a final volume of 21 µL (for 3-AP, FlUDP, FlUTP and control) or 57 µL (for ClADP and ClATP) contained 3 µM hRNR-α (for 3-AP, FlUDP, FlUTP and control) or 2 µM hRNR-α (for ClADP and ClATP), 3 mM ATP, 15 mM $MgCl_2$, 2 mM NADPH, 0.5 mM [5-^{3}H]-CDP, 100 µM *E. coli* Trx, 1 µM *E. coli* TrxR in 50 mM Hepes (pH 7.6). The IM without inhibitor was pre-incubated at 37 °C for 2 minutes prior to the addition of a particular inhibitor (or buffer for control). At the designated time points, 9 µL (for 3-AP, FlUDP, FlUTP and control) or 3 µL (for ClADP and ClATP) aliquots were removed from IM and subsequently diluted into the AM, which had been pre-incubated at 37 °C for 2 minutes. Subsequent to 3-minute incubation period, the reaction was quenched with 30 µL of 2% (v/v) $HClO_4$ and the pH was neutralized by adding 30 µL of 0.4 M NaOH. Dephosphorylation of [5-^{3}H]-dCDP was achieved by adding 410 µL (for 3-AP, FlUDP, FlUTP and control) or 380 µL (for ClADP and ClATP) of dephosphorylation mixture containing 10 units CIP, 1.2 mM dC, 100 mM Tris-HCl (pH 8.6). After 2-hour incubation period at 37 °C, the amount of [5-^{3}H]-dC was analyzed as described under *hRNR-α activity test*.

Fluorescence Resonance Energy Transfer (FRET)

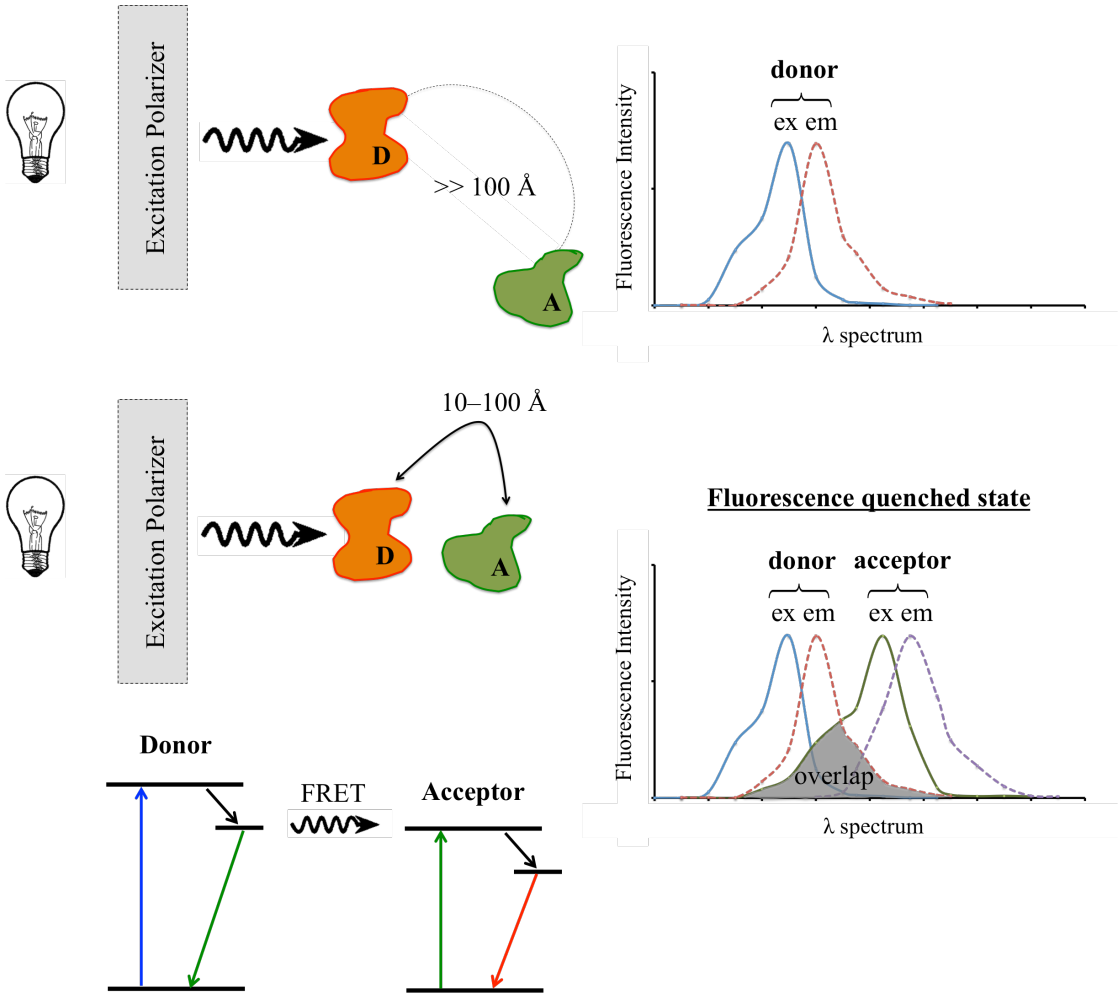

D, donor molecule; A, acceptor molecule; ex, excitation; em, emission.

Figure 3-15. Diagram depicting a FRET experiment. This figure is adapted from Ref. 40.

Clegg describes FRET as a spectroscopic process by which energy is non-radiatively transferred over long distances (10–100 Å) between molecules. In this process, the donor molecule, which must be a fluorophore, absorbs a photon from an external source and transfers this energy non-radiatively to the acceptor molecule.[40]

The efficiency of energy transfer really depends on the distance between the two interacting molecules as well as the overlap of the donor molecule emission and the acceptor molecule excitation spectra (Figure 3-15). The more overlap the spectra, the better the efficiency of energy transfer.

In general, the donor-acceptor pairs can be free in solution, one or both (covalently or noncovalently) bound to a macromolecule, or be an inherent part of the structure.[40] In 2014, Yuan *et al*[27] developed a FRET reporter platform using 5-IAF labeled hRNR-α as the donor molecule and 5-TMRIA labeled hRNR-α as the acceptor molecule to report hRNR-α hexamerization induced by dATP, ClFDP or ClFTP (Figure 3-16).

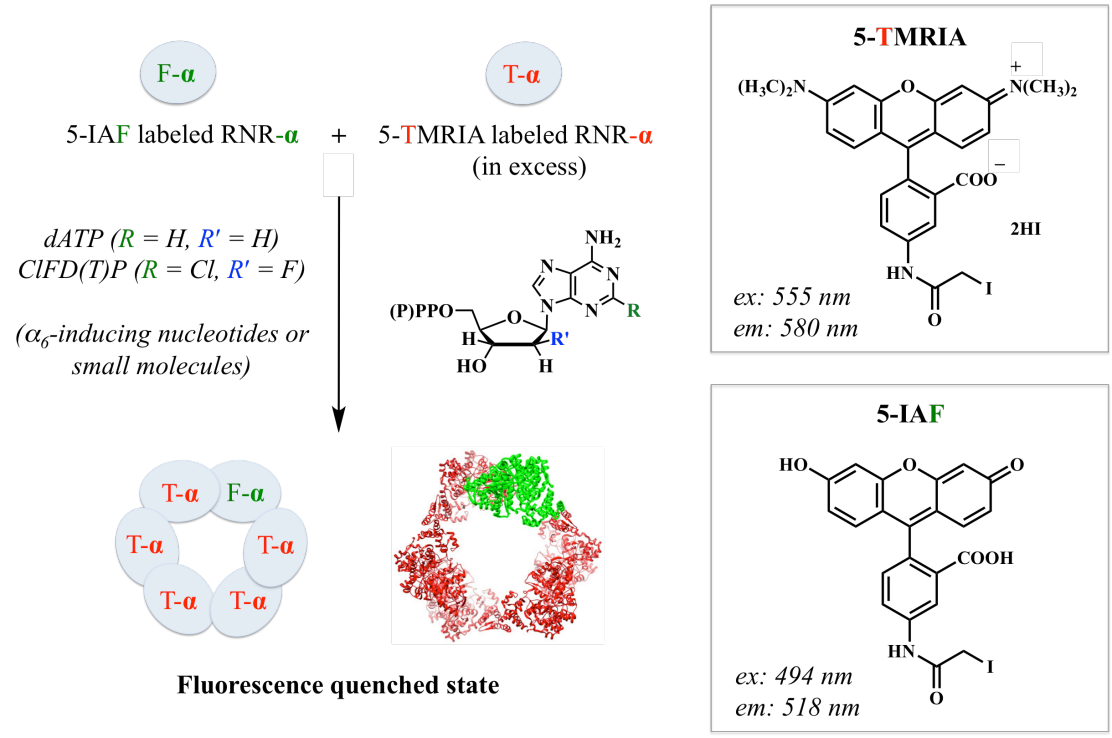

Figure 3-16. Introduction of the FRET-quenching assay reporting the ligand-driven hRNR-α oligomerization. The ribbon structure represents the known 9.01 Å dATP-bound human α_6 crystal structure (PDB: 5D1Y).[41]

Fluorescence dye labeling of hRNR-α. A labeling reaction mixture in a 250 μL final volume contained 10 μM hRNR-α, 30 μM 5-IAF or 30 μM 5-TMRIA, 15 mM $MgCl_2$, 1 mM DTT in 50 mM Hepes (pH 7.6). The reaction mixture was incubated under dark at RT for 20 minutes. The excess fluorescence dye was removed by using a PD-10 Sephadex G-25M column, which had been pre-equilibrated with AB [15 mM $MgCl_2$ and 5 mM DTT in 50 mM Hepes (pH 7.6)]. Upon adding AB, 5-IAF labeled hRNR-α (F-α) or 5-TMRIA labeled hRNR-α (T-α) was eluted out of the column. Labeled-protein containing fractions, judged by Bradford protein assay[31,32], were pooled and adjusted to a final concentration of 1 μM using AB. Labeled proteins were immediately carried out onto subsequent FRET assay.

Spectrofluorometer-based FRET assay. 220 μL of 0.2 μM fluorescence dye labeled protein was prepared by mixing F-α and T-α in a 1:5 ratio and adjusting the volume with AB. For titration experiments, a minimum volume of ClADP or ClATP was titrated into a 3 mm×3 mm path length quartz fluorescence microcuvette to make a final concentration of nucleotide inducer of 50, 100 and 250 μM. In control experiment, the same volume of nucleotide inducer was replaced with 20 mM Hepes (pH 7.6). Fluorescence intensities were measured using a Varian Cary Eclipse spectrofluorometer with the following settings: excitation wavelength, 480 nm; recorded emission spectra, 505–620 nm; excitation slit width, 20 nm; emission slit width, 10 nm. The emission spectra of oligomeric assembly were recorded after incubation at RT for 2, 4, 5, 6, and 8 minutes.

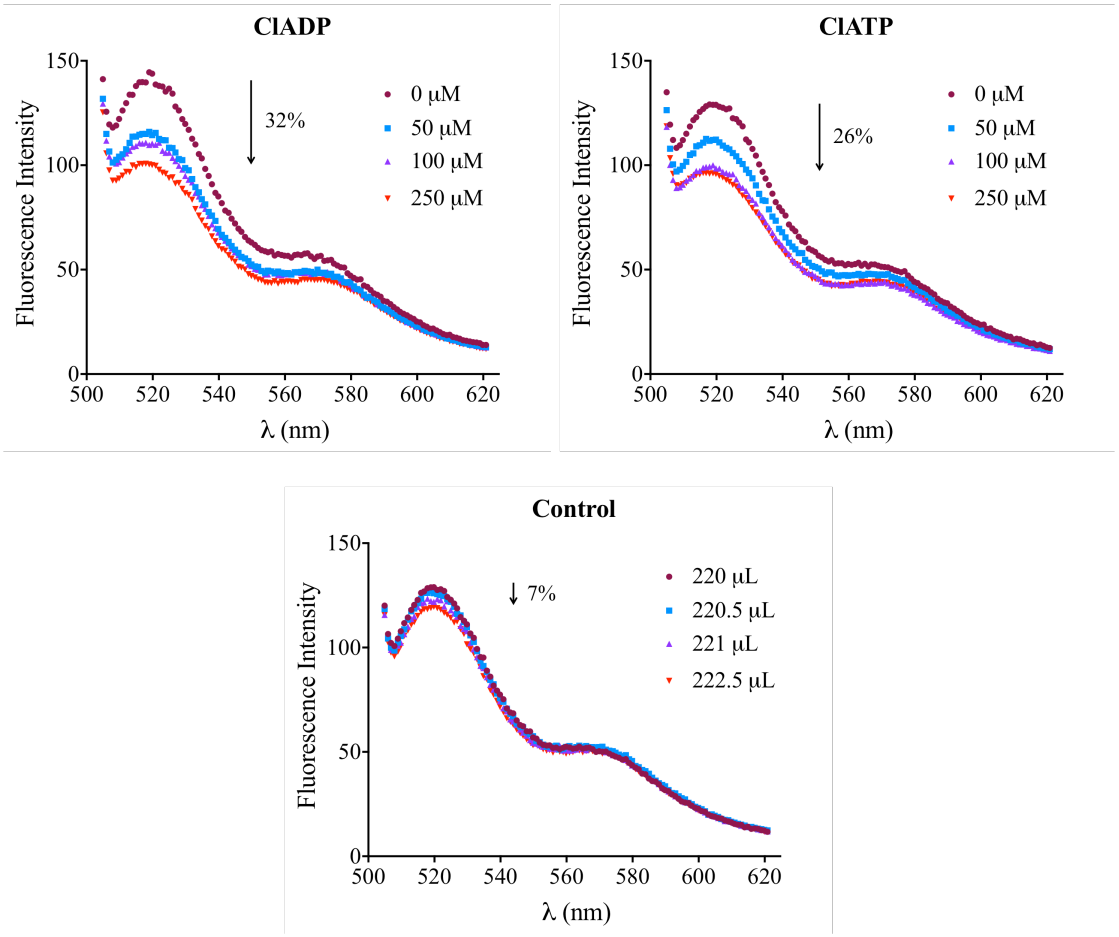

Figure 3-17. FRET quenching assays reporting ClAD(T)P-induced hRNR-α oligomerization. In control experiment, ClAD(T)P was replaced with the same volume of buffer to report fluorescence quenching caused by volume changes. These data were measured after incubation at RT for 5 minutes.

Upon titration of ClADP or ClATP up to 250 μM, fluorescence signal of F-α was quenched by 32% and 26%, respectively. On the other hand, only 7% of this quenching was from the change in assay volume (Figure 3-17). These results suggested that ClADP and ClATP were able to induce hRNR-α oligomerization. Various incubation time points (2, 4, 5, 6, or 8 minutes) were also examined; however, there was no significantly difference in fluorescence signals observed among each

time point (*see Appendix C*). This informed us that the nucleotide-induced hRNR-α oligomerization reached its equilibrium within 2-minute timescale. Even though we observed promising results from these preliminary experiments, performing FRET assays in the microcuvette might not be ideal since it requires a lot of enzyme and nucleotide inducers. We then took advantage of a Biotek Cytation™ 3 plate-reader in order to minimize the assay volume and, therefore, the amounts of protein and nucleotide analogues.

Biotek Cytation™ 3 plate-reader-based FRET assay (performed by Dr. Yi Zhao). The pre-mixed protein solution containing a 1:1 mixture of F-α:T-α (in equal concentrations and in equal volumes) was diluted with AB to a final protein concentration of 0.8 μM (for ClADP, FlUDP and FlUTP) or 0.4 μM (for ClATP). 100 μL of the diluted solution was aliquoted into an individual well of a Costar 96 half-area black opaque plate. 2 μL of each inhibitor stock solution (50x of various indicated concentrations) was added to a designated well. The 96-well plate was then placed into the Biotek Cytation™ 3 plate-reader, which was programmed with the following settings: shaking speed, 410 rpm; shaking time, 20 minutes (for ClADP, FlUDP and FlUTP) or 35 minutes (for ClATP); delay time, 5 seconds. Fluorescence intensities were measured using green filters: excitation, 485 ± 10 nm; emission, 528 ± 10 nm; top, 510 nm (optics position); gain, 35. Three replicates of these experiments were performed independently. By fitting the normalized fluorescence intensities and the inhibitor concentrations to equation 3.2 (Eq. 3.2), EC_{50} values of nucleotide-induced hRNR-α oligomerization were derived using Prism 6.0.

$$y = \frac{1}{1 + 10^{(X - \log(EC_{50}))}} \qquad \text{(Eq. 3.2)}$$

In this equation, y and x represent the normalized fluorescence intensity and the inhibitor concentration in log-scale, respectively.

Gel filtration analysis (SEC)

For Figure 3-25. The typical reaction mixture in a 150 μL final volume contained 5 mM DTT, 15 mM $MgCl_2$, 10 μM hRNR-α and 250 μM inhibitor (ClADP, ClATP, FlUDP and FlUTP) or 500 μM FlUTP in 50 mM Hepes (pH 7.6). The AM was incubated at 37 °C for 3 minutes prior to a 30-second centrifugation at 10,000×g at RT. The mixture was filtered using 0.22 μm Millex-GV syringe filter unit (Merck Millipore). 130 μL of the resultant filtrate was injected into a Superdex™ 200 10/300 GL column (24 mL, 10×300 mm, GE Healthcare), attached to a Prominence HPLC with a photodiode array (PDA) detector (SPD-M20A) (Shimadzu Corporation), which had been pre-equilibrated at RT at 0.5 mL/minute flow-rate of elution buffer [50 mM Hepes (pH 7.6), 15 mM $MgCl_2$, 150 mM NaCl]. The protein was eluted at 0.5 mL/minute flow-rate at RT. Protein M.W. standard curves were obtained by running GE Healthcare M.W. standards (thyroglobulin, ferritin, aldolase, conalbumin, and ovalbumin) under identical conditions at the end of each set of experiments. A_{280nm} and A_{260nm} were monitored. Additional M.W. standards: *β*-amylase, BSA, and alcohol dehydrogenase were also independently run. An additional experiment performed for FlUDP included 20 μM of FlUDP in the elution buffer under otherwise identical conditions.

For Figure 3-39A and 3-39B (right panel). Figure 3-39A, 10 μM hRNR-α was incubated with 4 mM dATP before splitting into two fractions. 300 μM ClADP and assay buffer were added to the first and the second fraction, respectively. Figure 3-39B

(right panel), samples were directly taken from fluorescence anisotropy (FA) assays. These samples were prepared and analyzed using the same conditions as described above for *Figure 3-25*. Note: 130 μL of samples from Figure 3-39A and 110 μL of samples from 3-39B (*left panel*) were injected into HPLC column.

EM data acquisition and rotational symmetry analysis

(*unpublished data; performed by Huma Inayat under the guidance of Professor Joaquin Ortega, McMaster University)*

The conditions used in our EM experiments were very similar, if not identical, to the conditions used in the FRET assays. For example, the incubation timescale of hRNR-α and indicated inhibitors was chosen based on the time-dependent FRET assays, which indicated when the oligomerization equilibrium was effectively reached (Figure 3-24A). More experimental details were described below.

Complexes were assembled by treating 10 μM recombinant hRNR-α with indicated nucleotide analogues [250 μM of ClADP, ClATP, FlUDP or FlUTP, or 100 μM ClFDP (for positive control)] in assembly buffer [50 mM Hepes (pH 7.6), 15 mM $MgCl_2$, and 5 mM DTT] for 2 minutes at ambient temperature. Then, sample was immediately diluted 100-fold with assembly buffer in the presence/absence of respective nucleotide analogues prior to depositing onto an EM grid fleshly coated with a continuous layer amorphous carbon. Grids were floated on a 5 μL drop of the diluted assembly reaction for 2 minutes immediately after a glow-discharge treatment of a 5 mA for 15 seconds. Excess of sample was blotted with filter paper and the grids were stained with 1% uranyl acetate for 1 minute. A JEOL 2010F electron microscope, operated at 200 kV at 50,000× magnification with a dose of ~15 electrons per $Å^2$, was used to collect images. Images were recorded on Kodak

SO-163 films and scanned on a Nikon Super COOLSCAN 9000 ED at 6.35 μm per pixel. Electron micrographs were binned 2-fold rendering images with a sampling of 2.54 Å per pixel.

Particle images in the electron micrographs were picked and extracted with Boxer from the EMAN package.[42] Averaged ~2,000 particle images were collected for each reaction and subjected to image analysis as described below.

To perform the symmetry analysis, groups of 200 particles were normalized, and then translationally aligned to a circularly symmetrical global average of all of the unaligned particle images in the group. Rotational symmetry analysis was determined using the spectral ratio product and Student's *t* statistical tests (*t*-tests) as implemented in the Rotastat software.[43] These tests were used to compare the rotational power spectra of particle images containing ring-shaped particles with that of background images of the same size.

To calculate the 2D averages of the ring-shaped particles with 3-fold rotational symmetry, particles were normalized and then rotationally and translationally aligned using cross-correlation-based methods as implemented in the Xmipp software package.[44-46] The reference used for alignments was constructed using a pyramidal combination of a subset of the images.[47] Particles with 3-fold rotational symmetry in this case were selected using self-organizing feature maps as implemented in the Xmipp software package. By using maximum-likelihood based classification approaches as implemented in the Xmipp software package[44-46], we were allowed to explore the conformational variability of the ring-shaped particles observed in the different reactions. For all reactions, the program was run with the number of expected classes equal to ten.

Trypsin activity assay in the presence and absence of nucleotide inhibitors

First, *N*-alpha-CBZ-arginine 7-amino-4-methylcoumarin hydrochloride (z-Arg-AMC) was used to determine the trypsin activity (Scheme 3-2). Given that the product of this protease cleavage is a fluorescence compound AMC, we can easily detect an amount of AMC produced, which refers to trypsin activity, by using a fluorescence plate reader.

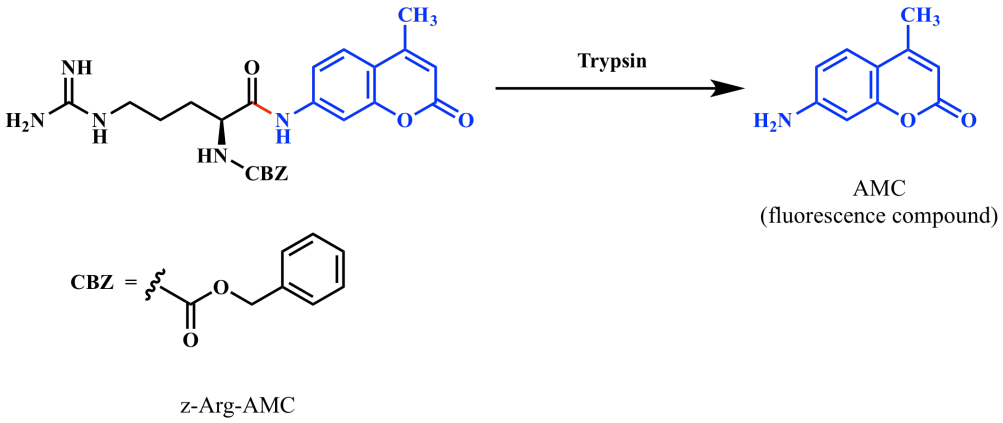

Scheme 3-2. Trypsin cleavage of z-Arg-AMC generates a fluorescence compound, AMC.

Standard curve of AMC (i.e., increase in fluorescence intensity as a function of AMC concentration). The AM in a 100 µL final volume contained 15 mM $MgCl_2$ and AMC at designated concentrations (as shown in Figure 3-18A) in 50 mM Hepes (pH 7.6). The fluorescence intensities were recorded using a Biotek Cytation™ 3 plate-reader (λ_{ex} = 380 nm and λ_{em} = 460 nm). The data were fit to a linear regression equation (Figure 3-18A).

K_m measurement of z-Arg-AMC for trypsin. The assay mixture in a final volume of 100 µL contained 10 nM trypsin (or 50 mM Hepes (pH 7.6) for background), 15 mM $MgCl_2$, and z-Arg-AMC at the indicated concentrations (as shown in Figure 3-18B) in 50 mM Hepes (pH 7.6). Fluorescence intensities were recorded over 17 minutes using a Biotek Cytation™ 3 plate-reader (λ_{ex} = 380 nm and λ_{em} = 460 nm). The rates of AMC production from the hydrolysis of z-Arg-AMC at the indicated concentrations were calculated using the linear regression equation obtained from the AMC standard curve (Figure 3-18A). The data were then fit to the Michaelis-Menten equation (Eq. 3.3) to yield $K_m \sim 84 \pm 15$ µM (Figure 3-18B).

$$y = \frac{V_{max} \times x}{K_m + x} \qquad \text{(Eq. 3.3)}$$

In this equation, V_{max} represents the maximum enzyme velocity in the same unit as y while K_m, the Michaelis-Menten constant, represents the substrate concentration needed to get a half-maximum enzyme velocity.

From these experiments, the activity of trypsin was affirmed. However, to ensure that the nucleotide inhibitors neither unexpectedly inhibit the trypsin activity nor quench the AMC fluorescence intensity, the following set of experiments was performed.

Trypsin activity in the presence of nucleotide inhibitors. The assay mixture in a final volume of 100 µL contained 10 nM trypsin, 15 mM $MgCl_2$, 110 µM z-Arg-AMC (~K_m value derived from Figure 3-18B), and nucleotide inhibitors at the concentrations at least 10-fold above K_i (Table 3-2) [ClFDP, 3 µM; ClADP, 14 µM; ClATP, 5 µM; FlUDP, 94 µM; FlUTP, 68 µM; or 50 mM Hepes (pH 7.6) for control] in 50 mM Hepes (pH 7.6). Fluorescence intensities were recorded over 10 minutes using a

Biotek Cytation™ 3 plate-reader (λ_{ex} = 380 nm and λ_{em} = 460 nm). The rates of AMC production from z-Arg-AMC hydrolysis in the absence or presence of each nucleotide inhibitor were calculated using the linear regression equation obtained from the AMC standard curve (Figure 3-18A). Each resultant trypsin activity was normalized by the trypsin activity obtained from the control experiment (Figure 3-18C).

Percentage of fluorescence quenching of AMC by nucleotide inhibitors. The assay mixture in a final volume of 100 μL contained 0.25 μM AMC, 15 mM $MgCl_2$, and nucleotide inhibitors [ClFDP, 3 μM; ClADP, 14 μM; ClATP, 5 μM; FlUDP, 94 μM; FlUTP, 68 μM; or 50 mM Hepes (pH 7.6) for control] in 50 mM Hepes (pH 7.6). Fluorescence intensities were recorded over 17 minutes using a Biotek Cytation™ 3 plate-reader (λ_{ex} = 380 nm and λ_{em} = 460 nm) (Figure 3-18D).

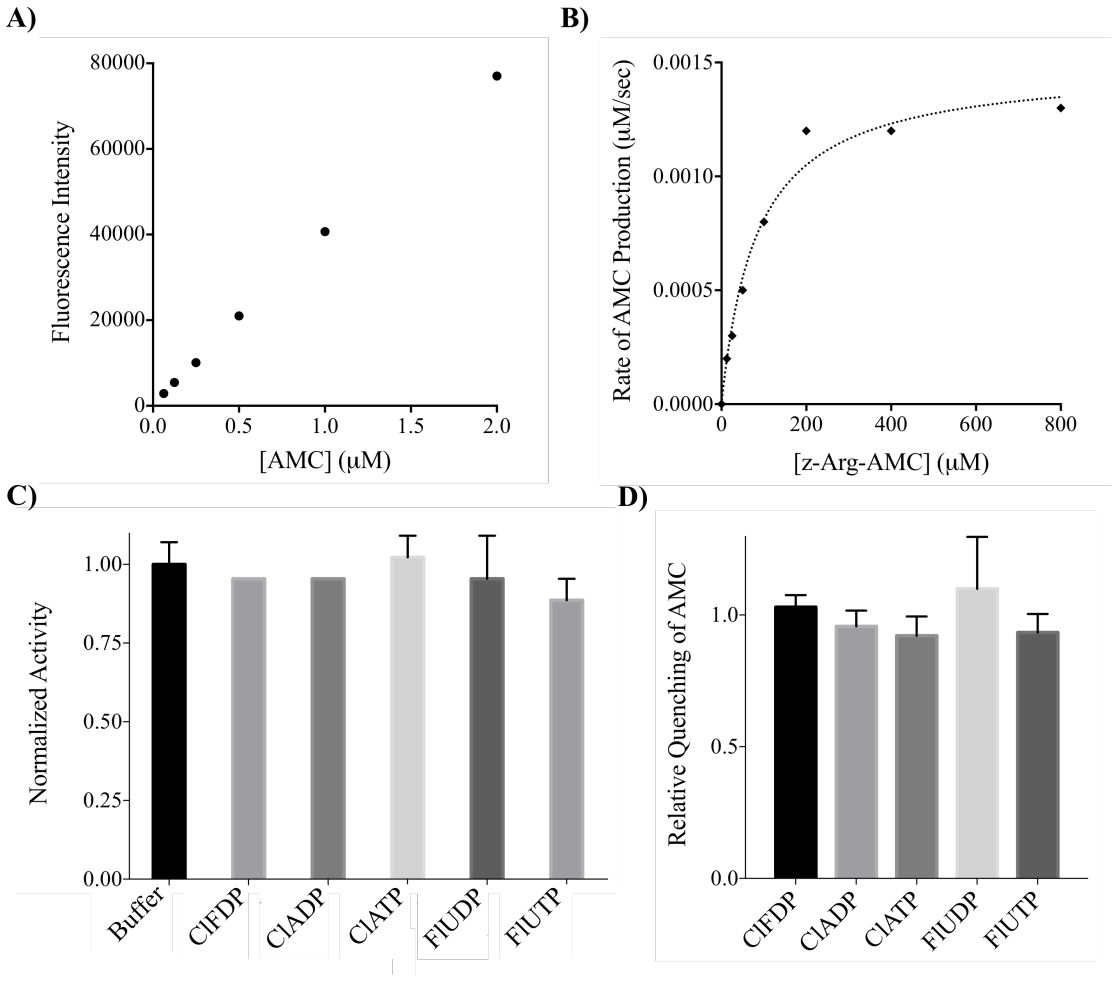

Figure 3-18. Trypsin activity and AMC fluorescence intensity are unaffected by nucleotide inhibitors. **A)** AMC standard curve. **B)** Determination of K_m of trypsin for z-Arg-AMC substrate by measuring fluorescence intensity of AMC formation, K_m ~ 84 ± 15 μM. **C)** Relative protease activity of 10 nM trypsin in hydrolysizing 110 μM z-Arg-AMC substrate in the presence of indicated inhibitors [ClFDP, 3 μM; ClADP, 14 μM; ClATP, 5 μM; FlUDP, 94 μM; or FlUTP, 68 μM]. **D)** Each nucleotide inhibitor showed no significant quenching of AMC fluorescence intensity. Error bars designate standard error from independent duplicates.

Figure 3-18C and 3-18D respectively confirmed the lack of trypsin inhibition and non-specific AMC-fluorophore quenching by nucleotides.

Trypsin digestion analysis of 1) hexamers induced by different nucleotide inhibitors and 2) hRNR-α in the presence of natural nucleotides. The AM in a final volume of 103 μL contained 3 μM hRNR-α, 15 mM $MgCl_2$, 0.5 mM DTT, 1 μM trypsin, and nucleotide inhibitors [ClFDP, 3 μM; ClADP, 14 μM; ClATP, 5 μM; FlUDP, 94 μM; or FlUTP, 68 μM] (Figure 3-29) or natural nucleotides at the concentrations at least 10-fold above reported K_d's[48,49] [dTTP, 18 μM; dGTP, 44 μM; dATP, 700 μM; or ATP, 3mM] (Figure 3-30) or buffer as control, in 50 mM Hepes (pH 7.6). The mixture without trypsin was pre-warmed at 37 °C for 3 minutes prior to an addition of trypsin to initiate the cleavage reaction. 18 μL aliquots were removed at 1, 5, 20 and 60 minute time points and immediately quenched with 10 μL of 4x Laemmli dye containing 8.4% BME. To deactivate the protease activity, the mixture was subsequently boiled at 100 °C for 10 minutes. The relative rates of trypsin digestion of hexamers induced by different nucleotide inhibitors were evaluated by standard SDS-PAGE analysis.

Recovery of ClADP subsequent to enzyme inhibition

The IM in a 200 μL final volume contained 25 μM hRNR-α, 25 μM hRNR-β, 5 mM DTT, 2.5 mM ATP, 15 mM $MgCl_2$, 0.5 mM CDP, and 25 μM ClADP in 50 mM Hepes (pH 7.6). For control experiment, hRNR-α and hRNR-β were replaced by ddH_2O. The IM was incubated at 37 °C for 10 minutes. To denature the enzymes, the sample was subsequently boiled at 100 °C for 2 minutes prior to centrifugation at 10,000×g for 30 seconds at RT. After the supernatant was collected, the remaining

residues were rinsed with 50 μL ddH_2O, followed by centrifugation at 10,000×g for 30 seconds at RT. The rinsing process was done twice. The combined supernatant was added to an ultracentrifugation device (YM-30 minicon) and spun at 6,000×g for 10 minutes at 4 °C. The flow-through was collected and the YM-30 minicon was topped up with additional 400 μL of ddH_2O before the ultracentrifugation was continued. This process was repeated for a total of five cycles. After removing the solvent of the combined flow-through using lyophilizer, the dry residue was redissolved in 130 μL ddH_2O, filtered with 0.22 μm Millex-GV syringe filter unit, and 100 μL of the final solution was injected onto the Ultra IBD (150×4.6 mm) column (Restek), which had been pre-equilibrated with 1% MeOH in buffer A [20 mM NH_4OAc (pH 5.8)] at 1 $mL.min^{-1}$ flow rate. The nucleotides were eluted isocratically with 1% MeOH in buffer A for 5 minutes, followed by linear gradients to 3% and 30% MeOH in buffer A over 25 minutes and 15 minutes, respectively. The percentage of MeOH in buffer A was brought up to 60% in the next 5 minutes and the last linear gradient to 100% MeOH was applied over 15 minutes. The diagnostic peak of ClADP appeared at ~21 minute retention time and the amounts of ClADP averaged over two runs were quantified using the known extinction coefficient (ε_{265}: 15,700 $M^{-1}.cm^{-1}$) against control experiments that were run under identical conditions.

Regain of hRNR-α reductase activity post dilution (estimation of off-rates)

To approximate the off-rates, the inhibited enzyme was rapidly diluted in dilution buffer to promote inhibitor dissociation. A regain of hRNR-α activity was subsequently measured as a function of time. The experimental details pertinent to each inhibitor are described below.

ClADP. The IM in a final volume of 20 μL contained 15 μM hRNR-α, 37.5 μM hRNR-β, 3 mM ATP, 15 mM $MgCl_2$, 5 mM DTT and 30 μM ClADP (or ddH_2O for control) in 50 mM Hepes (pH 7.6). The IM without the inhibitor was pre-warmed at 37 °C for 2 minutes before ClADP (or ddH_2O) was added. After incubation at 37 °C for another 2 minutes, the IM was diluted by an addition of 2,380 μL of pre-warmed buffer containing 15 mM $MgCl_2$, 5 mM DTT in 50 mM Hepes (pH 7.6). At this step, the IM was diluted 120 folds. 50 μL aliquots were removed from the diluted mixture at indicated time points, and subsequently mixed with 5 μL of 11x stock of AM to precede another 1.1-fold dilution. The 11x stock of AM was prepared in a 65 μL final volume containing 33 μM hRNR-β, 33 mM ATP, 15 mM $MgCl_2$, 11 mM NADPH, 1.1 mM Trx, 11 μM TrxR, and 5.5 mM [5-^{3}H]-CDP in 50 mM Hepes (pH 7.6). The individual aliquots of 11x AM stock were pre-warmed at 37 °C for 2 minutes prior to mixing with the respective aliquots of the diluted IM at each indicated time point. dCDP production was assayed over 9 minutes for each time point, followed by quenching with 30 μL of 2% (v/v) $HClO_4$. Standard neutralization, dephosphorylation, subsequent purification and scintillation counting procedure ensued (Figure 3-33A).

ClATP. The IM in a final volume of 15 μL contained 16.5 μM hRNR-α, 20 μM hRNR-β, 3 mM ATP, 15 mM $MgCl_2$, 5 mM DTT and 16.5 μM ClATP (or ddH_2O for control) in 50 mM Hepes (pH 7.6). The IM without the inhibitor was pre-warmed at 37 °C for 2 minutes at which point ClATP (or ddH_2O) was added. After incubation at 37 °C for another 2 minutes, the IM was diluted by an addition of 2,235 μL of pre-warmed buffer containing 15 mM $MgCl_2$, 5 mM DTT in 50 mM Hepes (pH 7.6). At this step, the IM was diluted 150 folds. 150 μL aliquots were removed from the diluted mixture at indicated time points, and subsequently mixed with 15 μL of 11x stock of AM to precede another 1.1-fold dilution. The 11x stock of AM was prepared in a

195 μL final volume otherwise identical conditions as described under *ClADP*. To analyze the amount of [5-^{3}H]-dC produced at each time point, the remaining steps listed above were followed (Figure 3-33B).

FlUDP and FlUTP. The IM in a final volume of 30 μL contained 2 μM hRNR-α, 5 μM hRNR-β, 3 mM ATP, 15 mM $MgCl_2$, 5 mM DTT and 90 μM FlUDP or FlUTP (or ddH_2O for control) in 50 mM Hepes (pH 7.6). The IM without the inhibitor was pre-warmed at 37 °C for 2 minutes at which point inhibitor (FlUDP or FlUTP) or ddH_2O was added. After incubation at 37 °C for another 2 minutes, the IM was diluted by an addition of 870 μL of pre-warmed buffer containing 15 mM $MgCl_2$, 5 mM DTT in 50 mM Hepes (pH 7.6). At this step, the IM was diluted 30 folds. 50 μL aliquots were then removed from the diluted mixture at indicated time points, and subsequently mixed with 5 μL of 11x stock of AM to precede another 1.1-fold dilution. The 11x stock of AM was prepared in a 65 μL final volume otherwise identical conditions as described under *ClADP*. The above-mentioned procedure was followed until the amount of [5-^{3}H]-dC produced at each time point was analyzed (Figure 3-33C and 3-33D).

Fluorescence Anisotropy (FA)

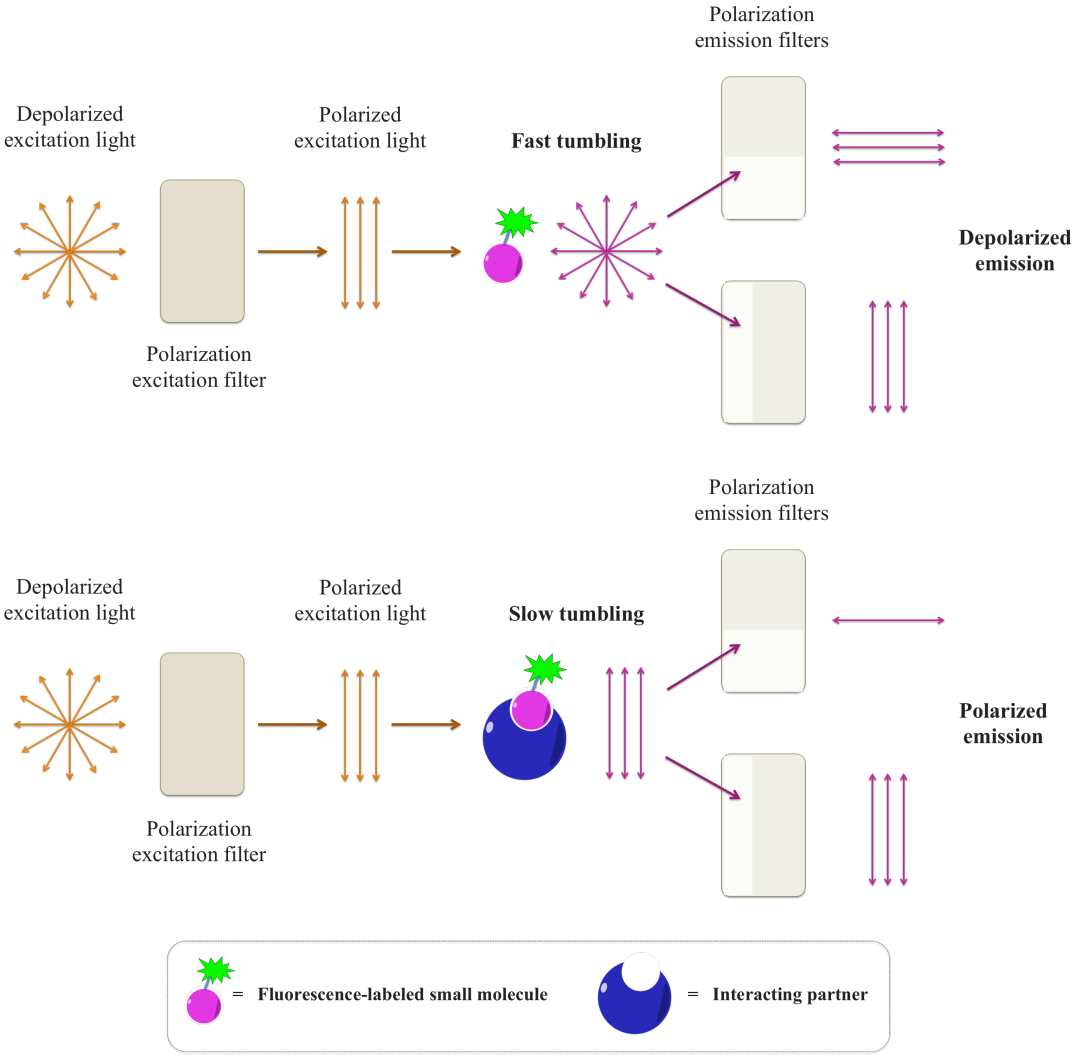

Figure 3-19. Fluorescence anisotropy (FA) as a tool to study molecular interactions. This figure is adapted from Ref. 50.

FA has been widely used for the study of molecular interactions in solution, *i.e.*, protein-DNA, DNA-DNA, carbohydrate-protein, and protein-protein interactions etc.[50,51] Figure 3-19 illustrates the principle of how FA is employed in the measurement of binding reactions. In solution, small molecules rotate and tumble

faster than larger molecules. When fluorescence-labeled small molecules in solution are excited with a plane-polarized light, they will tend to scramble the polarization of the incident light by radiating at a different direction (Figure 3-19, *top*), leading to the depolarization. However, when these fast-moving fluorescence-labeled small molecules bound to their interacting partners that have a large molecular mass, the movements of these complexes are restricted and become slower. These complexes will diminish the scrambling effect, and thus increase the polarization of the emitted light (Figure 3-19, *bottom*).[50]

Due to its known binding site specificity to RNR-α (S- and A-sites) and its commercial availability, Texas Red-5-dATP (or T*-dATP) was used as a fluorescence-labeled small molecule in these assays. We initially tried to study the binding of T*-dATP to the truncated N-terminal domain (NTD) of hRNR-α (H-NTD hereafter), in which only the A-site is available, and how this binding is affected by the ligands under study. If ClADP and FlUDP bind to the C-site, we would anticipate to observe an increase in FA upon treating the complex of H-NTD and T*-dATP with these inhibitors. However, it is also possible that the change in FA is too small until negligible since the M.W. of these inhibitors are relatively small compared to the M.W. of the protein. Thus, the difference between M.W. of protein-T*-dATP and of protein-T*-dATP-ligand complexes might be infinitesimal. Regardless, a drop in FA should not ever be expected under this assumption. Unfortunately, the sensitivity of the assays under these conditions was immensely low, which made the assays impractical. For instance, to observe a significant change in FA in a positive control, large amounts of H-NTD (100 μM) and dATP (8 mM) were required (data not shown). We, thus, replaced the H-NTD with either the wild-type hRNR-α or the D57N-α mutant and pre-blocked the S-site with an S-site exclusive binder, dTTP (Figure 3-34A). Under these conditions, T*-dATP can only bind to the A-site. Thus,

if an inhibitor binds to the A-site, an excessive amount of the corresponding inhibitor will compete over T*-dATP, leading to a release of T*-dATP to solution. The free-rotating/tumbling T*-dATP will consequently depolarize the incident plane-polarized light, leading to a drop in FA (Figure 3-19 (*bottom*) and 3-20). On the other hand, a slightly increase or no changes in FA would be expected if the inhibitor binds to the C-site.

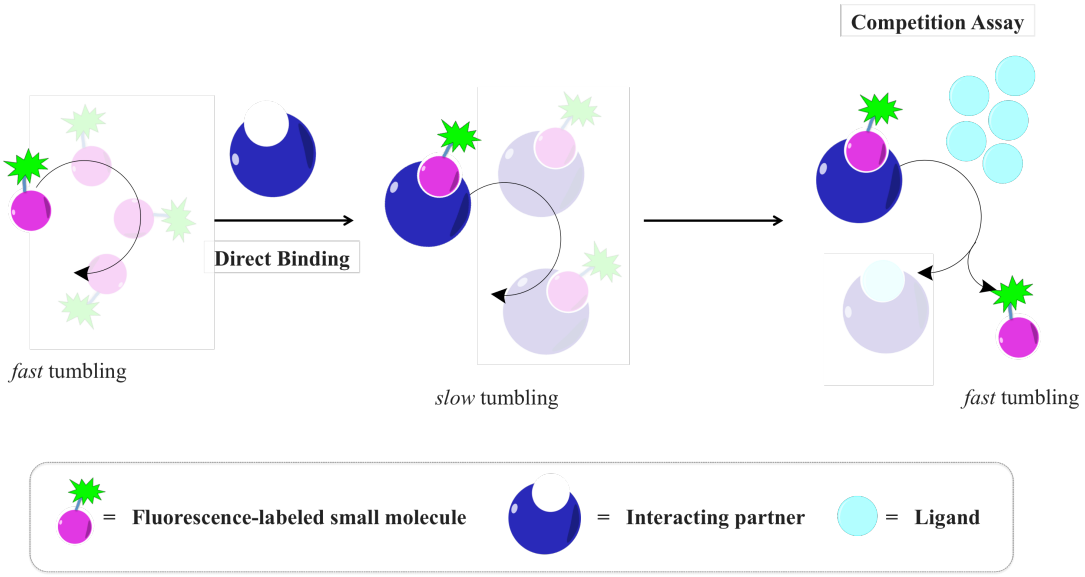

Figure 3-20. Fluorescence anisotropy (FA) assay principle. A direct binding of a fluorescence-labeled small molecule (fast tumbling) to its interacting partner will lead to a formation of a bigger fluorescence-labeled complex (slow tumbling). However, in the presence of an excessive amount of ligands, which specifically bind to the interacting partner, the fluorescence-labeled small molecule will be released to solution and freely rotate/tumble (fast tumbling). A drop of FA from slow tumbling state to fast tumbling state is then used as a readout for protein-ligand interactions.

Fluorescence anisotropy assays of T-dATP with either the wild-type hRNR-α or the D57N-α*. The AM in a 150 μL final volume contained either the wild-type hRNR-α or D57N-α (6 μM), T*-dATP (12 μM), KCl (100 mM), $MgCl_2$ (15 mM), DTT (5 mM), 5% glycerol and nucleotides of interest (dTTP, dATP, dGTP, ClADP or ClATP at 94, 700, 250, 75 and 31 μM, respectively, or assay buffer as control) (Figure 3-36A and 3-38) in Tris-HCl (50 mM) (pH = 7.6). The concentration of each nucleotide was judged by titration studies described below. The assay mixture was prepared by incubating T*-dATP with either hRNR-α or D57N-α for one minute before adding the nucleotide of interest at the indicated concentration, or assay buffer (for control). For the analysis of potential non-specific binding of T*-dATP (Figure 3-36C and 3-36E), the order of addition of T*-dATP or 700 μM dATP to the assay is designated on the x-axis of each plot. The mixture was thoroughly mixed and incubated for another minute. FA was then analyzed using a fluorescence spectrophotometer (Varian Cary Eclipse) (λ_{ex} = 580 nm, λ_{em} = 620 nm) and equation 3.4.[52-54]

$$r = \frac{I_{vv} - GI_{vh}}{I_{vv} + 2GI_{vh}} \quad \text{; whereas} \quad G = \frac{I_{hv}}{I_{hh}} \qquad \text{(Eq. 3.4)}$$

In this equation, r and G represent fluorescence anisotropy and the correction factor (G-factor), respectively. I_{ij} represents fluorescence intensity obtained after adjusting the polarization excitation and emission filters in *i*- and *j*-directions (h, horizontal or v, vertical), respectively.

For Figure 3-38A and 3-39B (*left panel*), the mixture without T*-dATP was pre-incubated for one minute with a saturating amount of the S-site exclusive binding nucleotide, dTTP, to pre-block the S-site or assay buffer (control). T*-dATP was then added to the mixture, which was subsequently mixed thoroughly. The nucleotide

inhibitor (ClADP or ClATP at indicated concentration) or assay buffer (control) was added prior to another minute incubation at RT. FA was measured as mentioned above. Thereafter, 110 μL of both samples from Figure 3-39B (*left panel*), hRNR-α and T*-dATP in the presence of dTTP alone, or in the presence of both dTTP and ClADP, was directly injected into the HPLC. This procedure further validated the resultant oligomeric state of hRNR-α subsequent to the FA measurements (Figure 3-39B, *right panel*).

For titration studies (Figure 3-36B, 3-36D and 3-37), the mixture without any nucleotides (dTTP, dATP, dGTP and ClATP) was pre-incubated with T*-dATP for one minute. Then, nucleotide of interest at indicated final concentrations; dTTP (3.5, 10.4, 31.3, 94 and 282 μM), dATP (87.5, 175, 350, 700 μM and 1.4 mM), dGTP (9.3, 27.8, 83.3, 250 and 750 μM) or ClATP (2, 4, 8, 16 and 31 μM) was added to the assay mixture. After incubating the mixture for another minute, the measurements were made as above.

3.3 Results and discussion

3.3.1 Determination of active phosphorylated forms of ClA and FlU in hRNR inhibition

hRNR inhibition was assessed by measuring CDP reduction after incubation the enzyme with di- and triphosphate forms of ClA and FlU for 3 minutes (Figure 3-21). As shown in Figure 3-22, a vast majority of the enzyme activity was inhibited after 3-minute incubation at 37 °C. However, there was no significantly further drop of enzyme activity observed when the incubation time increased. These results confirmed that hRNR-α activity was almost completely inhibited within 5-minute timescale.

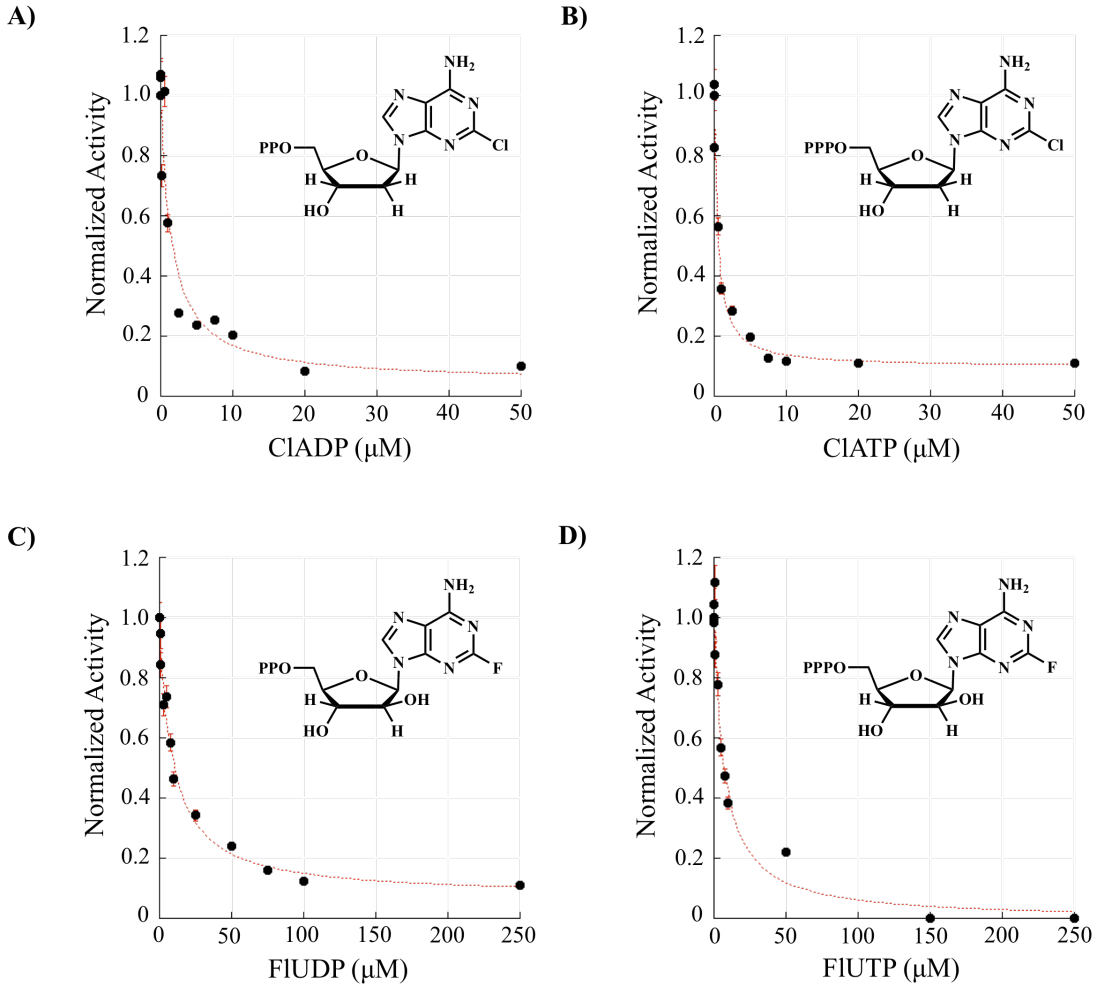

Figure 3-21. Dose-dependent of **A)** ClADP, **B)** ClATP, **C)** FlUDP, and **D)** FlUTP for hRNR-α-specific CDP/ATP reductase activity (assay duration: 3 minutes).

From Figure 3-21, hRNR activity was mostly inhibited by 50 μM of ClAD(T)P, or 250 μM of FlUD(T)P. By fitting these data to the tight-binding equation (Eq. 3.1)[39], an apparent K_i of each nucleotide analogue was derived and reported in Table 3-2.

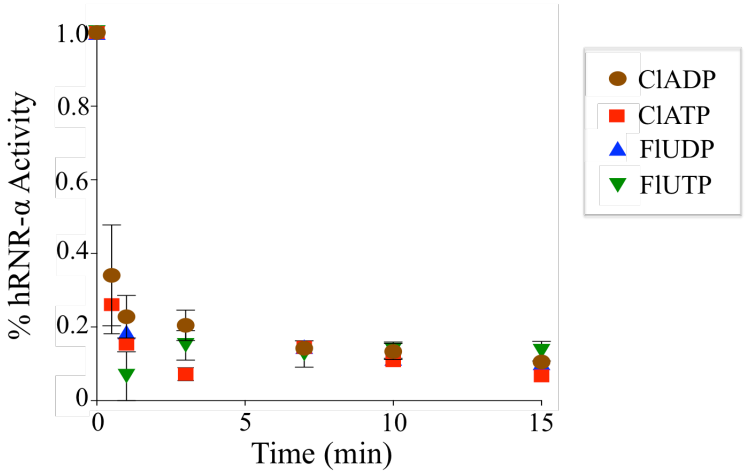

Figure 3-22. Time-dependent inhibition assay of hRNR-α-specific activity in the presence of ClADP (5 μM), ClATP (5 μM), FlUDP (50 μM) and FlUTP (12.5 μM).

Table 3-2. Inhibition constants of hRNR-α nucleotide–based inhibitors.

Nucleotide Analogue	K_i (μM)
ClADP	1.4 ± 0.7
ClATP	0.5 ± 0.1
FlUDP	9.4 ± 1.7
FlUTP	6.8 ± 1.3
ClFDP	0.017[16]
ClFTP	0.04[16]

All four nucleotide analogues [ClADP, ClATP, FlUDP and FlUTP] showed inhibitory effects on hRNR activity with their K_i values ranging from 0.5–10 μM. These results confirmed that both di- and triphosphate forms of ClA and FlU were active forms in hRNR inhibition. However, the binding affinities of these nucleotide analogues are not as good as of ClFDP and ClFTP (Table 3-2).[16]

In order to verify that hRNR inhibition induced by these nucleotide analogues is hRNR-α-subunit specific, we needed to prove that hRNR-β activity remains intact upon drug treatment.

3.3.2 Time-dependent inhibition assays for hRNR-β subunit

In the IM containing 1:1 hRNR-α:hRNR-β (2 μM), Mg•ATP, DTT, and the designated inhibitor (6 μM) in 50 mM Hepes (pH 7.6), the hRNR activity was inhibited by ~50–70% (in the case of nucleotide analogues) or ~100% (in the case of 3-AP). By removing aliquots from the IM at the indicated time points and immediately diluting into the AM, which contained excess hRNR-α, a recovery of the hRNR activity is expected if hRNR-β-specific activity remains unaffected. On the other hand, hRNR activity would remain inhibited if the inhibitor specifically affects hRNR-β-subunit activity.

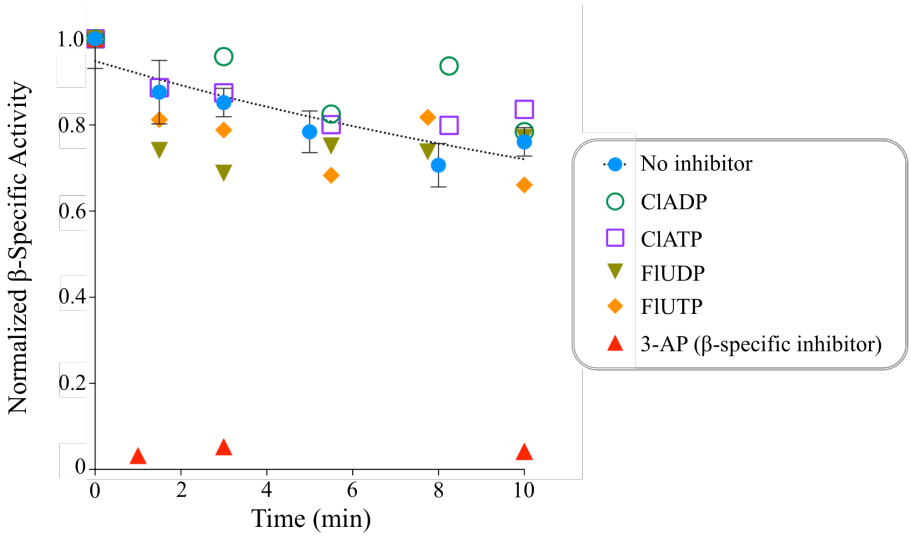

Figure 3-23. Effects of ClADP, ClATP, FlUDP, FlUTP and 3-AP on hRNR-β-subunit-specific activity. Normalized β-specific activity of 1.0 corresponds to the count of [5-^{3}H]-dC generated at zero time point.

While hRNR-β-specific activity remained unchanged in the case of 3-AP, the known RNR-β-subunit specific inhibitor, it was recovered in the case of ClADP, ClATP, FlUDP and FlUTP. These data suggested that both di- and triphosphate forms of ClA and FlU were the active hRNR-α-specific inhibitors. A decrease of the normalized β-specific activity over time, observed in Figure 3-23, was due to the known time-dependent intrinsic decay of diferric-tyrosyl radical cofactor-bearing mammalian RNR-β subunit.[34]

3.3.3 hRNR-α inhibition induced by ClA- and FlU-nucleotide analogues is coupled to α-subunit oligomerization

As mentioned in *chapter 2* that F2CDP and di- and triphosphate forms of ClF inhibit RNR activity via different mechanisms.[6,16,55] Here, we would like to identify the mechanism that ClA- and FlU-nucleotide analogues used to inhibit hRNR activity.

The RNR catalytic mechanism for NDP reduction at the C-site of RNR-α subunit is conserved from *E. coli* to *H. sapiens*.[6] The only active form of F2C in RNR inhibition, F2CDP, hijacks this conserved catalytic pathway from RNR $\alpha_2\beta_2$ holocomplex and irreversibly inactivates the enzyme activity. This mode of inhibition has been observed in both bacteria and eukaryotes. F2CTP, on the other hand, has no effects on either $\alpha_2\beta_2$ holocomplex activity or RNR-α oligomeric state.[56] In contrast to F2C, both di- and triphosphate forms of ClF are active RNR inhibitors. They inhibited eukaryotic RNR by inducing RNR-α-subunit hexamerization independent of RNR-β-subunit. Since both di- and triphosphate forms of ClA and FlU are active hRNR inhibitors and they specifically target hRNR-α subunit, we hypothesized that hRNR inhibition induced by ClAD(T)P and FlUD(T)P is directly linked to changes in hRNR-α oligomeric states. In order to test our hypothesis, two independent methods were used. We firstly made use of our in-house developed fluorescence resonance energy transfer (FRET) reporter platform to directly report on ligand-induced hRNR-α oligomerization.[27] Second, a formation of hRNR-α-hexamer was confirmed by using gel filtration analysis [Size Exclusion Chromatography (SEC)].

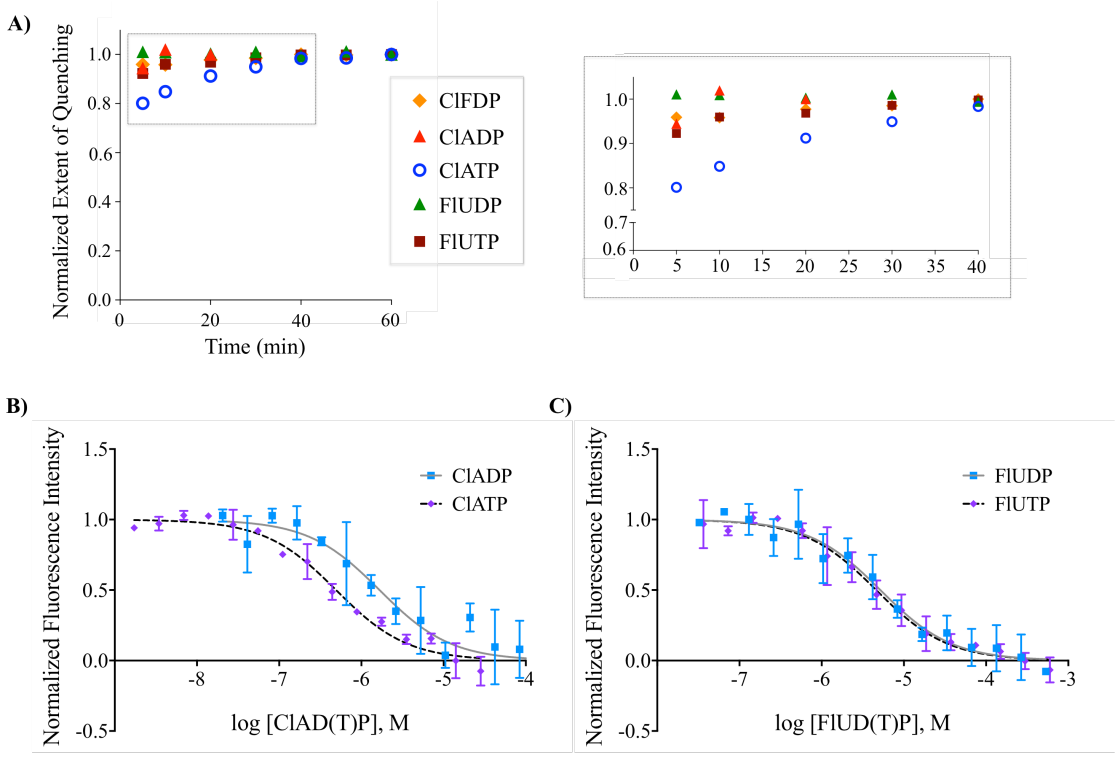

Figure 3-24. Biotek Cytation™ 3 plate-reader-based FRET assay *performed by Dr. Yi Zhao*. **A)** Time-dependent analysis of the extent of fluorescence quenching in the FRET assay. **B–C)** Dose-dependent analysis of hRNR-α-subunit-specific oligomerization induced by **B)** ClAD(T)P and **C)** FlUD(T)P.

In the time-dependent analysis (Figure 3-24A), the assay mixture contained 1:1 final concentrations of F-α:T-α in the presence of saturating amount of indicated inhibitors. The figure shows that hRNR-α oligomerization was complete induced within 5 minutes by ClADP, FlUDP and FlUTP or within 40 minutes by ClATP. In the case of ClADP, FlUDP and FlUTP, interestingly, this enzyme oligomerization timescale was similar to the enzyme inhibition timescale. EC_{50} values of inhibitor-induced hRNR-α-subunit-specific oligomerization derived from Figure 3-24B and Figure 3-24C were shown in Table 3-3. Even though these EC_{50} values fell into the

same range as their corresponding K_i values previously obtained (Table 3-2), they cannot necessarily be directly compared due to the differences in their assay settings. However, given that both K_i's and EC_{50}'s of FlUDP and FlUTP were higher than those of ClA nucleotides, these data suggested that inhibition potencies are positively correlated to the abilities of the inhibitors to induce hRNR-α-subunit oligomerization. Thus, the inhibition is likely coupled with hRNR-α oligomerization.

Table 3-3. EC_{50} values of hRNR-α nucleotide–induced oligomerization.

Nucleotide Analogue	EC_{50} (μM)
ClADP	1.7 ± 0.5
ClATP	0.5 ± 0.1
FlUDP	5.2 ± 1.2
FlUTP	4.6 ± 0.8
ClFDP	0.19[27]
ClFTP	0.07[27]

In order to confirm that these inhibitors can induce hRNR-α hexamerization, we measured the molecular weights of each nucleotide-induced hRNR-α oligomer using size exclusion chromatography (SEC).

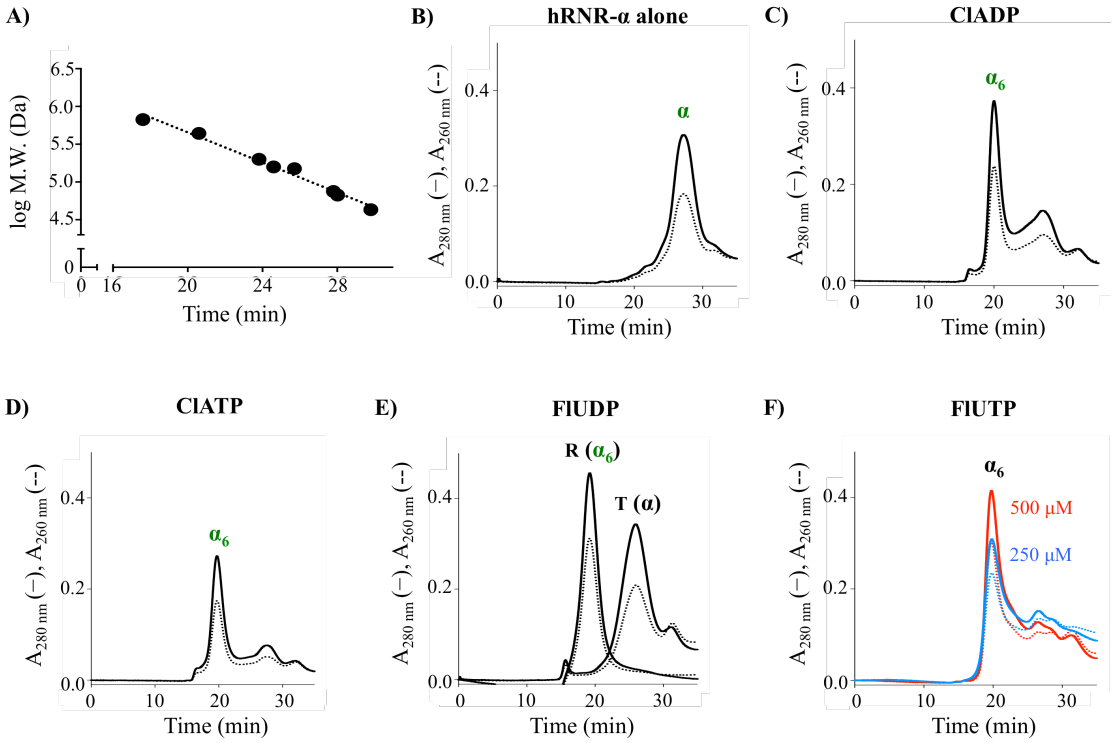

Figure 3-25. Representative gel filtration chromatograms. **A)** M.W. standard curve (M.W., retention time): thyroglobulin (669 kDa, 17.6 minute); ferritin (440 kDa, 20.6 minute); aldolase (158 kDa, 24.6 minute); conalbumin (75 kDa, 27.8 minute); ovalbumin (44 kDa, 29.8 minute). Additional M.W. standards: *β*-amylase (200 kDa, 23.8 minute); alcohol dehydrogenase (150 kDa, 25.7 minute); and BSA (66 kDa, 28.0 minute), were also shown. **B)** hRNR-α alone. **C–F)** hRNR-α treated with **C)** 250 μM ClADP; **D)** 250 μM ClATP; **E)** 250 μM of FlUDP when running buffer contained 20 μM FlUDP (trace labeled **R**), or no nucleotides (trace labeled **T**); **F)** 250 μM (blue) or 500 μM (red) of FlUTP.

Figure 3-25, B−D, showed that the persistent hRNR-α-hexamer was observed after incubating the enzyme with saturating amount of ClADP or ClATP at 37 °C for 3 minutes. Same hRNR-α-hexamer peak as well observed in the case of FlUTP. But,

in order to fully induce hRNR-α-hexamerization, 500 μM FlUTP was required (Figure 3-25F). Unexpectedly, upon treating the enzyme with saturating amount of FlUDP with no FlUDP in the running buffer, the nucleotide was insufficient to induce hRNR-α-hexamer. Only hRNR-α-monomer was eluted out of the column (Figure 3-25E, *trace* ***T***). But, once 20 μM FlUDP was added into the running buffer, exclusively hRNR-α_6 was observed (Figure 3-25E, *trace* ***R***). The capability of all four nucleotide analogues in inducing the hRNR-α-hexamerization expanded the generality of the novel ligand-driven hexamerization beyond the sole example, ClF.[16,56,57] However, given the dissimilar behavior of FlUDP-induced hexamer, it is surprising that the binding affinity of FlUDP to the enzyme is not significantly different from its analogue, FlUTP (Figure 3-21 (C−D), 3-24C, Table 3-2 and 3-3). Since ClFD(T)P-induced hexamers are kinetically stable beyond complete inhibition dissociation[57], whereas FlUDP-induced hexamer are unexpectedly low kinetically stable, this can be inferred that different nucleotide analogues induce different forms of hRNR-α-hexamers.

In collaboration with Huma Inayat and Professor Joaquin Ortega from McMaster University, Canada, we were able to further characterize the nucleotide-induced hRNR-α-hexamers using electron microscopy (EM) analysis.

3.3.4 Conformational heterogeneity within the hexamers induced by different nucleotide inhibitors

To simplify the experimental setup, we initially chose not to include excess nucleotide inhibitors in the dilution buffer. ClFDP, which is a known hRNR-α_6 inducer[16], was used as a positive control. Its electron micrograph (Figure 3-26A) showed ring-shaped structures, which were not observed in the control sample (Figure

3-26B). These results replicated Aye and coworkers' previous work.[57] ClAD(T)P and FlUD(T)P also showed similar electron micrographs with abundant ring-shaped particles (Figure 3-26, C–F (*left panels*)). All of these data are consistent with our previous SEC analysis. However, there is one worth mentioning difference in the case of FlUDP-induced hRNR-α_6 from both techniques. FlUDP was required in the SEC running buffer to maintain hRNR-α_6 stability while hRNR-α_6 was stable in the EM dilution buffer with no excess FlUDP. The differences in conditions and timescale of the EM and SEC analyses might play a role in these different outcomes.

In order to identify the symmetry of the observed rings, particles from the electron micrographs were selected, extracted, and their rotational symmetry was analyzed using statistic tests (*t*-test and the spectral ratio product[43] that pool the rotational power spectra of all particles in each of the samples tested). Results from these two tests are listed in Table 3-4.

In all cases, the ring-shaped particles exhibited both 3-fold and 6-fold rotational symmetries. We additionally observed 9-fold and 4-fold rotational symmetries with statistical significance in the case of the samples treated with ClATP and FlUDP, respectively. Because EM samples were prepared under similar conditions to FRET experiments, *i.e.*, reaction timescale and final protein concentrations, the EM samples were believed to be in the near-complete oligomerization state. We, thus, rationally interpreted the observed differences in rotational symmetries as differences in conformational flexibility among the hexamers induced by different inhibitors. In most cases, particles with 3-fold rotational symmetry showed the highest statistical significances, indicating that the particles with the trimer-of-dimers architecture were more abundant than those exhibiting 6-fold rotational symmetry. The ring radius of the 3-fold and 6-fold rotational symmetries were detected at ~50 Å and ~80 Å, respectively (Table 3-4).

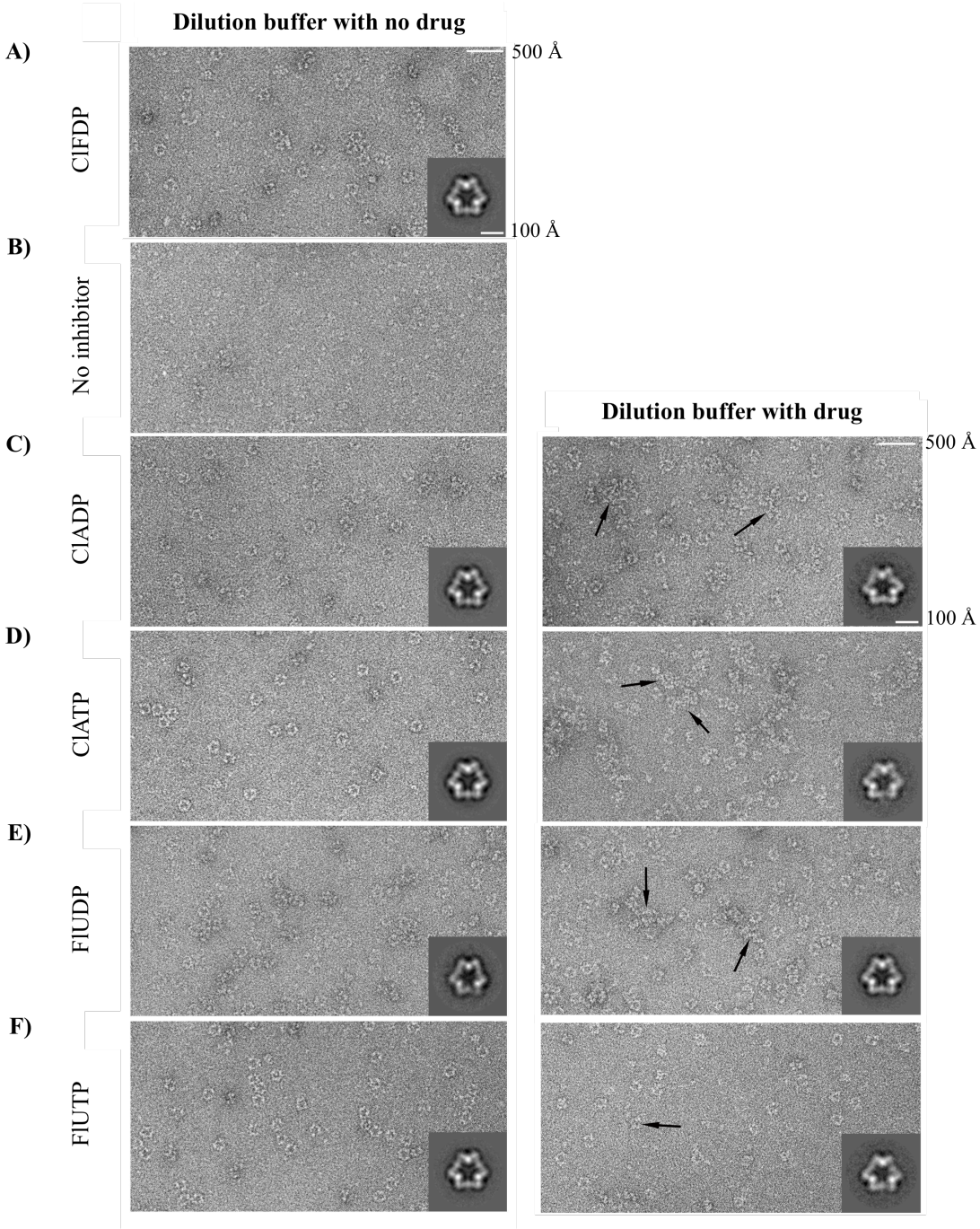

Figure 3-26. EM analysis of ring-shaped particles observed upon the treatments of hRNR-α with **A)** ClFDP (positive control), **B)** buffer alone (negative control), **C−D)** ClAD(T)P, or **E−F)** FlUD(T)P. Assembly reactions were immediately applied to the grid after performing a 100-fold dilution in buffer containing no inhibitor (*left panels*)

or 250 μM corresponding inhibitor (*right panels*). Samples were stained with 1% uranyl acetate and the images were taken using a transmission electron microscope (TEM). Insets in each panel show the 2D averages of the ring-shaped particles exhibiting 3-fold rotational symmetry induced by each inhibitor. Arrowheads indicate pleomorphic particles of different sizes accompanying the ring-shaped particles. *Data collection and analyses in this figure were performed by Huma Inayat under the guidance of Professor Joaquin Ortega.*

Table 3-4. Rotational symmetry analysis of ring-shaped hRNR-α particles induced by nucleotide analogues, and subsequently diluted with the dilution buffer containing no inhibitors. *Data collection and analyses were performed by Huma Inayat under the guidance of Professor Joaquin Ortega.*

Inhibitor	Symmetry detected	Radius (Å)	t-test significance level*	Spectral ratio product
ClFDP	3	48	p<0.000001	$3.79 \times 10^{+56}$
	6	81	p<0.000001	$3.19 \times 10^{+65}$
ClADP	3	50	p<0.000001	$3.12 \times 10^{+52}$
	6	83	p<0.000001	$1.85 \times 10^{+33}$
ClATP	3	43	p<0.000001	$9.91 \times 10^{+97}$
	6	78	p<0.000001	$8.07 \times 10^{+52}$
	9	81	p<0.000001	$5.75 \times 10^{+38}$
FlUDP	3	45	p<0.000001	$2.10 \times 10^{+32}$
	6	73	p<0.000001	$1.89 \times 10^{+34}$
	4	58	p<0.000001	$1.53 \times 10^{+25}$
FlUTP	3	50	p<0.000001	$1.01 \times 10^{+64}$
	6	81	p<0.000001	$4.56 \times 10^{+58}$

** These p-values indicate the confidence of the symmetry determined*

We also prepared EM samples under different conditions in which the 100-fold dilution was made into buffer containing saturating amount of respective nucleotide inhibitors (250 μM, or at least ~27-fold above the highest K_i (Table 3-2)). The aim of these experiments was to ensure that the distribution of hexameric states observed in Figure 3-26 (*left panels*) was not related to residence times of the different drugs. Interestingly, the efficiency of the assembly for the ring-shaped particles was reduced when the assembly reaction was 100-fold diluted with nucleotide-containing dilution buffer before applying the sample to the EM grids (Figure 3-26, *right panels*). The resulting electron micrographs showed pleomorphic particles of different sizes that accompany the ring-shaped particles (Figure 3-26, *right panels*, arrow heads). This led to a conclusion that the efficiency of hRNR-α to oligomerize into ring-shaped particles is lower in the buffer containing excess amount of nucleotide inhibitors. However, rotational symmetry analysis of these samples gave similar outcomes to what we previously observed from the samples prepared in the dilution buffer containing no inhibitors (Table 3-4 and 3-5).

Considering these two data sets together, it did not seem that the multiple types of rotational symmetries were simply due to the hexameric particles dissociating after the 100-fold dilution into the buffer containing no corresponding inhibitor; nor were they metastable states trapped along the hexamerization assembly pathway. Instead, they more likely represented end points of conformationally distinct hexamers with discrete rotational symmetries.

Table 3-5. Rotational symmetry analysis of ring-shaped hRNR-α particles induced by nucleotide analogues, and subsequently diluted with the dilution buffer containing saturating amount of respective inhibitor. *Data collection and analyses were performed by Huma Inayat under the guidance of Professor Joaquin Ortega.*

Inhibitor	Symmetry detected	Radius (Å)	t-test significance level*	Spectral ratio product
ClADP	3	50	p<0.000001	$3.96 \times 10^{+43}$
	6	83	p<0.000001	$1.85 \times 10^{+33}$
	4	81	p<0.000001	$1.61 \times 10^{+9}$
ClATP	3	50	p<0.000001	$6.24 \times 10^{+27}$
	4	68	p<0.000001	$3.50 \times 10^{+11}$
FlUDP	3	43	p<0.000001	$2.08 \times 10^{+47}$
	6	78	p<0.000001	$8.69 \times 10^{+35}$
FlUTP	3	43	p<0.000001	$2.90 \times 10^{+47}$
	6	81	p<0.000001	$2.69 \times 10^{+27}$
	4	71	p<0.000001	$9.27 \times 10^{+13}$

** These p-values indicate the confidence of the symmetry determined*

Interestingly, a higher proportion of particles exhibiting 4-fold rotational symmetry was detected in the samples prepared in the dilution buffer containing excess amount of inhibitors. This suggested that the ring-shaped particles displayed a larger degree of conformational flexibility under these conditions. Up to now, the reason why excess inhibitors in the dilution buffer resulted in this phenotype remains unclear.

We further characterized the drug-induced particles by selecting particle images from both conditions, with or without inhibitors in the dilution buffer, and

subjecting them to a correlation averaging to obtain two-dimensional (2D) averages. The projection structures of particles with 3-fold rotational symmetry, the most abundant particles, were first obtained. To this end, self-organizing featured maps were used to select for particles with 3-fold rotational symmetry. Subsequently, 2D averages were generated. For each inhibitor, a 2D average from the samples that were diluted in the buffer containing either no inhibitors or 250 μM of respective inhibitor was acquired (Figure 3-26 insets). These averages were similar across all of the four nucleotide inhibitors regardless of whether the dilution buffer containing respective inhibitor or not. These 2D averages revealed that the ClAD(T)P and FlUD(T)P induced trimer-of-dimers assemblies can be viewed as three straight rods measuring each ~100 Å in length (Figure 3-26 insets). Rods were connected with each other through their ends constructing a close structure with clear 3-fold symmetry. The three contact points between the rods displayed a clear globular density that defined the three vertices of a triangle.

Unfortunately, there was no crystal structure of mammalian RNR-α_6 complexes available by the time we obtained our projection structures. However, given that hRNR-α and ScRNR-α have a 66% sequence identity, it might be reasonable to compare our projection structures with the previously established 6.6 Å crystal structure of dATP-bound *S. Cerevisiae* (Sc)RNR-α_6 complexes.[58] The crystal packing of the dATP-bound ScRNR-α_6 can accommodate two possible hexameric assembly motifs, models A and B (Figure 3-27). Results from site-directed mutagenesis studies revealed that hexamers in solution most likely exhibited model B.[58] In order to determine the extent to which the ring-shaped particles of hRNR-α induced by ClA and FlU nucleotides structurally resembled, a 2D projection of each model, A and B, was generated along the rotational symmetry axis. The resulting projections were subsequently compared to the average of the experimental

projections obtained by TEM. Interestingly, the 2D projection obtained from model B was noticeably similar to the TEM average obtained from the 3-fold symmetry-preserving ClAD(T)P/FlUD(T)P-induced ring-shaped particles of hRNR-α. These results suggested that the newly characterized nucleotide-induced hRNR-α oligomers in their most abundant 3-fold symmetry (Figure 3-26, C−F) indeed adopt a trimer-of dimers architecture and the subunit arrangement was proposed as a solution model of ScRNR-α_6 (Figure 3-27, model B).

In 2016, Ando *et al*[41] successfully crystalized dATP-induced hRNR-α_6 at low resolution (9.01 Å). The obtained crystal structure is remarkably similar to the hexamer model B of ScRNR-α_6 (Figure 3-27, A and D). Even though a 2D projection of this hRNR-α_6 complex has not yet been generated, it looks promising that the hRNR-α-subunit arrangement in this case follows the pattern of what previously observed in model B of ScRNR-α_6 and our EM experimental projections (Figure 3-27, B−C).

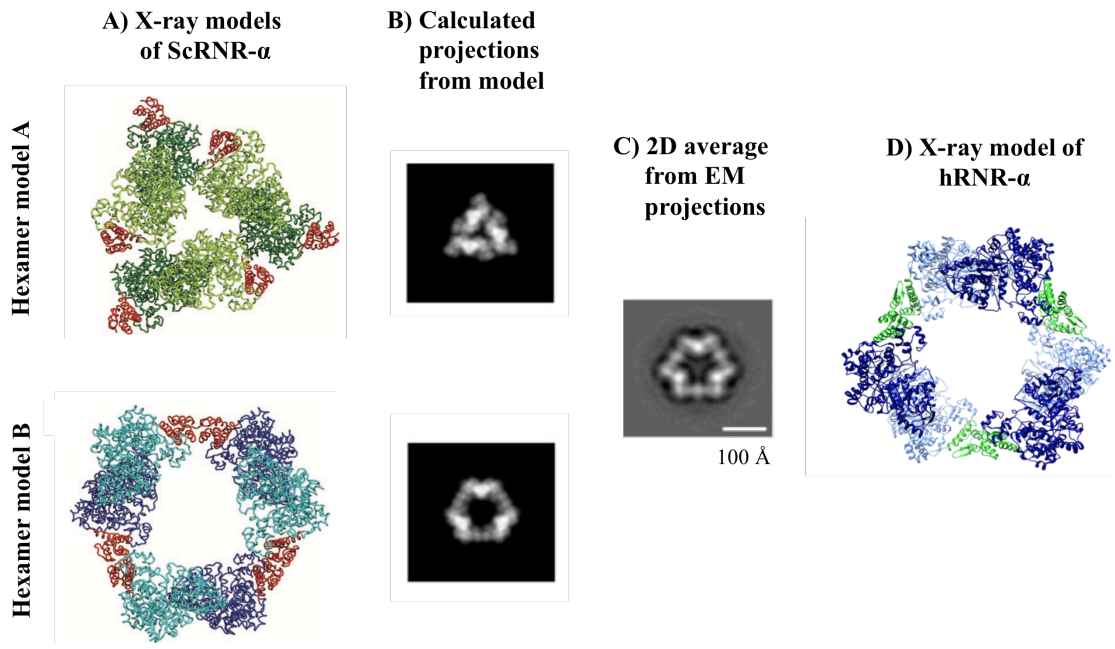

Figure 3-27. hRNR-α hexamers exhibit a trimer-of-dimers architecture. **A)** Hexamer models A and B show the ribbon representations, taken from Ref. 58, of the two hexameric layouts observed in the 6.6 Å crystal structure of ScRNR-α. The N-terminal domains within each ScRNR-α are shown in red. **B)** The corresponding 2D projections from each of the X-ray models A and B were generated along the rotational symmetry axis. The resolution of these projections was limited to 20 Å. **C)** The EM experimental projections of the hRNR-α ring-shaped particles obtained from ClATP treatment. **D)** The ribbon representation of dATP-induced hRNR-α_6 taken from Ref. 41. The N-terminal domains within each hRNR-α are shown in green. *Data analyses in **B–C)** were performed by Huma Inayat under the guidance of Professor Joaquin Ortega.*

Additionally, the conformational variability of the inhibitor-induced ring-shaped particles was examined using maximum-likelihood based classification

approaches[47] (Figure 3-28). The analysis was performed for both conditions of the dilution buffers, with and without respective inhibitor. In each data set, all particles were presented in the same orientation, *i.e.*, with the rotational symmetry axis perpendicular to the grid. Thus, the variation shown in the class averages is likely due to the existence of various conformations. Interestingly, homogenous populations of the ring-shaped particles were observed in the samples treated with the two triphosphates, ClATP (Figure 3-28C, *left panel*) and FlUTP (Figure 3-28E, *left panel*). The ten sub-populations obtained during the classification in each case of these two nucleoside triphosphates were structurally very similar, especially in the samples diluted in the dilution buffer containing no inhibitors. On the other hand, samples treated with the nucleoside diphosphates, ClADP (Figure 3-28B, *left panel*), FlUDP (Figure 3-28D, *left panel*), and the previously characterized ClFDP (Figure 3-28A) revealed ring-shaped particles with a much more obvious conformational variability. Some of the class averages significantly diverged from the class average obtained from the 3-fold symmetric particles. These differences further support the distinct conformational states of hRNR ring-shaped hexamers induced by the di- and triphosphate nucleosides. Some class averages obtained from the four inhibitors approximated the shape of a regular hexagon, or even a square in the case of FlUDP (Figure 3-28D, *right panel*). This last result was also consistent with the finding of the ring-shaped particles exhibiting 6-fold and 4-fold rotational symmetry from our previous rotational analysis (Table 3-4 and 3-5). It is also worth mentioning that the class averages acquired for the assembled rings obtained from the samples diluted in the buffer containing excess inhibitors (Figure 3-28, *right panels*) were more divergent compared to the another (Figure 3-28, *left panels*). Since the time-dependent FRET assay data (Figure 3-24A) suggested that all five inhibitors brought about a near-complete hRNR-α-subunit hexamerization under these conditions, we thus proposed

these populations of distinct conformations represent more likely the end points, instead of the intermediates, of the hexamer association.

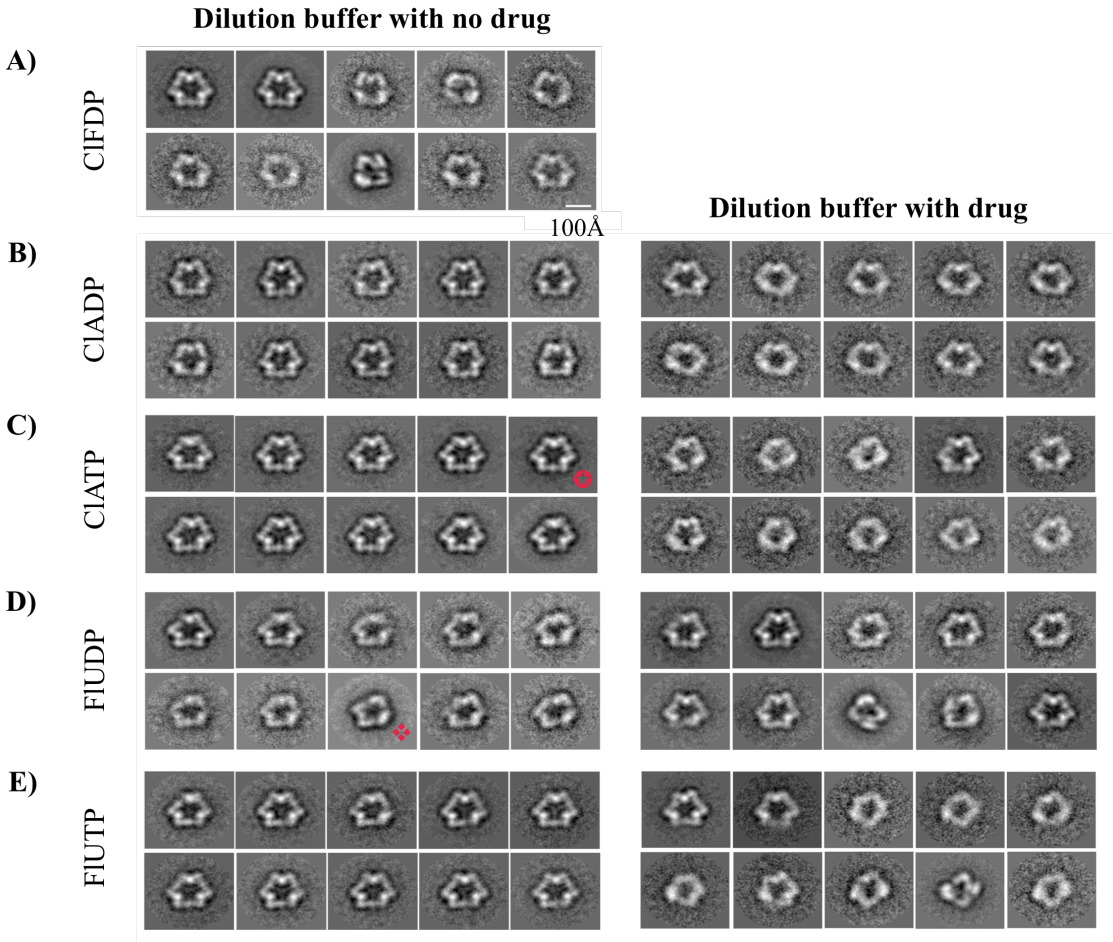

Figure 3-28. Conformational variability of the hRNR-α ring-shaped particles, *e.g.*, ✪ vs. ❖, induced by different nucleotide inhibitors; **A)** ClFDP, **B)** ClADP, **C)** ClATP, **D)** FlUDP, and **E)** FlUTP. In each case, a data set of ~2,000 particle images was subjected to a maximum likelihood classification approach[47], assuming the existence of ten classes. *Data collection and analyses were performed by Huma Inayat under the guidance of Professor Joaquin Ortega.*

3.3.5 Trypsin digestion assays confirmed conformationally distinct hexamers

To further validate conformational differences among each nucleotide-induced hRNR-α hexamers, we examined the extent to which individual hexamers are sensitive to protease cleavage. In this assay, we chose trypsin, a serine protease that cleaves peptide chain mainly at the carboxylic site of arginine or lysine[59], as our protease. We hypothesized that trypsin will cleave conformationally distinct hexamers with different rates, and/or generate different molecular weight fragments.

We found that the rates of trypsin cleavage were different among persistent hRNR-α-hexamers induced by the non-natural nucleotide inhibitors (Figure 3-29). Given that trypsin activity was unperturbed by these inhibitors under the same conditions (Figure 3-18C), the different rates observed must be directly due to conformationally distinct hexamers. Based on the comparable K_i values of FlUDP and FlUTP (Table 3-2), we initially expected these two nucleotide-induced hexamers were sensitive to trypsin to the same extent. Surprisingly, clear differences in trypsin cleavage rates were observed in FlUDP- and FlUTP-induced hRNR-α-hexamers (Figure 3-29). This finding, therefore, suggested that the differences in the observed trypsin cleavage rates were not associated with affinities or K_i values of the drugs. Or, in other words, this observation is not depending on hRNR-α structure stabilization caused by ligand binding.

In contrast to results from Figure 3-29, hRNR-α in the presence of natural nucleotides showed no appreciable sensitivity to the trypsin protease (Figure 3-30). Interestingly, the enzyme sensitivity was not also observed when hRNR-α was treated with dATP, a known RNR-α-hexamer inducer. This observation further supports the intrinsic differences between RNR-α hexameric states induced by dATP and other non-natural nucleotide inhibitors.[55]

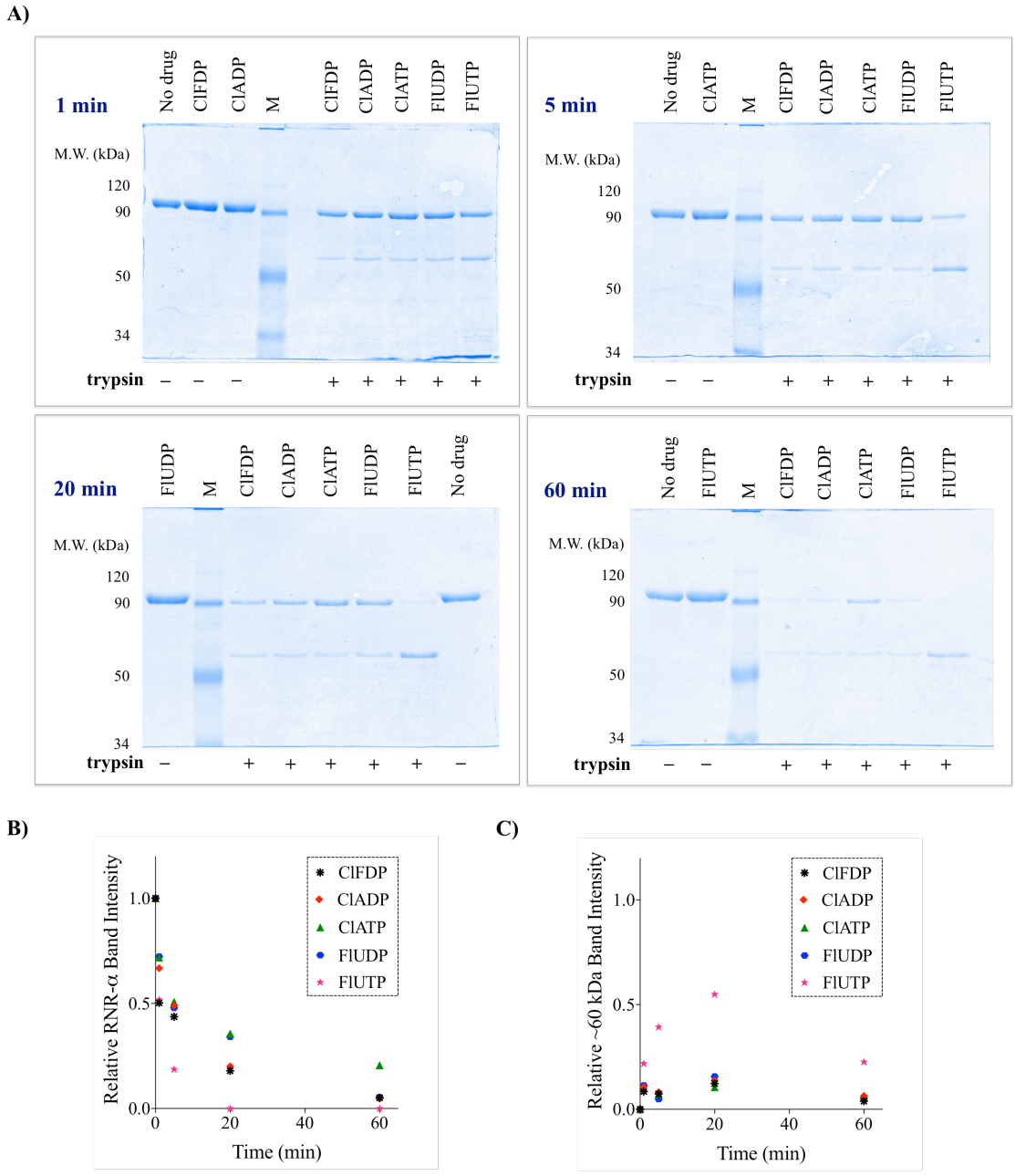

Figure 3-29. hRNR-α hexamers induced by different nucleotide inhibitors were cleaved by trypsin at different rates. **A)** SDS-PAGE analysis of the samples in which hRNR-α was pre-treated with buffer ("No drug") or indicated drugs prior to the addition of buffer containing no trypsin (−) or 1 $mg.mL^{-1}$ trypsin protease (+). M, M.W. marker. **B–C)** Relative hRNR-α (92 kDa, monomer) and ~60 kDa band

intensities of indicated drug-treated samples, respectively. To obtain the relative values, the designated band intensity of each drug-treated sample was compared to that of "No drug" sample of any particular gel.

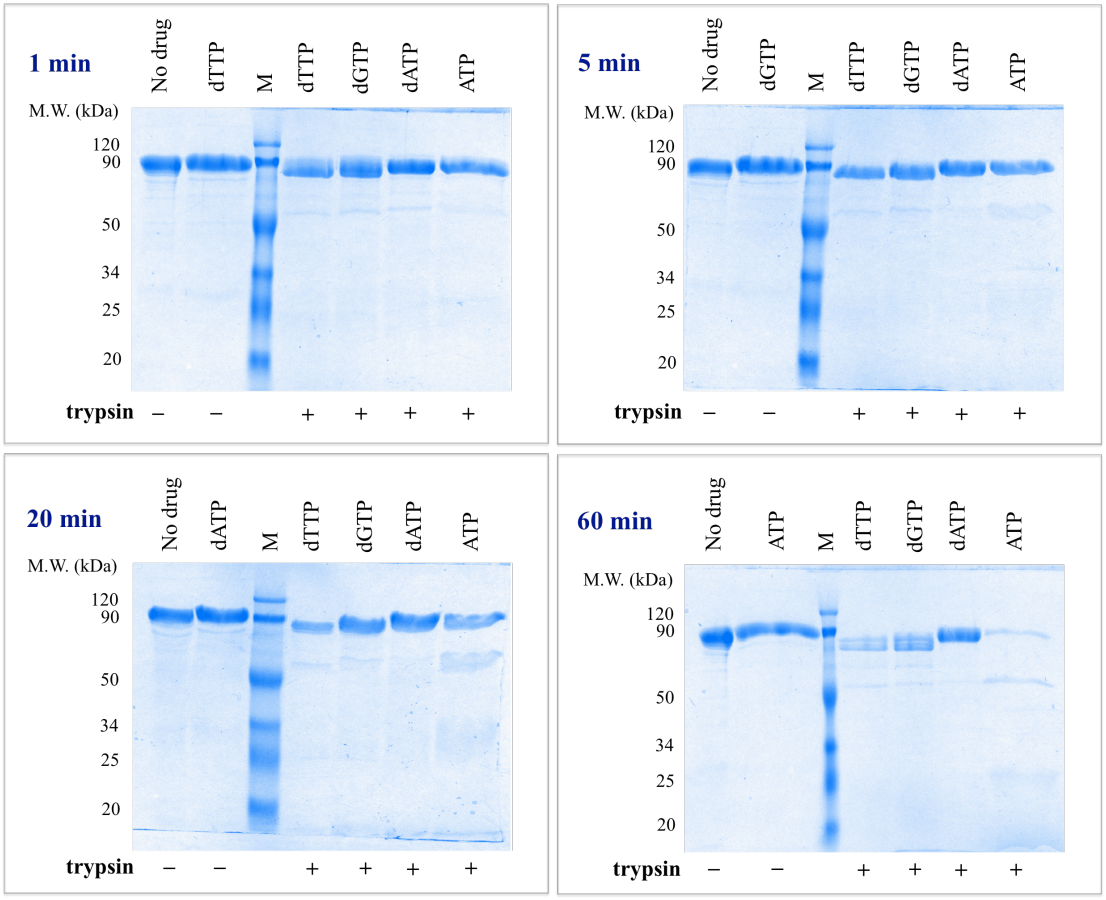

Figure 3-30. hRNR-α in the presence of natural nucleotides (dTTP, dGTP, dATP, and ATP) was resistant to trypsin. hRNR-α was pre-treated with buffer ("No drug") or natural nucleotides prior to the addition of buffer containing no trypsin (−) or 1 $mg.mL^{-1}$ trypsin protease (+). M, M.W. marker.

3.3.6 ClADP and FlUDP exhibit reversible mode of hRNR-α-specific inhibition

ClADP and FlUDP are anticipated to bind to the catalytic site (C-site) on the α-subunit as previously demonstrated for ClFDP[16] and F2CDP[6]. Similar to F2CDP and many other inactivators[6,55], the binding of ClADP and FlUDP to the C-site could possibly engage in a chemical reaction with the transient thiyl radical generated during the RNR catalytic cycle (Figure 3-31). Alternatively, like ClFDP[16], they could bind to the C-site without being chemically modified.

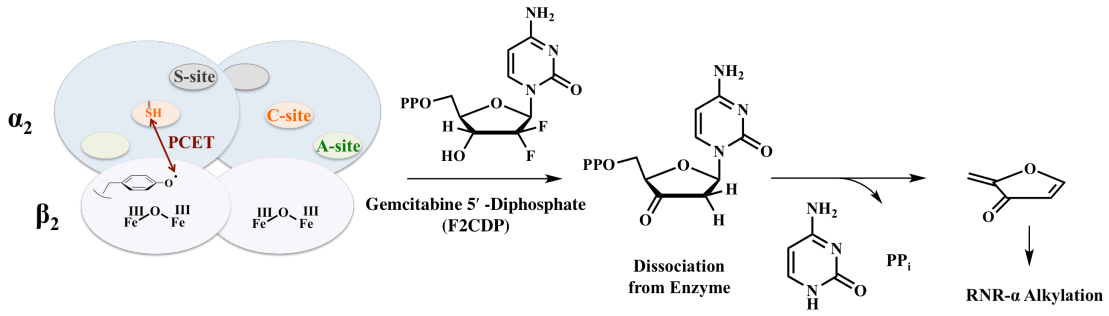

PCET, Proton-Coupled Electron Transfer.

Figure 3-31. The paradigm of irreversible RNR inactivation by F2CDP and other nucleotide analogues.[6,55]

In order to identify the mode of hRNR-α-specific inhibition by ClADP and FlUDP, we examined to what extent ClADP and FlUDP could be recovered post enzyme inhibition. A molar equivalent of ClADP was added to an assay mixture containing 1:1 hRNR-α and hRNR-β under turnover conditions to initiate enzyme inhibition. After heat-inactivation, denatured enzymes were removed, and small-molecule fraction was analyzed by HPLC (Figure 3-32).

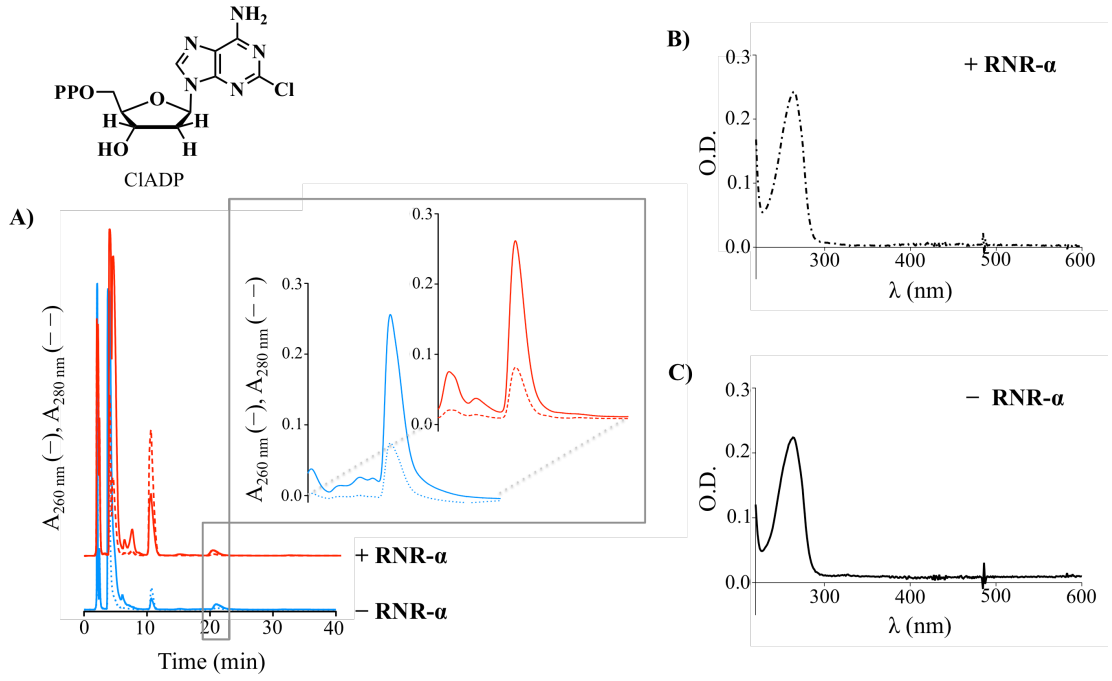

Figure 3-32. ClADP was recovered quantitatively post enzyme inhibition. **A)** HPLC diode array traces of nucleotide and other assay small-molecules extracted from inhibition mixture. Inset shows a comparison of ClADP peaks, of which retention time is ~21 minute, observed between the extracts from inhibition mixture (red) or control mixture (no enzymes, otherwise identical conditions) (blue). **B−C)** UV-visible absorbance spectra corresponding to the peak maxima at 21-minute retention time of the red (-·-·) and blue (−) HPLC traces, respectively. In both cases, λ_{max} shows at 265 nm.

If ClADP irreversibly bound to hRNR-α, we would not have been able to recover ClADP from this experiment since it would have been stuck to the enzyme and removed from the assay mixture prior to the injection into HPLC. From our two independent replicates, however, we found greater than 98% of ClADP was recovered (Figure 3-32A), which indicated the reversibility of hRNR-α inhibition induced by

ClADP. After trying the analogous experiment with FlUDP, unfortunately, FlUDP was not stable under the HPLC elution conditions.

To validate whether FlUDP reversibly induces hRNR-α inhibition, we measured the off-rate of FlUDP dissociation by monitoring a recovery of hRNR-α CDP-reductase activity upon dilution. The measurements were also extended to include FlUTP, ClADP, and ClATP. A time-dependent regain of hRNR-α activity was observed for each of the four inhibitors subsequent to dilution, and the half-lives of dissociation were all around 1–2 minutes (Figure 3-33).

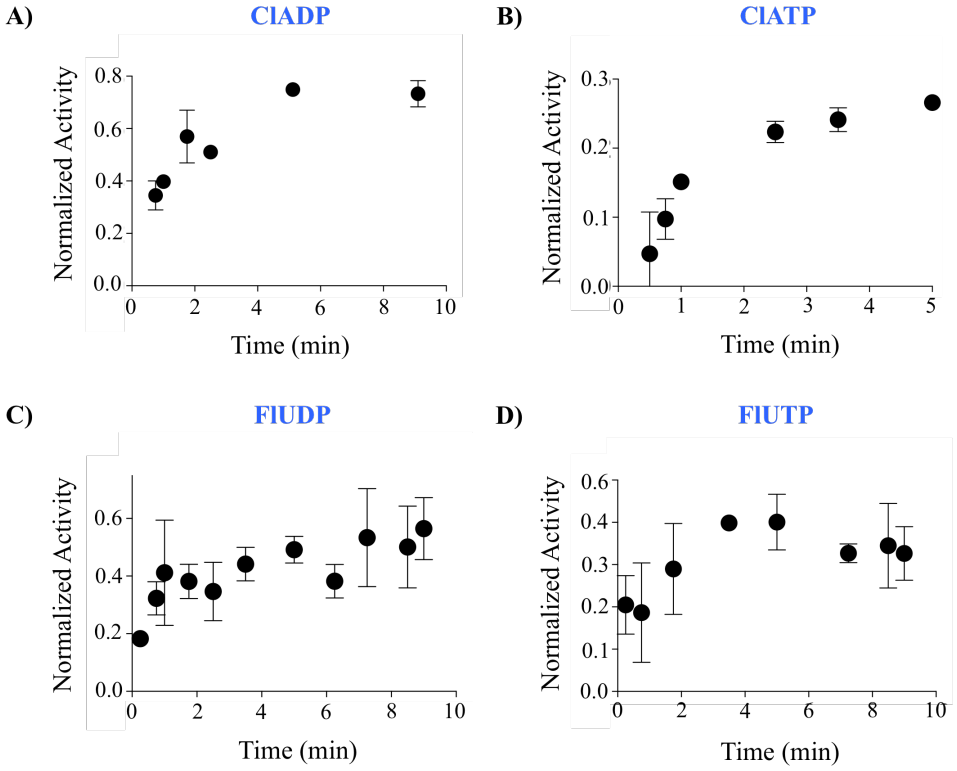

Figure 3-33. The time-dependent regain of hRNR-α-subunit-specific activity subsequent to dilution-assisted dissociations of **A)** ClADP **B)** ClATP **C)** FlUDP and **D)** FlUTP. Percentage activities were derived based on the results from control experiment where the inhibitor was replaced by assay buffer.

Based on the experimental conditions employed for inhibition and dilution, and the derived K_i values (Figure 3-21, Table 3-2), theoretical percentages of the inhibitor-bound form (E•I) formation and the E•I dissociation subsequent to dilution of each drug-treated sample were calculated and shown in Table 3-6.

Table 3-6. Theoretical percentages of the E•I formation and the E•I dissociation from each drug-treated sample. The percentages were calculated based on the estimated apparent K_i's of the inhibitors (Table 3-2) and the final concentrations of hRNR-α and respective inhibitors in the pre- or post-dilution samples.

Inhibitor	Theoretical Percentages (%)		Fold Dilution
	E•I Formation	E•I Dissociation	
ClADP	92	86	132
ClATP	85	83	165
FlUDP	90	75	33
FlUTP	93	70	33

The theoretical percentages shown in Table 3-6 represent the incompletion in E•I formation and E•I dissociation of each drug-treated sample under these conditions. Unfortunately, we were not able to increase the fold dilution due to low assay sensitivity and intrinsically low activity and stability of the mammalian enzyme.

These experimental limitations prevented us to achieve a full hRNR-α-specific activity regain (Figure 3-33). Nevertheless, we were able to observe a time-dependent regain of hRNR-α activity for each of the four inhibitors upon dilution. This affirms that these four nucleotide inhibitors reversibly inhibit hRNR-α-specific activity.

Because the hexamers induced by ClF nucleotides persist beyond inhibitor dissociation in the absence of other competitor nucleotides[57], these half-life values likely reflect off-rates of the inhibitor ligands rather than intrinsic stability of the hexamers. Since the ligand-off rate is 5–10-fold shorter than the retention time of hexameric state observed in gel filtration analysis (Figure 3-25), these data further support that the stability of different hexamers on gel filtration does not reflect different ligand residence times, but instead inherently different hRNR-α_6 states.

Thus far, we have shown that these four nucleotide analogues reversibly inhibit hRNR-α-specific activity by inducing distinct hRNR-α hexamers. We, next, investigated at which binding site(s) of the α-subunit that each inhibitor binds to.

3.3.7 Determination of binding site specificities of each nucleotide inhibitor

Based on the basis of the enzymatic activity of hRNR as an NDP reductase, binding of triphosphate nucleosides to the C-site is not possible. However, the α-subunit possesses two triphosphate-binding allosteric sites, S- and A-sites (Figure 3-34). We hence initially expected ClATP and FlUTP to bind to either the S- or the A-site, and the diphosphates of ClA and FlU to bind to the C-site at the α-subunit.

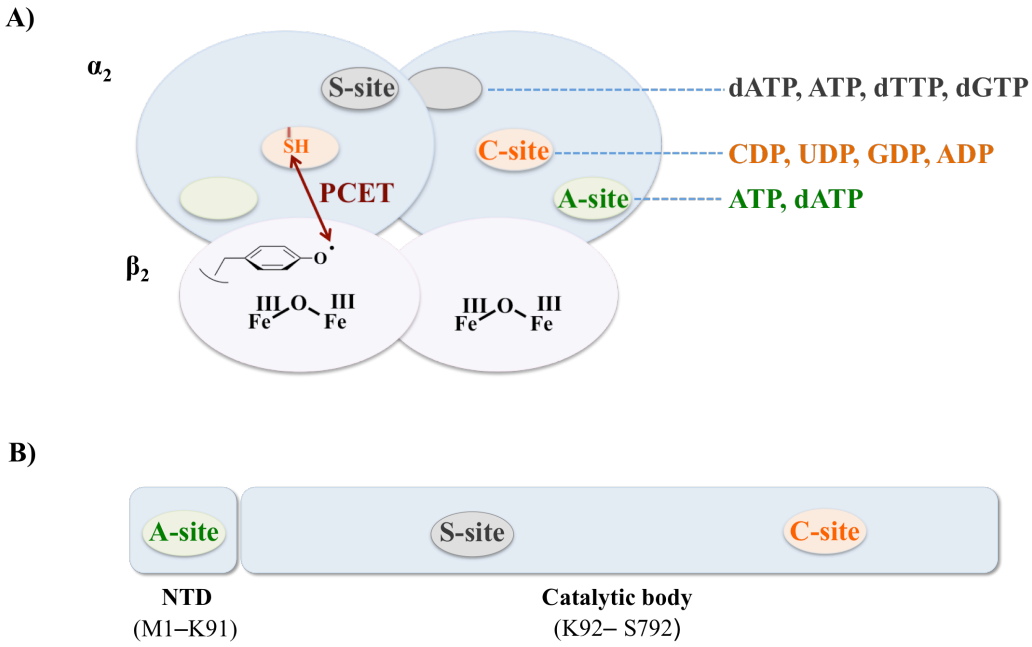

PCET, Proton-Coupled Electron Transfer; NTD, N-terminal Domain.

Figure 3-34. A) Human $\alpha_2\beta_2$ holocomplex and natural nucleotides that bind to specific site(s) at the α-subunit. **B)** Schematic representation of the two domains, NTD and catalytic body, of hRNR-α.

To verify whether or not these inhibitors bind to the A-site, we first unitized the previously characterized D57N-human RNR-α (D57N-α) mutant. A loss of the ability of the wild-type hRNR-α to discriminate between ATP and dATP at the A-site in this D57N point mutation is known.[48,58] For instance, D57N-α fails to hexamerize when treated with dATP under physiological conditions, only D57N-α-dimer is observed. Contrarily, it could still form hexamer when treated with ATP.[58] Due to the A-site defectiveness of D57N-α (Figure 3-34B), any A-site binding nucleotides hence assumed to no longer inhibit D57N-α activity. Under this assumption, the A-site

binding specificity of ClFTP was verified in 2011 by Aye and Stubbe.[16] We then examined the D57N-α-inhibiting ability of the four nucleotide inhibitors.

Under conditions where wild-typed hRNR-α was fully inhibited, the D57N-α point mutant was unresponsive to all four inhibitors at the final concentrations at least 10-fold above the measured K_i's for the wild-type (Figure 3-35). Since the binding of ClATP and FlUTP to the C-site is not possible as mentioned above, these data indicate that the triphosphates of ClA and FlU promote hRNR-α inhibition via the A-site binding, similar to ClFTP.[16] In the case of diphosphates of ClA and FlU, these observations were opposed to our expectations. Since the C-site of this mutant is known in literatures[16,60] and shown by our experimental results (Figure 3-8) to fully function, we expected to see the D57N-α inhibition upon the treatments of ClADP and FlUDP. Based on these unanticipated data (Figure 3-35, C–D), more information to inevitably identify the binding site specificity of these diphosphate inhibitors was needed. Nevertheless, these results are still striking for two reasons. First, it confirms that both ClADP and FlUDP are not mechanism-based inactivators, since the well-established mechanism-based inactivator, gemcitabine diphosphate (F2CDP), efficiently inhibits both D57N-α and the wild-type. Second, because the D57N-α is unable to adopt the deactivated α-hexameric state(s)[58,60], these data are consistent with our hypothesis that hexamerization is a prerequisite for RNR inhibition. In contrast to our results, the recently identified α_6-inducer ClFDP can inhibit D57N-α activity.[16] These differences likely reflect nuanced binding modes for the different ligands. In order to understand this phenomenon, further analyses beyond the scope of this project are required.

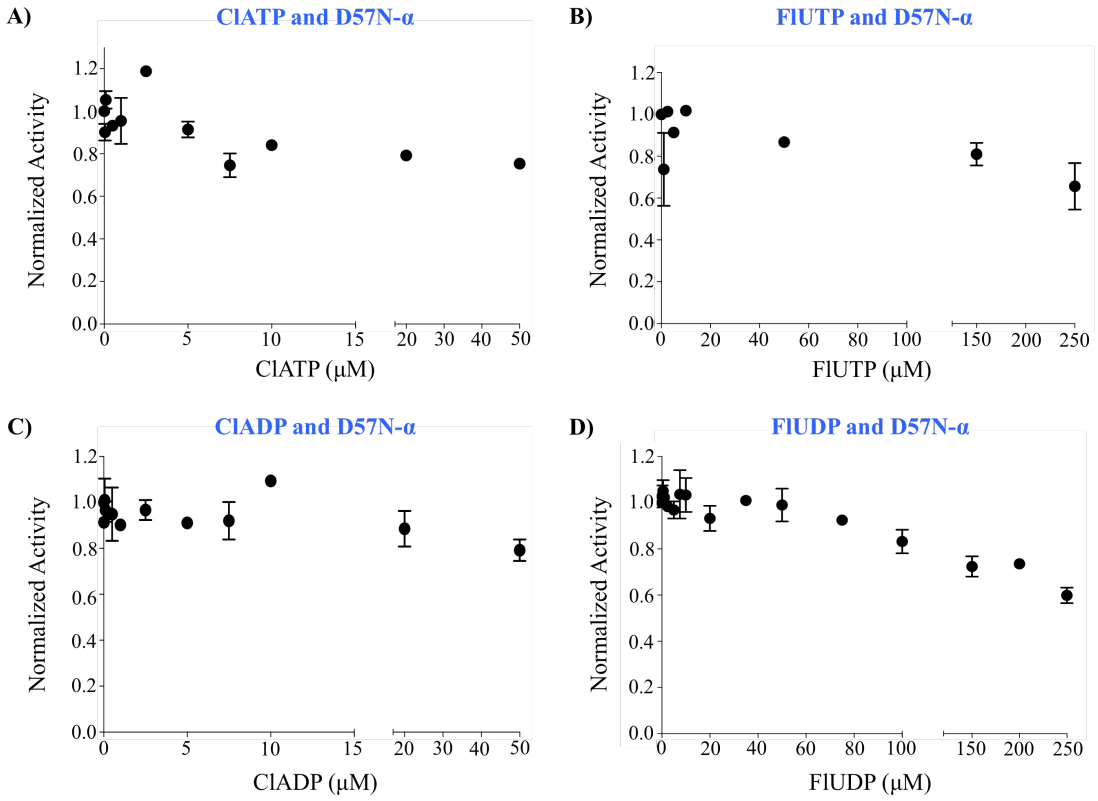

Figure 3-35. The recombinant D57N-α mutant remained largely uninhibited by **A)** ClATP, **B)** FlUTP, **C**) ClADP, and **D)** FlUDP under the conditions in which wild-type hRNR-α was inhibited (Figure 3-21). Percentage activities were calculated based on the results from control experiment where the inhibitor was replaced with assay buffer. The concentration ranges were identical to those known to sufficiently inhibit the wild-type hRNR-α (Figure 3-21, Table 3-2).

Next, we designed assays that combine fluorescence anisotropy (FA) and gel filtration analyses to further investigate the binding site specificity of ClADP and FlUDP. Because the lower K_i's of ClADP compared to FlUDP and of ClATP compared to FlUTP (Table 3-2), ClADP and ClATP were used as representative examples of FlUDP and FlUTP, respectively. We first introduced the wild-type

hRNR-α to a solution of free T*-dATP, which resulted in a significant increase in FA (Figure 3-36A). This result was consistent with the formation of a protein-ligand complex (Figure 3-20). Under these conditions in which there is no competing ligands, T*-dATP can independently bind to both S- and A-sites. Exclusive binding of nucleotide effectors to the S-site induces RNR-α dimerization. Regardless of S-site occupancy, A-site binding causes RNR-α hexamerization.[61] We next examined whether or not there is a nonspecific binding of T*-dATP to the enzymes (both wild-type and D57N-α mutant). A titration of non-labeled dATP to a solution of 6 μM of wild-type hRNR-α or D57N-α mutant and 1.2 μM of T*-dATP revealed that 700 μM dATP was sufficient to saturate both enzymes (Figure 3-36, B and D, the 4th bar from the left). However, not all of the labeled T*-dATP was displaced upon an addition of 700 μM dATP into a solution of hRNR-α and T*-dATP or D57N-α and T*-dATP. The same results were obtained even though the order of addition of T*-dATP and dATP was swapped (Figure 3-36, C and E). Even though this finding indicated the nonspecific binding of T*-dATP to the enzymes, it should not affect our assay interpretation because, in these experiments, only specific release of the dye from specific sites upon the addition of a competitive ligand matters.

Based on the inhibition assays of D57N-α, ClATP was shown to bind to the A-site at the α-subunit. We, thus, used ClATP to verify this FA assay reliability. First, saturating amount of dTTP (Figure 3-37A), an exclusive S-site binder, was introduced to a solution of hRNR-α treated with T*-dATP, in which an equilibrium of S- and A-site-bound forms was reached. We observed a 49 ± 1% drop in FA, which must represent a replacement of the S-site binding T*-dATP by the non-labeled dTTP because the S-site and the A-site are not coupled (Figure 3-38A). There is also a possibility of the compensatory binding of the displaced T*-dATP to the A-site. Subsequent addition of ClATP in a saturating amount (Figure 3-37C) to this mixture

resulted in a further 20 ± 1% decrease in FA (Figure 3-38A). The simplest explanation of these results is due to ClATP displacing some of the bound T*-dATP at the A-site. These outcomes not only added a further credence that ClATP binds to the A-site, but also validated the FA assay reliability.

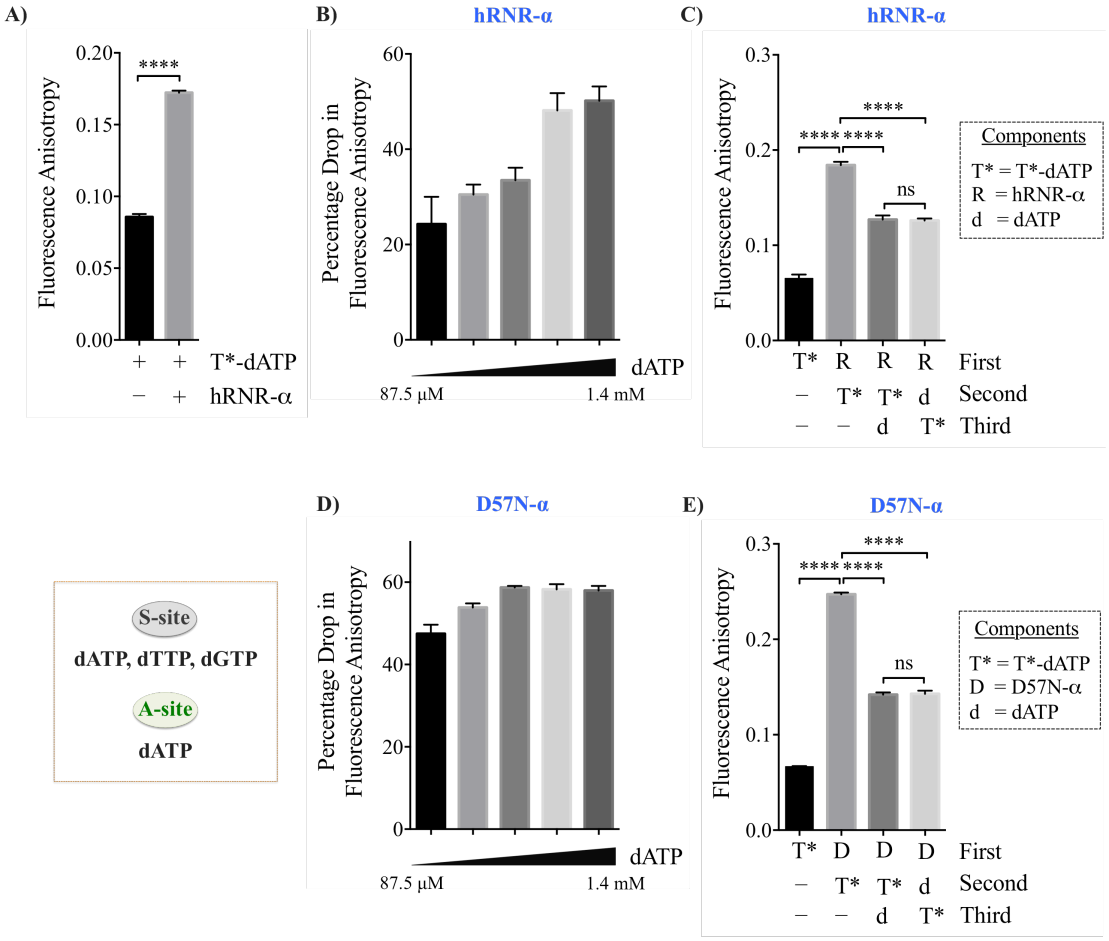

Figure 3-36. Fluorescence anisotropy (FA) studies with T*-dATP. The concentrations of T*-dATP and protein (hRNR-α or D57N-α) were kept consistent at 1.2 and 6 µM, respectively. **A)** Representative increase in FA upon addition of wild-type hRNR-α to a solution of T*-dATP. Since absolute values of FA fluctuate between different experiments, this measurement needs to be performed each time that the FA assays are

set up. However, a relative drop in FA is consistent for a given protein and ligand(s). **B**–**E)** The confirmation of nonspecific binding of T*-dATP to wild-type hRNR-α (**B**–**C**) or mutant (**D**–**E**). The saturating amount of dATP used in **C)** and **E)**, 700 μM, was judged by the titration results in **B)** and **D)**, respectively. The lowest concentration of dATP used was 87.5 μM and the concentration was doubled up to 1.4 mM. By comparing FA values from the systems in which the protein was sequentially incubated with T*-dATP and 700 μM dATP in a different order of addition, the existence of nonspecific binding of T*-dATP to these proteins was confirmed (**C** and **E**). Error bars designate SD (n=3). **Inset** shows the binding site specificities of the three natural nucleotide ligands used in these FA studies. The experimental data in this figure are interpreted on the assumption that T*-dATP binds to the same site as dATP.

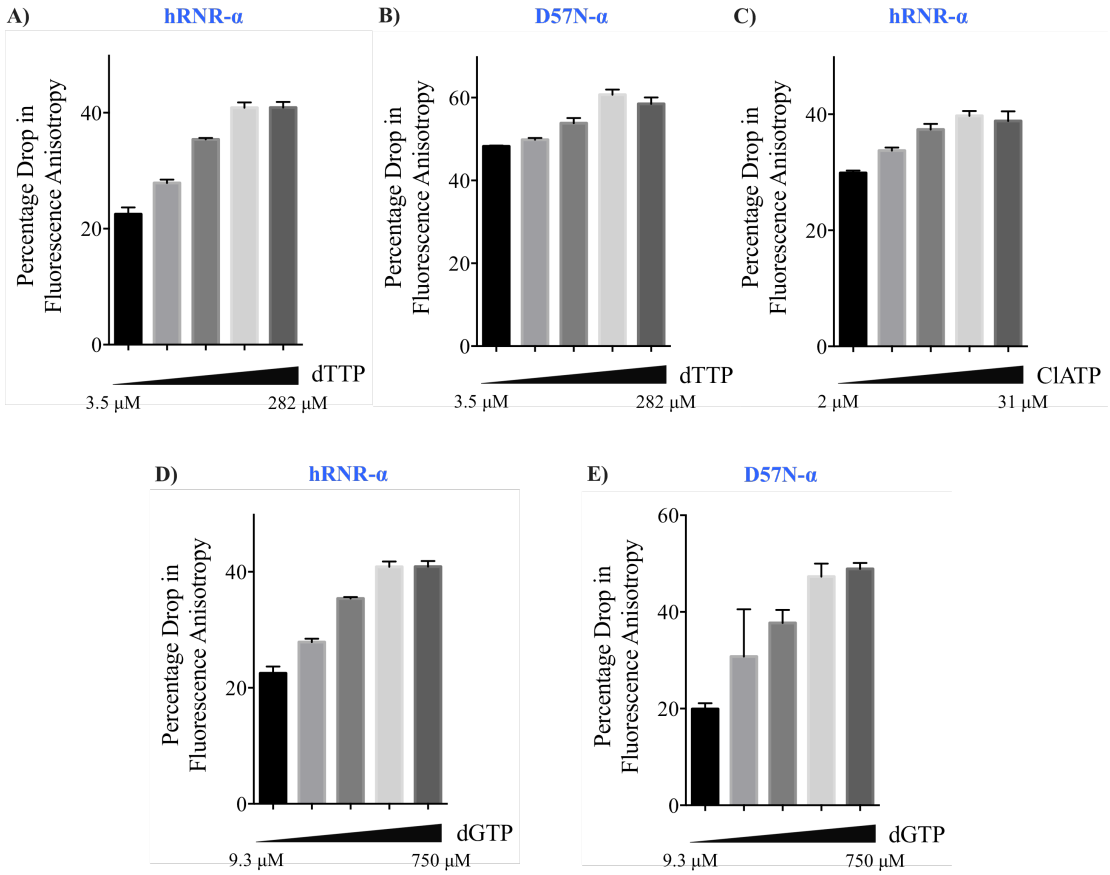

Figure 3-37. Titration studies of nucleotides into a solution of T*-dATP and wild-type hRNR-α or D57N-α. The concentrations of T*-dATP and protein (hRNR-α or D57N-α) were kept consistent at 1.2 and 6 μM, respectively. Five concentrations of each nucleotide were used (dTTP: 3.5, 10.4, 31.3, 94 and 282 μM; ClATP: 2, 4, 8, 16 and 31 μM; dGTP: 9.3, 27.8, 83.3, 250 and 750 μM). In **C)**, T*-dATP was added to hRNR-α, of which the S-site was pre-blocked with suturing amount of dTTP (94 μM, Figure 3-37A). Then, ClATP was added to the mixture prior to FA measurement. Error bars designate SD (n=3). The experimental data in this figure are interpreted on the assumption that T*-dATP binds to the same site as dATP.

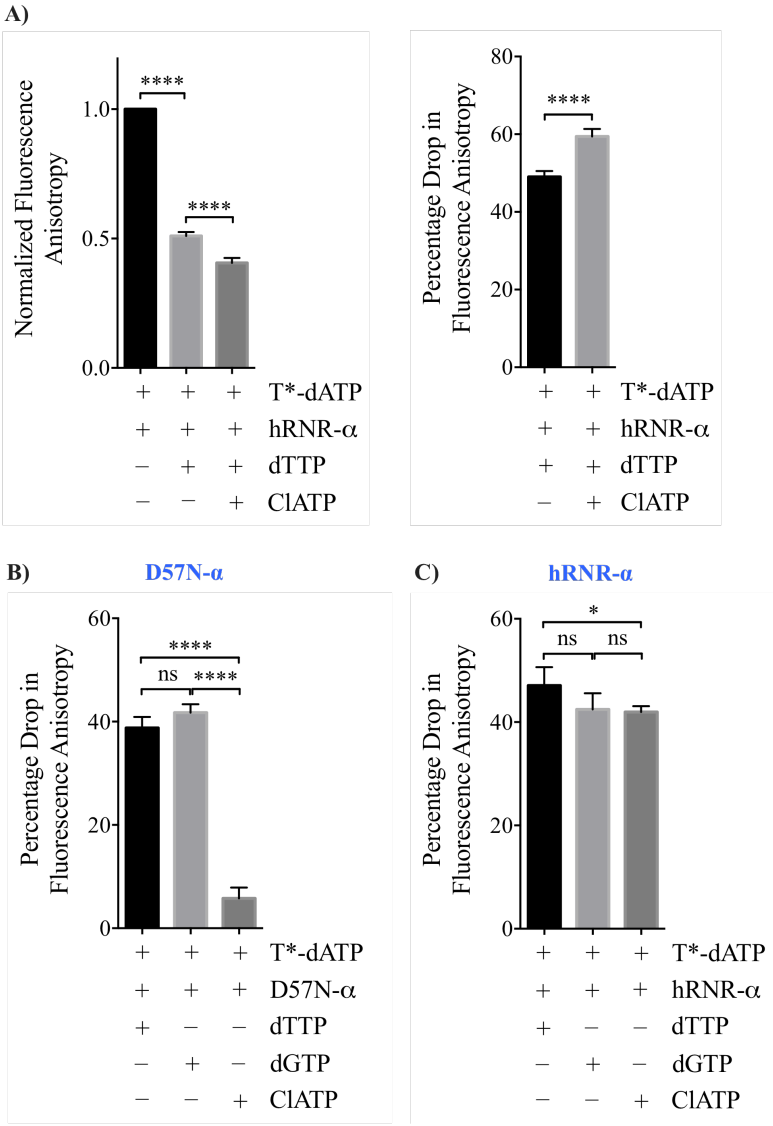

Figure 3-38. Determination of ClATP binding site specificity by fluorescence anisotropy (FA). The concentrations of T*-dATP, protein (hRNR-α or D57N-α), ClATP, dTTP, dGTP were 1.2, 6, 31, 94, and 250 μM, respectively. **A)** Addition of ClATP to a solution containing hRNR-α, T*-dATP (S- and A-site binder) and dTTP (S-site exclusive binder) resulted in a decrease in FA, suggesting ClATP binds to the A-site at the α-subunit. **B)** Addition of ClATP to a sample containing the defective-A-site-binding D57N-α mutant and T*-dATP, which exclusively binds to the S-site of

the mutant, led to a small decrease in FA compared to the values obtained when the S-site exclusive binders (dTTP or dGTP) were added. **C)** When wild-type hRNR-α was used in place of the mutant, T*-dATP can bind to both S- and A-sites. Thus, upon ClATP addition, a higher drop in FA compared to that shown in **B)** was observed. Error bars designate SD (n=3). The experimental data in this figure are interpreted on the assumption that T*-dATP binds to the same site as dATP.

In another set of experiments, we made use of both wild-type hRNR-α and D57N-α mutant. First, 6 μM of the A-site-defective D57N-α mutant was incubated with 1.2 μM T*-dATP. Since the A-site is not available in this mutant, the binding of T*-dATP was thus exclusive to the S-site. By adding a saturating amount of dTTP (94 μM, Figure 3-37B), we observed a 39 ± 1% drop in FA (Figure 3-38B). A same level of percentage drop in FA was observed when an alternative S-site-only binder, dGTP, was used in placed of dTTP. In contrast, the addition of ClATP gave a ~7-fold less decrease in FA compared to that observed in dTTP or dGTP (Figure 3-38B). Second, when these experiments were repeated with wild-type hRNR-α, ClATP gave rise to a significantly higher drop in FA (Figure 3-38C). This data set further confirmed the A-site-binding specificity of ClATP. Although the allosteric regulation of RNR is complicated, the FA data (Figure 3-38) together with the D57N-α inhibition analysis (Figure 3-35, A–B) are strongly consistent with the triphosphates of ClA and FlU bind to the A-site.

Next, we performed two independent sets of experiments to demonstrate that ClADP, a representative example of the diphosphate inhibitors, does indeed associate with the C-site. In the first set of experiments, wild-type hRNR-α was incubated with saturating amount of dATP (for both S- and A-sites) such that only the C-site was available for any newly added ligands. Under these conditions, hRNR-α adopts

hexameric states. After splitting the sample into two equal portions, ClADP and assay buffer were separately added to the first and second portions, namely sample A and B, respectively. Each sample was injected into a gel filtration column, which had been pre-equilibrated with running buffer containing no inhibitors, and the oligomeric state of eluted hRNR-α was evaluated. A hexameric peak was observed only in sample A (Figure 3-39A, magenta trace). Our gel filtration result in this study with ClADP (Figure 3-25C) showed that hRNR-α pre-treated with ClADP maintained its hexameric state, a remarkable feature of kinetic stability that unique to the drug-induced hexamers, even when there was no ClADP in the running buffer. Gel filtration results in previous studies with dATP from us[16] and others[3], on the other hand, have shown that in the absence of excess dATP in the running buffer, RNR-α pre-treated with excess dATP only elutes as low-order species. Thus, in the present experiment, the observation of any hexameric peaks in the gel filtration profile from sample A (and not in the control sample B) could only be a result from the interaction of ClADP with the C-site of hRNR-α, generating the observed kinetically stable hexamers.

In the second set of experiments, FA measurements were coupled with gel filtration analysis. Wild-type hRNR-α (6 μM) was incubated with T*-dATP (1.2 μM), and the S-site was subsequently blocked by dTTP in saturating amount (94 μM, Figure 3-37A). We first showed the similar decrease in FA (~50%, Figure 3-39B, *left panel*) compared to the change obtained in Figure 3-38A (*right panel*). Then, the sample mixture was either treated with the suturing amount of ClADP (75 μM) or assay buffer (for control). The addition of ClADP caused no statistically significant changes in FA (Figure 3-39B, *left panel*), unlike the addition of ClATP, which resulted in ~20% further drop in FA due to T*-dATP displacement (Figure 3-38A, *right panel*). These results suggested that ClADP interacts with neither S- nor A-sites. When these samples were separately analyzed by gel filtration analysis, the sample treated with

ClADP resulted in an appreciable fraction of hexamers, whereas the control sample eluted exclusively as a monomer (Figure 3-39B, *right panel*). Thus, T*-dATP and ClADP must occupy hRNR-α simultaneously under the conditions where ClADP site occupancy is appreciable, thereby leading to a significant proportion of α-hexameric state in the elution profile. These two sets of experiments (Figure 3-39) provided convincing evidence that ClADP induces hRNR-α hexamerization through interaction with the C-site only.

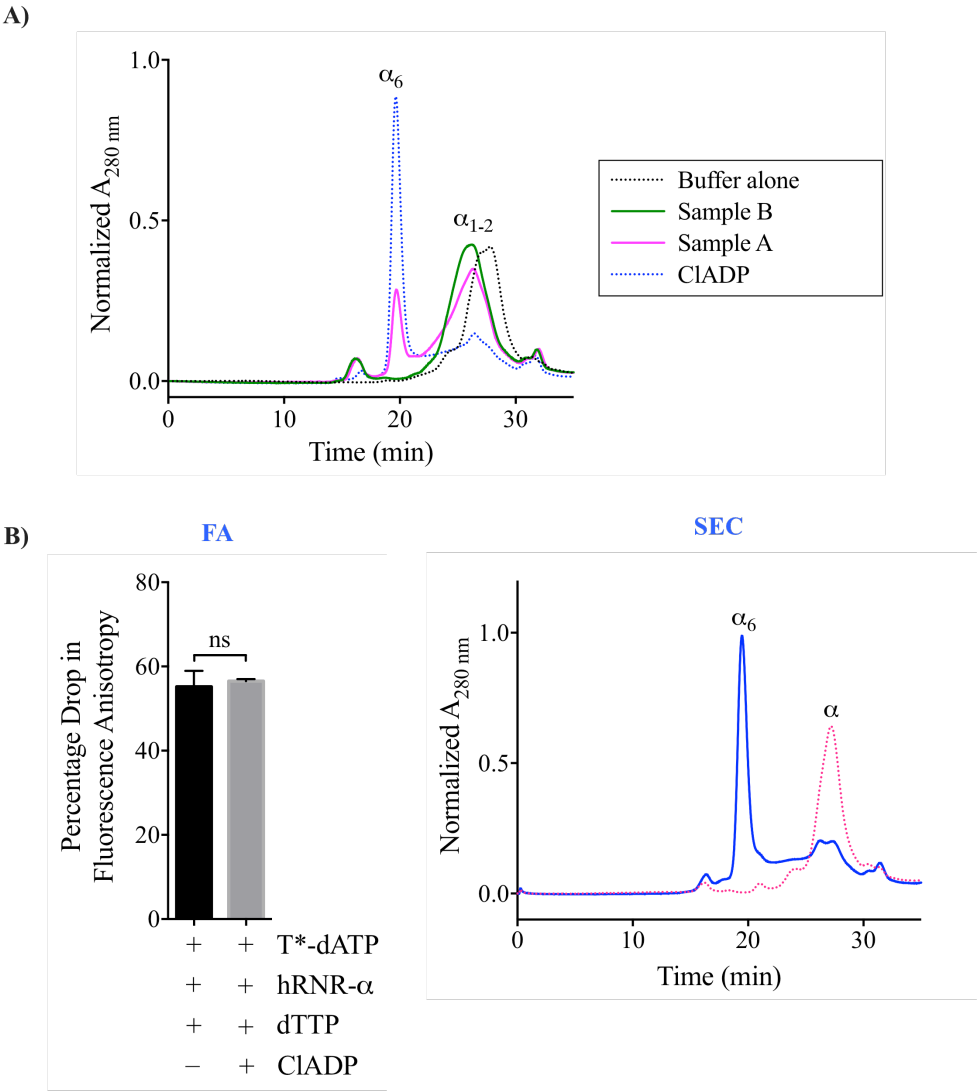

Figure 3-39. Determination of ClADP binding site specificity using both gel filtration analysis and fluorescence anisotropy (FA). **A)** ClADP C-site-binding specificity determined by size exclusion chromatography (SEC). Gel filtration analysis of hRNR-α treated with assay buffer alone (black trace), saturating amounts of dATP alone (green trace, *sample B*), ClADP alone (blue trace), or both (magenta trace, *sample A*). α_6 peak observed only when ClADP was additionally included, but not in the dATP-saturated sample where both S- and A-sites occupied. This suggested that

ClADP binds at the C-site. **B)** ClADP C-site-binding specificity determined by FA coupled with gel filtration analysis. ClADP caused no statistically significant changes in FA consistent with ClADP interacts with neither the S- nor A-sites (*left panel*). Upon direct injection of the sample treated with ClADP (the second bar in the plot), a considerable fraction of hRNR-α hexamers was observed, whereas a sole monomer peak was observed in the control sample (the first bar in the plot). Error bars designate SD (n=3). The experimental data in this figure are interpreted on the assumption that T*-dATP binds to the same site as dATP.

Conclusions

In this chapter, we have shown that hRNR enzyme inhibition is coupled with α-hexamerization. This coupling is insinuated by the fact that the K_i's for all of the inhibitors studied (Figure 3-21, Table 3-2) and the EC_{50}'s of oligomerization (Figure 3-24, Table 3-3) have similar values. This finding helps elucidate why the diphosphates of ClF, ClA, and FlU are not RNR mechanism-based inhibitors, because a binding of these diphosphates under this model requires rapid modulation of hRNR-α to a conformation that is incapable of PCET.

Our inhibition assays showed that ClA and FlU nucleotides bind to hRNR-α with diverse affinities (Table 3-2), which fairly dispersed in a range of 0.5–10 μM. These nucleotides also showed comparable off-rates within minutes time-scale, which is 5–10-fold shorter than a time-scale of our gel filtration experiments (Figure 3-25 and 3-33). Under the gel filtration time-scale, FlUDP eluted solely as a monomer unless FlUDP was also included in the running buffer. The hRNR-α-hexameric states from other drug-treated samples, on the other hand, did not require any inhibitor supplementation in the running buffer to maintain their hexameric states (Figure 3-25,

B–D, F and Figure 3-39, A and C). These data suggested that different nucleotide inhibitors induce structurally different hexamers, which were retained after ligand dissociation. The divergent conformations of these drug-induced hexameric states were further confirmed by the 2D averages of the drug-induced-ring-shaped particles obtained from our EM studies together with the different rates of trypsin protease cleavage among these hexamers (Figure 3-26, 3-28, 3-29 and 3-30).

The oligomerization-defective mutant, D57N-α, and fluorescence anisotropy (FA) were used as tools to determine binding site specificity of these nucleotide inhibitors. Even though the D57N-α mutant cannot hexamerized[58, 60], its C-site is still available and active[16] (Figure 3-8). As expected, ClATP and FlUTP failed to inhibit D57N-α under the conditions that they inhibited wild-type hRNR-α (Figure 3-35, A–B). This observation and the FA data (Figure 3-38) suggest that the triphosphates exclusively interact with the A-site. Unexpectedly, both ClADP and FlUDP, the enzyme-substrate analogues, failed to inhibit the mutant activity (Figure 3-35, C–D). This might be a result from a cross-talk between the C- and the A-sites upon a diphosphate-inhibitor binding. By performing FA assays coupled with gel filtration analysis, the C-site-binding specificity of these diphosphates was confirmed (Figure 3-39). Based on the results from these two independent sets of experiments, we proposed that ClADP and FlUDP must not only bind to the substrate-binding C-site but also induce the α-hexameric state.

REFERENCE

[1] Shao, J., Zhou, B., Chu, B., and Yen, Y. (2006) Ribonucleotide reductase inhibitors and future drug design. *Curr. Cancer Drug Targets 6*, 409-431.

[2] Kolberg, M., Strand, K. R., Graff, P., and Andersson, K. K. (2004) Structure, function, and mechanism of ribonucleotide reductases. *Biochim. Biophys. Acta. 1699*, 1-34.

[3] Hofer, A., Crona, M., Logan, D. T., and Sjoberg, B.-M. (2012) DNA building blocks: keeping control of manufacture. *Critical Reviews in Biochemistry and Molecular Biology 47*, 50-63.

[4] Robins, M. J. (2003) Ribonucleotide Reductases: Radical Chemistry and Inhibition at the Active Site. *Nucleosides, Nucleotides and Nucleic Acids 22*, 519-534.

[5] Cerqueira, N. M., Pereira, S., Fernandes, P. A., and Ramos, M. J. (2005) Overview of ribonucleotide reductase inhibitors: an appealing target in anti-tumour therapy. *Curr. Med. Chem. 12*, 1283-1294.

[6] Stubbe, J., and van der Donk, W. A. (1995) Ribonucleotide reductases: radical enzymes with suicidal tendencies. *Chem. Biol. 2*, 793-801.

[7] Plunkett, W., Huang, P., and Gandhi, V. (1997) Gemcitabine: Actions and Interactions. *NUcleosides and Nucleotides 16*, 1261-1270.

[8] Silva, D. J., Stubbe, J., Samano, V., and Robins, M. J. (1998) Gemcitabine 5'-triphosphate is a stoichiometric mechanism-based inhibitor of *Lactobacillus leichmannii* ribonucleoside triphosphate reductase: evidence for thiyl radical-mediated nucleotide radical formation. *Biochemistry 37*, 5528-5535.

[9] van der Donk, W. A., Yu, G., Perez, L., Sanchez, R. J., Stubbe, J., Samano, V., and Robins, M. J. (1998) Detection of a new substrate-derived radical during inactivation of ribonucleotide reductase from *Escherichia coli* by gemcitabine 5'-diphosphate. *Biochemistry 37*, 6419-6426.

[10] Xu, H., Faber, C., Uchiki, T., Racca, J., and Dealwis, C. (2006) Structures of eukaryotic ribonucleotide reductase I define gemcitabine diphosphate binding and subunit assembly. *Proc. Natl. Acad. Sci. U. S. A. 103*, 4028-4033.

[11] Xu, H., Faber, C., Uchiki, T., Fairman, J. W., Racca, J., and Dealwis, C. (2006) Structures of eukaryotic ribonucleotide reductase I provide insights into dNTP regulation. *Proc. Natl. Acad. Sci. U. S. A. 103*, 4022-4027.

[12] Ator, M. A., and Stubbe, J. (1985) Mechanism of inactivation of *Escherichia coli* ribonucleotide reductase by 2'-chloro-2'-deoxyuridine 5'-diphosphate: evidence for generation of a 2'-deoxy-3'-ketonucleotide via a net 1,2-hydrogen shift. *Biochemistry 24*, 7214-7221.

[13] Jordheim, L. P., Durantel, D., Zoulim, F., and Dumontet, C. (2013) Advances in the development of nucleoside and nucleotide analogues for cancer and viral diseases. *Nat. Rev. Drug Discov. 12*, 447-464.

[14] Damaraju, V. L., Damaraju, S., Young, J. D., Baldwin, S. A., Mackey, J., Sawyer, M. B., and Cass, C. E. (2003) Nucleoside anticancer drugs: the role of

nucleoside transporters in resistance to cancer chemotherapy. *Oncogene. 22*, 7524-7536.

[15] Xie, K. C., and Plunkett, W. (1996) Deoxynucleotide pool depletion and sustained inhibition of ribonucleotide reductase and DNA synthesis after treatment of human lymphoblastoid cells with 2-chloro-9-(2-deoxy-2-fluoro-β -D-arabinofuranosyl) adenine. *Cancer Res. 56*, 3030-3037.

[16] Aye, Y., and Stubbe, J. (2011) Clofarabine 5'-di and -triphosphates inhibit human ribonucleotide reductase by altering the quaternary structure of its large subunit. *Proc. Natl. Acad. Sci. U. S. A. 108*, 9815-9820.

[17] Jeha, S., Gandhi, V., Chan, K. W., McDonald, L., Ramirez, I., Madden, R., Rytting, M., Brandt, M., Keating, M., Plunkett, W., and Kantarjian, H. (2004) Clofarabine, a novel nucleoside analog, is active in pediatric patients with advanced leukemia. *Blood 103*, 784-789.

[18] Parker, W. B., Shaddix, S. C., Chang, C. H., White, E. L., Rose, L. M., Brockman, R. W., Shortnacy, A. T., Montgomery, J. A., Secrist, J. A., 3rd, and Bennett, L. L., Jr. (1991) Effects of 2-chloro-9-(2-deoxy-2-fluoro-β-D-arabinofuranosyl)adenine on K562 cellular metabolism and the inhibition of human ribonucleotide reductase and DNA polymerases by its 5'-triphosphate. *Cancer Res. 51*, 2386-2394.

[19] Galmarini, C. M., Mackey, J. R., and Dumontet, C. (2001) Nucleoside analogues: mechanisms of drug resistance and reversal strategies. *Leukemia 15*, 875-890.

[20] Keating, M. J., O'Brien, S., Plunkett, W., Robertson, L. E., Gandhi, V., Estey, E., Dimopoulos, M., Cabanillas, F., Kemena, A., and Kantarjian, H. (1994) Fludarabine phosphate: a new active agent in hematologic malignancies. *Semin. Hematol. 31*, 28-39.

[21] Krance, R. A., Hurwitz, C. A., Head, D. R., Raimondi, S. C., Behm, F. G., Crews, K. R., Srivastava, D. K., Mahmoud, H., Roberts, W. M., Tong, X., Blakley, R. L., and Ribeiro, R. C. (2001) Experience with 2-chlorodeoxyadenosine in previously untreated children with newly diagnosed acute myeloid leukemia and myelodysplastic diseases. *J. Clin. Oncol. 19*, 2804-2811.

[22] Chun, H. G., Leyland-Jones, B., and Cheson, B. D. (1991) Fludarabine phosphate: a synthetic purine antimetabolite with significant activity against lymphoid malignancies. *J. Clin. Oncol. 9*, 175-188.

[23] Dimopoulos, M. A., Kantarjian, H., Weber, D., O'Brien, S., Estey, E., Delasalle, K., Rose, E., Cabanillas, F., Keating, M., and Alexanian, R. (1994) Primary therapy of Waldenstrom's macroglobulinemia with 2-chlorodeoxyadenosine. *J Clin Oncol 12*, 2694-2698.

[24] Lindemalm, S., Liliemark, J., Gruber, A., Eriksson, S., Karlsson, M. O., Wang, Y., and Albertioni, F. (2003) Comparison of cytotoxicity of 2-chloro-2'-arabino-fluoro-2'-deoxyadenosine (clofarabine) with cladribine in mononuclear cells from patients with acute myeloid and chronic lymphocytic leukemia. *Haematologica 88*, 324-332.

[25] Seymour, J. F., Kurzrock, R., Freireich, E. J., and Estey, E. H. (1994) 2-chlorodeoxyadenosine induces durable remissions and prolonged suppression of $CD4^+$ lymphocyte counts in patients with hairy cell leukemia. *Blood 83*, 2906-2911.

[26] Steeper, J. R., and Steuart, C. D. (1970) A rapid assay for CDP reductase activity in mammalian cell extracts. *Anal. Biochem. 34*, 123-130.

[27] Fu, Y., Lin, H. Y., Wisitpitthaya, S., Blessing, W. A., and Aye, Y. (2014) A fluorimetric readout reporting the kinetics of nucleotide-induced human ribonucleotide reductase oligomerization. *ChemBioChem 15*, 2598-2604.

[28] Artin, E., Wang, J., Lohman, G. J., Yokoyama, K., Yu, G., Griffin, R. G., Bar, G., and Stubbe, J. (2009) Insight into the mechanism of inactivation of ribonucleotide reductase by gemcitabine 5'-diphosphate in the presence or absence of reductant. *Biochemistry 48*, 11622-11629.

[29] Fu, Y., Long, M. J., Rigney, M., Parvez, S., Blessing, W. A., and Aye, Y. (2013) Uncoupling of allosteric and oligomeric regulation in a functional hybrid enzyme constructed from *Escherichia coli* and human ribonucleotide reductase. *Biochemistry 52*, 7050-7059.

[30] Wang, J., Lohman, G. J., and Stubbe, J. (2007) Enhanced subunit interactions with gemcitabine-5'-diphosphate inhibit ribonucleotide reductases. *Proc. Natl. Acad. Sci. U. S. A. 104*, 14324-14329.

[31] Bradford, M. M. (1976) A rapid and sensitive method for the quantitation of microgram quantities of protein utilizing the principle of protein-dye binding. *Anal. Biochem. 72*, 248-254.

[32] Stoscheck, C. M. (1990) Quantitation of protein. *Methods Enzymol. 182*, 50-68.

[33] Bollinger, J. M., Jr., Tong, W. H., Ravi, N., Huynh, B. H., Edmondson, D. E., and Stubbe, J. A. (1995) Use of rapid kinetics methods to study the assembly of the diferric-tyrosyl radical cofactor of *E. coli* ribonucleotide reductase. *Methods Enzymol. 258*, 278-303.

[34] Aye, Y., Long, M. J., and Stubbe, J. (2012) Mechanistic studies of semicarbazone triapine targeting human ribonucleotide reductase *in vitro* and in mammalian cells: tyrosyl radical quenching not involving reactive oxygen species. *J. Biol. Chem. 287*, 35768-35778.

[35] Rova, U., Goodtzova, K., Ingemarson, R., Behravan, G., Graslund, A., and Thelander, L. (1995) Evidence by site-directed mutagenesis supports long-range electron transfer in mouse ribonucleotide reductase. *Biochemistry 34*, 4267-4275.

[36] Zhou, B., Shao, J., Su, L., Yuan, Y. C., Qi, C., Shih, J., Xi, B., Chu, B., and Yen, Y. (2005) A dityrosyl-diiron radical cofactor center is essential for human ribonucleotide reductases. *Mol. Cancer Ther. 4*, 1830-1836.

[37] Tamura, T., and Stadtman, T. C. (1996) A new selenoprotein from human lung adenocarcinoma cells: purification, properties, and thioredoxin reductase activity. *Proc. Natl. Acad. Sci. U. S. A. 93*, 1006-1011.

[38] Riddles, P. W., Blakeley, R. L., and Zerner, B. (1979) Ellman's reagent: 5,5'-dithiobis(2-nitrobenzoic acid)--a reexamination. *Anal. Biochem. 94*, 75-81.

[39] Copeland, R. A. (2009) *Evaluation of Enzyme Inhibitors in Drug Discovery: A Guide for Medicinal Chemists and Pharmacologists* (2nd Ed.), John Wiley & Sons Inc., New Jersey.

[40] Clegg, R. M. (1992) Fluorescence resonance energy transfer and nucleic acids. *Methods Enzymol. 211*, 353-388.

[41] Ando, N., Li, H., Brignole, E. J., Thompson, S., McLaughlin, M. I., Page, J. E., Asturias, F. J., Stubbe, J., and Drennan, C. L. (2016) Allosteric Inhibition of Human Ribonucleotide Reductase by dATP Entails the Stabilization of a Hexamer. *Biochemistry 55*, 373-381.

[42] Ludtke, S. J., Baldwin, P. R., and Chiu, W. (1999) EMAN: semiautomated software for high-resolution single-particle reconstructions. *J. Struct. Biol. 128*, 82-97.

[43] Kocsis, E., Cerritelli, M. E., Trus, B. L., Cheng, N., and Steven, A. C. (1995) Improved methods for determination of rotational symmetries in macromolecules. *Ultramicroscopy 60*, 219-228.

[44] Marabini, R., Masegosa, I. M., San Martin, M. C., Marco, S., Fernandez, J. J., de la Fraga, L. G., Vaquerizo, C., and Carazo, J. M. (1996) Xmipp: An Image Processing Package for Electron Microscopy. *J. Struct. Biol. 116*, 237-240.

[45] Sorzano, C. O., Marabini, R., Velazquez-Muriel, J., Bilbao-Castro, J. R., Scheres, S. H., Carazo, J. M., and Pascual-Montano, A. (2004) XMIPP: a new generation of an open-source image processing package for electron microscopy. *J. Struct. Biol. 148*, 194-204.

[46] Scheres, S. H., Nunez-Ramirez, R., Sorzano, C. O., Carazo, J. M., and Marabini, R. (2008) Image processing for electron microscopy single-particle analysis using XMIPP. *Nat. Protoc. 3*, 977-990.

[47] Scheres, S. H., Valle, M., Nunez, R., Sorzano, C. O., Marabini, R., Herman, G. T., and Carazo, J. M. (2005) Maximum-likelihood multi-reference refinement for electron microscopy images. *J. Mol. Biol. 348*, 139-149.

[48] Reichard, P., Eliasson, R., Ingemarson, R., and Thelander, L. (2000) Cross-talk between the allosteric effector-binding sites in mouse ribonucleotide reductase. *J. Biol. Chem. 275*, 33021-33026.

[49] Chimploy, K., and Mathews, C. K. (2001) Mouse ribonucleotide reductase control: influence of substrate binding upon interactions with allosteric effectors. *J. Biol. Chem. 276*, 7093-7100.

[50] Kakehi, K., Oda, Y., and Kinoshita, M. (2001) Fluorescence polarization: analysis of carbohydrate-protein interaction. *Anal. Biochem. 297*, 111-116.

[51] Lundblad, J. R., Laurance, M., and Goodman, R. H. (1996) Fluorescence polarization analysis of protein-DNA and protein-protein interactions. *Mol. Endocrinol. 10*, 607-612.

[52] Kimple, A. J., Yasgar, A., Hughes, M., Jadhav, A., Willard, F. S., Muller, R. E., Austin, C. P., Inglese, J., Ibeanu, G. C., Siderovski, D. P., and Simeonov, A. (2008) A high throughput fluorescence polarization assay for inhibitors of the GoLoco motif/G-α interaction. *Comb. Chem. High Throughput Screen 11*, 396-409.

[53] Rossi, A. M., and Taylor, C. W. (2011) Analysis of protein-ligand interactions by fluorescence polarization. *Nat. Protoc. 6*, 365-387.
[54] Lackowicz, J. R. (2006) *Principles of Fluorescence Spectroscopy* (3rd Ed.), pp 353-354, 361-364, Springer, New York.
[55] Licht, S., and Stubbe, J. (1999) *Mechanistic Investigations of Ribonucleotide Reductase* (Pourler, C. D., Ed.), pp 163-203, Elsevier, Amsterdam.
[56] Aye, Y., Li, M., Long, M. J., and Weiss, R. S. (2015) Ribonucleotide reductase and cancer: biological mechanisms and targeted therapies. *Oncogene. 34*, 2011-2021.
[57] Aye, Y., Brignole, E. J., Long, M. J., Chittuluru, J., Drennan, C. L., Asturias, F. J., and Stubbe, J. (2012) Clofarabine targets the large subunit (α) of human ribonucleotide reductase in live cells by assembly into persistent hexamers. *Chem. Biol. 19*, 799-805.
[58] Fairman, J. W., Wijerathna, S. R., Ahmad, M. F., Xu, H., Nakano, R., Jha, S., Prendergast, J., Welin, R. M., Flodin, S., Roos, A., Nordlund, P., Li, Z., Walz, T., and Dealwis, C. G. (2011) Structural basis for allosteric regulation of human ribonucleotide reductase by nucleotide-induced oligomerization. *Nat. Struct. Mol. Biol. 18*, 316-322.
[59] Olsen, J. V., Ong, S. E., and Mann, M. (2004) Trypsin cleaves exclusively C-terminal to arginine and lysine residues. *Mol. Cell Proteomics 3*, 608-614.
[60] Kashlan, O. B., and Cooperman, B. S. (2003) Comprehensive model for allosteric regulation of mammalian ribonucleotide reductase: refinements and consequences. *Biochemistry 42*, 1696-1706.
[61] Wisitpitthaya, S., Zhao, Y., Long, M. J., Li, M., Fletcher, E. A., Blessing, W. A., Weiss, R. S., and Aye, Y. (2016) Cladribine and Fludarabine Nucleotides Induce Distinct Hexamers Defining a Common Mode of Reversible RNR Inhibition. *ACS Chem. Biol. 11*, 2021-2032.

CHAPTER 4

In Cell Studies of Cladribine and Fludarabine

4.1 Introduction

Cladribine (ClA) and Fludarabine (FlU) are purine nucleoside analogues that are currently used in treatments of lymphoproliferative disorders.[1] These two drugs were developed after the discovery of an anticancer agent, 9-β-D-arabinofuranosyl-adenine (araA) (Figure 4-1).[2-5] Nowadays, araA is no longer used in clinic due to its poor solubility and rapid deamination by the ubiquitous adenosine deaminase (ADA), which leads to a loss of its pharmacological activity.[2,6] By having a halogen atom substituted at the C2 position of the adenosine moiety (Figure 4-1), ClA and FlU are resistant to the deamination by ADA.[2] In 1977, years after discoveries of ClA (1972)[3] and FlU (1968)[4], Carson *et al*[7] found that activities of deoxyadenosine kinase and deoxyguanosine kinase, crucial enzymes for many drugs' activation, are largely confined in lymphoid tissues, where ADA is present in high concentration[8]. They, therefore, proposed that an ADA-resistant deoxypurine analogue would be selectively toxic to lymphocytes.[7] This helps explain why ClA and FlU are effective in treating patients with non-Hodgkin's lymphoma and chronic lymphocytic leukemia.

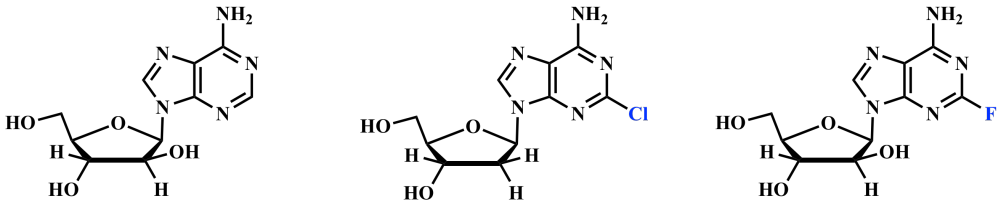

9-β-D-arabinofuranosyladenine Cladribine Fludarabine

Figure 4-1. Chemical structures of 9-β-D-arabinofuranosyladenine (araA), Cladribine (ClA) and Fludarabine (FlU).

The administered form of FlU in clinical use is fludarabine-5′-monophosphate, FlUMP, unlike ClA.[2,9,10] The phosphate group helps improve drug solubility, however, it will get hydrolyzed off by plasma phosphatase and ecto-5′-nucleotidase before entering cells. Nucleoside transporters are known to mediate the transport of these purine nucleosides into cells.[2]

In this chapter, we evaluated the ability of ClA and FlU to inhibit enzyme ribonucleotide reductase (RNR) activity in cells as well as drug toxicity in cell lines expressing wild-type RNR-α or oligomerization-defective D57N-α under inducible promoter.

4.2 Experimental

General Materials and Methods. Antibodies to mammalian ribonucleotide reductase α subunit (Ab81085), mammalian ribonucleotide reductase p53β (Ab8105), mammalian ribonucleotide reductase β subunit (Ab57653), mouse anti-rabbit IgG (HRP) (Ab99702) and goat anti-mouse IgG H&L (HRP) (Ab6789) were from Abcam. NH_4^+ salt of [5-^{3}H]-CDP (19.4 Ci/mmol) was from ViTrax. Fetal Bovine Serum (FBS) for cell experiments was from Sigma Aldrich. Other cell culture media, Bovine Calf

Serum (BCS) and Trypan Blue Stain (0.4%) were obtained from Gibco® Life Technologies. AlamarBlue® dye for cell viability assay was from Thermo Fisher Scientific. 96-well tissue culture plates with 0.33 cm^2 cell growth area and 60 mm×15 mm cell culture dishes were purchased from CELLTREAT® and Corning, respectively. Number of cells was counted by using Countess® II FL automated cell counter from Thermo Fisher Scientific. Cell viability assays were measured using Cytation™ 3 from BioTek®. Curve fitting and data analyses were performed using Prism v7.0 (Graphpad).

NIH-3T3 cell culture protocol

NIH-3T3 cells stably expressed with either wild-type or D57N mouse RNR-α (mRNR-α), generated by *Dr. Minxing Li*[11], were cultured at 37 °C under 5% CO_2 atmosphere. DMEM supplemented with 10% BCS, 100 μg/mL streptomycin sulfate, and 100 U/mL penicillin was used as media. Both cell lines were maintained and passaged in the presence of 1.25 μg/mL puromycin and the puromycin containing media were changed every two days. Cell passages were performed when the cells reached ~80% confluence by rinsing with 1x DPBS, followed by trypsinization, and centrifugation at 800×g at RT for 8 minutes.

Drugs treatment in cells

In a 150-mm tissue culture media dish (CELLTREAT®), either wild-type mRNR-α or D57N mRNR-α overexpressing 3T3 monolayer cultures at 80–100% confluence were treated with either DMSO (vehicle), Clofarabine (ClF), ClA, or FlUMP at indicated concentrations and incubated at 37 °C under 5% CO_2 atmosphere

for 3 hours. Cells originating from two 150-mm plates at 80–100% confluence were used for each set of *radioactive assays for cell lysate*. After cell harvesting, each pallet was subsequently lysed according to previously published protocols.[12,13] The resulting lysate was immediately used in *radioactive assays for cell lysate*.

Radioactive assays for cell lysate

Typical assay mixture (AM) of CDP reduction in a final volume of 135 μL contained 3 mM ATP, 10 mM DTT, 0.5 mM [5-^{3}H]-CDP (Specific activity (SA) = 25,000 cpm/nmol), and the lysate mentioned in *Drugs treatment in cells* in assay buffer (AB) [50 mM Hepes (pH 7.6), 15 mM $MgCl_2$]. The AM without [5-^{3}H]-CDP was pre-warmed at 37 °C for 2 minutes prior to the substrate addition. Four 30 μL-aliquots were removed at 40, 80, 130 and 180 second time-points post assay initiation, and immediately quenched with 2% (v/v) $HClO_4$ (30 μL). The mixture was subsequently neutralized with 30 μL of 0.4 M NaOH. Dephosphorylation of the resultant [5-^{3}H]-dCDP was achieved by adding 410 μL of dephosphorytion mixture containing 10 units CIP, 1.2 mM deoxycytidine (dC) in 100 mM Tris-HCl (pH 8.6) and incubating the mixture at 37 °C for 2 hours. Unreacted [5-^{3}H]-CDP was removed by loading the resultant mixture onto a borate column, which had been prepared by using method of Steeper and Steuart.[14] The amount of [5-^{3}H]-dCDP formed at each time-point was analyzed using liquid scintillation counting.

Western blot of cell lysates

Western blot analysis was carried out as previously reported.[12,13] Antibodies to mammalian ribonucleotide reductase α subunit (Ab81085) and goat anti-mouse IgG

H&L (HRP) (Ab6789) were used as primary and secondary antibodies at 1:1,000 and 1:5,000 dilutions, respectively. For loading controls, membranes were re-probed with mouse monoclonal anti-GAPDH-peroxidase (1:30,000 dilution) (monomer, 37 kDa) (Figure 4-3). For Figure 4-4A, antibodies to mammalian ribonucleotide reductase α subunit (Ab81085) and mouse anti-rabbit IgG (HRP) (Ab99702) were used for primary and secondary antibodies at 1:1,000 and 1:4,000 dilutions, respectively. In order to probe mammalian RNR-p53β, antibodies to mammalian RNR-p53β (Ab8105) at 1:2,000 dilution and mouse anti-rabbit IgG (HRP) (Ab99702) at 1:4,000 dilution were used for primary and secondary antibodies, respectively. Antibodies to mammalian ribonucleotide reductase β subunit (Ab57653) at 1:2,000 dilution and goat anti-mouse IgG H&L (HRP) (Ab6789) 1:4,000 dilution were used for primary and secondary antibodies to probe mammalian ribonucleotide reductase β subunit, respectively. Mouse monoclonal anti-GAPDH-peroxidase (1:2,000 dilution) was used for loading controls.

Cell viability assays

Flp-In T-REx HEK293 cell lines expressing RNR-α- (wild-type) or D57N-α-2×Flag were generated by *Dr. Marcus J. C. Long*. Flp-In T-REx HEK293 cells were cultured in MEM supplemented with 10% FBS, 1x pyruvate and non-essential amino acids, 100 μg/mL zeocin and 1x penicillin/streptomycin in a humidified atmosphere at 37 °C with 5% CO_2 atmosphere. 400,000 of the cells were seeded in 6-well plates. After 24 hours, plates were co-transfected with (A) 3:1 and (B) 6:1 plasmid mix containing the POG44 vector encoding the Flp recombinase and pcDNA5/FRT/TO-RNR-α- or D57N-α-2×Flag (2.5 μg total plasmid) using Mirus 2020 (7.5 μL) in 6-well plates as per manufacturer's instructions. Two days after transfection or when the cells

reached confluence, the cells were trypsinized. The two separate transfection conditions (A and B) were pooled and plated in 10 cm dishes. After 1–1.5 days, the cells were changed to selective media containing 150 μg/mL Hygromycin B. After 1.5–2 weeks, single colonies had formed. Once the colonies were large enough to pick, individual clones were selected using cloning cylinders. Individual clones were grown in 12-well plates, and verified for expression using anti-flag western blot (+/− 200 ng/mL tetracycline, 24 hours) and immunofluorescence (which showed cytosolic Flag-tagged wild-type or D57N-α upon tetracycline induction). For passaging lines post selection, 100 μg/mL Hygromycin B was used.

Flp-In T-REx HEK293 cells expressed with either wild-type or D57N RNR-α were seeded in 60 mm×15 mm cell culture dishes (Corning) at 37 °C under 5% CO_2 atmosphere. The media used was DMEM supplemented with 10% FBS, 100 μg/mL streptomycin sulfate and 100 U/mL penicillin. After cells attached to the dishes (1–2 days), Hygromycin B was added to a final concentration of 50 μg/mL. Cells were trypsinized after they reached ~80% confluence and the number of cells was counted using Trypan Blue Stain (Gibco® Life Technologies) and Countess® II FL automated cell counter (Thermo Fisher Scientific). 2,500 cells, in 100 μL media, were seeded in 96 well plates (CELLTREAT®) without Hygromycin B. 50 μL of 300 ng/mL tetracycline or media alone (without tetracycline) was added into each well. Cells were cultured at 37 °C under 5% CO_2 atmosphere for 11 hours. 50 μL of indicated drugs at 4x of indicated concentrations or media alone (for control) were added into designated wells. Cells were left at 37 °C under 5% CO_2 atmosphere for 45 hours before 90 μL of media was removed. 11 μL of alamarBlue® dye was subsequently added into each well. After 48 hours of drug treatment, cell viabilities were determined using Cytation™ 3 (BioTek®) (λ_{ex} = 560 nm, λ_{em} = 590 nm). Normalized fluorescence intensities (y-axis) were plotted against log values of drug concentrations in molar

scale (x-axis). The data were fit into equation 4.1 using Prism v7.0 and EC_{50} values were derived.

$$y = 1 - \frac{1}{1 + 10^{(\log(EC_{50}) - x)}} \qquad \text{Eq. 4.1}$$

4.3 Results and discussion

4.3.1 ClA and FlU inhibit wild-type mRNR-α but not the oligomerization-defective mD57N-α in NIH-3T3 fibroblasts

Tumors are classically considered as wounds that do not heal, which implies that cells that are responsible in the response of injury and angiogenesis, such as fibroblasts and endothelial cells, have an important role in the progression, growth and spread of cancers.[15] Also, elevated RNR expression is one of cancer-characteristics.[16] We thus chose to assess the ability of ClA and FlU to inhibit RNR in NIH-3T3 fibroblast cells stably expressing with either wild-type or D57N mRNR-α, which were generated by *Dr. Minxing Li. (See Ref. 11 for more details)*

In 1981, Weinberg *et al*[17] first identified D57N-α, a single point mutation at the A-site of RNR (Figure 4-2), during their studies of the effects of natural nucleotide pool imbalance in mouse (m) T-lymphosarcoma cells. By mutating aspartic acid (D) at position 57 to asparagine (N), dATP-mediated RNR enzyme inhibition is disrupted. Later, Reichard *et al*[18] and Kashlan *et al*[19] confirmed that the D57N point mutation renders mRNR-α resistant to dATP-driven RNR inhibition. Furthermore, in 2006, Rofougaran *et al*[20] discovered that mRNR forms an inactive $\alpha_6\beta_2$ octomer in the presence of dATP. Based on this evidence, it is most likely that the mD57N mutant is not inhibited by dATP due to its incapability to form α-hexamers. Thus, if there is any

connection between RNR-α hexamerization and RNR inhibition promoted by ClA and FlU nucleotides, we expected ClA and FlU to inhibit wild-type mRNR-α but not the mD57N-α in NIH-3T3 fibroblasts.

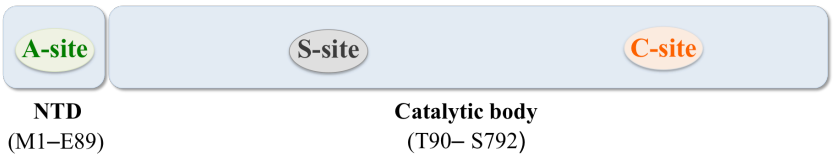

Figure 4-2. Schematic representation of the two domains, NTD and catalytic body, of mRNR-α.

We first treated NIH-3T3 cells stably expressing wild-type mRNR-α with a known RNR-α-hexamerization inducer, ClF[13,21,22], ClA, FlUMP or DMSO (vehicle) at the concentrations similar to those used in previous pharmacological studies[23-25] for 3 hours. The mRNR-α subunit-specific activity after drug treatment was evaluated by measuring the rate of [5-^{3}H]-dCDP product formation in cell lysates. Similar to the results observed in the positive control (ClF-treated cells), lysates from ClA- and FlUMP-treated cells showed potent RNR inhibition (Figure 4-3, *top*).

Next, we investigated the effects of these compounds on cells stably expressing the oligomerization-defective point mutation D57N-α[19], which we found to be resistant to a known RNR-α-hexamerization inducer ClFTP[21] but not to the mechanism-based inactivator gemcitabine 5′-diphosphate (F2CDP). The in cell and *in vitro* data for the latter drug were provided by *Dr. Yuan Fu (See Ref. 11 for more details)*. The CDP/ATP-reductase-activity of mRNR in NIH-3T3 expressing mD57N-α lines was not suppressed by either ClA or FlUMP (Figure 4-3, *bottom*). These results showed an inhibition signature that involves protein hexamerization similar to the allosteric RNR-inhibitor, ClF.[13,21] Given that the D57N-α-expressing mutant lines

showed resistance to ClF, whereas they were sensitive to F2C[11], an important hint about potential links between RNR inhibition promoted by ClA/FlU nucleotides and α-hexamerization was provided by this set of experiments.

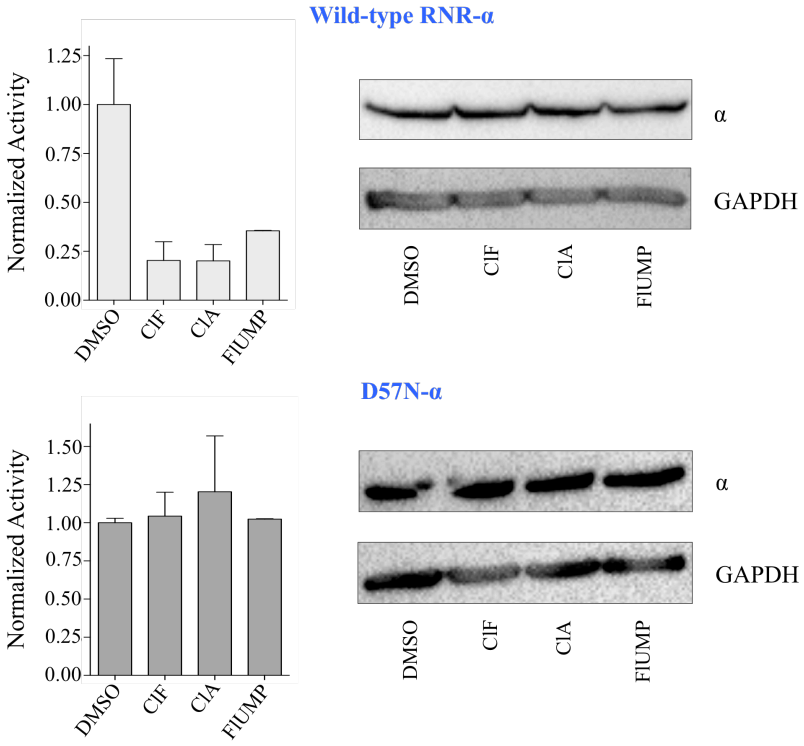

Figure 4-3. Evaluation of the ability of ClA and FlUMP to inhibit mRNR-α subunit-specific CDP/ATP-reductase-activity from NIH-3T3 cell lysates. NIH-3T3 cells stably expressing either wild-type mRNR-α (*top*) or D57N mRNR-α (*bottom*) were treated with DMSO (vehicle), 5 μM ClF[23], 50 μM ClA[25] or 300 μM FlUMP[24] for 3 hours prior to cell harvesting and lysis. The mRNR-α subunit-specific activity of 500 μg of total lysate was determined by immediately measuring the rate of [5-^{3}H]-dCDP product formation over 4 time-points. Error bars designate SD (n=2).

4.3.2 RNR-α oligomerization plays a role in cytotoxic activity of ClA and FlU

We have shown in *chapter 3* that ClA- and FlU-nucleotide-induced RNR inhibition is coupled to RNR-α-oligomerization. We next evaluated to what extent the oligomeric mode of RNR inhibition plays a role in drug cytotoxic profiles.

Flp-In HEK293 T-REx cells that can stably incorporate a single copy of a selectable transgene at a defined genomic locus upon transient transfection with a plasmid encoding flippase (FLIP) recombinase, and an appropriate donor plasmid containing flippase recognition target (FRT) sites were used in the following experiments. Even though, the toxicity of these nucleosides to normal cells versus cancer cells depends on various parameters, we here focused on gaining initial insights into the importance of oligomeric regulation in the ultimate cytotoxic activity of these nucleosides. The Flp-In HEK293 T-REx cells constitutively express the tetracycline (tet)-repressor to facilitate the tet-inducible expression of the transgene of interest. Isogenic lines stably expressing either RNR-α-Flag or D57N-α-Flag under a tet-controlled CMV-promoter were established. By using this system, we can thus temporally control the protein expression, which allows us to spotlight the effects from (wild-typed and mutant) RNR-α alone against a native background.

As evidenced by Flag blot, these clonogenic lines showed undetectable expression of ectopic RNR-α. But, upon 11-hour tet-exposure, the total RNR-α levels were upregulated approximately 2–3 folds relative to the endogenous protein. However, the levels of RNR-β and RNR-p53β, the two isoforms of RNR-β subunit, were unaffected under these conditions (Figure 4-4).

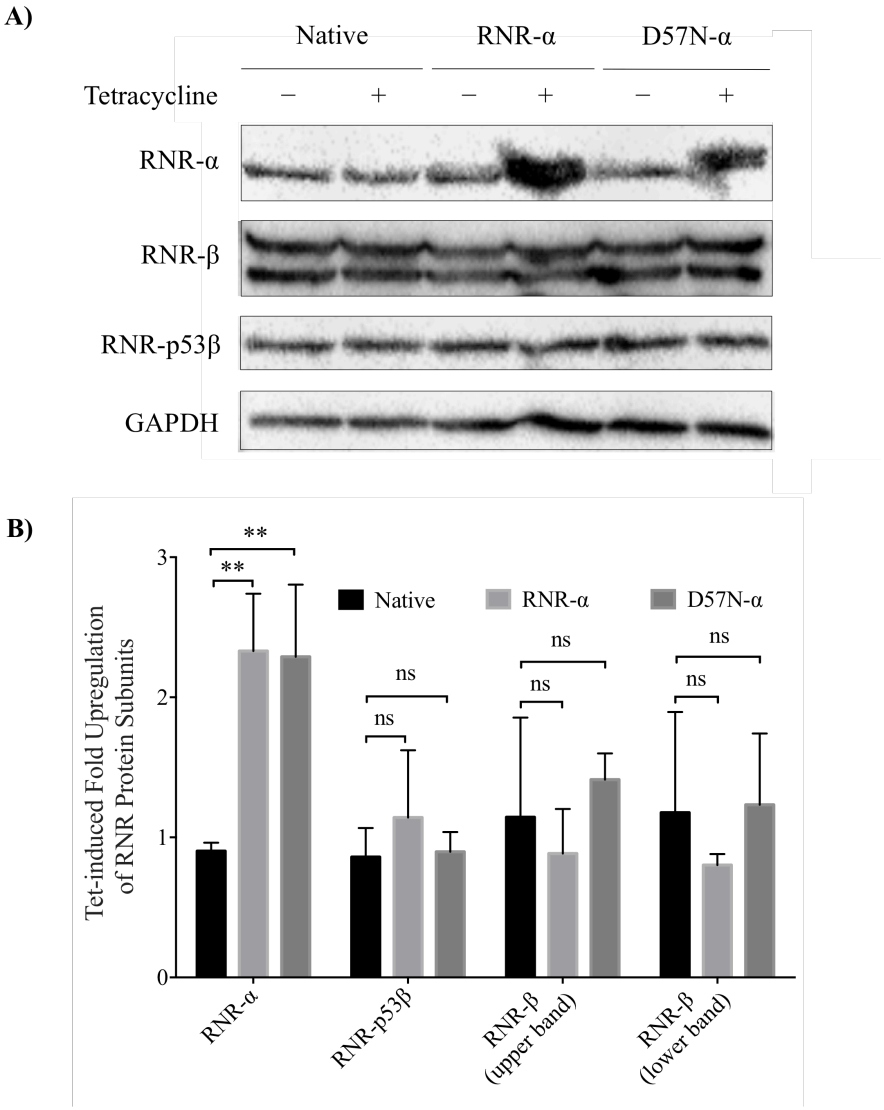

Figure 4-4. Validation of tetracycline (tet)-induced RNR-α or D57N-α overexpression in Flp-In T-REx HEK293 cell lines. **(A)** A representative western blot. Protein level was analyzed using indicated antibodies to RNR-α subunit and the two isoforms of RNR-β subunit. GAPDH was used as a loading control. ***Note:*** Since mammalian RNR-β is known to be labile for cleavage at the N-terminal PEST domain[26], multiple bands always observed when an RNR-β containing protein blot is probed with anti-RNR-β. **(B)** Quantification of protein fold upreguration normalized over GAPDH.

We next set up a proliferation inhibition assay in which cells were seeded at 10% confluence in 96-well plates, then treated with tet for 11 hours prior to the drug addition. After 48 hours (approximately 2.5 doubling time) of drug treatment, total viable cells were measured using alamarBlue® reagent. AlamarBlue® is widely used as an indicator of metabolic and cellular health in cell viability bioassays.[27] This dye is non-toxic, water-soluble, stable in culture media and permeable through cell membranes. The dye acts as an intermediate electron acceptor in the electron transport chain without any interference of the normal transfer of electrons.[28] By comparing oxidation-reduction potentials of alamarBlue® and other electron carriers in the electron transport chain at 25 °C, pH 7.0 (Table 4-1), alamarBlue® can be reduced by NADPH, FADH, FMNH, NADH, as well as the cytochromes.[27] Once the indicator dye accepts electrons, it changes from its non-fluorescent, blue-colored-oxidized state to the fluorescent, pink-colored-reduced state.[28]

Table 4-1. Oxidation-reduction potentials in the electron transport system.[27]

Half-Reaction	E_0 (mV) at 25°C, pH 7.0
$O_2 + 4H^+ + 4e^- \longrightarrow 2H_2O$	+820
alamarBlue®$_{OX}$ + $2H^+ + 2e^- \longrightarrow$ alamarBlue®$_{RED}$	+380
cytochromes®$_{OX}$ + $e^- \longrightarrow$ cytochromes$_{RED}$	+290 to +80
$FMN + 2H^+ + 2e^- \longrightarrow FMNH_2$	-210
$FAD + 2H^+ + 2e^- \longrightarrow FADH_2$	-220
$NAD^+ + 2H^+ + 2e^- \longrightarrow NADH + H^+$	-320
$NADP^+ + 2H^+ + 2e^- \longrightarrow NADPH + H^+$	-320

Measurements of this color change are quantitative (colorimetric and/or fluorometric readings). Based on our *in vitro* data in *chapter 3*, we would expect that overexpression of RNR-α and D57N-α would similarly protect HEK293 cells from gemcitabine (F2C) for three reasons. First, F2CDP (the only active form of gemcitabine that inhibits RNR) targets the C-site of both wild-type RNR-α and the reduced-affinity-A-site-binding mutant D57N-α.[11] Second, as shown in Figure 4-4, RNR-α overexpression is similar in both lines. Third, the specific activities of D57N-α and wild-type RNR-α are comparable. For the RNR-α inhibitors, that inhibit the enzyme activity by inducing RNR-α-hexamerization, we hypothesized that over-expression of oligomerization-defective D57N-α should rescue cell toxicity, whereas overexpression of wild-type RNR-α should elicit some protection in cases where the K_i value of the inhibitor under study is lower or not much greater than the wild-type RNR-α cellular concentrations. Our experimental hypothesis is shown in Figure 4-5.

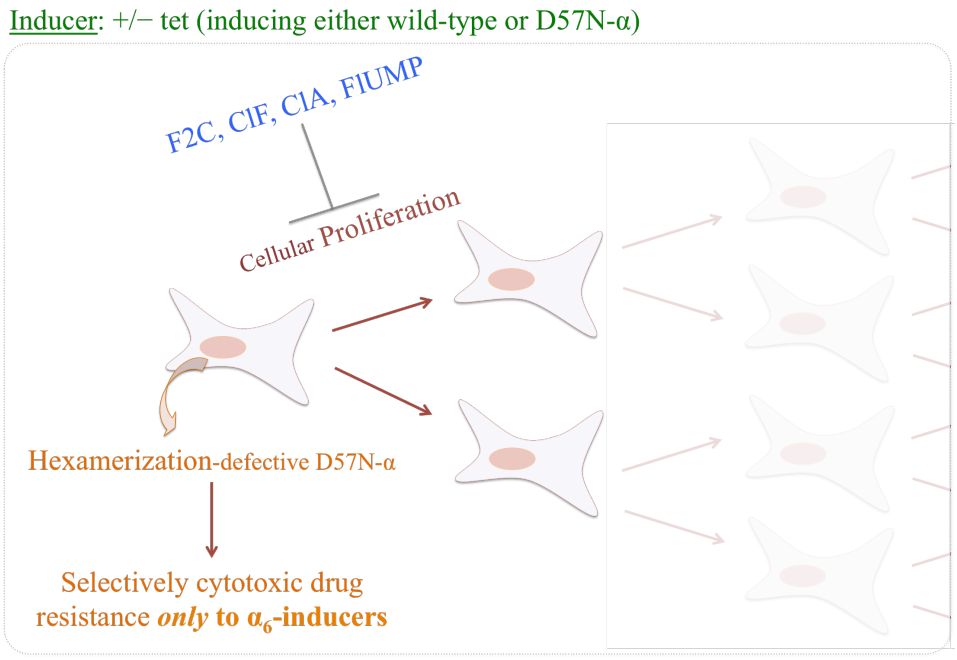

Figure 4-5. The experimental hypothesis of cell viability assays.

Over three separate runs, each with quadruplicate data, we observed modest protection against F2CDP cytotoxicity upon tet-induction of RNR-α or D57N-α relative to the noninduced samples (Figure 4-6A and 4-7). As we expected, the fold protections observed in RNR-α and D57N-α overexpression were not significantly different, and the magnitude of protection (3–5 folds, Figure 4-7) was on the order of the RNR-α overexpression we observed in Figure 4-4B.

In the case of ClF and ClA, RNR-α overexpression cells elicited a small effect on the EC_{50} value relative to the noninduced cells (Figure 4-6, B–C and 4-7), similar to the results with F2C. In contrast, D57N-α overexpression showed almost complete protection (>20 folds in each case) against both ClF and ClA treatment (Figure 4-7). These results were not from an unlikely scenario that the global nucleotide pool is being perturbed by D57N-α overexpression since RNR-α and D57N-α expressing cells were still sensitive to artificial nucleotide-induced toxicity. We can thus conclude that ClF and ClA selectively target RNR-α through oligomeric downregulation as we initially expected. In the case of FlUMP, no protection was observed in both RNR-α and D57N-α overexpression (Figure 4-6D and 4-7). By considering the higher K_i's of FlUDP and FlUTP, compared to those of ClFD(T)P and ClAD(T)P, together with the relatively low amount of protein overexpression we observed in this system (Figure 4-4), any rescue upon RNR-α overexpression would be unlikely. These observations implied that RNR-α is a low-priority target of FlU-nucleotides, whereas it is the principal target of ClF- and ClA-nucleotides.

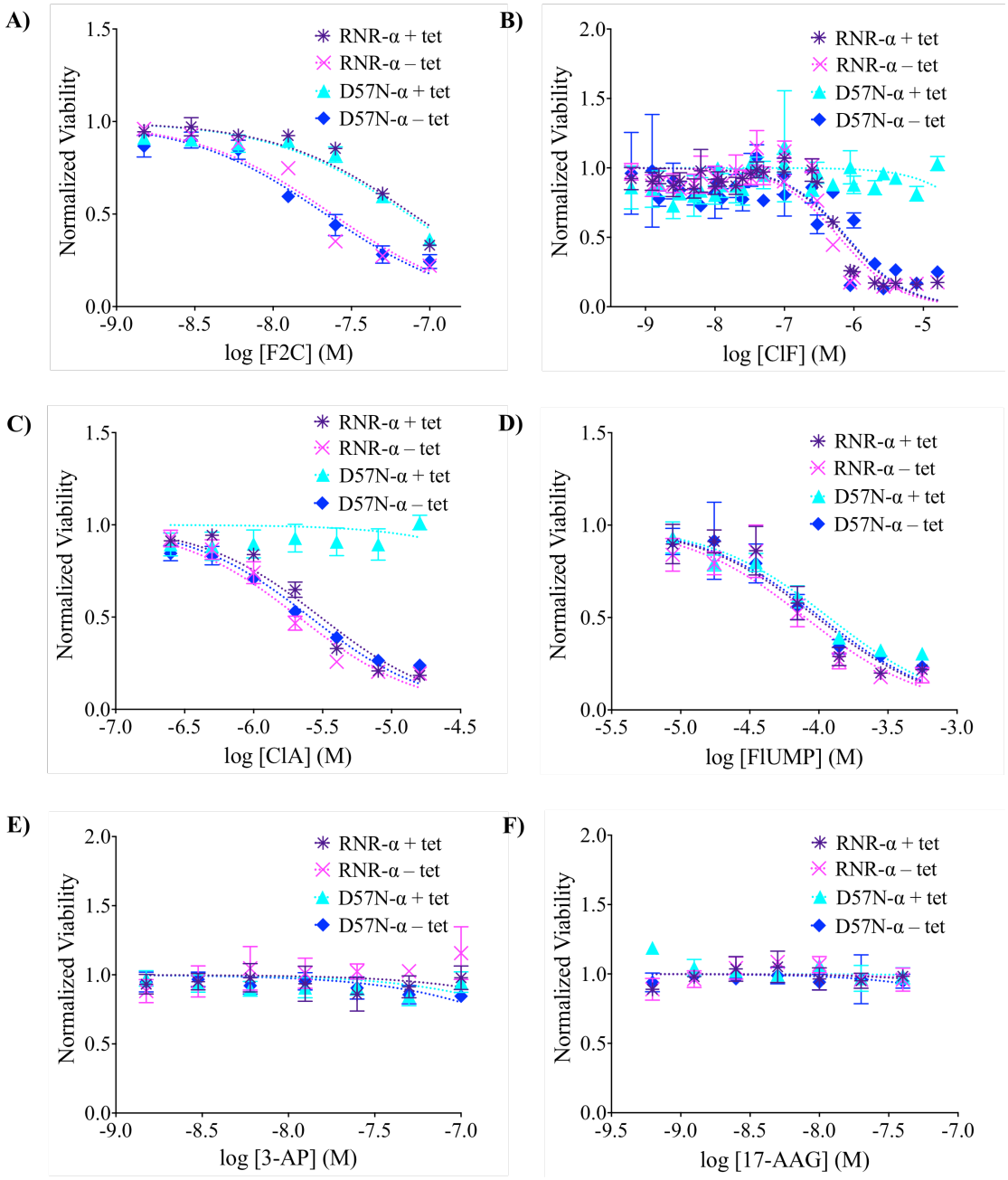

Figure 4-6. Dose-dependent viability assays of **(A)** F2C, **(B)** ClF, **(C)** ClA, **(D)** FlUMP, **(E)** an RNR-β-specific inhibitor, Triapine (3-AP)[29], and **(D)** an HSP90 inhibitor, 17-AAG.[30] Since neither 3-AP nor 17-AAG targets RNR-α, no protection was observed in either RNR-α or D57N-α overexpression.

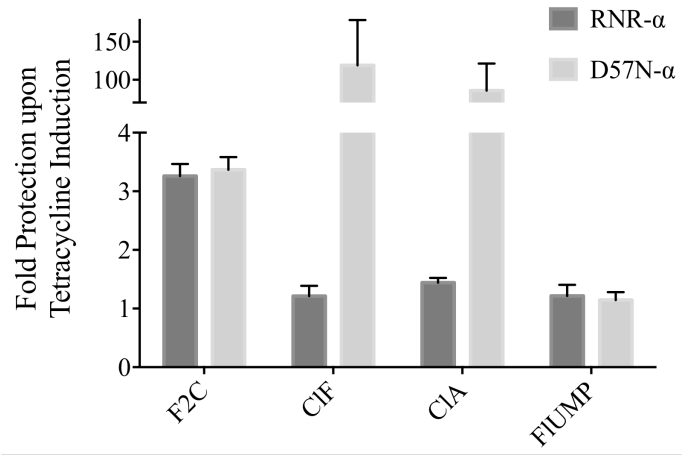

Figure 4-7. Quantification of fold protection upon tet-induction of samples treated with F2C, ClF, ClA, or FlUMP (data from Figure 4-6).

Conclusions

Chemotherapy is one of the key modes of cancer treatment. However, the effectiveness of nucleotide chemotherapy is limited by drug resistance.[31] Conventional views mostly attribute mechanisms of nucleotide drug resistance to a reduction of intracellular concentration of drug active species and/or a suppression of apoptosis induction.[1,31] In this chapter, we investigated the functional impacts of defective oligomeric regulation of RNR-α under conditions where drug uptake and metabolism, interaction with other targets, and apoptosis pathway induction processes are unaltered. Our in-cell data showed that RNR-α hexamerization is potentially an additional pathway to cytotoxic resistance to RNR-α_6-inducer nucleotides such as those of ClF and ClA. This finding differentiates these nucleotides from the more well-characterized conventional suicide inactivators such as F2C.

REFERENCE

[1] Galmarini, C. M., Mackey, J. R., and Dumontet, C. (2001) Nucleoside analogues: mechanisms of drug resistance and reversal strategies. *Leukemia 15*, 875-890.

[2] Damaraju, V. L., Damaraju, S., Young, J. D., Baldwin, S. A., Mackey, J., Sawyer, M. B., and Cass, C. E. (2003) Nucleoside anticancer drugs: the role of nucleoside transporters in resistance to cancer chemotherapy. *Oncogene. 22*, 7524-7536.

[3] Sigal, D. S., Miller, H. J., Schram, E. D., and Saven, A. (2010) Beyond hairy cell: the activity of cladribine in other hematologic malignancies. *Blood 116*, 2884-2896.

[4] Sneader, W. (2005) *Drug Discovery: A History*, pp 258, John Wiley & Sons Ltd., West Sussex.

[5] Lee, W. W., Benitez, A., Goodman, L., and Baker, B. R. (1960) POTENTIAL ANTICANCER AGENTS. XL. SYNTHESIS OF THE β-ANOMER OF 9-(D-ARABINOFURANOSYL)-ADENINE. *J. Am. Chem. Soc. 82*, 2648-2649.

[6] Peters, G. J. (2006) *Deoxynucleoside Analogs in Cancer Therapy*, pp 307, Humana Press Inc., New Jersey

[7] Carson, D. A., Kaye, J., and Seegmiller, J. E. (1977) Lymphospecific toxicity in adenosine deaminase deficiency and purine nucleoside phosphorylase deficiency: possible role of nucleoside kinase(s). *Proc. Natl. Acad. Sci. U. S. A. 74*, 5677-5681.

[8] Adams, A., and Harkness, R. A. (1976) Adenosine deaminase activity in thymus and other human tissues. *Clin. Exp. Immunol. 26*, 647-649.

[9] Gandhi, V., and Plunkett, W. (2002) Cellular and clinical pharmacology of fludarabine. *Clin. Pharmacokinet 41*, 93-103.

[10] Foran, J. M., Oscier, D., Orchard, J., Johnson, S. A., Tighe, M., Cullen, M. H., de Takats, P. G., Kraus, C., Klein, M., and Lister, T. A. (1999) Pharmacokinetic study of single doses of oral fludarabine phosphate in patients with "low-grade" non-Hodgkin's lymphoma and B-cell chronic lymphocytic leukemia. *J. Clin. Oncol. 17*, 1574-1579.

[11] Wisitpitthaya, S., Zhao, Y., Long, M. J., Li, M., Fletcher, E. A., Blessing, W. A., Weiss, R. S., and Aye, Y. (2016) Cladribine and Fludarabine Nucleotides Induce Distinct Hexamers Defining a Common Mode of Reversible RNR Inhibition. *ACS Chem. Biol. 11*, 2021-2032.

[12] Aye, Y., Long, M. J., and Stubbe, J. (2012) Mechanistic studies of semicarbazone triapine targeting human ribonucleotide reductase *in vitro* and in mammalian cells: tyrosyl radical quenching not involving reactive oxygen species. *J. Biol. Chem. 287*, 35768-35778.

[13] Aye, Y., Brignole, E. J., Long, M. J., Chittuluru, J., Drennan, C. L., Asturias, F. J., and Stubbe, J. (2012) Clofarabine targets the large subunit (α) of human ribonucleotide reductase in live cells by assembly into persistent hexamers. *Chem. Biol. 19*, 799-805.

[14] Steeper, J. R., and Steuart, C. D. (1970) A rapid assay for CDP reductase activity in mammalian cell extracts. *Anal. Biochem. 34*, 123-130.
[15] Kalluri, R., and Zeisberg, M. (2006) Fibroblasts in cancer. *Nat. Rev. Cancer 6*, 392-401.
[16] Aye, Y., Li, M., Long, M. J., and Weiss, R. S. (2015) Ribonucleotide reductase and cancer: biological mechanisms and targeted therapies. *Oncogene. 34*, 2011-2021.
[17] Weinberg, G., Ullman, B., and Martin, D. W., Jr. (1981) Mutator phenotypes in mammalian cell mutants with distinct biochemical defects and abnormal deoxyribonucleoside triphosphate pools. *Proc. Natl. Acad. Sci. U. S. A. 78*, 2447-2451.
[18] Reichard, P., Eliasson, R., Ingemarson, R., and Thelander, L. (2000) Cross-talk between the allosteric effector-binding sites in mouse ribonucleotide reductase. *J. Biol. Chem. 275*, 33021-33026.
[19] Kashlan, O. B., and Cooperman, B. S. (2003) Comprehensive model for allosteric regulation of mammalian ribonucleotide reductase: refinements and consequences. *Biochemistry 42*, 1696-1706.
[20] Rofougaran, R., Vodnala, M., and Hofer, A. (2006) Enzymatically active mammalian ribonucleotide reductase exists primarily as an $\alpha_6\beta_2$ octamer. *J. Biol. Chem. 281*, 27705-27711.
[21] Aye, Y., and Stubbe, J. (2011) Clofarabine 5'-di and -triphosphates inhibit human ribonucleotide reductase by altering the quaternary structure of its large subunit. *Proc. Natl. Acad. Sci. U. S. A. 108*, 9815-9820.
[22] Fu, Y., Lin, H. Y., Wisitpitthaya, S., Blessing, W. A., and Aye, Y. (2014) A fluorimetric readout reporting the kinetics of nucleotide-induced human ribonucleotide reductase oligomerization. *ChemBioChem 15*, 2598-2604.
[23] Bonate, P. L., Arthaud, L., Cantrell, W. R., Jr., Stephenson, K., Secrist, J. A., 3rd, and Weitman, S. (2006) Discovery and development of clofarabine: a nucleoside analogue for treating cancer. *Nat. Rev. Drug Discov. 5*, 855-863.
[24] Robertson, L. E., Denny, A. W., Huh, Y. O., Plunkett, W., Keating, M. J., and Nelson, J. A. (1996) Natural killer cell activity in chronic lymphocytic leukemia patients treated with fludarabine. *Cancer Chemother Pharmacol. 37*, 445-450.
[25] Mansson, E., Spasokoukotskaja, T., Sallstrom, J., Eriksson, S., and Albertioni, F. (1999) Molecular and biochemical mechanisms of fludarabine and cladribine resistance in a human promyelocytic cell line. *Cancer Res. 59*, 5956-5963.
[26] Mann, G. J., Graslund, A., Ochiai, E., Ingemarson, R., and Thelander, L. (1991) Purification and characterization of recombinant mouse and herpes simplex virus ribonucleotide reductase R2 subunit. *Biochemistry 30*, 1939-1947.
[27] Rampersad, S. N. (2012) Multiple applications of Alamar Blue as an indicator of metabolic function and cellular health in cell viability bioassays. *Sensors (Basel) 12*, 12347-12360.

[28] Page, B., Page, M., and Noel, C. (1993) A new fluorometric assay for cytotoxicity measurements *in-vitro*. *Int. J. Oncol. 3*, 473-476.

[29] Popovic-Bijelic, A., Kowol, C. R., Lind, M. E., Luo, J., Himo, F., Enyedy, E. A., Arion, V. B., and Graslund, A. (2011) Ribonucleotide reductase inhibition by metal complexes of Triapine (3-aminopyridine-2-carboxaldehyde thiosemi-carbazone): a combined experimental and theoretical study. *J. Inorg. Biochem. 105*, 1422-1431.

[30] Sauvageot, C. M., Weatherbee, J. L., Kesari, S., Winters, S. E., Barnes, J., Dellagatta, J., Ramakrishna, N. R., Stiles, C. D., Kung, A. L., Kieran, M. W., and Wen, P. Y. (2009) Efficacy of the HSP90 inhibitor 17-AAG in human glioma cell lines and tumorigenic glioma stem cells. *Neuro. Oncol. 11*, 109-121.

[31] Holohan, C., Van Schaeybroeck, S., Longley, D. B., and Johnston, P. G. (2013) Cancer drug resistance: an evolving paradigm. *Nat. Rev. Cancer 13*, 714-726.

APPENDIX A

ZRANB3: A Binding Partner of RNR α-subunit

Dr. Yuan Fu discovered a binding interaction between zinc finger Ran-binding domain-containing protein 3 (ZRANB3) (Figure A-1) and RNR-α subunit while screening a random-primed cDNA library from HeLa cells using a fusion protein RNR1-GAL4BD as bait; the cDNA library was constructed in pP6 vector, and RNR1-GAL4BD constructed in pB43. This hit clone was subsequently verified by immunoprecipitation (unpublished data).

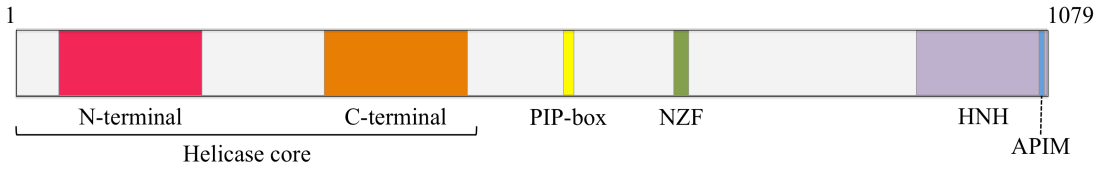

Figure A-1. Modular structure of ZRANB3.[1] ZRANB3 possesses several functional domains, *i.e.*, 1) a helicase core at its N-terminus is a characteristic for the SNF2 ATPase family members, 2) a PCNA-interacting protein motif (PIP-box), 3) an unusual zinc finger of the NZF-type (Npl4 zinc finger)[2], 4) a putative HNH-type endonuclease domain at the C-terminal, and 5) APIM (AlkB homologue 2 PCNA-interacting motif)[3], residues 1074–1078[1], which is part of the HNH domain. This Figure is adapted from Ref. 1.

To identify which domain(s) of ZRANB3 (Figure A-1) that RNR-α interacts with, we first examined the HNH domain, whose name derived from the three most conserved histidine (H) and asparagine (N) residues in the degenerate motif[1].

As the APIM domain is part of the HNH domain in ZRANB3 and can interact with PCNA (a protein that controls RNR activity during DNA synthesis)[4], we designed two truncated proteins: (1) His_6-HA-HNH and (2) His_6-$flag_2$-HNHΔAPIM, to investigate whether the APIM domain is necessary for interaction(s) (if any) between RNR-α and the HNH domain of ZRANB3.

Generation of His_6-HA-HNH and His_6-$flag_2$-HNHΔAPIM plasmids

HNH and HNHΔAPIM were separately amplified from the plasmid encoding flag-ZRANB3, a generous gift from Weston et al[1], using the primers shown in Table A-1. The result gene was finally cloned into an empty pET28a vector. The genes were confirmed by sequencing at the Cornell University Life Science Core Laboratories Center (Figure A-2).

Table A-1. Primers used for the construction of His_6-HA-HNH and His_6-$flag_2$-HNHΔAPIM.

		Primer sequence (5′ ⟶ 3′)
His_6-HA-HNH	Fwd	GGTAGCCATTACCCATACGATGTTCCAGATTACGCTCTTCTTGA AGATGGAGCCTGTGTC
	Rev	AACTCAGCTTCCTTTCGGGCTTTGTTACTTCTTTACCAAAAAT CGTGTGATGTCTGATCC
His_6-$flag_2$-HNHΔAPIM	Fwd	GATGACGACAAGGACTACAAAGACGATGACGACAAGCTTCTT GAAGATGGAGCCTGTGTC
	Rev	GCCAACTCAGCTTCCTTTCGGGCTTTGTTACTTTGTGATGTCT GATCCATGCTTTGA
	Fwd extender	AGCGGCCTGGTGCCTCGTGGTAGCCATGACTACAAAGACGAT GACGACAAGGACTACAAA
	Rev extender	TATGCTAGTTATTGCTCAGCGGTGGCAGCAGCCAACTCAGCTT CCTTTCGGGCTTTGTTA

A) His_6-HA-HNH

MGSSHHHHHHSSGLVPRGSHYPYDVPDYALLEDGACVPFLNPYTVQADLTVKPSTSKGYL
QAVDNEGNPLCLRCQQPTCQTKQACKANSWDSRFCSLKCQEEFWIRSNNSYLRAKVFETE
HGVCQLCNVNAQELFLRLRDAPKSQRKNLLYATWTSKLPLEQLNEMIRNPGEGHFWQVDHIKPVY
GGGGQCSLDNLQTLCTVCHKERTARQAKERSQVRRQSLASKHGSDITRFLVKK

B) His_6-$flag_2$-HNHΔAPIM

MGSSHHHHHHSSGLVPRGSHDYKDDDDKDYKDDDDKLLEDGACVPFLNPYTVQADLTVKPSTSK
GYLQAVDNEGNPLCLRCQQPTCQTKQACKANSWDSRFCSLKCQEEFWIRSNNSYRAKVFETE
HGVCQLCNVNAQELFLRLRDAPKSQRKNLLYATWTSKLPLEQLNEMIRNPGEGHFWQVDH
IKPVYGGGGQCSLDNLQTLCTVCHKERTARQAKERSQVRRQSLASKHGSDITK

Figure A-2. Amino acid sequences of **A)** His_6-HA-HNH, and **B)** His_6-$flag_2$-HNHΔAPIM. Sequences of His_6-tag, HA-tag, $flag_2$-tag, HNH, and APIM are colored in black, green, orange, purple, and blue, respectively.

Recombinant protein expression and purification

His_6-HA-HNH and His_6-$flag_2$-HNHΔAPIM proteins were expressed and purified as previously described for hRNR-α (*chapter 3*) with the following modifications: 450 μM and 150 μM IPTG were used to induce the expression of His_6-HA-HNH and His_6-$flag_2$-HNHΔAPIM, respectively. The obtained cell pellet was lysed in lysis buffer (50 mM Tris-HCl, pH 8.0, 800 mM NaCl, 10 mM imidazole, 5 mM BME, 1 mM PMSF, 10% glycerol and 0.2% Triton X-100). After a removal of DNA by adding 2% (wt/v) streptomycin sulfate, the supernatant was incubated with TALON® metal affinity resin, which was pre-equilibrated with 10 column volumes (CV) of lysis buffer, for 1 hour. The suspension was then re-loaded on the column, and the resin was washed with 1 bed volume (BV) (×2) of wash 1 buffer (50 mM Tris-HCl, pH 8.0, 800 mM NaCl, 15 mM imidazole, 5 mM BME, and 0.2% Triton X-100), followed by 1 BV of wash 2 buffer (50 mM Tris-HCl, pH 8.0, 800 mM NaCl, 20 mM imidazole, 5 mM BME, and 0.2% Triton X-100). The desired protein was then eluted

out with elution buffer (50 mM Tris-HCl, pH 8.0, 300 mM NaCl, 125 mM imidazole, and 1 mM BME). The protein-containing fractions were pooled and injected into a fast protein liquid chromatography (FPLC), which had been pre-equilibrated with at least 5 BV of storage buffer (30 mM Hepes, pH 7.8, 50 mM NaCl, 0.25 mM EDTA, 1 mM DTT, 0.01% NP40, and 10% glycerol). According to the resulting chromatogram, the protein-containing fractions were pooled and subsequently concentrated using centricons (10 kDa M.W. cut-off). Protein purity was determined using SDS-PAGE.

His_6-$flag_2$-HNHΔAPIM.

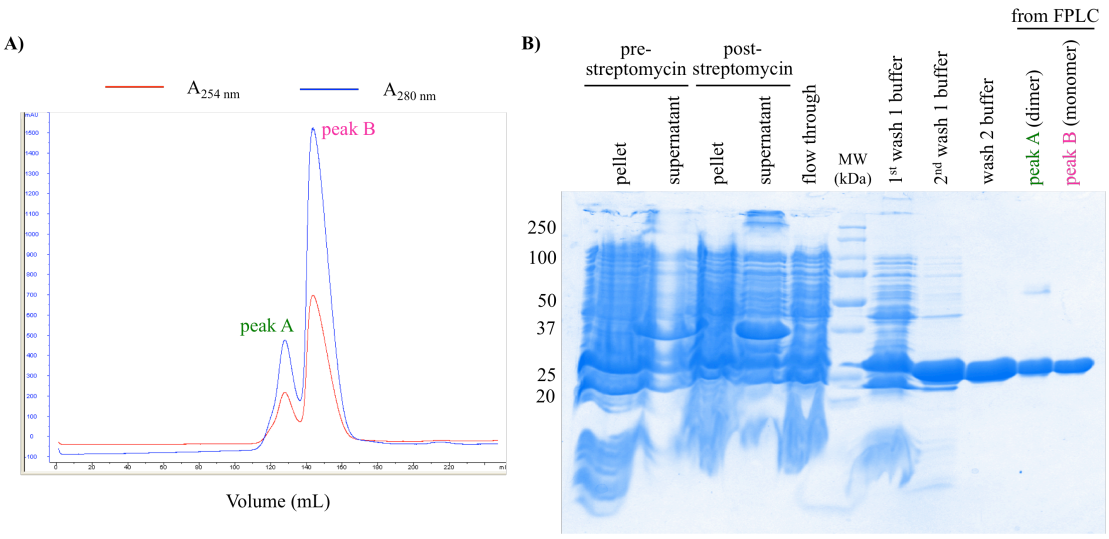

Figure A-3. A) FPLC chromatogram of His_6-$flag_2$-HNHΔAPIM with high imidazole concentration and **B)** 15% SDS-PAGE gel of purified His_6-$flag_2$-HNHΔAPIM (27 kDa).

His$_6$-HA-HNH.

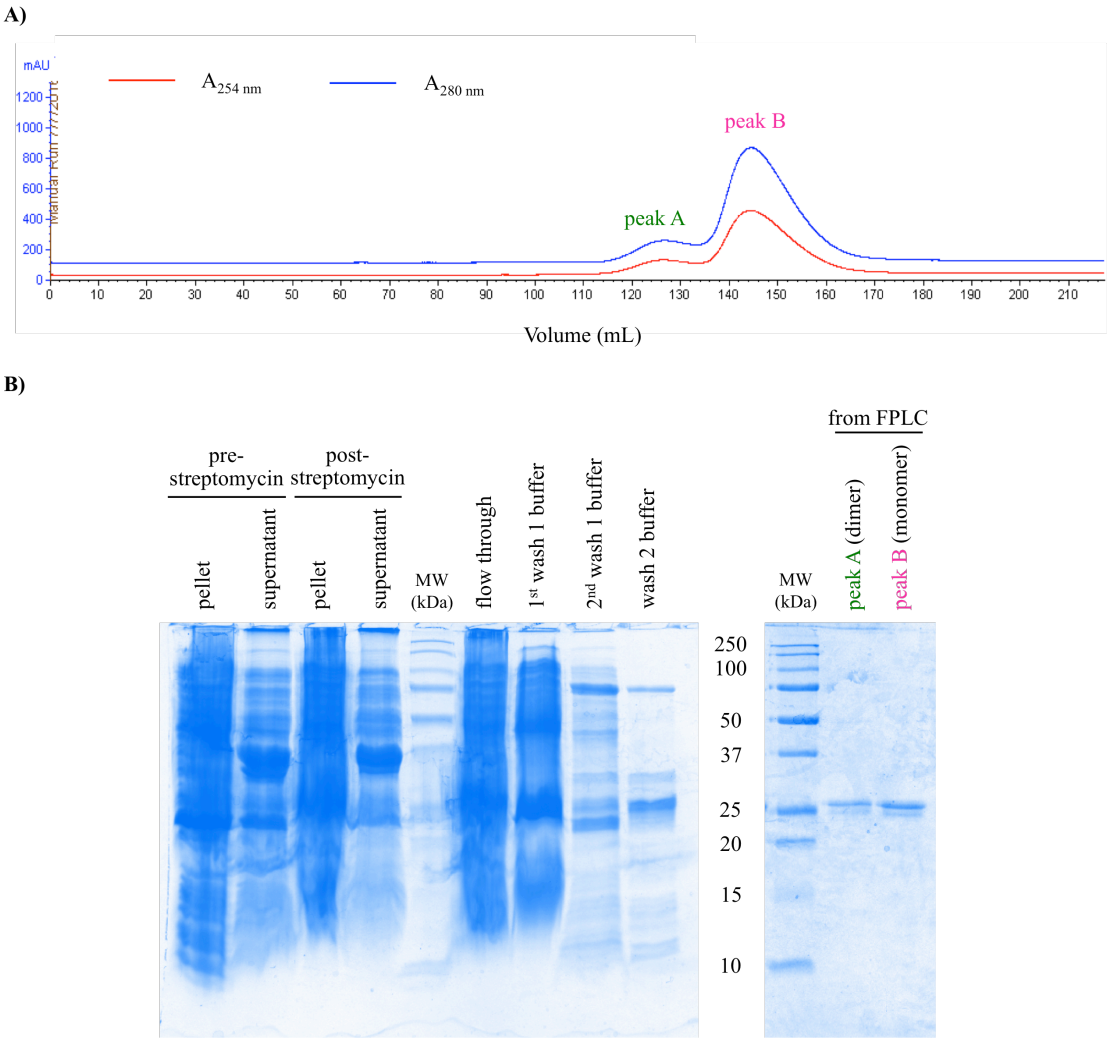

Figure A-4. A) FPLC chromatogram of His$_6$-HA-HNH with high imidazole concentration and **B)** 15% SDS-PAGE gel of purified His$_6$-HA-HNH (27 kDa).

Examination of protein interactions

Binding interactions between (1) hRNR-α and HNH, and (2) hRNR-α and HNHΔAPIM were preliminary tested by using gel filtration analysis [Size Exclusion Chromatography (SEC)]. In this study, we evaluated two oligomeric states of hRNR-α, monomers and ClFDP-induced-hexamers (hRNR-α_6). The typical reaction mixture in a 150 μL final volume contained 50 μM HNH (or HNHΔAPIM) protein, 10 μM hRNR-α, 15 mM $MgCl_2$, 5 mM DTT, 15.5 μM ClFDP (for the ClFDP-induced-hRNR-α_6) or assay buffer (for the monomers) in 50 mM Hepes (pH 7.6). For the hRNR-α monomers, the reaction mixture was incubated at 37 °C for 3 minutes prior to filtration and injection into a column as previous described in *Gel filtration analysis (SEC)* (*chapter 3*). For the ClFDP-induced-hexamers, the reaction mixture without HNH (or HNHΔAPIM) was pre-incubated at 37 °C for 2 minutes prior to addition of the protein of interest and subsequent incubation at 37 °C for another 3 minutes, filtration, and injection onto a column; 1 mL fractions were collected and 2% from each fraction was used for SDS-PAGE analysis. Protein bands were visualized by silver staining (Figure A-5 and A-6).

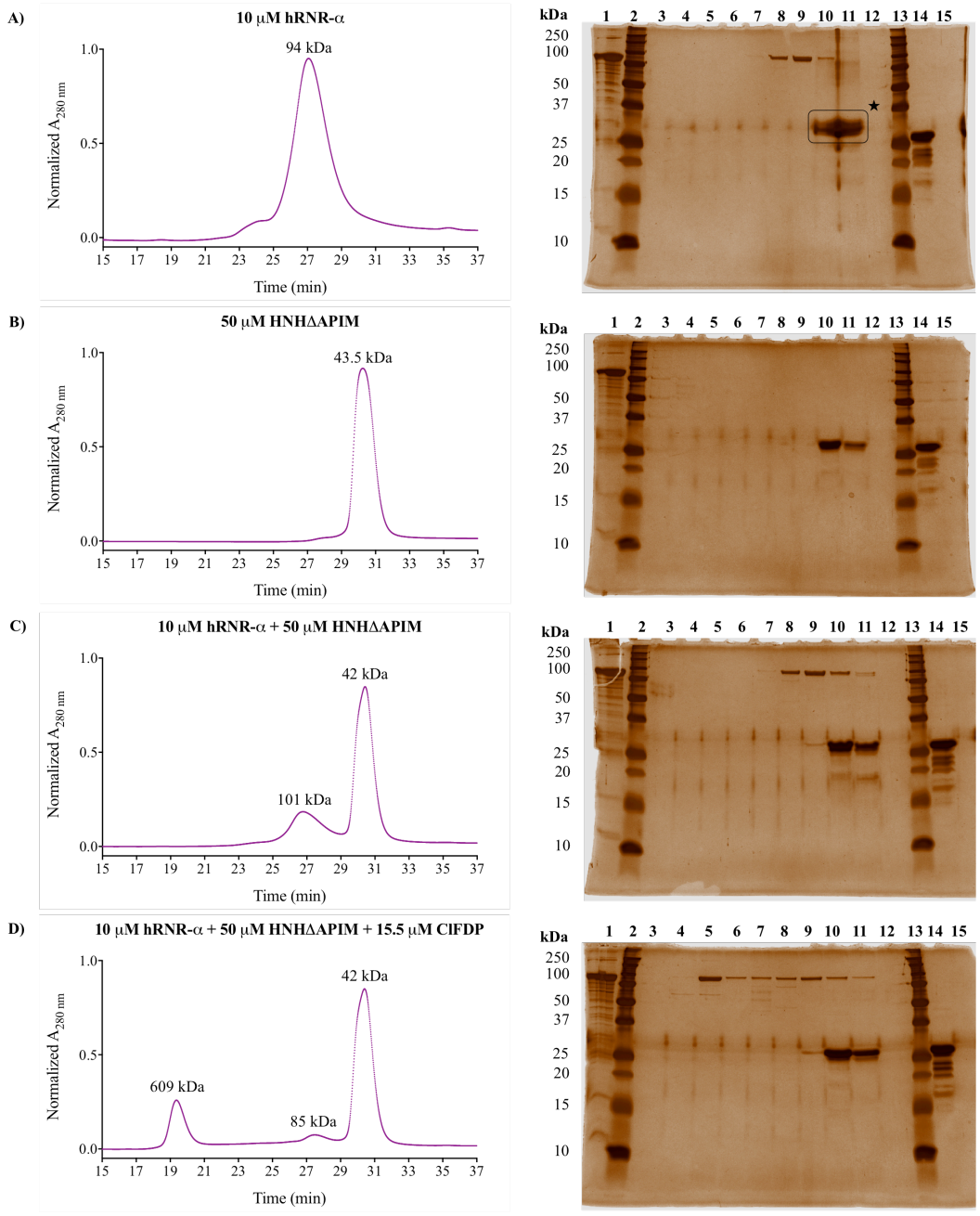

Lane		Lane		Lane	
1	Recombinant hRNR-α	6	Fraction from 21–23 min	11	Fraction from 31–33 min
2	M.W. marker	7	Fraction from 23–25 min	12	Fraction from 33–35 min
3	Fraction from 15–17 min	8	Fraction from 25–27 min	13	M.W. marker
4	Fraction from 17–19 min	9	Fraction from 27–29 min	14	Recombinant HNHΔAPIM
5	Fraction from 19–21 min	10	Fraction from 29–31 min	15	Empty

Figure A-5. Examination of the interactions between hRNR-α (90 kDa) and HNHΔAPIM (27 kDa). **A–B** show characteristic profiles of purified recombinant

hRNR-α and HNHΔAPIM, respectively. **C–D** show profiles of the reaction mixture of HNHΔAPIM and two oligomeric states of hRNR-α; **C**) the monomers and **D**) the ClFDP-induced-hRNR-α_6. *Right panels* show SDS-PAGE gel analyses of fractions obtained from the corresponding SEC chromatograms shown on the *left panels*. Note: A smear observed on the SDS-PAGE gel of the hRNR-α alone sample (★) was not from the recombinant protein, but most likely from a contaminant on the gel cassette.

Shown in Figure A-5A, the purified recombinant hRNR-α eluted from the column during 25–31 minute retention time, while the purified recombinant HNHΔAPIM eluted during 29–33 minutes (Figure A-5B). However, incubation of HNHΔAPIM with hRNR-α and subsequent SEC analysis yielded an additional band ~90 kDa, which corresponds to hRNR-α, in fraction 11 (Figure A-5C, *right panel*). This band was not observed in the recombinant hRNR-α alone control (Figure A-5A, *right panel*). Likewise, upon incubation of HNHΔAPIM with the ClFDP-induced-hRNR-α_6, hRNR-α eluted during 19–33 minutes retention time (Figure A-5D, *right panel*). From our previous data, however, ClFDP-induced-hRNR-α_6 alone in the absence of the HNHΔAPIM normally eluted as a single peak around 19–21 minute retention time (data not shown). Similar results were also observed when HNH was used instead of HNHΔAPIM (Figure A-6). Under an assumption that the similar results observed from these two independent sets of experiments are from protein-protein interactions, the APIM domain does not seem to be an essential factor for the binding between the HNH domain and hRNR-α (either in monomeric or hexameric states). Since we cannot exclude the possibility that these two proteins just co-elute, further experiments (*i.e.,* pull-down assays using specific affinity resins) are needed to confirm their binding interactions.

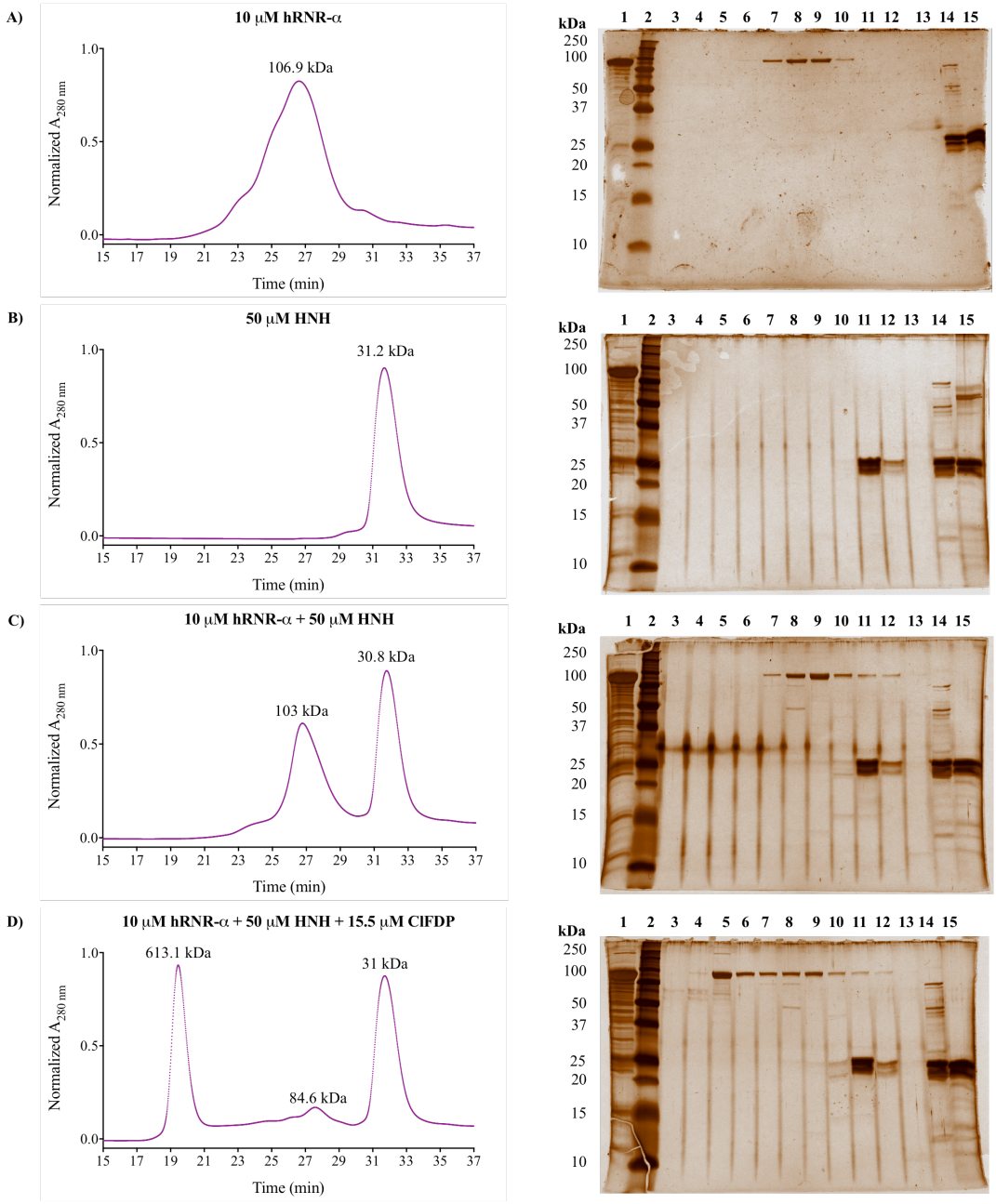

Lane		Lane		Lane	
1	Recombinant hRNR-α	**6**	Fraction from 21–23 min	**11**	Fraction from 31–33 min
2	M.W. marker	**7**	Fraction from 23–25 min	**12**	Fraction from 33–35 min
3	Fraction from 15–17 min	**8**	Fraction from 25–27 min	**13**	Fraction from 35–37 min
4	Fraction from 17–19 min	**9**	Fraction from 27–29 min	**14**	Recombinant HNH (monomer)
5	Fraction from 19–21 min	**10**	Fraction from 29–31 min	**15**	Recombinant HNH (dimer)

Figure A-6. Examination of the interactions between hRNR-α (90 kDa) and HNH (27 kDa). **A–B** show characteristic profiles of purified recombinant hRNR-α and

HNH, respectively. **C–D** show profiles of the reaction mixture of HNH and two oligomeric states of hRNR-α; **C**) the monomers and **D**) the ClFDP-induced-hRNR-α_6. *Right panels* show SDS-PAGE gel analyses of fractions obtained from the corresponding SEC chromatograms shown on the *left panels*. Note: this set of experiments and the one from Figure A-5 were independently performed.

REFERENCE

[1] Weston, R., Peeters, H., and Ahel, D. (2012) ZRANB3 is a structure-specific ATP-dependent endonuclease involved in replication stress response. *Genes Dev. 26*, 1558-1572.

[2] Wang, B., Alam, S. L., Meyer, H. H., Payne, M., Stemmler, T. L., Davis, D. R., and Sundquist, W. I. (2003) Structure and ubiquitin interactions of the conserved zinc finger domain of Npl4. *J. Biol. Chem. 278*, 20225-20234.

[3] Gilljam, K. M., Feyzi, E., Aas, P. A., Sousa, M. M., Muller, R., Vagbo, C. B., Catterall, T. C., Liabakk, N. B., Slupphaug, G., Drablos, F., Krokan, H. E., and Otterlei, M. (2009) Identification of a novel, widespread, and functionally important PCNA-binding motif. *J. Cell. Biol. 186*, 645-654.

[4] Salguero, I., Guarino, E., Shepherd, M. E., Deegan, T. D., Havens, C. G., MacNeill, S. A., Walter, J. C., and Kearsey, S. E. (2012) Ribonucleotide reductase activity is coupled to DNA synthesis via proliferating cell nuclear antigen. *Curr. Biol. 22*, 720-726.

APPENDIX B

^{1}H and ^{31}P NMR Spectra of ClA(M/D/T)P and FlU(D/T)P

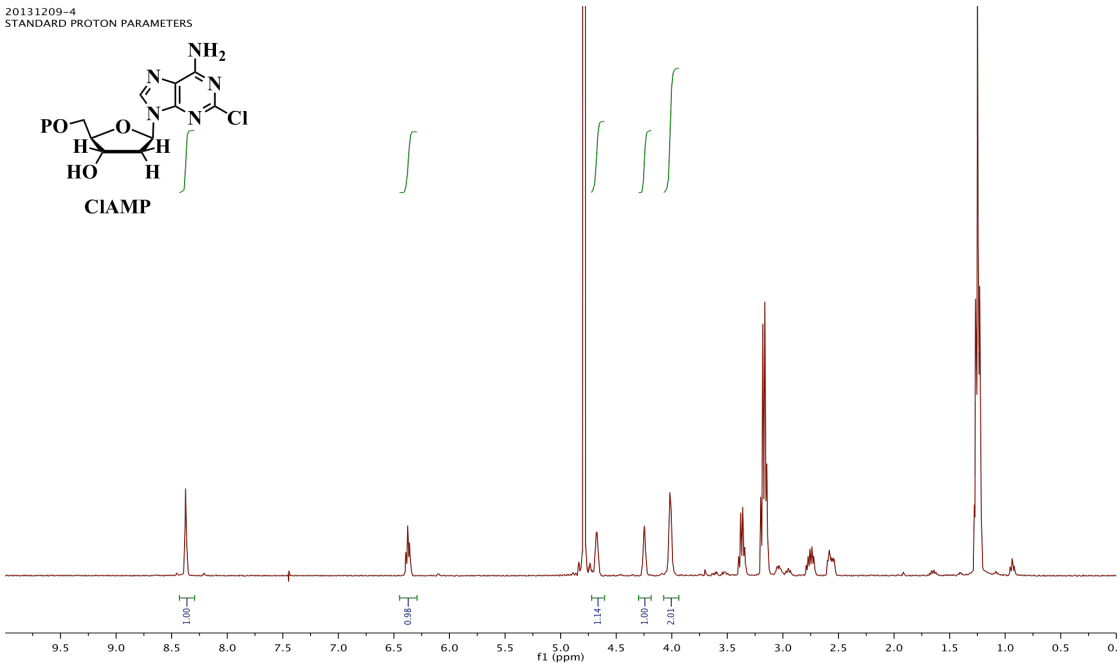

Figure A-7. ^{1}H-NMR spectrum of ClAMP (600 MHz, D_2O).

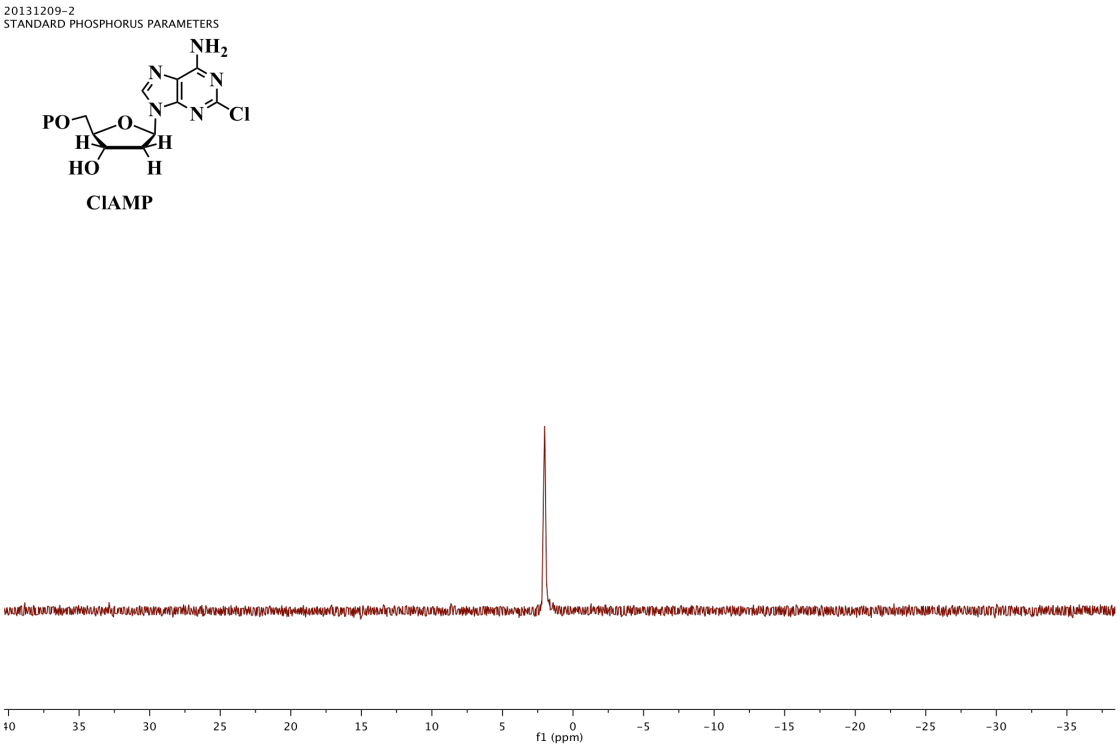

Figure A-8. ^{31}P-NMR spectrum of ClAMP (501 MHz, D_2O, H_3PO_4 external reference).

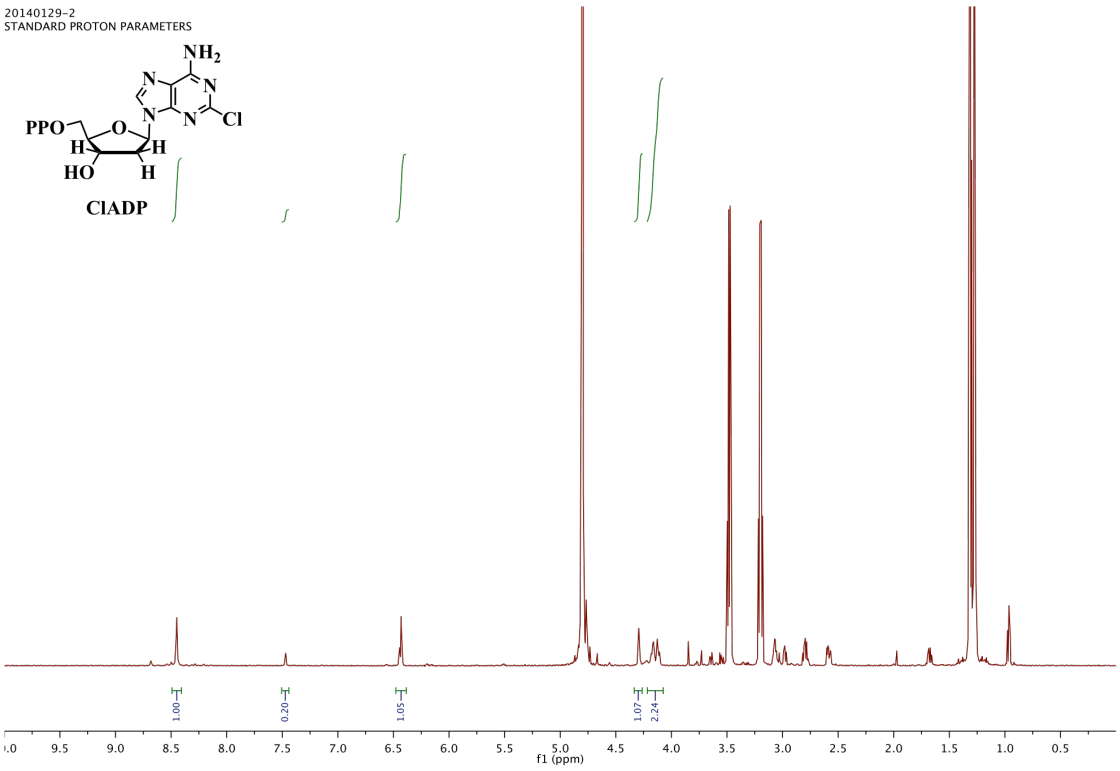

Figure A-9. ^{1}H-NMR spectrum of ClADP (600 MHz, D_2O).

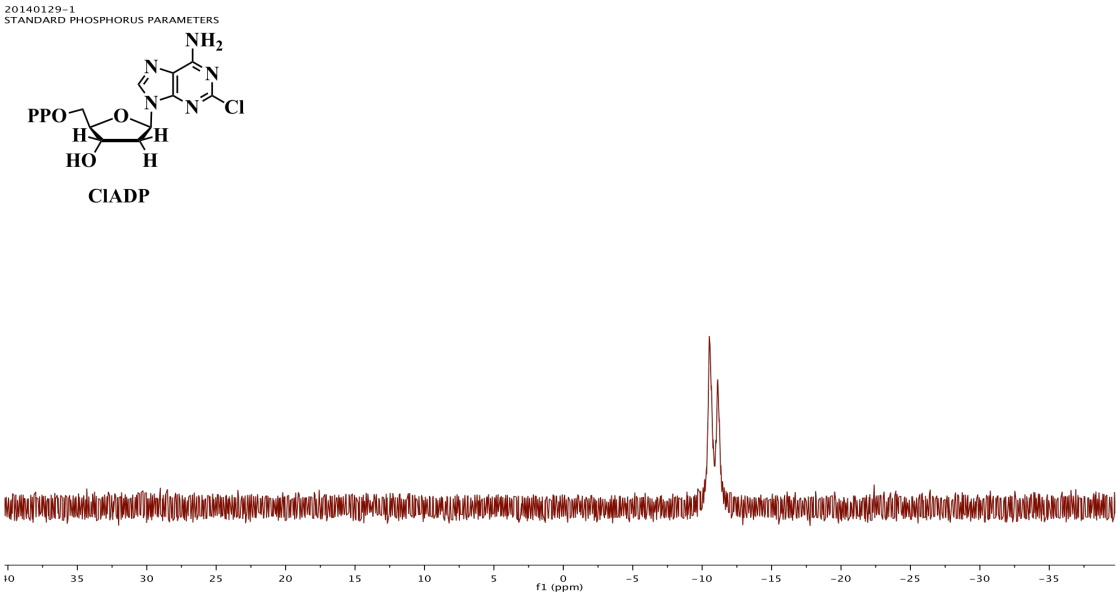

Figure A-10. ^{31}P-NMR spectrum of ClADP (501 MHz, D_2O, H_3PO_4 external reference).

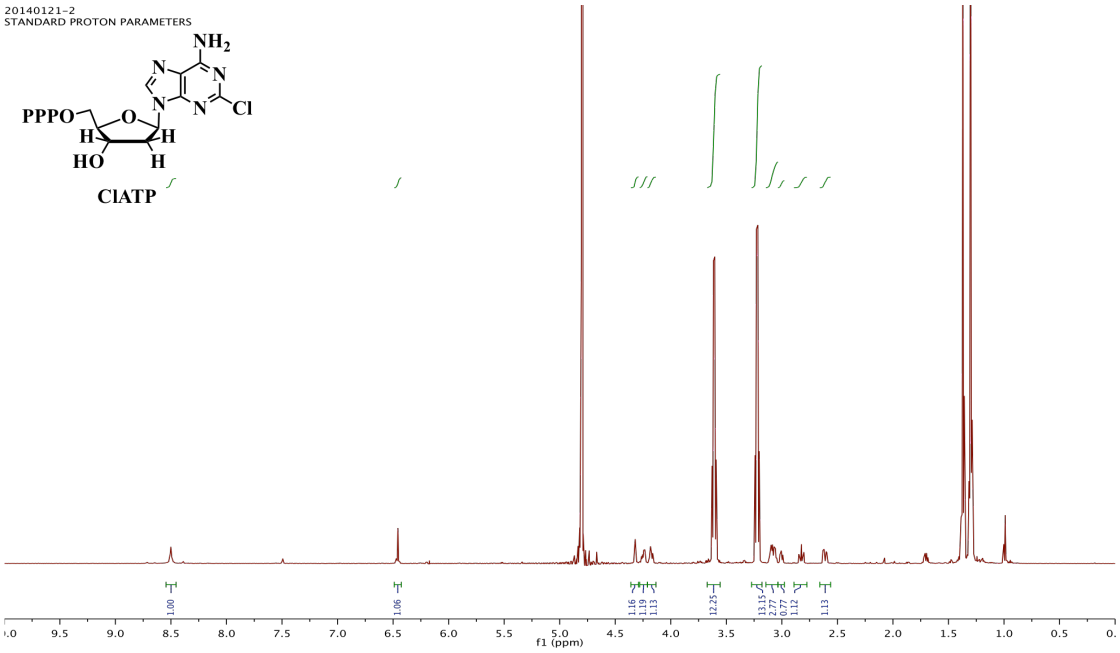

Figure A-11. ^{1}H-NMR spectrum of ClATP (600 MHz, D_2O).

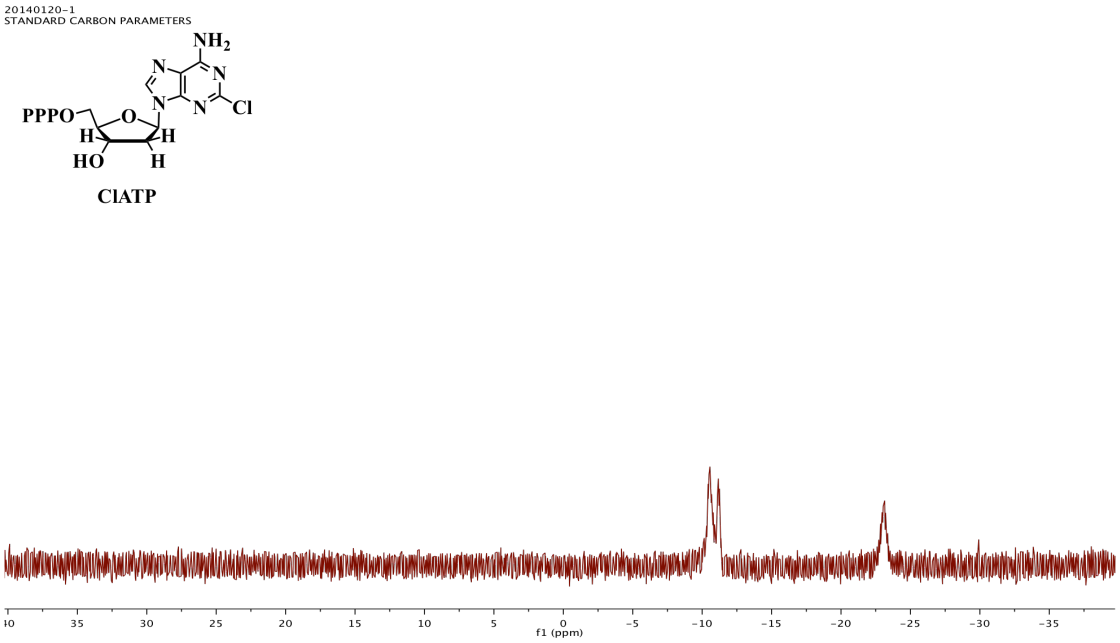

Figure A-12. ^{31}P-NMR spectrum of ClATP (400 MHz, D_2O, H_3PO_4 external reference).

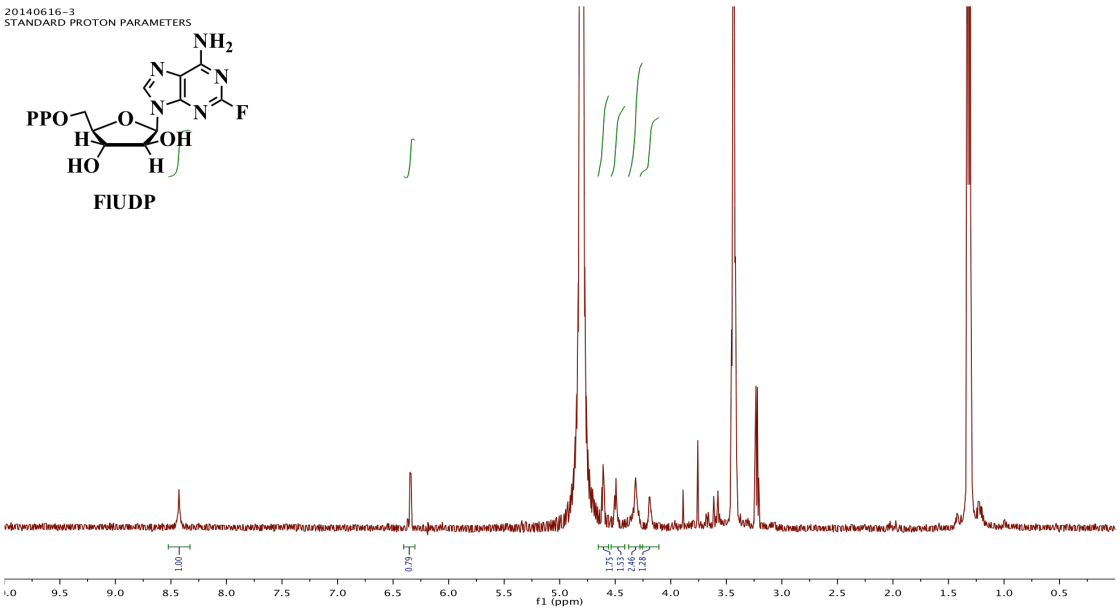

Figure A-13. ^{1}H-NMR spectrum of FlUDP (600 MHz, D_2O)

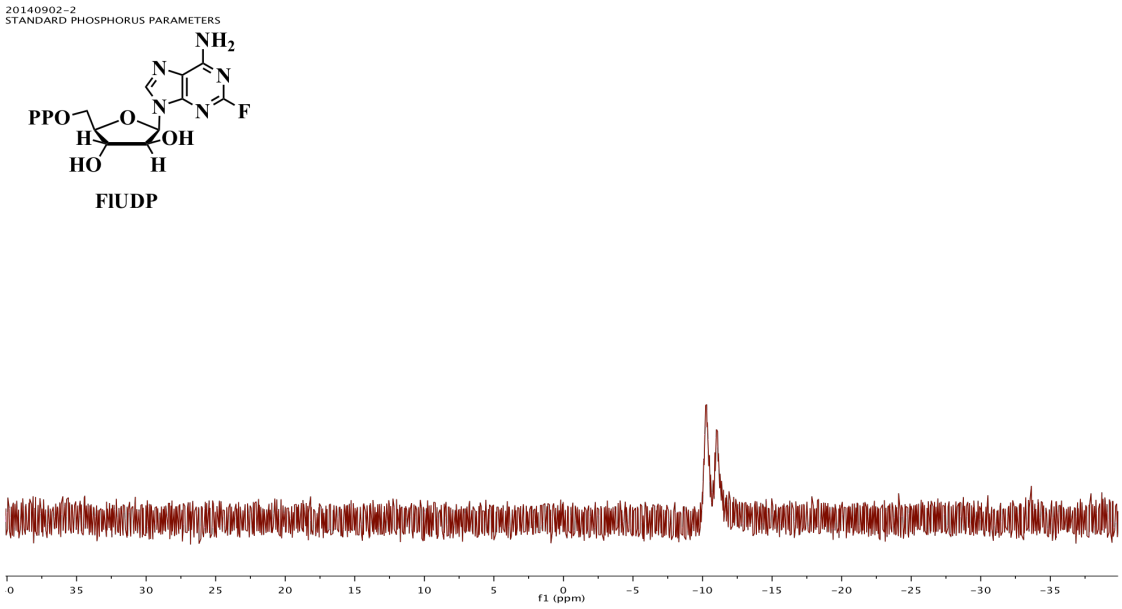

Figure A-14. ^{31}P-NMR spectrum of FlUDP (501 MHz, D_2O, H_3PO_4 external reference).

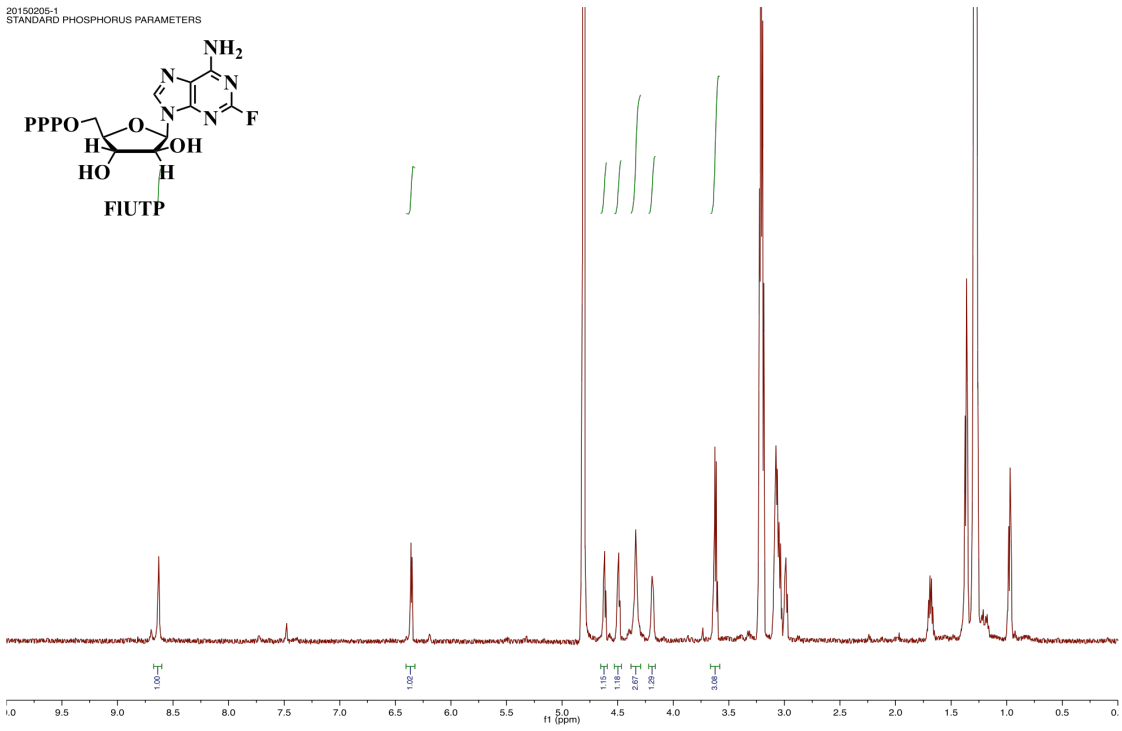

Figure A-15. ^{1}H-NMR spectrum of FlUTP (600 MHz, D_2O)

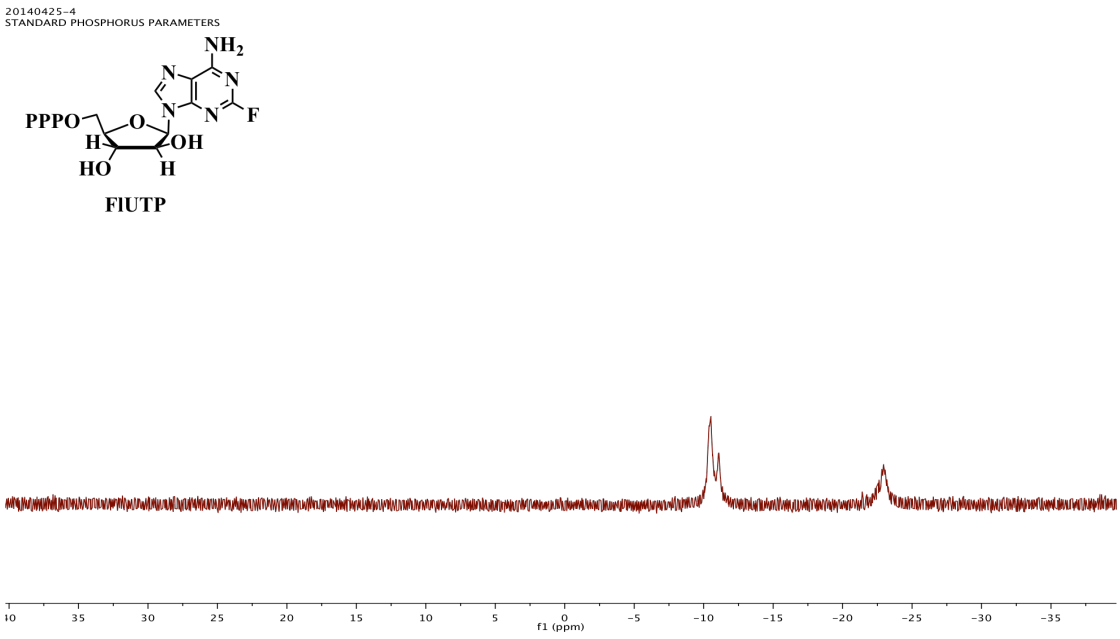

Figure A-16. ^{31}P-NMR spectrum of FlUTP (501 MHz, D_2O, H_3PO_4 external reference).

APPENDIX C

Fluorescence Resonance Transfer (FRET) Quenching Assays

Supporting Information

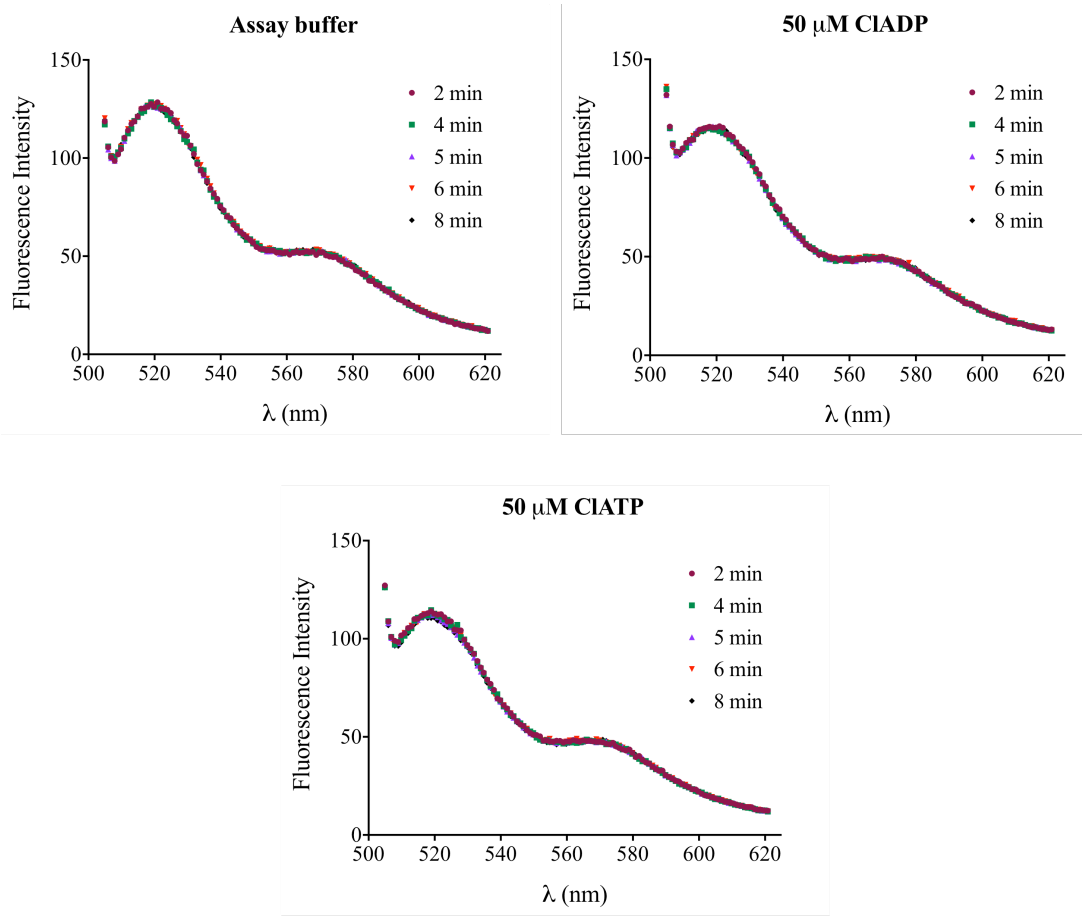

Figure A-17. Fluorescence intensities measured after adding 0.5 μL of either assay buffer (20 mM Hepes, pH 7.6) for a control, 22 mM ClADP, or 22 mM ClATP into the original assay mixture (220 μL) containing F-α and T-α in a 1:5 ratio at the indicated time points post incubation at RT. (Assay final volume = 220.5 μL) Final concentrations were calculated under an assumption that changes in volume was negligible.

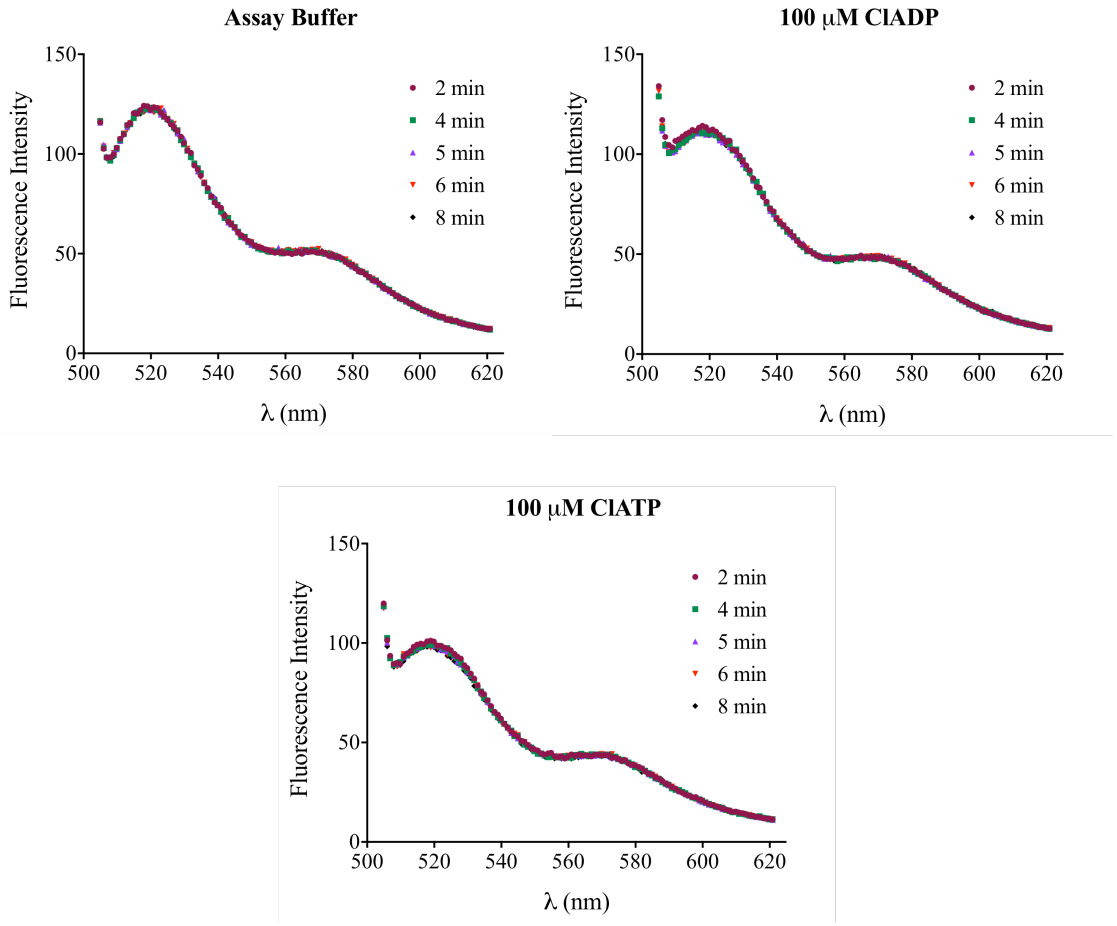

Figure A-18. Fluorescence intensities measured after directly adding 0.5 μL of either assay buffer (20 mM Hepes, pH 7.6) for a control, 22 mM ClADP, or 22 mM ClATP into the mixture obtained from Figure A-17 at the indicated time points post incubation at RT. (Assay final volume = 221 μL) Final concentrations were calculated under an assumption that changes in volume were negligible.

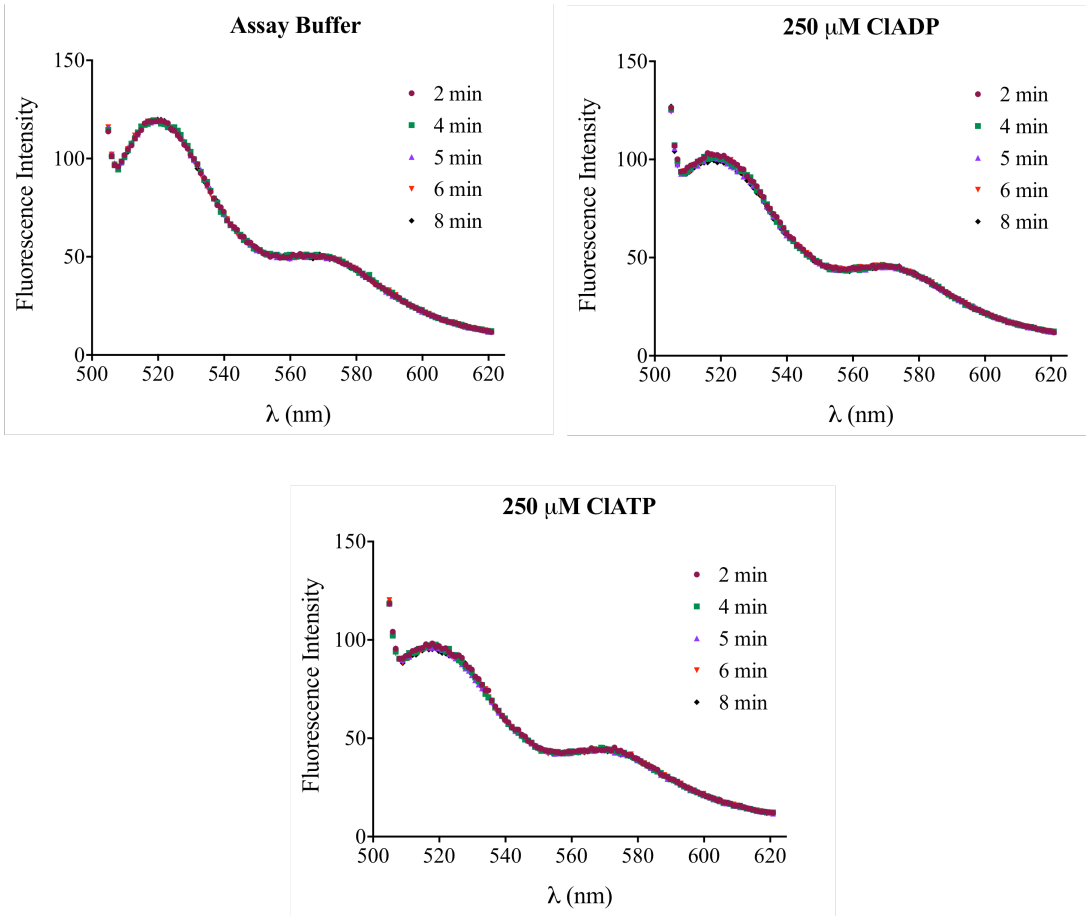

Figure A-19. Fluorescence intensities measured after directly adding 1.5 μL of either assay buffer (20 mM Hepes, pH 7.6) for a control, 22 mM ClADP, or 22 mM ClATP into the mixture obtained from Figure A-18 at the indicated time points post incubation at RT. (Assay final volume = 222.5 μL) Final concentrations were calculated under an assumption that changes in volume were negligible.